HIERARCHICAL STRUCTURAL MODELS OF PORTFOLIO CREDIT RISK

by

Junming Huang

B.S. in Applied Mathematics, Sun Yat-sen University, 2006

M.S. in Mathematical Finance, University of Pittsburgh, 2008

Submitted to the Graduate Faculty of

the Department of Mathematics in partial fulfillment

of the requirements for the degree of

Doctor of Philosophy

University of Pittsburgh

2013

UNIVERSITY OF PITTSBURGH

DEPARTMENT OF MATHEMATICS

This dissertation was presented

by

Junming Huang

It was defended on

April 8, 2013

and approved by

Professor John Chadam, Department of Mathematics

Professor Xinfu Chen, Department of Mathematics

Professor Brent Doiron, Department of Mathematics

Professor Satish Iyengar, Department of Statistics

Professor Jean-François Richard, Department of Economics

Dissertation Director: Professor John Chadam, Department of Mathematics

HIERARCHICAL STRUCTURAL MODELS OF PORTFOLIO CREDIT RISK

Junming Huang, PhD

University of Pittsburgh, 2013

In this thesis, we will study hierarchical structural models of portfolio credit defaults that incorporate cyclical dependence and contagion to capture market phenomena such as multi-humped loss distributions. We will use both analytical methods and Monte Carlo simulations in our study. Some of these new models will be calibrated to standard market models to illustrate their effectiveness in pricing single-name CDS's and CDO tranches simultaneously.

Keywords: Hierarchical Structural Models, Cyclical Dependence, Contagion, Multi-humped Loss Distribution, Monte Carlo Simulations, Large Portfolio Approximation, Calibration, Credit Default Swaps, Collateralized Debt Obligations.

TABLE OF CONTENTS

LIST OF TABLES

LIST OF FIGURES

1.0 INTRODUCTION

1.1 MOTIVATION

The recent financial crisis has posed a significant challenge for the mathematical modeling of credit default. Many of the credit derivatives that incurred substantial losses, including CDOs, are based on the credit worthiness of a large number of obligors (typically 100-125 names). As shown by empirical study, defaults are correlated, and it is extremely important to derive an appropriate model for this dependence structure. In particular, credit defaults typically exhibit cyclical correlation and default contagion. According to Giesecke and Weber (2004) [14], cyclical correlation is due to the dependence of firms on common economic factors. Contagion, on the other hand, is associated with the local interaction of firms with their business partners. These two types of dependence structures lead to market phenomena such as default clustering and a multi-humped distribution of portfolio loss (i.e., the occurrence of larger losses with higher probability) which have not been well captured in the current literature. Hence, modeling default correlation and contagion is a growing research topic in credit risk modeling that has a significant impact on industrial practice. In this thesis, we study hierarchical (factor) structural credit default models that attempt to capture both the cyclical dependence and contagion effects.

A structural model provides a causal relationship between a firm's asset values (later referred to as the default index, credit quality, credit worthiness) and its liabilities (later referred to as the default barrier). In such a model, a firm defaults on its debt if its asset value drops below its debt value; that is, the firm becomes insolvent. Here, there are two approaches in defining the default time. When it comes to multiple firms, a hierarchical structure correlates the credit qualities of different companies through a systematic factor (e.g., the state of the economy) so that each firm's

default index can be decomposed into a (common) systematic factor and an idiosyncratic component which are independent of each other. Though economically intuitive, within the hierarchical structural modeling framework, more realistic models beyond the basic model need to be developed for pricing single-name CDS contracts and CDO tranches consistently. With the modeling complexity of both the cyclical dependence and the contagion as well as the high dimensionality, it is in general difficult to derive analytical results on interesting quantities such as the first-to-default (FtD) probability and the loss distribution needed to understand and price these credit instruments. Monte Carlo simulations are therefore needed to study these models combined with the aid of asymptotic analysis as the size of the portfolio becomes large. As a direct application of our models to the financial market, a selection of these new models are calibrated to establish their effectiveness.

1.2 LITERATURE SURVEY ON CREDIT DEFAULT MODELS

Currently, there are three basic types of credit default models: the copula model, the intensity model, and the structural model. In this thesis, we will focus on structural models. On the other hand, copula models will be used as an alternative to generate data to be calibrated to some of the new structural models that we develop. Before we discuss the literature on structural models in detail, we would like to briefly describe the copula and the intensity approaches.

1.2.1 Copula Models and Intensity Models

Before the (subprime) credit crisis, the most popular model for multi-name credit defaults was the copula model. A copula model is a tool to separate the dependence structure between different obligors from their marginal default probabilities, with minor insight into the "real correlation structure". These copula models, including the Gaussian copula model, the pre-crisis market standard, were used extensively in pricing complex credit instruments such as the collateralized debt

obligations (CDO's) which typically consist of 125 companies. The CDO's have a complicated structure, including tranching of default risks associated with obligors that have a variety of credit ratings. Hence, a careful treatment of the correlation structure is necessary for understanding and pricing of CDO's. However, as the copula model lacks intuition and appropriate dynamics on the correlation structure, their misuse had a significant contribution to the recent credit crisis. More details of copula models are discussed in section 6.2 and in Schönbucher (2003) [37] or O'Kane (2008) [34].

Intensity models, on the other hand, are based on modeling the default time as the first arrival time of a counting process (e.g., a Poisson process). From an intuitive point of view, default can occur as a complete surprise. This approach focuses on modeling the "hazard rate" or "intensity" (which can be constant, time-dependent, random, or even stochastic) of the counting process. These intensity models are calibrated to directly fit the market data. In the multivariate case, some intensity models rely on the conditional independence assumption; that is, conditioned on the realization of default intensities, defaults are independent. Some other intensity models focus on modeling simultaneous jumps in such a way that the intensity of an obligor can be decomposed into a "crisis" intensity and an idiosyncratic intensity (see Duffie and Singleton (1999) [8]). Other intensity models follow the "top-down" approach in the sense that the intensity of the portfolio loss process is modeled as opposed to modeling individual defaults and then building the dependence structure as in the "bottom-up" approach. More on intensity models can be found in Schönbucher (2003) [37] or O'Kane (2008) [34].

1.2.2 Structural Models

In structural models, default occurs when the value of the firm falls below its liabilities. In the original Merton (1974) [32] setting, default can only occur at the maturity of the credit instrument. On the other hand, the Black-Cox approach (1976) [3] allows firms to default at any time on or before maturity; i.e., default is defined as the first-crossing-time that the value process drops below the firm's liability. Zhou (2001) [47] extended this approach to two dimensions, where he studied

the following model:

$$d\,lnV_{i,t} = \mu_i\,dt + \sigma_i\,dW_{i,t} \tag{1.1}$$

$$dW_{i,t}\,dW_{j,t} = \rho_{ij}\,dt \tag{1.2}$$

with $\tau_i = \inf\{t > 0 : V_{i,t} < K_i \exp(\lambda_i t)\}$ for $i = 1, 2$ and expressed the joint survival probability as an infinite series involving modified Bessel functions. Here, $V_{i,t}$ is the asset value process of firm i, μ_i is the expected growth rate of the asset value, $K_i \exp(\lambda_i t)$ is the debt value (liability), λ_i is the growth rate of the liability, and τ_i is the default time. Zhou (2001) [47] focused on the study of the (computationally less intensive) case where $\mu_i = \lambda_i$, after illustrating that the difference in expected asset and liability growth rate has little effect on default correlations with 1 or 2 year horizons and relatively small effect with 5 to 10 year horizons. Here, default correlation is taken to be the correlation between the default trigger indicators of firm i and firm j:

$$Corr[I\{\tau_i \le T\}, I\{\tau_j \le T\}] = \frac{E[I\{\tau_i \le T\}\,I\{\tau_j \le T\}] - E[I\{\tau_i \le T\}]E[I\{\tau_j \le T\}]}{\sqrt{Var[I\{\tau_i \le T\}]}\,\sqrt{Var[I\{\tau_j \le T\}]}} \tag{1.3}$$

For more than two names (firms, obligors), Vasicek (1987) [43] proposed a one-factor structural model for a homogeneous portfolio with a similar definition of default at maturity as Merton (1974) [32]:

$$X_{i,T} = \rho\,Y + \sqrt{1-\rho^2}\,\epsilon_i \tag{1.4}$$

with $\tau_i \le T$ if $X_{i,T} < K$, where $X_{i,T}$ is a credit index (for instance, the logarithm of the asset value) of firm i at maturity, Y is the "systematic factor" and ϵ_i is the "idiosyncratic component", ρ is the correlation between the asset of firm i and the systematic factor, and the barrier K is the same for all firms. Here, $(Y, \epsilon_1, ..., \epsilon_N)$ are taken to be independent standard normal random variables. Hence, conditional on the systematic state variable Y, defaults are independent. This allows for easy calculation of the portfolio loss distribution. Indeed, given the systematic factor Y, the marginal default probability for firm i is

$$\Pr(\tau_i \le T | Y = y) = \Phi\left(\frac{K - \rho\,y}{\sqrt{1-\rho^2}}\right) \tag{1.5}$$

In addition, with a zero recovery rate, the conditional probability distribution of the portfolio loss in this equally weighted setting $L = \frac{1}{N}\sum_{i=1}^{N} I\{\tau_i \le T\}$ (fraction of defaulted securities in

the portfolio) given $Y = y$ has a binomial distribution with probability mass function $\binom{N}{n} p^n (1-p)^{N-n}$ where $p = \Pr(\tau_i \leq T | Y = y)$ from equation (1.5) since the default indication $I\{\tau_i \leq T\} : \ i = 1, ..., N$ are independent Bernoulli random variables conditioned on Y. Hence, the unconditional loss distribution is

$$\Pr(L = \frac{n}{N}) = \int_{-\infty}^{\infty} \binom{N}{n} (\Phi(\frac{K - \rho\, y}{\sqrt{1-\rho^2}}))^n (1 - \Phi(\frac{K - \rho\, y}{\sqrt{1-\rho^2}}))^{N-n} \phi(y)\, dy \tag{1.6}$$

where n is the number of defaults in the portfolio and N is the portfolio size. Vasicek also derived a large portfolio approximation to the loss distribution as $N \to \infty$:

$$\Pr(L \leq x) = \Phi(\frac{1}{\rho}(\sqrt{1-\rho^2}\Phi^{-1}(x) - K)) \tag{1.7}$$

While structural models are intuitive, one disadvantage is that the default time as a stopping time in a diffusion-based structural model is predictable, namely, one can predict the occurrence of default as the asset value gets closer and closer to the default barrier. As a consequence, short-term credit spreads are unrealistically low in this setup.

Several authors have proposed remedies for this. One way is to consider alternative scenarios for the firm value process. Zhou (2001) [48] suggested a jump-diffusion model for the asset value process. Ruf and Scherer (2009) [35] provided an improved Brownian-bridge based Monte Carlo scheme for pricing corporate bonds in an arbitrary jump-diffusion model as well as an explicit formula for the time-zero limit of short-term spread. Siu et al. (2008) [39] considered a Markovian regime-switching geometric Brownian motion model for the asset of a single-name where both the drift and the volatility are governed by a two-state hidden Markov chain. All of the above three models are one-dimensional. Kim et al. (2008) [29] extended this regime-switching model to two dimensions. They found that CDS spreads are higher in economic recession than expansion, and increase regardless of maturity as the difference of volatilities between bear and bull markets increases. In addition, the spreads for basket defaults are higher when the intensity shifts from a bull to bear a market increases. Fouque et al. (2006) [10] studied the effect of stochastic volatility on the yield spread curve, in particular, the effect of volatility time scales. They proposed a two-factor volatility structure with both fast and slow stochastic volatilities for calibration to both short and long maturity spreads. Fouque et al. (2008) [11] proposed a multivariate first-crossing

model with stochastic volatility where default correlation is generated by correlation between the Brownian motions driving the individual names as well as through common stochastic volatility factors, and provided an approximation to the loss distribution using perturbation techniques. Metzler (2008) [33] argued that the lack of the capability of describing market data in multi-name structural models is due to the wrong "location" of systematic risk. He suggested that one should move the systematic risk from the correlated driving Brownian motions to the trend and volatility, and proposed a general factor model:

$$d\,X_{i,t} = \mu_i(M_t)\,dt + \sigma_i(V_t)\,dW_{i,t} \tag{1.8}$$

which includes Siu et al. (2008) [39], Kim et al. (2008) [29], Fouque et al. (2006) [10], Fouque et al. (2008) [11] as special cases. Here, the pair of processes (M, V) are (not necessarily independent) systematic factors which are independent of the independent sequence of idiosyncratic Brownian motions $W_1, ..., W_N$. He then studied three specific models in this framework: a random drift model, a linear model and a dynamic model, and was able to calibrate to both non-distressed (2006) and distressed (2008) tranche data. Hurd (2009) [22] considered using time-changed Brownian motions for the firms' value processes and introduced a notion of "first-crossing-time of the second kind" as the definition of default time. He also extended this approach to multi-firms by introducing a one-factor time-change model.

Other authors consider the effect of incomplete information and many of them are able to build the connection between structural models and reduced-form models within this framework. Duffie and Lando (2001) [9] considered a structural model with incomplete accounting information. In their model, investors cannot observe the assets directly, and can only receive periodic and noisy accounting reports. They showed that with imperfect information, credit spreads are strictly positive at zero maturity, and they derived a default-arrival intensity process for this model. While the market sees the manager's information with noise in Duffie and Lando (2001) [9], Çetin et al. (2004) [5] obtained a reduced-form model from the structural model by constructing an economy where the market sees a reduction of the manager's information set. Jarrow and Protter (2004) [25] argued that the difference between structural and reduced-form models should be characterized not in terms of the accessibility of the default time, but in terms of the information assumed known

by the modeler. In particular, they showed that if one reduces the information set available to the modeler, a structural model can be transformed into a hazard rate model. Giesecke (2006) [15] analyzed the role of information in structural models through a model definition of default time and a model filtration. He showed that when default is not observable with respect to the model filtration, the model admits a generalized reduced-form pricing formula in terms of the cumulative intensity. He also studied several types of incomplete information models and determined whether each model admits an intensity. Guo et al. (2009) [18] rigorously defined incomplete information with the notion of "delayed filtrations" that translates structural models into reduced-form models. Jarrow et al. (2007) [26] proposed a model where the market only observes the firm's asset value when it crosses certain levels, interpreted as changes significant enough for the firm's management to make a public announcement. Frey and Schmidt (2010) [13] studied structural and reduced-form models under incomplete information using a stochastic filtering approach. They also discussed the construction of a dynamic reduced-form model via nonlinear filtering as well as pricing, calibration and hedging in that model. Valužis (2008) [42] considered incomplete information due to interest-rate and liquidity risk and generalized the model of Zhou (2001) [47] by allowing the default thresholds to be stochastic for two firms. In his model, the default time is still predictable. While all of the above models consider incomplete information in the firm's value process and/or the default boundary, Jackson et al. (2009) [24] studied a randomized initial distance-to-default first-crossing model that makes the matching distribution problem analytically tractable. On the other hand, Katz and Shokhirev (2010) [28] captured uncertainty related to the firm's ability to avoid default even if its liabilities momentarily exceed its assets by replacing the absorbing boundary condition in the diffusion with the radiation boundary condition, which produces an unpredictable default time. A related model was given by Yildirim (2006) [46] that defined default time (more precisely, liquidation time) as the first time the asset crosses the barrier and the area under the barrier is greater than a prespecified exogenous level. In particular, Yildirim defined A_t as the cumulative area of the firm value process below an exhaust level b, representing the total loss in firm value with respect to b:

$$A_t = \int_0^t V_s \, I\{V_s < b\} \, ds \tag{1.9}$$

Default (liquidation) time is defined as (given the exogenous level $\bar{b}$ independent of b):

$$\tau = \inf\{t > 0 : A_t > \bar{b}\} \tag{1.10}$$

To address contagion effects, Haworth (2006) [19] proposed a structural model with default contagion. She first developed a two-dimensional first-crossing model with contagion. In this model, company one (the subsidiary) defaults if the asset of either company goes below its barrier. Then she incorporated a more realistic contagion structure by increasing the volatility of the other companies by a factor if one company defaults. She also investigated the effect of contagion decay on basket credit spreads; that is, the volatility jumps if one of the companies defaults and then decays back to the original level exponentially.

1.3 OUTLINE OF THESIS

The remaining part of the thesis is arranged as follows.

Chapter 2 studies the simplest hierarchical structural model analytically as a tool for validating the Monte Carlo methods in chapter 3. There are two approaches in defining default in a structural model. In Merton (1974) [32] and Vasicek (1987) [43], default occurs if the company cannot payoff its debt at the maturity. In contrast, Black and Cox (1976) [3] defines default as the first time that the firm become insolvent, which has more dynamics. These two types of definitions will be compared for the models we study. In section 2.1, existing results on the first-to-default probability (needed to price first-to-default swaps) in 2 dimensions (i.e., a portfolio of two firms) are stated and analytic formulas in higher dimensions are given for both the uncorrelated and the perfectly correlated cases. In section 2.2, the loss distribution (needed to price CDO's) is studied with several of the existing results stated for the large homogeneous portfolio approximation in the Vasicek setting. In addition, we will derive the following new results:

- The peak of the loss distribution when the correlation is 0 (section 2.2.1).

- The behavior of the large homogeneous loss density at the extreme losses (when all firms survive and when all firms default) (section 2.2.2.1).
- The behavior of the large homogeneous loss density at the extreme correlations (when all firms are independent and when all firms are perfectly correlated) (section 2.2.2.2).
- The monotonicity of the large homogeneous loss density with respect to the portfolio loss (section 2.2.2.3).
- The large portfolio approximation for a heterogeneous portfolio will be studied in section 2.2.2.4 with the desired multi-hump feature generated by the heterogeneity.

Section 2.3 is a chapter summary.

Chapter 3 describes the Monte Carlo methods to be used to study the more sophisticated models in chapters 4 and 5. Section 3.1 is a brief description of Monte Carlo estimates for boundary crossing probabilities. In particular, the barrier-shifting techniques (BAST) in Gobet (2008) [17] for estimating first-crossing probabilities in high dimensions will be described in detail. The standard deviation of the Monte Carlo estimator will also be given in section 3.1. In section 3.2, these Monte Carlo methods especially Gobet's BAST will be tested against the analytic results studied in chapter 2. In particular, we will validate the BAST by matching the following analytic results:

- The first-to-default probability appearing in section 2.1 for a homogeneous portfolio will be validated in section 3.2.1.1.
- The first-to-default probability appearing in section 2.1 for a heterogeneous portfolio will be validated in section 3.2.1.2.
- The effect of the number of simulations and stepsize will be studied in section 3.2.1.3.
- The peak of the loss distribution when the correlation is 0 appearing in section 2.2.1 will be validated in section 3.2.2.1.
- The extreme loss behavior of the large homogeneous portfolio approximation appearing in section 2.2.2.1 will be validated in section 3.2.2.2.
- The large portfolio approximation for a heterogeneous portfolio appearing in section 2.2.2.4 will be validated in section 3.2.2.3.

Section 3.3 is a chapter summary.

Chapter 4 studies financially more realistic models with a focus on the cyclical dependence (dependence of credit qualities on macroeconomic factors), using the Monte Carlo methods validated in chapter 3. In section 4.1, we will examine a model in which the default barrier switches between a "good" state and a "bad" state, reflecting the possibility of a false liability report. In section 4.2, we will study models in which the correlation switches between a low value when the economy is good and a high value when the economy is bad. In section 4.3, models with financially motivated drift behavior will be investigated. In particular, a drift switching model in section 4.3.1 is able to generate a multi-humped loss distribution which can be seen analytically as an application of the principle of the large portfolio approximation (see Schönbucher (2003) [37]) and Levy's arcsin law (see Steele (2000) [40]). Based on this, in section 4.3.2, we develop an analytically more tractable random drift model which is essentially a good analytic approximation of the drift switching model that allows for a fast calculation of the loss distribution using a recursive algorithm. Section 4.4 is devoted to models with a random initial state to address the issue of low short-term spreads in structural models. The models in section 4.4 will be calibrated in chapter 6 to data generated by a standard market model. In particular, a gamma initial state model with a switching correlation will be studied in section 4.4.2 and a truncated normal initial state model with a random correlation will be studied in section 4.4.3. Both models are able to generate a multi-humped loss distribution. In section 4.5, we will study mean-reverting models. In section 4.5.1, a mean-reverting stochastic correlation model will be examined that allows for the correlation to revert to its long-term mean with a random fluctuation which is anti-cyclical (i.e., the correlation increases as the economy gets worse). In section 4.5.2, a model with a mean-reverting systematic factor proposed to reflect business cycles is investigated. Section 4.6 is a chapter summary.

Chapter 5 studies contagion models using Monte Carlo simulations. In section 5.1, we will examine a structural model with contagion similar to Haworth (2006) [19] which increases the volatility of the surviving firms whenever a default occurs in the same industry. In section 5.2, we propose a jump diffusion model with an infectious jump size for which the sizes of both the up-jumps and down-jumps depend on the number of defaults that have occurred in the same sec-

tor. In section 5.3, we will investigate a jump diffusion model with an infectious jump intensity for which the frequency of the down-jumps increases as the number of defaults in that sector increases. Section 5.4 combines the drift switching in section 4.3.1, the cyclical (mean-reverting) economy in section 4.5.2, and the infectious volatility in section 5.1 into a "hybrid" model to capture both the cyclical dependence and the contagion. Section 5.5 is a chapter summary.

In chapter 6, we will apply the models in section 4.4 directly to the financial market by calibrating them to a standard market model. Section 6.1 will be an introduction pointing out the inconsistency prevalent in real markets between the single-name CDS spreads and the multi-name tranche spreads due to liquidity and investor preferences. As a preliminary exercise, the common random initial state model in section 4.4.1 will be calibrated to market quotes of CDO tranches in 125 dimensions. In section 6.2, we will introduce the pre-crisis standard copula models, including the mixing copula model in O'Kane (2008) [34]. This model will be used to generate data for a 5-dimensional bespoke portfolio that we will use for calibration. In section 6.3, we will calibrate the correlation switching with a gamma random initial model in 4.4.2 to the bespoke data. In section 6.4, the same set of data will be calibrated to the random correlation model with a truncated normal initial in section 4.4.3. We will see that the model in 4.4.3 is able to simultaneously calibrate to the single-name and multi-name bespoke data. Section 6.5 is a chapter summary.

In chapter 7, we will conclude the thesis and discuss some future work.

2.0 A SIMPLE HIERARCHICAL STRUCTURAL MODEL

For background and later comparison, we begin with a simple hierarchical structural model with one systematic factor for a portfolio of N credits (later referred to as the Toy Model) in which the default index is governed by the following stochastic differential equation (SDE) (note: throughout the thesis, we implicitly assume that regulatory conditions are satisfied to ensure the existence and uniqueness of solutions to SDE's used in the thesis):

$$d\,X_{i,t} = \rho_i\,dW_t + \sqrt{1-\rho_i^2}\,dB_{i,t}, \quad X_{i,0} = 0 \tag{2.1}$$

with the default time in the first-crossing setup defined by

$$\tau_i = \inf\{t > 0 : X_{i,t} < K_i\} \tag{2.2}$$

where $W, B_1, ..., B_N$ are independent standard Brownian motions, and $\rho_1, ..., \rho_N$ are constants. We interpret the default index $X_{i,t}$ as the "credit quality" of firm i which can be some function of the firm's asset value, W_t as the systematic factor, $B_{i,t}$ as the idiosyncratic component, K_i as the default barrier, and ρ_i as the "correlation" between firm i and the "market". Hence, $X_{i,t} - K_i$ can be understood as the log solvency ratio or the distance-to-default. This is the basic "hierarchical structure" in which individual risk factors are modeled through correlation to some systematic factor(s). In this one-factor setting, the asset correlation between firm i and firm j is $\rho_i\,\rho_j$. More precisely,

$$Corr[X_{i,t}, X_{j,t}] = \frac{E[X_{i,t}\,X_{j,t}] - E[X_{i,t}]E[X_{j,t}]}{\sqrt{Var[X_{i,t}]}\,\sqrt{Var[X_{j,t}]}} = \frac{\rho_i\,\rho_j\,t}{t} = \rho_i\,\rho_j \tag{2.3}$$

Notice that the asset correlation in this model is a known constant. In later chapters, we will investigate more sophisticated models in which the asset correlation can be time-dependent, random

and stochastic. There will also be models where the barrier K or equivalently the initial distance-to-default X_0 is random. Also, the systematic factor may be modeled by a more sophisticated process other than the simple Brownian motion. We shall also study contagion models where a default event in one industry increases another firm's default risk in the same industry. These models are much more difficult to study analytically and hence need to be studied using Monte Carlo simulations. Before we discuss Monte Carlo methods, we state existing analytical results and derive new analytical results for these simple structural models in order to have guidelines for validating the Monte Carlo methods we will use in later chapters when we study more realistic models.

2.1 FIRST-TO-DEFAULT PROBABILITY

The first quantity we are interested in is the first-to-default (FtD) probability which is used in pricing and hedging basket derivatives such as First-to-Default Swaps. When there are only two firms, the first-to-default probability in the first-crossing setup is known explicitly (Zhou (2001) [47]).

$$\begin{aligned}&\Pr(\min\{\tau_1,\tau_2\}\le T)\\&=1-\frac{2r_0}{\sqrt{2\pi T}}\exp\{-\frac{r_0^2}{4T}\}\sum_{n=1,3,\ldots}\frac{1}{n}\sin(\frac{n\pi\theta_0}{\alpha})\left[I_{\frac{1}{2}(\frac{n\pi}{\alpha}+1)}(\frac{r_0^2}{4T})+I_{\frac{1}{2}(\frac{n\pi}{\alpha}-1)}(\frac{r_0^2}{4T})\right]\end{aligned}\tag{2.4}$$

where $I_\nu(z)$ is the modified Bessel function of the first kind with order ν, and

$$\alpha=\begin{cases}\arctan(-\frac{\sqrt{1-\rho_1^2\rho_2^2}}{\rho_1\rho_2}), & \text{if } \rho_1\rho_2<0\\ \pi+\arctan(-\frac{\sqrt{1-\rho_1^2\rho_2^2}}{\rho_1\rho_2}), & \text{otherwise}\end{cases}\tag{2.5}$$

$$\theta_0=\begin{cases}\arctan(-\frac{K_2\sqrt{1-\rho_1^2\rho_2^2}}{K_1-\rho_1\rho_2K_2}), & \text{if } (\cdot)<0\\ \pi+\arctan(-\frac{K_2\sqrt{1-\rho_1^2\rho_2^2}}{K_1-\rho_1\rho_2K_2}), & \text{otherwise}\end{cases}\tag{2.6}$$

$$r_0=\frac{-K_2}{\sin(\theta_0)}\tag{2.7}$$

In order to get a general idea of the difference between the first crossing and Vasicek definitions of default, we compare the two-dimensional exact FtD probability in these two setups.

Recall that in the Vasicek setting, $\tau_i^{Vasicek} \leq T$ if $X_{i,T} < K_i$. For two firms, the first-to-default probability is

$$\begin{aligned} &\Pr(\min\{\tau_1^{Vasicek}, \tau_2^{Vasicek}\} \leq T) \\ &= \Pr(X_{1,T} \leq K_1, X_{2,T} \leq K_2) \\ &= \Phi(\frac{K_1}{\sqrt{T}}) + \Phi(\frac{K_2}{\sqrt{T}}) - \Phi_2(\frac{K_1}{\sqrt{T}}, \frac{K_2}{\sqrt{T}}; \rho_1\rho_2) \end{aligned} \tag{2.8}$$

where $\Phi_2(x_1, x_2; \rho)$ denotes the two-dimensional normal CDF with mean $[0 \;\; 0]$ and covariance matrix $\begin{bmatrix} 1 & \rho \\ \rho & 1 \end{bmatrix}$, i.e.,

$$\Phi_2(x_1, x_2; \rho) = \int_{-\infty}^{x_1} \int_{-\infty}^{x_2} \frac{1}{2\pi\sqrt{1-\rho^2}} \exp\{-\frac{1}{2(1-\rho^2)}(u_1^2 - 2\rho u_1 u_2 + u_2^2)\} \, du_2 \, du_1 \tag{2.9}$$

For specificity in the comparison, we fix $K = -3$, $T = 5$ and vary $\rho_2 = -1, ..., 1$, and plot (figure 1 in Appendix B) the FtD probabilities (equations (2.4) and (2.8)) for different levels of $\rho_1 = 0.1, 0.5, 0.9$, represented by red, green and blue curves, respectively, where plain and asterisk represent first-crossing and Vasicek, respectively.

It is clear that the FtD probability in the first-crossing setup is much greater than for the Vasicek setup. This is an indication of modeling differences leading to significant changes in probability of default. For 100-125 names (the typical number involved in a CDO), these differences are enhanced. For more than two names, there is no explicit formula for the FtD probability in the first-crossing setting in general, except for $\rho = 0, 1$ in a homogeneous portfolio where $K_i = K : i = 1, ..., N$ and $\rho_i = \rho : \; i = 1, ..., N$. For such a homogeneous portfolio, only nonnegative ρ is considered, since the asset correlation is ρ^2 (equation (2.3) with $\rho_i = \rho_j$). The homogeneous FtD probability in the first-crossing setting for $\rho = 0$ is

$$\Pr(\min\{\tau_1, ..., \tau_N\} \leq T)|_{\rho=0} = 1 - (1 - 2\Phi(\frac{K}{\sqrt{T}}))^N \tag{2.10}$$

and for $\rho = 1$ is

$$\Pr(\min\{\tau_1, ..., \tau_N\} \leq T)|_{\rho=1} = 2\Phi(\frac{K}{\sqrt{T}}) \tag{2.11}$$

For an inhomogeneous portfolio with 2 sectors, where sector 1 contains 1 credit and sector 2 contains $N-1$ credits ($N > 2$). The firms in sector 2 has a common default barrier K_2 and a common correlation with the market ρ_2, the FtD probability is only known for $\rho_2 = -1, 0, 1$:

$$\Pr(\min\{\tau_1, ..., \tau_N\} \leq T)|_{\rho_2=\pm 1} = F(T; \rho_1, \pm 1) \tag{2.12}$$

where $F(T; \rho_1, \rho_2)$ is the FtD probability for two firms in equation (2.4), and

$$\Pr(\min\{\tau_1, ..., \tau_N\} \leq T)|_{\rho_2=0} = 1 - (1 - 2\Phi(\frac{K_1}{\sqrt{T}}))\,(1 - 2\Phi(\frac{K_2}{\sqrt{T}}))^{N-1} \tag{2.13}$$

2.2 PORTFOLIO LOSS DISTRIBUTION

We also contrast the portfolio loss distribution which is essential in understanding and pricing CDO's in the first-crossing setting versus the Vasicek setting. For a homogeneous portfolio, as mentioned in the introductory section 1.3, the portfolio loss distribution in the Vasicek setting is

$$\begin{aligned} P^{Vasicek}(L^{(N)} = \frac{n}{N}) = \int_{-\infty}^{\infty} \binom{N}{n} (\Phi(\frac{K - \rho\sqrt{T}\,z}{\sqrt{(1-\rho^2)\,T}}))^n \\ (1 - \Phi(\frac{K - \rho\sqrt{T}\,z}{\sqrt{(1-\rho^2)\,T}}))^{N-n} \phi(z)\,dz \end{aligned} \tag{2.14}$$

where $L^{(N)}$ denotes the fraction of loss for a portfolio of size N.

2.2.1 Peaks When $\rho = 0$

In the Vasicek setting we have

$$P^{Vasicek}(L^{(N)} = \frac{n}{N})|_{\rho=0} = \binom{N}{n} \Phi(\frac{K}{\sqrt{T}})^n \, (1 - \Phi(\frac{K}{\sqrt{T}}))^{N-n} \tag{2.15}$$

and

$$P^{Vasicek}(L^{(N)} = 1)|_{\rho=1} = \Phi(\frac{K}{\sqrt{T}}), \quad P^{Vasicek}(L^{(N)} = 0)|_{\rho=1} = 1 - \Phi(\frac{K}{\sqrt{T}}) \tag{2.16}$$

On the other hand, the exact loss distributions in the first-crossing model with $\rho = 0, 1$ are

$$P(L^{(N)} = \frac{n}{N})|_{\rho=0} = \binom{N}{n} (2\Phi(\frac{K}{\sqrt{T}}))^n \, (1 - 2\Phi(\frac{K}{\sqrt{T}}))^{N-n} \tag{2.17}$$

and

$$P(L^{(N)} = 1)|_{\rho=1} = 2\Phi(\frac{K}{\sqrt{T}}), \quad P(L^{(N)} = 0)|_{\rho=1} = 1 - 2\Phi(\frac{K}{\sqrt{T}}) \tag{2.18}$$

Let us denote $p_n^{L,Vasicek}|_{\rho=0} = P^{Vasicek}(L^{(N)} = \frac{n}{N})|_{\rho=0}$ and $p_n^L|_{\rho=0} = P(L^{(N)} = \frac{n}{N})|_{\rho=0}$. Then,

$$\frac{p_n^{L,Vasicek}|_{\rho=0}}{p_{n-1}^{L,Vasicek}|_{\rho=0}} = \frac{N-n+1}{n} \frac{\Phi(\frac{K}{\sqrt{T}})}{1 - \Phi(\frac{K}{\sqrt{T}})} \tag{2.19}$$

and

$$\frac{p_n^{L}|_{\rho=0}}{p_{n-1}^{L}|_{\rho=0}} = \frac{N-n+1}{n} \frac{2\Phi(\frac{K}{\sqrt{T}})}{1 - 2\Phi(\frac{K}{\sqrt{T}})} \tag{2.20}$$

So

$$\frac{p_n^{L,Vasicek}|_{\rho=0}}{p_{n-1}^{L,Vasicek}|_{\rho=0}} \geq 1 \iff n \leq (N+1)\Phi(\frac{K}{\sqrt{T}}) \tag{2.21}$$

and

$$\frac{p_n^{L}|_{\rho=0}}{p_{n-1}^{L}|_{\rho=0}} \geq 1 \iff n \leq 2(N+1)\Phi(\frac{K}{\sqrt{T}}) \tag{2.22}$$

Thus, if $\rho = 0$, the loss distribution in the Vasicek setting has a peak at $n = \lfloor (N+1)\Phi(\frac{K}{\sqrt{T}}) \rfloor$, while the peak is at $n = \lfloor 2(N+1)\Phi(\frac{K}{\sqrt{T}}) \rfloor$ in the first-crossing model, where $\lfloor x \rfloor$ is the largest integer less than or equal to x, as can be seen in equations (2.21) and (2.22). In the next subsection, we will investigate a large portfolio approximation of the loss distribution which we will use frequently in later chapters for studying more complicated models.

2.2.2 Large Portfolio Approximation

In order to get a better understanding of the behavior of the loss distribution, we study a large portfolio approximation when the portfolio size of a homogeneous portfolio (where all individual credits have the same notional and marginal default probability) grows to infinity. As $N \to \infty$, we can apply a version of the strong law of large numbers to conclude that (Schönbucher (2002) [36] & (2003) [37], Frey and McNeil (2003) [12], Metzler (2008) [33], McLeish and Metzler (2011) [31]) the asymptotic loss fraction converges almost surely to the individual (marginal) default probability given the systematic factor W_T in the Vasicek setup:

$$L^{(\infty)} = \Phi(\frac{K - \rho\sqrt{T}\,z}{\sqrt{(1-\rho^2)\,T}}), \quad \Pr(\,\cdot\,|\frac{W_T}{\sqrt{T}} = z) - a.s. \tag{2.23}$$

Hence, by iterated expectation, Schöbucher (2002) [36] et. al. calculated the asymptotic loss distribution

$$\begin{aligned}
&\Pr(L^{(\infty)} \le x) \\
&= E[\Pr(L^{(\infty)} \le x|\frac{W_T}{\sqrt{T}})] \\
&= \int_{-\infty}^{\infty} \Pr(L^{(\infty)} = \Phi(\frac{K - \rho\sqrt{T}\,z}{\sqrt{(1-\rho^2)\,T}}) \le x|\frac{W_T}{\sqrt{T}} = z)\,\phi(z)\,dz \\
&= \int_{-\infty}^{\infty} I\{\Phi(\frac{K - \rho\sqrt{T}\,z}{\sqrt{(1-\rho^2)\,T}}) \le x\}\,\phi(z)\,dz \\
&= \int_{\frac{K-\sqrt{(1-\rho^2)T}\Phi^{-1}(x)}{\rho\sqrt{T}}}^{\infty} \phi(z)\,dz \\
&= \Phi(\frac{\sqrt{(1-\rho^2)T}\Phi^{-1}(x) - K}{\rho\sqrt{T}})
\end{aligned} \tag{2.24}$$

and the loss density for the large portfolio approximation in the Vasicek setting is

$$p^{Vasicek}(x) = \frac{\sqrt{1-\rho^2}}{\rho}\,\exp\{\frac{1}{2}[(\Phi^{-1}(x))^2 - \frac{(\sqrt{(1-\rho^2)T}\,\Phi^{-1}(x) - K)^2}{\rho^2\,T}]\} \tag{2.25}$$

2.2.2.1 Extreme Loss Behavior As an addition to the previous work (Schöbucher (2002) [36] et. al.), we investigate the tail behavior of the asymptotic loss density.

$$p^{Vasicek}(x) = \frac{\sqrt{1-\rho^2}}{\rho}\, exp\{\frac{1}{2}[(1+\frac{\sqrt{1-\rho^2}}{\rho})\,\Phi^{-1}(x) - \frac{K}{\rho\sqrt{T}}][(1-\frac{\sqrt{1-\rho^2}}{\rho})\,\Phi^{-1}(x) + \frac{K}{\rho\sqrt{T}}]\} \tag{2.26}$$

Hence, we have

$$p^{Vasicek}(0) = \begin{cases} \infty, & \text{if } \rho^2 \in [\frac{1}{2}, 1) \\ 0, & \text{if } \rho^2 \in (0, \frac{1}{2}) \end{cases} \tag{2.27}$$

and

$$p^{Vasicek}(1) = \begin{cases} \infty, & \text{if } \rho^2 \in (\frac{1}{2}, 1) \\ 0, & \text{if } \rho^2 \in (0, \frac{1}{2}] \end{cases} \tag{2.28}$$

So the asymptotic loss density at the two extremes depends on the correlation ρ.

In figures 2, 3, and 4 (see Appendix B), we compare the asymptotic loss density using equation (2.25) for a large homogeneous portfolio with 5-year maturity and different levels of $\rho = 0.1, 0.3, 0.5, 0.7, 0.9$, represented by the red, green, blue, cyan and magenta curves, respectively, and $K = -3, -1, -0.1$.

As expected, the asymptotic density at both extremes tends to zero for low levels of ρ^2 and tends to infinity for high levels of ρ^2.

To be more precise, we look at the asymptotic densities at $x = 10^{-i}, i = 1, ..., 16$ for a maturity of five years. The results are shown in tables 1, 2, 3, and 4 (see Appendix B).

Now it is clear that the asymptotic loss density converges to zero at both 0% loss and 100% loss when $\rho^2 < 0.5$, and diverges to infinity at both 0% loss and 100% loss when $\rho^2 > 0.5$.

Next, we look more closely at what happens when ρ^2 is close to 0.5, i.e., ρ is close to $\sqrt{0.5} \approx 0.707$. In figure 5 (see Appendix B), we compare the asymptotic loss density for a large homogeneous portfolio of 10000 names with $K = -0.01$, $T = 5$ and different levels of $\rho = 0.7, \sqrt{0.5}, 0.71$, represented by the red, green and blue curves, respectively. We find that for $\rho = 0.7 < \sqrt{0.5}$, the asymptotic loss density tends to zero at both extremes; for $\rho = \sqrt{0.5}$, the asymptotic loss density tends to infinity at no loss and zero at entire loss; for $\rho = 0.71 > \sqrt{0.5}$, the asymptotic loss density tends to infinity at both extremes, consistent with our theoretical results.

2.2.2.2 Extreme Correlation Behavior Notice also that the asymptotic loss cumulative distribution function (2.24) and probability density function (2.25) can be rewritten as

$$\Pr(L^{\infty} \leq x) = \Phi\left(\frac{\sqrt{1-\rho^2}\Phi^{-1}(x) - \Phi^{-1}(q)}{\rho}\right) \tag{2.29}$$

$$p^{Vasicek}(x) = \frac{\sqrt{1-\rho^2}}{\rho} \exp\left\{\frac{1}{2}(\Phi^{-1}(x))^2 - \frac{1}{2\rho^2}(\sqrt{1-\rho^2}\,\Phi^{-1}(x) - \Phi^{-1}(q))^2\right\} \tag{2.30}$$

where $q = \Pr(X_{i,T} < K) = \Phi(\frac{K}{\sqrt{T}})$ is the marginal probability of default. We should note that in the Vasicek setup, $q < 0.5$ and $\Phi^{-1}(q) = \frac{K}{\sqrt{T}} < 0$.

We then investigate how the asymptotic loss density behaves for extreme values of the correlation ρ. We first show that as $\rho \to 0^+$, the asymptotic loss density approaches a Dirac mass at q. We need to show that for any test function $f \in C([0,1])$,

$$\lim_{\rho \to 0^+} \int_0^1 p^{Vasicek}(x)\, f(x)\, dx = f(q) \tag{2.31}$$

Indeed, fix $\varepsilon > 0$, choose $\eta \in (0, \min\{q, 1-q\})$ such that $|f(x) - f(q)| < \varepsilon$ if $|x - q| \leq \eta$. We have that

$$
\begin{aligned}
&|\int_0^1 p^{Vasicek}(x)\, f(x)\, dx - f(q)| = |\int_0^1 p^{Vasicek}(x)\, (f(x) - f(q))\, dx| \\
&\leq (\int_0^{q-\eta} + \int_{q-\eta}^{q+\eta} + \int_{q+\eta}^1)\, p^{Vasicek}(x)\, |f(x) - f(q)|\, dx \\
&< 2\, \|f\|_{L^\infty} \int_0^{q-\eta} p^{Vasicek}(x)\, dx + \varepsilon \int_{q-\eta}^{q+\eta} p^{Vasicek}(x)\, dx + 2\, \|f\|_{L^\infty} \int_{q+\eta}^1 p^{Vasicek}(x)\, dx \\
&< \varepsilon + 2\, \|f\|_{L^\infty}\, [\, \Phi(\frac{\sqrt{1-\rho^2}\, \Phi^{-1}(q-\eta) - \Phi^{-1}(q)}{\rho}) + 1 - \Phi(\frac{\sqrt{1-\rho^2}\, \Phi^{-1}(q+\eta) - \Phi^{-1}(q)}{\rho})\,] \\
&= \varepsilon + 2\, \|f\|_{L^\infty}\, [\, \Phi(\frac{\sqrt{1-\rho^2}\, \Phi^{-1}(q-\eta) - \Phi^{-1}(q)}{\rho}) + \Phi(\frac{\Phi^{-1}(q) - \sqrt{1-\rho^2}\, \Phi^{-1}(q+\eta)}{\rho})\,]
\end{aligned}
\tag{2.32}
$$

Since $\Phi^{-1}(q-\eta) < \Phi^{-1}(q) < \Phi^{-1}(q+\eta)$, we have $\lim_{\rho \to 0^+} \Phi(\frac{\sqrt{1-\rho^2}\Phi^{-1}(q-\eta) - \Phi^{-1}(q)}{\rho}) = 0$ and $\lim_{\rho \to 0^+} \Phi(\frac{\Phi^{-1}(q) - \sqrt{1-\rho^2}\Phi^{-1}(q+\eta)}{\rho}) = 0$. Hence, for some $\rho_\varepsilon \in (0,1)$, we have $|\int_0^1 p^{Vasicek}(x)\, f(x)\, dx - f(q)| < 2\, \varepsilon$ if $\rho \in (0, \rho_\varepsilon)$. The proof is complete.

Alternatively, as $\rho \to 0^+$, $\frac{\sqrt{1-\rho^2}\Phi^{-1}(x) - \Phi^{-1}(q)}{\rho}$ goes to $-\infty$ if $x \in [0, q]$ and goes to ∞ if $x \in (q, 1]$. Since Φ is continuous, we have

$$
\begin{aligned}
&\lim_{\rho \to 0^+} \Pr(L^\infty \leq x) \\
&= \lim_{\rho \to 0^+} \Phi(\frac{\sqrt{1-\rho^2}\, \Phi^{-1}(x) - \Phi^{-1}(q)}{\rho}) \\
&= \Phi(\lim_{\rho \to 0^+} \frac{\sqrt{1-\rho^2}\, \Phi^{-1}(x) - \Phi^{-1}(q)}{\rho}) \\
&= I\{x > q\}
\end{aligned}
\tag{2.33}
$$

Hence, $\lim_{\rho \to 0^+} p^{Vasicek}(x) = \delta(x - q)$.

Now we know that $\lim_{\rho \to 0^+} p^{Vasicek}(x) = \delta(x - q)$, namely, the asymptotic loss density becomes more and more concentrated at q as ρ gets closer and closer to zero. Intuitively, the loss fraction approaches the individual default probability as the portfolio consists of a large number of

nearly independent defaultable assets, as the law of large numbers would predict.

At the other extreme, as $\rho \to 1^-$, we have for $x \in (0,1)$,

$$\begin{aligned}
&\lim_{\rho\to 1^-} \Pr(L^\infty \le x) \\
&= \lim_{\rho\to 1^-} \Phi\Big(\frac{\sqrt{1-\rho^2}\,\Phi^{-1}(x) - \Phi^{-1}(q)}{\rho}\Big) \\
&= \Phi\Big(\lim_{\rho\to 1^-} \frac{\sqrt{1-\rho^2}\,\Phi^{-1}(x) - \Phi^{-1}(q)}{\rho}\Big) \\
&= \Phi(-\Phi^{-1}(q)) \\
&= 1 - \Phi(\Phi^{-1}(q)) \\
&= 1 - q
\end{aligned} \tag{2.34}$$

Since $\Pr(L^\infty \le 0) = 0$ and $\Pr(L^\infty \le 1) = 1$, we have

$$\lim_{\rho\to 1^-} \Pr(L^\infty \le x) = (1-q)\, I\{x > 0\} \,+\, q\, I\{x \le 1\} \tag{2.35}$$

and

$$\lim_{\rho\to 1^-} p^{Vasicek}(x) = (1-q)\,\delta(x) + q\,\delta(x-1) \tag{2.36}$$

The intuition is that when $\rho \to 1^-$, the assets in the credit portfolio become perfectly dependent. Either the entire portfolio survives with survival probability $1-q$ or the entire portfolio defaults with default probability q.

To be more rigorous, we should prove that $\lim_{\rho\to 1^-} \int_0^1 p^{Vasicek}(x)\, f(x)\, dx = (1-q)\, T(0) + q\, f(1)$ for any test function $f \in C([0,1])$. To do this, fix $\varepsilon > 0$, choose $\eta \in (0, \frac{1}{2})$ such that

$|f(x) - f(0)| < \varepsilon$ if $0 \leq x \leq \eta$ and $|f(x) - f(1)| < \varepsilon$ if $0 \leq 1 - x \leq \eta$. We have

$$
\begin{aligned}
&| \int_0^1 p^{Vasicek}(x)\, f(x)\, dx - [\,(1-q)\, f(0) + q\, f(1)\,]\,| \\
&= | \int_0^\eta p^{Vasicek}(x)\, f(x)\, dx - (1-q)\, f(0)| + | \int_\eta^{1-\eta} p^{Vasicek}(x)\, f(x)\, dx| \\
&\qquad + | \int_{1-\eta}^1 p^{Vasicek}(x)\, f(x)\, dx - q\, f(1)| \\
&\leq |f(\xi_0) \int_0^\eta p^{Vasicek}(x)\, dx - (1-q)\, f(0)| + \|f\|_{L^\infty} \int_\eta^{1-\eta} p^{Vasicek}(x)\, dx \\
&\qquad + |f(\xi_1) \int_{1-\eta}^1 p^{Vasicek}(x)\, dx - q\, f(1)|
\end{aligned}
$$

with $\xi_0 \in (0, \eta)$ and $\xi_1 \in (1-\eta, 1)$ in the mean value theorem for integration

$$
\begin{aligned}
&= |f(\xi_0)\, (\int_0^\eta p^{Vasicek}(x)\, dx - (1-q)) + (1-q)\, (f(\xi_0) - f(0))| \\
&\qquad + \|f\|_{L^\infty}\, [\, \Phi(\frac{\sqrt{1-\rho^2}\, \Phi^{-1}(1-\eta) - \Phi^{-1}(q)}{\rho}) - \Phi(\frac{\sqrt{1-\rho^2}\, \Phi^{-1}(\eta) - \Phi^{-1}(q)}{\rho})\,] \\
&\qquad + |f(\xi_1)\, (\int_{1-\eta}^1 p^{Vasicek}(x)\, dx - q) + q\, (f(\xi_1) - f(1))| \\
&\leq \|f\|_{L^\infty}\, | \int_0^\eta p^{Vasicek}(x)\, dx - (1-q)| + (1-q)\, \varepsilon \\
&\qquad + \|f\|_{L^\infty}\, [\, \Phi(\frac{\sqrt{1-\rho^2}\, \Phi^{-1}(1-\eta) - \Phi^{-1}(q)}{\rho}) - \Phi(\frac{\sqrt{1-\rho^2}\, \Phi^{-1}(\eta) - \Phi^{-1}(q)}{\rho})\,] \\
&\qquad + \|f\|_{L^\infty}\, | \int_{1-\eta}^1 p^{Vasicek}(x)\, dx - q| + q\, \varepsilon
\end{aligned}
$$

$$
\begin{aligned}
&= \varepsilon + \|f\|_{L^\infty} \, [\, | \int_0^\eta p^{Vasicek}(x)\, dx - (1-q)| \\
&\quad + |\Phi(\frac{\sqrt{1-\rho^2}\,\Phi^{-1}(1-\eta) - \Phi^{-1}(q)}{\rho}) - \Phi(\frac{\sqrt{1-\rho^2}\,\Phi^{-1}(\eta) - \Phi^{-1}(q)}{\rho})| \\
&\quad + | \int_{1-\eta}^1 p^{Vasicek}(x)\, dx - q| \,] \\
&= \varepsilon + \|f\|_{L^\infty} \, [\, |\Phi(\frac{\sqrt{1-\rho^2}\,\Phi^{-1}(\eta) - \Phi^{-1}(q)}{\rho}) - (1-q)| \\
&\quad + |\Phi(\frac{\sqrt{1-\rho^2}\,\Phi^{-1}(1-\eta) - \Phi^{-1}(q)}{\rho}) - \Phi(\frac{\sqrt{1-\rho^2}\,\Phi^{-1}(\eta) - \Phi^{-1}(q)}{\rho})| \\
&\quad + |1 - \Phi(\frac{\sqrt{1-\rho^2}\Phi^{-1}(1-\eta) - \Phi^{-1}(q)}{\rho}) - q| \,] \\
&= \varepsilon + \|f\|_{L^\infty} \, [\, |\Phi(\frac{\sqrt{1-\rho^2}\,\Phi^{-1}(\eta) - \Phi^{-1}(q)}{\rho}) - (1-q)| \\
&\quad + |\Phi(\frac{\sqrt{1-\rho^2}\,\Phi^{-1}(1-\eta) - \Phi^{-1}(q)}{\rho}) - \Phi(\frac{\sqrt{1-\rho^2}\,\Phi^{-1}(\eta) - \Phi^{-1}(q)}{\rho})| \\
&\quad + |\Phi(\frac{\Phi^{-1}(q) - \sqrt{1-\rho^2}\,\Phi^{-1}(1-\eta)}{\rho}) - q| \,]
\end{aligned}
\tag{2.37}
$$

Since

$$
\lim_{\rho \to 1^-} \Phi(\frac{\sqrt{1-\rho^2}\,\Phi^{-1}(\eta) - \Phi^{-1}(q)}{\rho}) = \Phi(-\Phi^{-1}(q)) = 1 - \Phi(\Phi^{-1}(q)) = 1 - q \tag{2.38}
$$

$$
\lim_{\rho \to 1^-} |\Phi(\frac{\sqrt{1-\rho^2}\,\Phi^{-1}(1-\eta) - \Phi^{-1}(q)}{\rho}) - \Phi(\frac{\sqrt{1-\rho^2}\,\Phi^{-1}(\eta) - \Phi^{-1}(q)}{\rho})| = 0 \tag{2.39}
$$

$$
\lim_{\rho \to 1^-} \Phi(\frac{\Phi^{-1}(q) - \sqrt{1-\rho^2}\,\Phi^{-1}(1-\eta)}{\rho}) = \Phi(\Phi^{-1}(q)) = q \tag{2.40}
$$

we can find some $\rho_\varepsilon \in (0,1)$ such that $| \int_0^1 p^{Vasicek}(x)\, f(x)\, dx - [\, (1-q)\, f(0) + q\, f(1)\,] \,| < 2\,\varepsilon$ if $\rho \in (\rho_\varepsilon, 1)$. The proof is complete.

In figures 6 and 7 (see Appendix B), we plot the asymptotic cumulative loss distributions for a homogeneous portfolio of 100 names with individual default probability $q = 0.1$ for ρ close to 0 and ρ close to 1 to illustrate our previous analytic results. The red and green curves in figure 6

represent the asymptotic cumulative loss distributions for $\rho = 0.1, 0.01$, respectively. We can see that the asymptotic cumulative loss distribution behaves like a Heaviside function at q. The red, green, blue and cyan curves in figure 7 represent the asymptotic cumulative loss distributions for $\rho = 0.9, 0.99, 0.999, 0.9999$, respectively. It is clear that the asymptotic cumulative loss distribution behaves like a linear combination of two Heaviside functions at 0 and 1 with weights $1-q$ and q, respectively.

2.2.2.3 Monotonicity Next, we check the monotonicity of the asymptotic loss density by looking at its derivative with respect to x:

$$\begin{aligned}
&\frac{d}{dx}\, p^{Vasicek}(x) \\
&= p^{Vasicek}(x)\, [\Phi^{-1}(x)\frac{d\Phi^{-1}(x)}{dx} - \frac{1}{\rho^2}(\sqrt{1-\rho^2}\Phi^{-1}(x) - \Phi^{-1}(q))\sqrt{1-\rho^2}\frac{d\Phi^{-1}(x)}{dx}] \\
&= p^{Vasicek}(x)\, \frac{1}{\phi(\Phi^{-1}(x))}\, [(1 - \frac{1-\rho^2}{\rho^2})\Phi^{-1}(x) + \frac{1}{\rho^2}\Phi^{-1}(q)] \\
&= \frac{\sqrt{2\pi(1-\rho^2)}}{\rho^3}\, [(2\rho^2 - 1)\Phi^{-1}(x) + \Phi^{-1}(q)] \\
&\qquad \exp\{(\Phi^{-1}(x))^2 - \frac{1}{2\rho^2}(\sqrt{1-\rho^2}\Phi^{-1}(x) - \Phi^{-1}(q))^2\}
\end{aligned} \tag{2.41}$$

Hence, we have that when $\rho^2 \in (0, 0.5)$, $\frac{d}{dx}\, p^{Vasicek}(x) > 0, \quad x \in [0, \Phi(\frac{\Phi^{-1}(q)}{1-2\rho^2}))$, $\frac{d}{dx}\, p^{Vasicek}(x) < 0, \quad x \in (\Phi(\frac{\Phi^{-1}(q)}{1-2\rho^2}), 1]$. So when $\rho^2 \in (0, 0.5)$, the asymptotic loss density is strictly increasing for $x < \Phi(\frac{\Phi^{-1}(q)}{1-2\rho^2})$ and strictly decreasing for $x > \Phi(\frac{\Phi^{-1}(q)}{1-2\rho^2})$, and attains its maximum at $x = \Phi(\frac{\Phi^{-1}(q)}{1-2\rho^2})$. As ρ^2 approaches 0, the maximum approaches q. On the other hand, as ρ^2 gets larger but less than 0.5, the maximum tends to 0, as confirmed by figures 2, 3, and 4 (see Appendix B) and also observed in Schönbucher (2002) [36] who stated the behavior without proving it.

When $\rho^2 = 0.5$, we have

$$\frac{d}{dx}\, p^{Vasicek}(x) = \sqrt{8\pi}\Phi^{-1}(q)\, \exp\{(\Phi^{-1}(x))^2 - (\frac{1}{\sqrt{2}}\Phi^{-1}(x) - \Phi^{-1}(q))^2\} < 0. \tag{2.42}$$

So when $\rho^2 = 0.5$, the asymptotic loss density is strictly decreasing.

Finally, when $\rho^2 \in (0.5, 1)$, $\frac{d}{dx} p^{Vasicek}(x) < 0, \quad x \in [0, \Phi(\frac{\Phi^{-1}(q)}{1-2\rho^2}))$, $\frac{d}{dx} p^{Vasicek}(x) > 0, \quad x \in (\Phi(\frac{\Phi^{-1}(q)}{1-2\rho^2}), 1]$. So when $\rho^2 \in (0.5, 1)$, the asymptotic loss density is strictly decreasing for $x < \Phi(\frac{\Phi^{-1}(q)}{1-2\rho^2})$ and strictly increasing for $x > \Phi(\frac{\Phi^{-1}(q)}{1-2\rho^2})$, and attains the minimum at $x = \Phi(\frac{\Phi^{-1}(q)}{1-2\rho^2})$.

2.2.2.4 Large Portfolio Approximation for Heterogeneous Portfolio The above large portfolio approximation can be extended to heterogeneous portfolios with the Vasicek definition of default. For a heterogeneous portfolio with N obligors in J sectors, each sector with weight $w_{j,N} > 0$ satisfying $\sum_{j=1}^{J} w_{j,N} = 1$ and the same $\rho_j > 0$ and $K_j < 0$ within each sector (within-sector homogeneity), we have that, as $N \to \infty$, provided that $w_j = \lim_{N\to\infty} w_{j,N}$ is well defined for each j (the proportion of obligors in each sector is asymptotically stable) (Frey and McNeil (2003) [12], Metzler (2008) [33], McLeish and Metzler (2011) [31])

$$L^{(\infty)} = E[\frac{1}{N}\sum_{i=1}^{N} I\{\tau_i \le T\}|W_T], \quad \Pr(\cdot|\frac{W_T}{\sqrt{T}} = z) - a.s. \tag{2.43}$$

We apply the principle of large portfolio approximation in Frey and McNeil (2003) [12] et. al. to our model to get

$$L^{(\infty)} = \sum_{j=1}^{J} w_j \, \Phi(\frac{K_j - \rho_j \sqrt{T}\, z}{\sqrt{(1-\rho_j^2)\, T}}) = G(z), \quad \Pr(\cdot|\frac{W_T}{\sqrt{T}} = z) - a.s. \tag{2.44}$$

Since

$$G'(z) = -\sum_{j=1}^{J} \frac{w_j \rho_j}{\sqrt{1-\rho_j^2}} \, \phi(\frac{K_j - \rho_j \sqrt{T}\, z}{\sqrt{(1-\rho_j^2)\, T}}) < 0 \tag{2.45}$$

where we use the fact that $\rho_j > 0$ for all j, G is strictly decreasing with $G(\infty) = 0$ and $G(-\infty) = \sum_{j=1}^{J} w_j = 1$. Hence, G has an inverse denoted by G^{-1}. By iterated expectation,

$$\begin{aligned}
&\Pr(L^{(\infty)} \leq x) \\
&= E[\Pr(L^{(\infty)} \leq x | \frac{W_T}{\sqrt{T}})] \\
&= \int_{-\infty}^{\infty} \Pr(L^{(\infty)} = G(z) \leq x | \frac{W_T}{\sqrt{T}} = z)\, \phi(z)\, dz \\
&= \int_{-\infty}^{\infty} I\{G(z) \leq x\}\, \phi(z)\, dz \\
&= \int_{G^{-1}(x)}^{\infty} \phi(z)\, dz
\end{aligned} \tag{2.46}$$

and the loss density for the large portfolio approximation is

$$\begin{aligned}
&p^{Vasicek}(x) = -\frac{\phi(G^{-1}(x))}{G'(G^{-1}(x))} \\
&= \frac{\exp\{-\frac{1}{2}[G^{-1}(x)]^2\}}{\sum_{j=1}^{J} \frac{w_j \rho_j}{\sqrt{1-\rho_j^2}} \exp\{-\frac{1}{2}[\frac{K_j - \rho_j \sqrt{T} G^{-1}(x)}{\sqrt{(1-\rho_j^2)T}}]^2\}} \\
&= \frac{1}{\sum_{j=1}^{J} \frac{w_j \rho_j}{\sqrt{1-\rho_j^2}} \exp\{\frac{1}{2}[(1 + \frac{\rho_j}{\sqrt{1-\rho_j^2}}) G^{-1}(x) - \frac{K_j}{\sqrt{(1-\rho_j^2)T}}][(1 - \frac{\rho_j}{\sqrt{1-\rho_j^2}}) G^{-1}(x) + \frac{K_j}{\sqrt{(1-\rho_j^2)T}}]\}}
\end{aligned} \tag{2.47}$$

It is easy to see that the term in the denominator

$$H_j(x) = \exp\{\frac{1}{2}[(1 + \frac{\rho_j}{\sqrt{1-\rho_j^2}}) G^{-1}(x) - \frac{K_j}{\sqrt{(1-\rho_j^2)T}}][(1 - \frac{\rho_j}{\sqrt{1-\rho_j^2}}) G^{-1}(x) + \frac{K_j}{\sqrt{(1-\rho_j^2)T}}]\} \tag{2.48}$$

satisfies

$$H_j(0) = \begin{cases} \infty, & \text{if } \rho_j^2 \in [0, \frac{1}{2}) \\ 0, & \text{otherwise} \end{cases} \tag{2.49}$$

and

$$H_j(1) = \begin{cases} \infty, & \text{if } \rho_j^2 \in [0, \frac{1}{2}] \\ 0, & \text{otherwise} \end{cases} \tag{2.50}$$

where we use the fact that $G^{-1}(0) = \infty$ and $G^{-1}(1) = -\infty$.

Hence, we have

$$p^{Vasicek}(0) = \begin{cases} \infty, & \text{if } \rho_j^2 \in [\frac{1}{2}, 1) \text{ for all } j \\ 0, & \text{otherwise} \end{cases} \tag{2.51}$$

and

$$p^{Vasicek}(1) = \begin{cases} \infty, & \text{if } \rho_j^2 \in (\frac{1}{2}, 1) \text{ for all } j \\ 0, & \text{otherwise} \end{cases} \tag{2.52}$$

Next, we study the monotonicity of $p^{Vasicek}(x)$ by taking the derivative with respect to x:

$$\begin{aligned} \frac{d}{dx}p^{Vasicek}(x) &= \frac{d}{dx}\frac{1}{\sum_{j=1}^{J}\frac{w_j\rho_j}{\sqrt{1-\rho_j^2}}\exp\{\frac{1}{2}[\frac{1-2\rho_j^2}{1-\rho_j^2}(G^{-1}(x))^2 + \frac{2\rho_j K_j}{(1-\rho_j^2)\sqrt{T}}G^{-1}(x) - \frac{K_j^2}{(1-\rho_j^2)T}]\}} \\ &= -\frac{\sum_{j=1}^{J}\frac{w_j\rho_j}{\sqrt{1-\rho_j^2}}\exp\{\frac{1}{2}[\frac{1-2\rho_j^2}{1-\rho_j^2}(G^{-1}(x))^2 + \frac{2\rho_j K_j}{(1-\rho_j^2)\sqrt{T}}G^{-1}(x) - \frac{K_j^2}{(1-\rho_j^2)T}]\}\,[\frac{1-2\rho_j^2}{1-\rho_j^2}G^{-1}(x) + \frac{\rho_j K_j}{(1-\rho_j^2)\sqrt{T}}]}{G'(G^{-1}(x))\,[\sum_{j=1}^{J}\frac{w_j\rho_j}{\sqrt{1-\rho_j^2}}\exp\{\frac{1}{2}[\frac{1-2\rho_j^2}{1-\rho_j^2}(G^{-1}(x))^2 + \frac{2\rho_j K_j}{(1-\rho_j^2)\sqrt{T}}G^{-1}(x) - \frac{K_j^2}{(1-\rho_j^2)T}]\}]^2} \end{aligned} \tag{2.53}$$

First, assume that $\rho_j^2 \leq \frac{1}{2}$ for all j and that there exists k such that $\rho_k^2 < \frac{1}{2}$. In this case, $\frac{1-2\rho_j^2}{1-\rho_j^2} \geq 0$ for all j and $\frac{1-2\rho_k^2}{1-\rho_k^2} > 0$. Since G is strictly decreasing, $G' < 0$ and G^{-1} is strictly decreasing. Denote the numerator of $\frac{d}{dx}p^{Vasicek}(x)$ by

$$A(x) = \sum_{j=1}^{J}\frac{w_j\rho_j}{\sqrt{1-\rho_j^2}}\,B(x)\,[\frac{1-2\rho_j^2}{1-\rho_j^2}G^{-1}(x) + \frac{\rho_j K_j}{(1-\rho_j^2)\sqrt{T}}] \tag{2.54}$$

where $B(x) = \exp\{\frac{1}{2}[\frac{1-2\rho_j^2}{1-\rho_j^2}(G^{-1}(x))^2 + \frac{2\rho_j K_j}{(1-\rho_j^2)\sqrt{T}}G^{-1}(x) - \frac{K_j^2}{(1-\rho_j^2)T}]\}$. It is easy to see that $A(0) = \infty$ and $A(1) = -\infty$ with the fact that $G^{-1}(0) = \infty$ and $G^{-1}(1) = -\infty$. In addition,

$$\frac{dA}{dx} = \frac{\sum_{j=1}^{J}\frac{w_j\rho_j}{\sqrt{1-\rho_j^2}}\,B(x)\,\{[\frac{1-2\rho_j^2}{1-\rho_j^2}G^{-1}(x) + \frac{\rho_j K_j}{(1-\rho_j^2)\sqrt{T}}]^2 + \frac{1-2\rho_j^2}{1-\rho_j^2}\}}{G'(G^{-1}(x))} < 0 \tag{2.55}$$

Hence, A is strictly decreasing from ∞ to $-\infty$. With the continuity of $\frac{d}{dx}p^{Vasicek}(x)$, we have that there exist some x^* such that $\frac{d}{dx}p^{Vasicek}(x) > 0$ for $x < x^*$ and $\frac{d}{dx}p^{Vasicek}(x) < 0$ for $x > x^*$. Therefore, if $\rho_j^2 \leq \frac{1}{2}$ for all j and $\rho_k^2 < \frac{1}{2}$ for some k (i.e., all within-sector correlations are less than or equal to 0.5 with at least one within-sector correlation strictly less than 0.5), the

asymptotic loss density starts from $p^{Vasicek}(0) = 0$ and increases up to some point, then decreases back to $p^{Vasicek}(1) = 0$ (one-humped shape). For example, consider a two-sector portfolio with $w_1 = w_2 = 0.5$, $\rho_1 = 0.1$, $\rho_2 = 0.6$, $K_1 = K_2 = -1$, $T = 5$. Numerical experiments show that the asymptotic density has a hump at $x = 0.2236$ corresponding to $G^{-1}(x) = 0.6684$

Next, assume that $\rho_j^2 > \frac{1}{2}$ for all j. We have already shown that $p^{Vasicek}(0) = \infty$ and $p^{Vasicek}(1) = \infty$. A typical portfolio with this correlation structure would have an asymptotic density that decreases from ∞ to some point and then increases back to ∞.

In the special case where $\rho_j^2 = \frac{1}{2}$ for all j,

$$A(x) = \sum_{j=1}^{J} \frac{\sqrt{2} w_j K_j}{\sqrt{T}} \exp\{\frac{\sqrt{2} K_j}{\sqrt{T}} - \frac{K_j^2}{T}\} < 0 \tag{2.56}$$

Hence, $\frac{d}{dx} p^{Vasicek}(x) < 0$, and the asymptotic loss density is monotonically decreasing from $p^{Vasicek}(0) = \infty$ to $p^{Vasicek}(1) = 0$.

Now assume that $\rho_j^2 < \frac{1}{2}$ for some j and $\rho_j^2 > \frac{1}{2}$ for some other j. In this case, $\frac{1-2\rho_j^2}{1-\rho_j^2} G^{-1}(x) + \frac{\rho_j K_j}{(1-\rho_j^2)\sqrt{T}}$ is strictly decreasing from ∞ to $-\infty$ for $\rho_j^2 < \frac{1}{2}$ and strictly increasing from $-\infty$ to ∞ for $\rho_j^2 > \frac{1}{2}$. Thus, it is possible that $\frac{d}{dx} p^{Vasicek}(x)$ changes sign multiple times which implies that the asymptotic density has multiple humps. For specificity, consider a two-sector portfolio with $w_1 = w_2 = 0.5$, $\rho_1 = .1$, $\rho_2 = 0.9$, $K_1 = K_2 = -1$, $T = 5$. Numerical experiments show that $\frac{d}{dx} p^{Vasicek}(x) > 0$ when $x \in (0, 0.1457)$ ($G^{-1}(x) \in (1.0202, \infty)$); $\frac{d}{dx} p^{Vasicek}(x) < 0$ when $x \in (0.1457, 0.4911)$ ($G^{-1}(x) \in (-0.6594, 1.0202)$); $\frac{d}{dx} p^{Vasicek}(x) > 0$ when $x \in (0.4911, 0.6962)$ ($G^{-1}(x) \in (-1.83, -0.6594)$); $\frac{d}{dx} p^{Vasicek}(x) < 0$ when $x \in (0.6962, 1)$ ($G^{-1}(x) \in (-\infty, -1.83)$). Hence, the asymptotic loss density for this portfolio has two humps. The above locations of the local extremes are found by solving $\frac{d}{dx} p^{Vasicek}(x) = 0$ for $G^{-1}(x)$ and recovering x by $x = G(G^{-1}(x))$. Figure 8 (see Appendix B) plots the numerator of $\frac{d}{dx} p^{Vasicek}(x)$ ($i.e., A(x)$) against $G^{-1} \in (-3, 3)$ to illustrate the locations of G^{-1} that make $\frac{d}{dx} p^{Vasicek}(x) = 0$:

It is also interesting to notice that while the standard normal random variable Z has a maximum density (likelihood) at 0 and the conditional asymptotic loss $L^{\infty} = G(Z)$, the asymptotic

loss density in the above large portfolio does not attain its maximum at $x = G(0) = 0.2395$ corresponding to $z = 0$. Rather, the maximum of the asymptotic loss density is located at $x = G(1.0202) = 0.1457$ corresponding to $z = 1.0202$. This might seem puzzling at first, especially when we recall the Monte Carlo method for estimating the asymptotic loss density: generate 10000 independent standard normal random variables Z, simulate the conditional asymptotic loss $L^{\infty} = G(Z)$, and perform the Gaussian kernel density estimation. The resolution is obtained by examining

$$p^{Vasicek}(x) = \frac{\Pr(L^{(\infty)} \in (x, x+dx))}{dx} = \frac{\int_{z \in G^{-1}((x,x+dx))} \phi(z)\, dz}{dx} = -\frac{\phi(G^{-1}(x))}{G'(G^{-1}(x))} \tag{2.57}$$

Although the numerator $\phi(G^{-1}(x))$ attains its maximum at $G^{-1}(x) = 0$, the denominator $G'(G^{-1}(x))$ in the above large portfolio also has a much larger magnitude at $G^{-1}(x) = 0$ ($G'(0) = -0.2614$) than at $G^{-1}(x) = 1.0202$ ($G'(1.0202) = -0.0207$) where the asymptotic loss density attains its maximum. It is the transformation from z to x through $x = G(z)$ that changes the relative scales of dx and dz and the shape of the asymptotic loss density. While the numerator is symmetric about $G^{-1}(x) = 0$, a plot of the denominator below (figure 9 in Appendix B) shows that the denominator is asymmetric and $|G'(z)| < |G'(-z)|$ for $z > 0$, which explains the result that the asymptotic loss density attains its maximum at a loss corresponding to $z = G^{-1}(x) > 0$ instead of $z = G^{-1}(x) < 0$.

2.3 CHAPTER SUMMARY

In summary, we introduced a simple one-factor model that has the basic "hierarchical structure". In this context, we studied analytically the first-to-default probability, portfolio loss distribution, and large portfolio approximation for both homogeneous and heterogeneous portfolios. These analytic results will be used to validate the Monte Carlo methods that we discuss in the next chapter.

3.0 MONTE CARLO METHODS

Since the models we study throughout the thesis are high dimensional ($100 - 125$ dimensions) by nature, it is very difficult to derive, in a general framework, analytic formulas for the first-to-default probability and the loss distribution needed to price credit derivatives. In order to examine some specific models, using Monte Carlo methods, we first describe the numerical schemes and the approximations we use to handle first-crossing problems in high dimensions.

3.1 INTRODUCTION TO MONTE CARLO METHODS

Monte Carlo approximations for boundary-crossing probabilities have been well studied for one-dimensional diffusion processes. In the classical textbook of Glasserman (2004) [16], boundary-crossing probabilities are approximated using "Brownian interpolation", as opposed to the naive idea of "linear interpolation" which has an obvious low bias in estimating the hitting probabilities for continuous-time processes. The method in Glasserman (2004) [16] first approximates the one-dimensional diffusion process

$$d\,X_t = \mu(t, X_t)\,dt + \sigma(t, X_t)\,dW_t, \quad X_0 = x_0 \tag{3.1}$$

by an Euler scheme

$$\hat{X}_0 = X_0, \quad \hat{X}_{t_{i+1}} = \hat{X}_{t_i} + \mu(t_i, \hat{X}_{t_i})\,\delta t + \sigma(t, \hat{X}_{t_i})\,\sqrt{\delta t} Z_{i+1} \tag{3.2}$$

where $\delta t = T/N$ and $Z_1, ..., Z_N$ are independent standard Gaussian random variables. He then approximates the barrier-crossing probability using the first-crossing distribution of a Brownian bridge without simulating the trigger event,

$$P(\hat{\tau} \leq T) = 1 - \prod_{i=1}^{N}(1 - p(\hat{X}_{t_i}, \hat{X}_{t_{i+1}}, \delta t, K, \sigma(t, \hat{X}_{t_i}))) \tag{3.3}$$

where

$$p(x, y, \delta t, K, \sigma) = \begin{cases} exp(-\frac{2(x-K)(y-K)}{\sigma^2 \delta t}) & \text{if } x > K \text{ and } y > K \\ 1 & \text{otherwise} \end{cases} \tag{3.4}$$

and then taking the average. Alternatively, one can simulate the trigger event by drawing an independent uniform random variable U at each simulation and taking

$$I\{\hat{\tau} \leq T\} = I\{U \leq \max_i p(\hat{X}_{t_i}, \hat{X}_{t_{i+1}}, \delta t, K, \sigma(t, \hat{X}_{t_i}))\} \tag{3.5}$$

The boundary-crossing probability is then the average of the trigger indicators for a sufficiently large number of simulations.

On the other hand, Broadie et al. (1997) [4] proposed a continuity correction to discretely sampled barrier options that suggested shifting the barrier up from K to $K + 0.5826\sigma\sqrt{\delta t}$ to compensate for the bias.

However, in higher dimensions, the first-crossing distribution is not known in closed-form in general. Even in two dimensions, as mentioned in section 2.1, the first-crossing probability for correlated Brownian motions with flat absorbing boundaries is very complicated and involves series of modified Bessel functions (Iyengar (1985) [23], Zhou (2001) [47]). The "Brownian interpolation" technique is not directly applicable in more than two dimensions, yet we are interested in very high (100-125) dimensional problems. Metzler (2008) [33] proposed a remedy by treating the conditioned processes

$$X^{i,k} = \{ X_{i,u} : u \in [t_{k-1}, t_k], X_{i,t_{k-1}} = x_{i,k-1}, X_{i,t_k} = x_{i,k} \} \tag{3.6}$$

as if they were independent for small time step δt and applying the one-dimensional first-crossing distribution for a Brownian bridge. However, Metzler (2008) [33] did not study the convergence

of this scheme. On the other hand, Gobet (2008) [17] generalized the method of Broadie et al. (1997) [4] to multi-dimensions and proposed "optimal" boundary correction schemes with well-studied convergence results, improving the $O(\sqrt{\delta t})$ convergence of the "linear interpolation" scheme to $o(\sqrt{\delta t})$. In this barrier shifting technique (BAST), instead of checking whether or not $\min_k\{\hat{X}_{i,t_k}\} < K_i$, we check whether or not $\min_k\{\hat{X}_{i,t_k} - \bar{y}(\infty)|n\sigma|n\sqrt{\delta t}\} < K_i$, where n is the inward unit normal vector, σ is the volatility, and $\bar{y}(\infty) \approx 0.5826$ is the expected asymptotic renormalized overshoot (Broadie et al. (1997) [4]). In our model, $\bar{y}(\infty)|n\sigma|n\sqrt{\delta t} = \bar{y}(\infty)\sqrt{\delta t}$ and hence we should check whether or not $\min_k\{\hat{X}_{i,t_k}\} < K_i + \bar{y}(\infty)\sqrt{\delta t}$. Notice that in the multi-dimensional problem, we shift the barriers separately without the need to take into account the correlations. If the process is close to the barrier or the stepsize is relatively large, we should use $\bar{y}(-\frac{K}{\sqrt{\delta t}})$ with the expected overshoot $\bar{y}(u) = E[s_{\tau^u} - u] \approx 0.5826 + 0.1245exp\{-2.7u^{1.2}\}$ instead of $\bar{y}(\infty)$, where s_i is a Gaussian random walk and $\tau^u = \inf\{i > 0 : s_i > u\}$. This is called the adjusted barrier shifting technique (ABAST) (Gobet (2008) [17]).

We can show that the standard deviation of the Monte Carlo estimator $\hat{p}$ of $p = p(A)$ is $\sqrt{\frac{p(1-p)}{M}}$ which is dominated by $0.5\sqrt{\frac{1}{M}}$ where p is the exact probability that event A happens (e.g., the First-to-Default event happens), and M is the number of simulations. Indeed, denote by $\hat{\tau}_i^m$ the simulated individual trigger time for firm i in simulation m. In all of the schemes above, we compute the indicator of the (First-to-Default) event I_{A^m} where A^m is the event that at least one firm defaults by T; i.e., $\hat{\tau}^m \leq T$ with $\hat{\tau}^m = min\{\hat{\tau}_i^m : i = 1, ..., N\}$. Finally, we set

$$\hat{p} = \frac{1}{M}\sum_1^M I_{A^m} \tag{3.7}$$

Since each I_{A^m} is a Bernoulli random variable that takes value 1 with probability p and 0 with probability $1-p$, $Var(I_{A^m}) = p(1-p)$. Since they are independent,

$$Var(\hat{p}) = \frac{p(1-p)}{M} \leq \frac{(\frac{p+(1-p)}{2})^2}{M} = \frac{1}{4M} \tag{3.8}$$

Hence, if we do 10000 simulations, the standard deviation of the BAST estimator will be less than 0.005, which is often small compared to the simulation bias (expected error) with a stepsize

$\delta t = 0.01$. The above argument remains valid if we replace A and the corresponding A^m by arbitrary events; e.g., the n^{th}-to-Default events.

In what follows, we compare these various numerical methods. We will find with numerical experiments that for low-dimensional problems, increasing the number of simulations leads to more improvement than increasing the sampling frequency; for high-dimensional problems, increasing the sampling frequency leads to more improvement than increasing the number of simulations.

3.2 VALIDATION OF MONTE CARLO METHODS

Before we apply the Monte Carlo methods to the sophisticated models we examine in later chapters, we need to validate the Monte Carlo schemes by comparison with the analytic results in Chapter 2.

3.2.1 First-to-Default Probability

We first examine the MC approximation for FtD probability which is essential in pricing FtD basket swaps. The analytic results for FtD probability were studied in section 2.1. In particular, the two-dimensional FtD probabilities in both the first-crossing and Vasicek settings were given by equations (2.4) and (2.8).

3.2.1.1 Homogeneous Portfolio We look at the case when the portfolio of N firms is homogeneous; i.e., when $\rho_i = \rho$, and $K_i = K$. In this case, only nonnegative ρ would matter since $Corr[X_{i,t}X_{j,t}] = \rho^2$ (equation (2.3) with $\rho_i = \rho_j$). For $N = 2$, figures 10, 11, 12, 13 (see Appendix C) compare the exact two-dimensional FtD probability (red) (equation (2.4)) with the Monte Carlo results using "linear interpolation" (green), "Brownian interpolation" (blue), BAST (cyan) and

ABAST (magenta). The next two plots in figures 14 and 16 compare the 100-dimensional Monte Carlo approximations and the exact solutions at $\rho = 0, 1$ (red asterisk, yellow asterisk). Recall that the exact result is only known at $\rho = 0, 1$ (equations (2.10) and (2.11)).

It is clear from the plots that for two-dimensional problems, both "Brownian interpolation" and BAST work well, even for large stepsize $\delta t = 0.25$. However, when the dimension of the problem is very high, e.g., 100, then BAST seems to work better for large ρ because "Brownian interpolation" does not reflect the high correlation in the scheme and no known convergence results exist, while the convergence rate of the BAST does not depend on the correlation. In addition, only in the case when δt is large and the barrier $K = -0.5$ is close to the initial value of the process do the BAST and ABAST make a difference.

3.2.1.2 Heterogeneous Portfolio We now introduce some inhomogeneity by considering a portfolio consisting of credits from two sectors. More precisely, all credits in the same sector share a common $\rho_i : \ i = 1, 2$, while credits from different sectors have different $\rho's$. For simplicity and to focus on the impact of correlation, we assume $K_i = K$. We choose several fixed correlations for the first sector and let the correlations for the second sector vary from -1 to 1. The first six figures 17, 18, 19, 20, 21, and 22 (see Appendix C) compare the exact two-dimensional FtD probability (red) (equation (2.4) with $\rho = \rho_1\rho_2$) with the Monte Carlo results using "linear interpolation" (green), "Brownian interpolation" (blue), BAST (cyan) and ABAST (magenta) with one firm in the first sector and the other firm in the second sector. The second set of these figures 23 and 24 (see Appendix C) compare the exact results at $\rho_2 = -1, 0, 1$ (asterisk) and the Monte Carlo approximations in 100 dimensions with one firm in the first sector and the other 99 firms in the second sector. Here, the exact results in the first-crossing setting are given by equation (2.4) with $\rho = \rho_1\rho_2$ for $\rho_2 = -1, 1$, and the exact result is $1 - (1 - 2\Phi(\frac{K}{\sqrt{T}}))^{100}$ (equation (2.13) with $K_1 = K_2 = K$) for $\rho_2 = 0$.

Again, we can see that for the 100-dimensional problem, BAST and ABAST match the exact values at $\rho_2 = -1, 0, 1$ better than "Brownian interpolation" and as long as the barrier is not too

close to the process, BAST and ABAST will coincide. Hence we will focus on BAST in what follows. Furthermore, the plots appear to suggest that all of the above Monte Carlo methods work better for positive correlations than for negative correlations.

3.2.1.3 Effects of Stepsize and Number of Simulations As mentioned in section 3.1, the standard deviation (equation (3.8)) of the Monte Carlo estimator depending on the number of simulations is often small compared with its bias $o(\sqrt{\delta t})$ depending on the sampling frequency (e.g., if $NumSim = 10000$ and $\delta t = 0.01$). We illustrate this by varying the number of replications and the stepsize and comparing the results.

The figures 26 and 27 (see Appendix C) compare a homogeneous portfolio consisting of 100 names using BAST with $\delta t = 0.25, 0.01, 0.001$, and $NumSim = 10000, 50000$ for $T = 1$. It appears that increasing $NumSim$ from 10000 to 50000 does not significantly improve the results apart from smoothing the FtD probability a little bit by reducing the variance, while reducing the stepsize from 0.25 to 0.01 does make an improvement. On the other hand, reducing the stepsize further from 0.01 to 0.001 improves the result but the difference is usually less than 0.001. Hence, it seems that a stepsize of 0.01 and 10000 simulations would be a reasonable choice for an error tolerance of 0.01. Indeed, taking $N = 100, K = -3, T = 1$, for instance, the l^∞ norm of the error $\|P_{MC} - P_{Exact}\|_{l^\infty}^{\rho=0,1} = \max\{|P_{MC}(\rho = 0) - P_{Exact}(\rho = 0)|, |P_{MC}(\rho = 1) - P_{Exact}(\rho = 1)|\}$ at $\rho = 0, 1$ (where the exact values are known: see equations (2.12) and (2.13)) is given in table 5 (see Appendix C).

In the non-homogeneous case, we compare the Monte Carlo approximations using BAST for two names with the exact solutions (red) (equation (2.4)), one in the first sector and one in the second sector, with $K = -3, T = 5$, and different values of $\rho_1 = 0.1, 0.5, 0.9$, $\delta t = 0.25$, $NumSim = 10000$ (green), $\delta t = 0.01$, $NumSim = 10000$ (blue), $\delta t = 0.25$, $NumSim = 50000$ (cyan), $\delta t = 0.01$, $NumSim = 50000$ (magenta). These are shown in figures 28, 29, and 30 (see Appendix C).

The l^∞ norms of the errors with varying stepsizes $\delta t = 0.25, 0.01$ and number of simulations $NumSim = 10000, 50000$ for different correlations $\rho_1 = 0.1, 0.5, 0.9$ are shown in table 6 (see Appendix C). The l^∞ norm of the error with specified ρ_1 is defined as $\|P_{MC} - P_{Exact}\|_{l^\infty} = \max\{|P_{MC}(\rho_2) - P_{Exact}(\rho_2)| : \rho_2 \in \{-1, -0.9, ..., -0.1, 0, 0.1, ..., 0.9, 1\}\}$. Again, we can see that with a stepsize $\delta t = 0.01$ and 10000 simulations, we are able to obtain reasonably good approximation. From now on throughout the dissertation, these will be the stepsize and number of simulations we use, unless otherwise stated.

3.2.2 Portfolio Loss Distribution

We compare the loss distribution between the Vasicek model with numerical integration (equation (2.14)) and the first-crossing model with BAST Monte Carlo approximation. In figure 31 (see Appendix C), the red, blue, magenta curves are the Vasicek loss distributions for $\rho = 0, 0.5, 1$, while the green, cyan, black curves are the first-crossing loss distributions for $\rho = 0, 0.5, 1$ in a portfolio of 50 credits. It is clear from both the definitions of default and the numerical experiment that the first-crossing setting generates larger losses than the Vasicek setting.

3.2.2.1 Peaks When $\rho = 0$ In section 2.2, we learned from equations (2.21) and (2.22) that if $\rho = 0$, the loss distribution in the Vasicek setting has a peak at $n = \lfloor (N+1)\Phi(\frac{K}{\sqrt{T}}) \rfloor$, while the peak is at $n = \lfloor 2(N+1)\Phi(\frac{K}{\sqrt{T}}) \rfloor$ in the first-crossing model, where $\lfloor x \rfloor$ is the largest integer less than or equal to x. Thus, if $\rho = 0$, for parameters $N = 50$, $K = -3$, $T = 5$, the loss distribution in the Vasicek setting has a peak at $n = 4$, while the peak is at $n = 9$ in the first-crossing model. These observations are confirmed in figure 31.

3.2.2.2 Extreme Loss Behavior Figure 31 also confirms the behavior of the loss distribution at the tails studied in equations (2.27) and (2.28). That is, the tails of the loss distribution vanish when $\rho^2 < 0.5$ (e.g., $\rho = 0$ and $\rho = 0.5$) and blow up when $\rho^2 > 0.5$ (e.g., $\rho = 1$).

3.2.2.3 Heterogeneous Portfolio, Large Portfolio Approximation, and Multiple Humps In section 2.2.2.4, we studied the large portfolio approximation for a heterogeneous portfolio, including its tail behavior (equations (2.51) and (2.52)) and its monotonicity under different conditions on parameters. We showed that when $\rho_j^2 \leq \frac{1}{2}$ for all j and there exists k such that $\rho_k^2 < \frac{1}{2}$, then the asymptotic density starts from zero and increases to some point and then decreases back to zero with only one hump. Using 10000 Monte Carlo simulations and a time stepsize 0.01, we compare the first-crossing and Vasicek loss densities (using Gaussian kernel density estimation for smoothing) for a finite-size two-sector portfolio with 50 names in each sector and the same within-sector structure as the above large portfolio (see figure 32 in Appendix C). It is obvious that the loss in the first-crossing setting is significantly larger than in the Vasicek setting.

We also compare the Gaussian kernel loss density (a smoothing density estimation method) for the above finite-size portfolio with the asymptotic loss density in the Vasicek setting in figure 33 (see Appendix C). The asymptotic loss density is calculated in two ways: the first uses the analytic formula $p^{Vasicek}(x) = \frac{1}{\sum_{j=1}^{J} \frac{w_j \rho_j}{\sqrt{1-\rho_j^2}} H_j(x)}$ with a numerical root finding algorithm for calculating $G^{-1}(x)$ appearing in $H_j(x)$; the second uses Monte Carlo to generate 10000 independent standard normal random variables Z, simulate the conditional asymptotic loss $L^{\infty} = G(Z)$, and then estimate the Gaussian kernel density of the asymptotic loss. It turns out that they match to a very high degree, except that the finite portfolio loss density has slightly fatter tails and the asymptotic loss density has a slightly higher peak (part of the reason is that Gaussian kernel density estimation smooths out the density). The location of the hump also agrees with the previous calculation.

When $\rho_j^2 > \frac{1}{2}$ for all j, a typical portfolio with this correlation structure would have an asymptotic density that decreases from ∞ to some point and then increases back to ∞. For a concrete example, consider a two-sector portfolio with $w_1 = w_2 = 0.5$, $\rho_1 = 0.8$, $\rho_2 = 0.9$, $K_1 = K_2 = -1$, $T = 5$. We compare the analytic asymptotic loss density with the normalized histogram for loss density estimation for a finite portfolio with 50 obligors in each of the two sectors and the same within-sector structure as the large portfolio. We use a normalized histogram instead of Gaussian kernel density estimation, since the Gaussian kernel density would smooth out the blow-up at 0% loss and 100% loss. Figure 34 (see Appendix C) confirms the monotonicity and clearly shows that

the asymptotic loss density and the finite-sample estimation match almost exactly.

When there exist $j \neq k$ such that $\rho_j^2 < \frac{1}{2}$ and $\rho_k^2 > \frac{1}{2}$, we showed that the model is able to generate multiple humps. In figures 35 and 36 (see Appendix C), we illustrate the multi-humped feature by comparing the first-crossing and Vasicek loss distributions and loss densities (using Gaussian kernel smooth density estimation) for the finite-size portfolio specified in section 2.2.2.4 with 50 names in each of the two sectors and the same within-sector structures with $w_1 = w_2 = 0.5$, $\rho_1 = 0.1$, $\rho_2 = 0.9$, $K_1 = K_2 = -1$, $T = 5$. Numerical experiments show that $\frac{d}{dx}p^{Vasicek}(x) > 0$ when $x \in (0, 0.1457)$; $\frac{d}{dx}p^{Vasicek}(x) < 0$ when $x \in (0.1457, 0.4911)$; $\frac{d}{dx}p^{Vasicek}(x) > 0$ when $x \in (0.4911, 0.6962)$; $\frac{d}{dx}p^{Vasicek}(x) < 0$ when $x \in (0.6962, 1)$ ($G^{-1}(x) \in (-\infty, -1.83)$). Hence, the two humps are located at 0.1457 and 0.6962. It is clear that the location of the big hump in the first-crossing setting is much larger than in the Vasicek setting.

In figure 37 (see Appendix C), we also compare the normalized histogram (used for density estimation) and the Gaussian kernel loss density with the Vasicek definition of default for the above finite-size portfolio. We can see that they agree to a high degree (the Gaussian kernel density estimation smooths out the histogram).

To illustrate the goodness of the large portfolio approximation, we compare the asymptotic loss densities (using both analytic and MC methods previously described) with the Gaussian kernel loss density (using 10000 MC simulations with a time stepsize 0.01) for the above finite-size portfolio (see figure 38 in Appendix C). It turns out that the locations of the humps are close except that the asymptotic loss density is more concentrated (steeper) at the two humps, while the finite portfolio loss density is flatter and wider (i.e., has heavier tails) (again, part of the reason is that the Gaussian kernel density estimation smooths out the density). In addition, the large portfolio approximation is much faster. Indeed, the Gaussian kernel loss density estimation using Monte Carlo takes 38.49286 seconds; while the analytic asymptotic loss density estimation only takes 0.391843 second, the MC asymptotic loss density estimation with 10000 simulations takes only 0.039277 second. The previous calculation of the locations of the humps (0.1457 and 0.6962) in the asymptotic loss density is also confirmed.

If $\rho_j > 0$ for some j and $\rho_k < 0$ for some k, it is possible for the toy model to generate a multi-humped loss distribution, especially when the between-sector correlations are large and negative. This is illustrated in figures 39 and 40 (see Appendix C) by comparing the first-crossing and Vasicek loss distributions and densities for a two-sector portfolio with 50 names in each sector and $\rho_1 = 0.5$, $K_1 = K_2 = -1$, $T = 5$ and different negative values of ρ_2.

3.2.3 Perturbation Approximation for the First-to-Default Probability

In the previous sections of this chapter, we investigated the MC methods in calculating the first-to-default probability and loss distribution for pricing basket default swaps and collateralized debt obligations. However, a disadvantage of the MC method is that it is relatively slow. In this and the next subsection, we explore the possibility of alternative approximations which allow for fast calculation of the first-to-default probability in the first-crossing setting. Metzler (2008) [33] applied the argument of Wise and Bhansali (2008) [44] to derive a perturbation approximation to the joint survival probability:

$$Q(T) = \Pr(\min\{\tau_1, ..., \tau_N\} > T) = \prod_{i=1}^{N} Q_i(T) \left[1 + \frac{1}{2} \sum_{j \neq i} \left(\frac{Q_{i,j}(T)}{Q_i(T) Q_j(T)} - 1\right)\right] \tag{3.9}$$

where $Q_i(T) = \Pr(\tau_i > T)$ is the marginal survival probability and $Q_{i,j}(T) = \Pr(\min\{\tau_i, \tau_j\} > T)$ is the bivariate survival probability.

Thus, the first-to-default probability can be approximated by

$$\Pr(\min\{\tau_1, ..., \tau_N\} \leq T) = 1 - \prod_{i=1}^{N} (1 - P_i(T)) \left[1 + \frac{1}{2} \sum_{j \neq i} \left(\frac{1 + P_{i,j}(T) - P_i(T) - P_j(T)}{(1 - P_i(T))(1 - P_j(T))} - 1\right)\right] \tag{3.10}$$

given the marginal default probability $P_i(T)$ and the bivariate default probability $P_{i,j}(T)$.

3.2.4 Bonferroni-type Bounds for the First-to-Default Probability

Many authors have studied the upper and lower bounds for the probability of a union of events in terms of individual and bivariate probabilities. Dawson and Sankoff (1967) [6] provided a lower bound on the probability that at least one out of N events occurs in terms of the sum of individual probabilities, $S1$, and the sum of bivariate probabilities, $S2$. Kwerel (1975) [30] provided "stringent" upper and lower bounds on the probability that exactly n out of N events occur based on $S1$ and $S2$ using linear programming, and claimed that the lower bound for the union of events obtained is equivalent to the one in Dawson and Sankoff (1967) [6]. Hunter (1976) [21] obtained an upper bound for the union of events based on specific individual and bivariate probabilities in terms of some maximizing spanning tree. That is,

$$\Pr(\bigcup A_i) \leq \sum \Pr(A_i) - \max_{\tau \in T} \sum_{\tau} \Pr(A_i A_j) \tag{3.11}$$

where $\tau = \{i, j\}$ is some spanning tree of the $\{A_i\}$, in the set T of such spanning trees.

In figure 41 (see Appendix C), we apply these bounds and compare them with the perturbation approximation and Monte Carlo simulation of the First-to-Default probability for a homogeneous portfolio of 100 credit names with parameters $\rho = 0, ..., 1$, $K = -3$, $T = 3$ in the first-crossing setting. The red curve is an upper bound, the green curve is the lower bound, the blue curve is the perturbation approximation, the cyan curve is the Monte Carlo simulation, and the magenta asterisks are the exact FtD probability when $\rho = 0, 1$. It appears that both the upper and the lower bounds coincide with the exact probability at $\rho = 1$, that the upper bound performs relatively well with small ρ, the perturbation approximation is good when ρ is small, as might be expected since the perturbation expansion is around $\rho = 0$. The above comparison shows that the perturbation expansion and the Bonferroni-type estimates are inadequate for use in pricing and hedging complex credit derivatives.

3.3 CHAPTER SUMMARY

In conclusion, with the basic "hierarchical structure" in the toy model, one is able to generate a multi-humped loss distribution when there are two or more sectors with certain specifications of heterogeneous correlations. However, as pointed out by Hull et al. (2005) [20] and O'Kane (2008) [34], the toy model fails to capture certain market features such as "correlation smiles". This leads us to introduce more financially motivated features in our models (i.e., cyclical correlation (correlation through sharing the same macroeconomic environment) and contagion (default interaction between firms in the same industry)). In what follows, we will study these more sophisticated models using Monte Carlo approximation and analytic results (including asymptotic analysis) whenever possible.

4.0 MODELS WITH CYCLICAL CORRELATION

In this chapter, we investigate models that are able to capture certain market features through inclusion of financially more realistic dynamics on macroeconomic correlation (referred to as cyclical correlation). The financially motivated dynamics that we study in this chapter include barrier switching (section 4.1), correlation switching (section 4.2), stochastic (or random) drift (section 4.3), random initial state (section 4.4), and mean-reverting models of correlation and macroeconomic factor (section 4.5).

4.1 A BARRIER SWITCHING MODEL

We begin with a new one-factor structural model which includes regime switching on the barrier. The dynamics of the firm's credit index is the same as equation (2.1). However, the barrier now is governed by a Markov chain that is independent of W and B, with instantaneous transition probabilities:

$$\begin{aligned} &\Pr(K_{i,t} = k_i^b | K_{i,t-} = k_i^g) = \lambda_b \, dt, \quad \Pr(K_{i,t} = k_i^g | K_{i,t-} = k_i^g) = 1 - \lambda_b \, dt \\ &\Pr(K_{i,t} = k_i^g | K_{i,t-} = k_i^b) = \lambda_g \, dt, \quad \Pr(K_{i,t} = k_i^b | K_{i,t-} = k_i^b) = 1 - \lambda_g \, dt \end{aligned} \tag{4.1}$$

where λ_g, λ_b are interpreted as "intensities" that the firm's liability switches between the good state and bad state, and $k_i^b = k_i^g \kappa_i$ with $\kappa_i \in (0, 1)$.

This model reflects the phenomenon that some firms (like Enron during 1990's) might purposely misrepresent their liabilities, and this manifests itself through randomness on the liability

barriers.

From the dynamics of the barrier, we can find the finite-time transition probability matrix:

$$\begin{aligned}
\begin{bmatrix} P^K_{gg}(t) & P^K_{gb}(t) \\ P^K_{bg}(t) & P^K_{bb}(t) \end{bmatrix} &= \exp\left\{ \begin{bmatrix} -\lambda_b & \lambda_b \\ \lambda_g & -\lambda_g \end{bmatrix} t \right\} \\
&= \exp\left\{ \begin{bmatrix} 1 & \lambda_b \\ 1 & -\lambda_g \end{bmatrix} \begin{bmatrix} 0 & 0 \\ 0 & -(\lambda_g+\lambda_b) \end{bmatrix} \begin{bmatrix} 1 & \lambda_b \\ 1 & -\lambda_g \end{bmatrix}^{-1} t \right\} \\
&= \begin{bmatrix} 1 & \lambda_b \\ 1 & -\lambda_g \end{bmatrix} \exp\left\{ \begin{bmatrix} 0 & 0 \\ 0 & -(\lambda_g+\lambda_b) \end{bmatrix} t \right\} \begin{bmatrix} 1 & \lambda_b \\ 1 & -\lambda_g \end{bmatrix}^{-1} \\
&= \begin{bmatrix} 1 & \lambda_b \\ 1 & -\lambda_g \end{bmatrix} \begin{bmatrix} \exp\{0\} & 0 \\ 0 & \exp\{-(\lambda_g+\lambda_b)t\} \end{bmatrix} \begin{bmatrix} 1 & \lambda_b \\ 1 & -\lambda_g \end{bmatrix}^{-1} \\
&= \tfrac{1}{\lambda_g+\lambda_b} \begin{bmatrix} \lambda_g + \lambda_b \exp\{-(\lambda_u+\lambda_d)t\} & \lambda_b(1-\exp\{-(\lambda_g+\lambda_b)t\}) \\ \lambda_g(1-\exp\{-(\lambda_g+\lambda_b)t\}) & \lambda_b + \lambda_g \exp\{-(\lambda_g+\lambda_b)t\} \end{bmatrix}
\end{aligned} \tag{4.2}$$

This is the solution of the Kolmogorov backward equation

$$\frac{d}{dt}P^K(t) = Q\,P^K(t), \quad P^K(0) = I \tag{4.3}$$

where $P^K(t) = \begin{bmatrix} P^K_{gg}(t) & P^K_{gb}(t) \\ P^K_{bg}(t) & P^K_{bb}(t) \end{bmatrix}$, $Q = \begin{bmatrix} -\lambda_b & \lambda_b \\ \lambda_g & -\lambda_g \end{bmatrix}$, $P^K_{ij}(t) = \Pr(K_t = k_j | K_0 = k_i)$.

In addition, the steady-state distribution of the barrier is

$$\begin{bmatrix} P^K_{gg}(\infty) & P^K_{gb}(\infty) \\ P^K_{bg}(\infty) & P^K_{bb}(\infty) \end{bmatrix} = \tfrac{1}{\lambda_g+\lambda_b} \begin{bmatrix} \lambda_g & \lambda_b \\ \lambda_g & \lambda_b \end{bmatrix} \tag{4.4}$$

Suppose initially, the barrier is in a good state, that is, $K_{i,0} = k^i_g$. In the Vasicek setting, the probability that firm i defaults given the systematic factor W_T and the barrier $K_{i,T}$ is

$$\Pr(X_{i,T} < K_{i,T} | W_T, K_{i,T}) = \Phi\left(\frac{K_{i,T} - \rho_i W_T}{\sqrt{(1-\rho_i^2)\,T}}\right) \tag{4.5}$$

Thus, with good initial barriers, the probability that firm i defaults, given the systematic factor W_T, can be calculated using equation (4.2)

$$\begin{aligned}\Pr(X_{i,T} < K_{i,T}|W_T) = &\frac{1}{\lambda_g+\lambda_b}\left(\lambda_g + \lambda_b \exp\{-(\lambda_g+\lambda_b)T\}\right)\Phi\left(\frac{k_i^g - \rho_i W_T}{\sqrt{(1-\rho_i^2)\,T}}\right)\\ &+\frac{\lambda_b}{\lambda_g+\lambda_b}\left(1-\exp\{-(\lambda_g+\lambda_b)T\}\right)\Phi\left(\frac{k_i^b - \rho_i W_T}{\sqrt{(1-\rho_i^2)\,T}}\right)\end{aligned} \tag{4.6}$$

We denote by $p_i^{Vasicek}(w) = \Pr(X_{i,T} < K_{i,T}|W_T = w)$.

Since in the Vasicek setting, defaults are independent given W_T, we have the loss distribution and the n^{th}-to-default probability to be

$$\begin{aligned}P^{Vasicek}(L = \frac{n}{N}) = &\frac{1}{\sqrt{2\pi T}}\int_{-\infty}^{\infty}\sum_{1\le i_1<\ldots<i_n\le N}\prod_{k=1}^{n} p_{i_k}^{Vasicek}(w)\\ &\prod_{l\neq i_1,\ldots,i_n}\left(1-p_l^{Vasicek}(w)\right)\,\exp\left\{-\frac{w^2}{2T}\right\}dw\end{aligned} \tag{4.7}$$

$$\begin{aligned}P^{Vasicek}(L \ge \frac{n}{N}) = &\frac{1}{\sqrt{2\pi T}}\int_{-\infty}^{\infty}\sum_{j=n}^{N}\sum_{1\le i_1<\ldots<i_j\le N}\prod_{k=1}^{j} p_{i_k}^{Vasicek}(w)\\ &\prod_{l\neq i_1,\ldots,i_j}\left(1-p_l^{Vasicek}(w)\right)\,\exp\left\{-\frac{w^2}{2T}\right\}dw\end{aligned} \tag{4.8}$$

If the portfolio is homogeneous, $i.e., p_i^{Vasicek}(w) = p^{Vasicek}(w),\ i = 1,...,n$, we obtain the simpler expressions:

$$\begin{aligned}P^{Vasicek}(L = \frac{n}{N}) = &\frac{1}{\sqrt{2\pi T}}\int_{-\infty}^{\infty}\binom{N}{n} p^{Vasicek}(w)^n\\ &\left(1-p^{Vasicek}(w)\right)^{N-n}\,\exp\left\{-\frac{w^2}{2T}\right\}dw\end{aligned} \tag{4.9}$$

$$\begin{aligned}P^{Vasicek}(L \ge \frac{n}{N}) = &\frac{1}{\sqrt{2\pi T}}\int_{-\infty}^{\infty}\sum_{j=n}^{N}\binom{N}{j} p^{Vasicek}(w)^j\\ &\left(1-p^{Vasicek}(w)\right)^{N-j}\,\exp\left\{-\frac{w^2}{2T}\right\}dw\end{aligned} \tag{4.10}$$

As a special case, the first-to-default probability in the Vasicek setting is

$$\begin{aligned} & P^{Vasicek}(L \geq \frac{1}{N}) = 1 - P^{Vasicek}(L = 0) \\ & = \int_{-\infty}^{\infty} \prod_{i=1}^{N} (1 - p_i^{Vasicek}(w)) \, \exp\{-\frac{w^2}{2T}\} \, dw \end{aligned} \tag{4.11}$$

for an inhomogeneous portfolio and

$$\begin{aligned} & P^{Vasicek}(L \geq \frac{1}{N}) = 1 - P^{Vasicek}(L = 0) \\ & = \int_{-\infty}^{\infty} (1 - p^{Vasicek}(w))^N \, \exp\{-\frac{w^2}{2T}\} \, dw \end{aligned} \tag{4.12}$$

for a homogeneous portfolio.

We compare the first-to-default probability in the toy model and in the barrier switching model both in the first-crossing setting and in the Vasicek setting with $k_g = -3$, $\kappa = 0.5$ (so $k_b = -1.5$) and $T = 5$, for different levels of barrier switching intensities. In figure 42 (see Appendix D), there are two firms, with $\rho_1 = 0.5$ for the first firm, and we let the correlation of the second firm ρ_2 vary from -1 to 1. The red curves represent the FtD probabilities in the toy model where there is no barrier switching (known from equation (2.4)), while the green, blue, cyan and magenta curves represent the FtD probability with $\lambda_g = \lambda_b = 10, 1, 0.1, 0.01, 0.01$, respectively. The lines, circles and asterisks represent the first-crossing, Vasicek exact, Vasicek MC approximations, respectively. As expected, the FtD probability (both in the first-crossing and Vasicek settings) converges to the case of no barrier switching (in the corresponding first-crossing and Vasicek settings) as the switching intensities vanish. It is also clear that increasing the intensity increases the first-to-default probability.

Next, we focus on the first-crossing setting, and plot (see figure 43 in Appendix D) the first-to-default probability with $\rho_1 = 0.5$, $\rho_2 = -1...1$, $\lambda_g = \lambda_b = 1$ and $\kappa_1 = \kappa_2 = 1, 0.75, 0.5, 0.25$, represented by the red, green, blue and cyan curves, respectively, to see the effect of different levels of a bad liability report. It is clear that less reliable liability reports (i.e., smaller κ) increase the first-to-default probability.

Next, we look at the effect of changing ρ_1 and compare the FtD probability in the barrier switching model with $\rho_2 = -1...1$, $\kappa_1 = \kappa_2 = 0.5$, $\lambda_g = \lambda_b = 1$ and $\rho_1 = 0.1, 0.5, 0.9$, represented by the red, green and blue curves, respectively in figure 44 (see Appendix D). Notice that the barrier switching model has a similar behavior to the toy model in that the first-to-default probabilities both in the first-crossing and the Vasicek setups are decreasing functions of $\rho_1\rho_2$, the correlation between the two firms (compare figures 44 and 1).

We now look at the FtD probability in the barrier switching model for a two-sector portfolio with 50 names in each sector. In figure 45 (see Appendix D), we fix $\kappa_1 = \kappa_2 = 0.5$, $\lambda_g = \lambda_b = 1$ and vary $\rho_1 = 0.1, 0.5, 0.9$, and plot the FtD probability for different levels of $\rho_1 = 0.1, 0.5, 0.9$, represented by the red, green and blue, respectively. The first-crossing Monte Carlo, Vasicek Monte Carlo and the Vasicek exact solution (equation (4.11)) are represented by the plain, circle, and asterisk marks, respectively. It seems that when $\rho_2 = \pm 1$ the FtD probability is a decreasing function of ρ_1 in both the first-crossing and the Vasicek setups.

Finally, we compare the loss distribution for a homogeneous portfolio of 50 names and investigate the effect of changing ρ, κ and λ for fixed $K = -3$, $T = 5$.

In figure 46 (see Appendix D), the red, green and blue curves represent the loss distribution for fixed $\kappa = 0.5$ and $\lambda = 1$, and $\rho = 0.1, 0.5, 0.9$, respectively. The plain and asterisk marks represent the first-crossing Monte Carlo and Vasicek exact solution (equation (4.9)), respectively. It seems that increasing the correlation spreads out the loss distribution to the two extremes, and, in fact, the loss density tends to blow up at the two ends for large ρ^2, for instance, for $\rho = 0.9$, and vanish at the two ends for small ρ^2, similar to the toy model (compare figures 46 and 31).

In figure 47 (see Appendix D), the red, green, blue and cyan curves represent the loss distribution for fixed $\rho = 0.5$ and $\lambda = 1$, and $\kappa = 1, 0.75, 0.5, 0.25$, respectively. The plain and asterisk marks represent the first-crossing Monte Carlo and Vasicek exact solution, respectively. As expected, decreasing κ (decreasing the true distance-to-default) shifts the loss distribution to the right.

In figure 48 (see Appendix D), the red, green, blue and cyan curves represent the loss distribution for fixed $\rho = 0.5$ and $\lambda = 1$, and $\lambda = 0, 0.1, 1, 10$, respectively. The plain and asterisk marks represent the first-crossing Monte Carlo and Vasicek exact solution, respectively. Again, as expected, increasing λ (increasing the frequency of barrier switch) shifts the loss distribution to the right.

In summary then, this barrier switching model, introduced to capture uncertainty (unreliability) in a firm's reporting of its liability, manifests the following behavior in the loss distribution in that larger losses become more likely.

4.2 A CORRELATION SWITCHING MODEL

According to empirical studies, correlations tend to increase in bad economy, and decrease in good economy. We next consider hierarchical structural models where correlation is a decreasing function of the market factor M, in particular, models with a two-state correlation (low when the market is good and high when the market is bad). In particular, we will study the one-factor model:

$$d\,X_{i,t} = \rho_i\,dM_t + \sqrt{1-\rho_i^2}\,dB_{i,t}, \quad X_{i,0} = 0 \tag{4.13}$$

where the market index M_t can be taken as any appropriate processes, e.g., Brownian motion, regime-switching, poisson jump, mean-reverting, etc. In this section, we will examine two special case: when M is a Brownian motion (section 4.2.1), and when M is a two-state Markov chain (section 4.2.2).

4.2.1 Brownian Macroeconomic Factor

We first look at a model with a Brownian motion market index and correlation switching.

$$d\,X_{i,t} = \rho_{i,t}\,dW_t + \sqrt{1-\rho_{i,t}^2}\,dB_{i,t}, \quad X_{i,0} = 0 \tag{4.14}$$

$$\rho_{i,t} = \rho_{i,0}\,I\{W_t \geq 0\} + sgn(\rho_{i,0})\,(\kappa_i + (1-\kappa_i)|\rho_{i,0}|)\,I\{W_t < 0\} \tag{4.15}$$

In this model, correlation increases in magnitude as the market goes bad, i.e., $W_t < 0$, and goes back to the original level as the market returns to normal. Here, $\kappa_i \in [0,1]$ controls the level of increase in the correlation $\rho_{i,0}$. Notice that

$$\kappa_i + (1-\kappa_i)|\rho_{i,0}| = |\rho_{i,0}| + \kappa_i(1-|\rho_{i,0}|) \in [|\rho_{i,0}|, 1] \tag{4.16}$$

Also, if $|\rho_{i,0}| = 1$, then $|\rho_{i,t}| \equiv 1$. Hence, perfect correlation with the market remains perfect subsequently. On the other hand, if $|\rho_{i,0}| = 0$, then $|\rho_{i,t}| = \kappa_i$ when $W_t < 0$, which is consistent with the phenomenon that seemingly uncorrelated assets in a normal economy may become highly correlated in a market crash.

In figure 49 (see Appendix D), we compare the FtD probability of a two-firm portfolio for different levels of $\kappa_i = \kappa$, with fixed $\rho_{1,0} = 0.5$ and varying $\rho_{2,0} = -1, ..., 1$: The red, green, blue, cyan, magenta curves represent the FtD probability for $\kappa = 0, 0.25, 0.5, 0.75, 1$, respectively.

It is clear that when $\rho_{2,0} > 0$, increasing κ decreases the FtD probability. This makes sense because the FtD probability without correlation switching is a decreasing function of $\rho_1\rho_2$ (see figure 1 in Appendix B). Increasing κ (the correlation switching level) increases both ρ_1 and ρ_2 when $\rho_{1,0} = 0.5 > 0$ and $\rho_{2,0} > 0$, and hence increases $\rho_1\rho_2$ and decreases the FtD probability.

We also compare the FtD probability in figure 50 (see Appendix D) for different κ when there are 15 obligors in each of the two sectors, with the same set of parameters. Again, the red, green, blue, cyan, magenta curves represent the FtD probability for $\kappa = 0, 0.25, 0.5, 0.75, 1$, respectively. It appears that in this case, increasing the level of κ decreases the first-to-default probability.

Furthermore, we compare the portfolio loss distribution for different κ when there are 15 obligors in each of the two sectors, with the same set of parameters. In figure 51 (see Appendix D), the red, green, blue, cyan, magenta curves represent the portfolio loss distribution for $\kappa = 0, 0.25, 0.5, 0.75, 1$, respectively. It appears that increasing κ increases the probabilities of both very small loss and very large loss, and decreases the probability of mid-size loss.

4.2.2 Two-State Macroeconomic Factor

Next, we consider the case when the market index is a jump process:

$$\begin{aligned} \Pr(M_t = -1 | M_{t-} = 0) = \lambda_d \, dt, \quad \Pr(M_t = 0 | M_{t-} = 0) = 1 - \lambda_d \, dt \\ \Pr(M_t = 0 | M_{t-} = -1) = \lambda_u \, dt, \quad \Pr(M_t = -1 | M_{t-} = -1) = 1 - \lambda_u \, dt \end{aligned} \tag{4.17}$$

The market now has two states, normal and bad, corresponding to two correlation states, normal and high:

$$\rho_{i,t} = \rho_{i,0} \, I\{M_t = 0\} + sgn(\rho_{i,0}) \left(\kappa_i + (1 - \kappa_i)|\rho_{i,0}|\right) I\{M_t = -1\} \tag{4.18}$$

In figure 52, 53, and 54 (see Appendix D), we compare the FtD probability for a portfolio of two names with parameters $\lambda_u = \lambda_d = 10, ..., 0.01$, $\kappa = 0.5$, $\rho_{1,0} = 0.1, 0.5, 0.9$, $\rho_{2,0} = -1, ..., 1$, $K = -3$, $T = 5$, $\delta t = 0.01$, $NumSim = 10000$. It is interesting to note that if the switching rate is high, the FtD probability with positive $\rho_{1,0}$ shrinks sharply to 0 for positive $\rho_{2,0}$. In fact, with $\lambda_u = \lambda_d = 10$, that is, there is about $\lambda \delta t = 0.1$ probability that the economy will switch regimes in a time-step of size 0.01 year, the FtD probability starts at 0 when $\rho_{2,0} = -1$, then grows dramatically as $\rho_{2,0}$ gets close to 0 from the negative side, and attains a peak at $\rho_{2,0} = -0.1$, and finally vanishes with a big jump-down when $\rho_{2,0}$ becomes positive. On the other hand, when the switching rate is very low, the FtD probability tends to spread out for varying $\rho_{2,0}$.

We now look at the case when $\rho_{1,0}$ is negative. With the same set of parameters except $\rho_{1,0} = -0.1, -0.5, -0.9$, we plot the FtD probability in figures 55, 56, and 57 (see Appendix D). It seems that when $\rho_{1,0}$ is negative, with high switching rate, the FtD probability stays high for varying $\rho_{2,0}$ except for very highly negative $\rho_{1,0}$. Another observation is that all FtD probabilities

seem to attain peak values near $\rho_{2,0} = 0$, regardless of the values of $\rho_{1,0}$, whether positive or negative, and regardless of the switching intensities.

4.3 MODELS WITH DRIFT

In the previous sections of this chapter, we focused on models without drift. In this section, we investigate the impact of the drift as a stochastic process.

4.3.1 A Drift Switching Model

We propose a model that has a drift which switches depending on the state of the economy:

$$d\,X_{i,t} = \rho_i\,\mu_i\,sgn(W_t)\,dt + \sigma_i\,\sqrt{1-\rho_i^2}\,dB_{i,t}, \quad X_{i,0} = 0 \tag{4.19}$$

In this model, $\mu > 0$, so the credit quality of a firm in this model has a positive drift away from the negative default boundary when the economy is in good shape, i.e., $W_t > 0$, and has a negative drift otherwise.

We now apply Levy's Arcsin Law (see Steele (2000) [40]) to this new model:

$$\begin{aligned}
&\Pr(\int_0^T sgn(W_t)\,dt \le y)\\
&= \Pr(\int_0^T (I\{W_t>0\} - I\{W_t<0\})\,dt \le y)\\
&= \Pr(\int_0^T (I\{W_t>0\} - (1-(I\{W_t>0\} + I\{W_t=0\})))\,dt \le y)\\
&= \Pr(\int_0^T (2I\{W_t>0\} + I\{W_t=0\} - 1)\,dt \le y)\\
&= \Pr(\int_0^T I\{W_t>0\}\,dt \le \frac{y+T}{2})\\
&= \frac{2}{\pi}\arcsin\sqrt{\frac{y+T}{2T}}
\end{aligned} \tag{4.20}$$

with probability density function

$$\Pr(\int_0^T sgn(W_t)\,dt \in dy) = \frac{1}{\pi\sqrt{(T-y)(y+T)}}\,dy, \quad y \in (-T,T) \tag{4.21}$$

Hence, we have

$$E[\int_0^T sgn(W_t)\,dt] = \int_{-T}^{T} \frac{y}{\pi\sqrt{(T^2-y^2)}}\,dy = 0 \tag{4.22}$$

$$\begin{aligned}
&Var[\int_0^T sgn(W_t)\,dt] \\
&= \int_{-T}^{T} \frac{y^2}{\pi\sqrt{(T^2-y^2)}}\,dy \\
&= 2\int_0^{T} \frac{y^2}{\pi\sqrt{(T^2-y^2)}}\,dy \\
&= 2\int_0^{\frac{\pi}{2}} \frac{T^2\sin^2\theta}{\pi T\cos\theta}\,T\cos\theta\,d\theta \\
&= \frac{2T^2}{\pi}\int_0^{\frac{\pi}{2}} \sin^2\theta\,d\theta \\
&= \frac{T^2}{\pi}\int_0^{\frac{\pi}{2}} (1-\cos 2\theta)\,d\theta \\
&= \frac{T^2}{\pi}\,(\theta - \frac{1}{2}\sin 2\theta)|_0^{\frac{\pi}{2}} \\
&= \frac{T^2}{2}
\end{aligned} \tag{4.23}$$

With the independence of W and B, the correlation between firm i and j $(i \neq j)$ is

$$\begin{aligned}
&Corr[X_{i,T}, X_{j,T}] \\
&= \frac{E[X_{i,T}\,X_{j,T}] - E[X_{i,T}]\,E[X_{j,T}]}{\sqrt{Var[X_{i,T}]}\,\sqrt{Var[X_{j,T}]}} \\
&= \frac{\rho_i\rho_j\mu_j\mu_j\,E[(\int_0^T sgn(W_t)\,dt)^2]}{\sqrt{\rho_i^2\mu_i^2\frac{T^2}{2} + \sigma_i^2(1-\rho_i^2)T}\,\sqrt{\rho_j^2\mu_j^2\frac{T^2}{2} + \sigma_j^2(1-\rho_j^2)T}} \\
&= \frac{\rho_i\rho_j\mu_i\mu_j\frac{T^2}{2}}{\sqrt{\rho_i^2\mu_i^2\frac{T^2}{2} + \sigma_i^2(1-\rho_i^2)T}\,\sqrt{\rho_j^2\mu_j^2\frac{T^2}{2} + \sigma_j^2(1-\rho_j^2)T}} \\
&= \frac{\rho_i\,\rho_j\,\mu_i\,\mu_j\,T}{\sqrt{[\rho_i^2\mu_i^2T + 2\sigma_i^2(1-\rho_i^2)]\,[\rho_j^2\mu_j^2T + 2\sigma_j^2(1-\rho_j^2)]}}
\end{aligned} \tag{4.24}$$

It is interesting to notice that the magnitude of the asset correlation is an increasing function of time, as opposed to the static asset correlation in the toy model. Moreover,

$$\lim_{T\to\infty} Corr[X_{i,T}, X_{j,T}] = sgn(\rho_i\,\rho_j) \tag{4.25}$$

Thus, as time goes to infinity, the magnitude of the asset correlation approaches 1 as long as none of them are uncorrelated with the market.

On the other hand, the magnitude of the asset correlation is also increasing as a function of ρ, since

$$Corr[X_{i,T}, X_{j,T}] = \frac{sgn(\rho_i\,\rho_j)\,mu_i\,\mu_j\,T}{\sqrt{[\mu_i^2 T + 2\sigma_i^2(\frac{1}{\rho_i^2}-1)]\,[\mu_j^2 T + 2\sigma_j^2(\frac{1}{\rho_j^2}-1)]}} \tag{4.26}$$

Since $\int_0^T sgn(W_t)\,dt$ and $B_{i,T}$ are independent, we have that in the Vasicek setting, the individual default probability conditioned on the value of $\int_0^T sgn(W_t)\,dt$ is

$$\Pr(X_{i,T} < K_i | \int_0^T sgn(W_t)\,dt) = \Phi(\frac{K_i - \rho_i\,\mu_i \int_0^T sgn(W_t)\,dt}{\sigma_i\,\sqrt{(1-\rho_i^2)T}}) \tag{4.27}$$

Denote by $p_i^{Vasicek}(y) = \Pr(X_{i,T} < K_i | \int_0^T sgn(W_t)\,dt = y)$. The portfolio loss distribution and the n^{th}-to-default probability are

$$\begin{aligned} P^{Vasicek}(L^{(N)} = \frac{n}{N}) = \int_{-T}^{T} \sum_{1\le i_1<\ldots<i_n\le N} \prod_{k=1}^{n} p_{i_k}^{Vasicek}(y) \\ \prod_{l\neq i_1,\ldots,i_n} (1 - p_l^{Vasicek}(y))\,\frac{1}{\pi\sqrt{(T-y)(y+T)}}\,dy \end{aligned} \tag{4.28}$$

$$\begin{aligned} P^{Vasicek}(L^{(N)} \ge \frac{n}{N}) = \int_{-T}^{T} \sum_{j=n}^{N} \sum_{1\le i_1<\ldots<i_j\le N} \prod_{k=1}^{j} p_{i_k}^{Vasicek}(y) \\ \prod_{l\neq i_1,\ldots,i_j} (1 - p_l^{Vasicek}(y))\,\frac{1}{\pi\sqrt{(T-y)(y+T)}}\,dy \end{aligned} \tag{4.29}$$

If the portfolio is homogeneous, $i.e., p_i^{Vasicek}(y) = p^{Vasicek}(y),\ i = 1, ..., n$, we obtain the simpler expressions:

$$P^{Vasicek}(L^{(N)} = \frac{n}{N}) = \int_{-T}^{T} \binom{N}{n} p^{Vasicek}(y)^n \\ (1 - p^{Vasicek}(y))^{N-n} \frac{1}{\pi\sqrt{(T-y)(y+T)}}\, dy \tag{4.30}$$

$$P^{Vasicek}(L^{(N)} \geq \frac{n}{N}) = \int_{-T}^{T} \sum_{j=n}^{N} \binom{N}{j} p^{Vasicek}(y)^j \\ (1 - p^{Vasicek}(y))^{N-j} \frac{1}{\pi\sqrt{(T-y)(y+T)}}\, dy \tag{4.31}$$

We compare the loss distribution for a homogeneous portfolio of 50 names in this model in the Vasicek setting and in the first-crossing setting, with $\mu = 1$, $K = -3$, $T = 5$. In figure 58 (see Appendix D), the red, green, blue, cyan and magenta curves represent the loss distributions for $\rho = 0, 0.25, 0.5, 0.75, 1$, respectively, and the plain, circle and asterisk curves represent the MC approximation in the first-crossing setting, the exact analytic result (equation (4.30)) and the MC approximation in the Vasicek setting, respectively.

Next, we compare the loss distribution in the toy model against the drift switching model for the same homogeneous portfolio (see figure 59 in Appendix D) with $\rho = 0.25, 0.5, 0.75$, respectively, in the first-crossing setting and in the Vasicek setting (asterisk).
Then we compare the loss distribution in the drift switching model against the toy model (asterisk) for a two-sector portfolio with 50 names in each sector in the first-crossing setting with $\rho_1 = 0.9, \rho_2 = 0.1$. In figure 60 (see Appendix D), the red (plain, asterisk), green (plain, asterisk) and blue (plain, asterisk) curves represent the loss distribution with different liabilities $K_i = -3, -4, -2$ in the drift switching and the toy model, respectively. It is clear that this model can generate a two-humped loss distribution which is of interest in the finance industry.

We are interested in knowing how the two-humped loss distribution is generated. Notice that in the toy model, the market is Gaussian and has a density function centered at 0, while in the drift switching model, the market has a density function that blows up at $\pm T$. We suspect that this is the

source of the two humps. We study this in more detail analytically by looking at the large portfolio limit in the Vasicek setting.

By applying a version of the strong law of large numbers, we have, for a homogeneous portfolio,

$$L^{(\infty)} = \Phi(\frac{K-\rho\mu y}{\sqrt{(1-\rho^2)T}}), \quad \Pr(\cdot \mid \int_0^T sgn(W_t)\,dt = y) - a.s. \tag{4.32}$$

Hence,

$$\begin{aligned}
&\Pr(L^{(\infty)} \le x) \\
&= E[\Pr(L^{(\infty)} \le x \mid \int_0^T sgn(W_t)\,dt)] \\
&= \int_{-\infty}^{\infty} \Pr(L^{(\infty)} = \Phi(\frac{K-\rho\mu y}{\sqrt{(1-\rho^2)T}}) \le x \mid \int_0^T sgn(W_t)\,dt = y)\ \Pr(\int_0^T sgn(W_t)\,dt \in dy) \\
&= \int_{-\infty}^{\infty} I\{\Phi(\frac{K-\rho\mu y}{\sqrt{(1-\rho^2)T}}) \le x\}\ \Pr(\int_0^T sgn(W_t)\,dt \in dy) \\
&= \int_{\frac{K-\sqrt{(1-\rho^2)T}\Phi^{-1}(x)}{\rho\mu}}^{\infty} \Pr(\int_0^T sgn(W_t)\,dt \in dy)
\end{aligned} \tag{4.33}$$

and the asymptotic loss density is

$$p^{Vasicek}(x) = \begin{cases} \sqrt{\dfrac{2(1-\rho^2)T}{\pi(\rho^2\mu^2T^2 - (K-\sqrt{(1-\rho^2)T}\Phi^{-1}(x))^2)}}\ \exp\{\dfrac{1}{2}(\Phi^{-1}(x))^2\}, \\ \quad \text{if } x \in (\Phi(\dfrac{K-\rho\mu T}{\sqrt{(1-\rho^2)T}}), \Phi(\dfrac{K+\rho\mu T}{\sqrt{(1-\rho^2)T}})) \\ 0, \quad \text{otherwise} \end{cases} \tag{4.34}$$

So the asymptotic density blows up at $\Phi(\frac{K-\rho\mu T}{\sqrt{(1-\rho^2)T}})$ and $\Phi(\frac{K+\rho\mu T}{\sqrt{(1-\rho^2)T}})$. This explains the two-hump phenomenon in the loss distribution. In addition, this captures the clustering phenomenon of credit defaults; that is, defaults cluster at certain percentages of portfolio loss.

We study the location of the two humps where the asymptotic loss density blows up as we increase the values of parameters. Since they are located at $\Phi(\frac{K\pm\rho\mu T}{\sqrt{(1-\rho^2)T}})$ and Φ is an increasing function, we simply need to check the monotonicity of $\frac{K\pm\rho\mu T}{\sqrt{(1-\rho^2)T}}$. We provide some analysis and

numerical illustrations by plotting the asymptotic loss density in the drift switching model in the Vasicek setup for a homogeneous portfolio of 100 names.

First, both humps occur at larger loss with increasing K, that is, if the initial distance-to-default is smaller. Indeed,

$$\frac{\partial}{\partial K}\frac{K \pm \rho\mu T}{\sqrt{(1-\rho^2)T}} = \frac{1}{\sqrt{(1-\rho^2)T}} > 0 \tag{4.35}$$

In figure 61 (see Appendix D), $\rho = 0.5$, $\mu = 1$, $T = 5$ and $K = -5, -4, -3, -2, -1$ are represented by the red, green, blue, cyan and magenta curves, respectively. We can see that the loss density shifts to larger loss as the distance-to-default decreases.

Second, if we increase μ, the two peaks spread out, since

$$\frac{\partial}{\partial \mu}\frac{K \pm \rho\mu T}{\sqrt{(1-\rho^2)T}} = \pm\frac{\rho\sqrt{T}}{\sqrt{(1-\rho^2)}} \tag{4.36}$$

In figure 62 (see Appendix D), $\rho = 0.5$, $K = 3$, $T = 5$, $\mu = 1, 2, 3$ are represented by the red, green and blue curves, respectively. It is easy to see that the loss density spreads out as μ gets large. Intuitively, if the drift becomes large, the systematic factor gets larger, either in the positive or negative direction, and since the mass of $\int_0^T sgn(W_t)\,dt$ is concentrated at the two ends, increasing the drift gives larger masses on the two ends.

Third, since

$$\frac{\partial}{\partial T}\frac{K \pm \rho\mu T}{\sqrt{(1-\rho^2)T}} = \frac{-K \pm \rho\mu T}{2\sqrt{(1-\rho^2)T^3}} \tag{4.37}$$

as T increases, the second peak occurs at larger loss, while the first peak occurs at larger loss if $T < \frac{-K}{\rho\mu}$ and at smaller loss if $T > \frac{-K}{\rho\mu}$.

In figure 63 (see Appendix D), $\rho = 0.5$, $\mu = 1$, $K = -3$, $T = 3, 5, 7, 9$ are represented by the red, green, blue and cyan curves, respectively. It is clear that the second peak moves to larger loss for longer maturity, while the first peaks are indistinguishable, since $\Phi(\frac{K \pm \rho\mu T}{\sqrt{(1-\rho^2)T}})$ $= 0.0013, 0.0023, 0.0023, 0.0019$ for $T = 3, 5, 7, 9$, respectively. In figure 64 (see Appendix D), $\rho = 0.1$, $\mu = 1$, $K = -3$, $T = 10, 20, 30, 40, 50$ are represented by the red, green, blue, cyan and magenta curves, respectively. While the second peak still moves to larger loss for longer maturity,

this plot clearly shows that the first peak moves to larger loss at first as time to maturity increases and then moves to smaller loss as time to maturity becomes very large, larger than $\frac{-K}{\rho\mu} = 30$ in this case.

Finally, since

$$\frac{\partial}{\partial\rho}\frac{K \pm \rho\mu T}{\sqrt{(1-\rho^2)T}} = \frac{\rho K \mp \mu T}{\sqrt{(1-\rho^2)^3 T}} \tag{4.38}$$

as ρ increases, the first peak occurs at smaller loss. Regarding the second peak, when $\frac{\mu T}{-K} < 1$, then the second peak occurs at larger loss if $\rho < \frac{\mu T}{-K}$ and at smaller loss if $\rho > \frac{\mu T}{-K}$; while the second peak occurs at larger loss when $\frac{\mu T}{-K} \geq 1$.

In figures 65 and 66 (see Appendix D), we plot the asymptotic loss density in the drift switching model in the Vasicek setup for a homogeneous portfolio of 100 names with $\mu = 1$, $T = 5$ for $K = -1, -3$ and different levels of $\rho = 0.1, 0.3, 0.5, 0.7, 0.9$ are represented by the red, green, blue, cyan and magenta curves, respectively. We can easily see that the asymptotic density has two peaks. As K gets closer to 0, the loss density shifts to larger loss, as expected. As ρ gets larger, the first peak is located at smaller loss. The second peak occurs at larger loss as ρ increases since $\frac{\mu T}{-K} = 5, \frac{5}{3}$ for $K = -1, -3$, respectively.

Furthermore, we look at the limits of the locations of the two humps as the values of the parameters get very small or very large.

First, since

$$\lim_{K\to-\infty} \Phi(\frac{K \pm \rho\mu T}{\sqrt{(1-\rho^2)T}}) = 0 \tag{4.39}$$

the two peaks approach 0% losses as the initial distance-to-default is extremely large. On the other hand, we have

$$\lim_{K\to 0^-} \Phi(\frac{K \pm \rho\mu T}{\sqrt{(1-\rho^2)T}}) = \Phi(\frac{\pm \rho\mu T}{\sqrt{(1-\rho^2)T}}) \tag{4.40}$$

Second, we have

$$\lim_{\mu\to 0^+} \Phi(\frac{K \pm \rho\mu T}{\sqrt{(1-\rho^2)T}}) = \Phi(\frac{K}{\sqrt{(1-\rho^2)T}}) \tag{4.41}$$

$$\lim_{\mu\to\infty} \Phi(\frac{K-\rho\mu T}{\sqrt{(1-\rho^2)T}}) = 0 \tag{4.42}$$

$$\lim_{\mu\to\infty} \Phi(\frac{K+\rho\mu T}{\sqrt{(1-\rho^2)T}}) = 1 \tag{4.43}$$

As the drift goes to zero, the systematic part vanishes and we are back to the independent Gaussian case where there is only one peak. As the drift goes to infinity, on the other hand, the two peaks spread out to 0% loss and 100% loss.

Third, we have

$$\lim_{T\to 0^+} \Phi(\frac{K\pm\rho\mu T}{\sqrt{(1-\rho^2)T}}) = 0 \tag{4.44}$$

$$\lim_{T\to\infty} \Phi(\frac{K-\rho\mu T}{\sqrt{(1-\rho^2)T}}) = 0 \tag{4.45}$$

$$\lim_{T\to\infty} \Phi(\frac{K+\rho\mu T}{\sqrt{(1-\rho^2)T}}) = 1 \tag{4.46}$$

As time-to-maturity goes to zero, both peaks approach zero, since the firm is healthy initially. As time-to-maturity goes to infinity, the systematic factor grows extremely large, either in the positive or negative direction, since most mass of $\int_0^T sgn(W_t)\,dt$ is concentrated at $\pm T$, the two peaks spread out to 0% loss and 100% loss.

Finally, we have

$$\lim_{\rho\to 0^+} \Phi(\frac{K\pm\rho\mu T}{\sqrt{(1-\rho^2)T}}) = \Phi(\frac{K-x_0}{\sqrt{T}}) \tag{4.47}$$

$$\lim_{\rho\to 1^-} \Phi(\frac{K-\rho\mu T}{\sqrt{(1-\rho^2)T}}) = 0 \tag{4.48}$$

$$\lim_{\rho\to 1^-} \Phi(\frac{K+\rho\mu T}{\sqrt{(1-\rho^2)T}}) = \begin{cases} 0, & \text{if } K+\mu T<0 \\ 1, & \text{if } K+\mu T>0 \end{cases} \tag{4.49}$$

As ρ goes to zero, both peaks approach to $\Phi(\frac{K}{\sqrt{T}})$. The intuition is that when ρ is close to zero, the systematic factor vanishes and the defaultable assets in the portfolio become almost independent,

hence the loss distribution becomes concentrated at the marginal default probability with only the idiosyncratic components. On the other hand, as ρ gets close to 1, the assets in the portfolio become almost perfectly dependent, so either 0% loss or 100% loss will be most likely.

Now we would like to add the systematic fluctuation dW term to the model and investigate its effects.

$$d\,X_{i,t} = \rho_i\,(\mu_i\,sgn(W_t)\,dt + dW_t) + \sqrt{1-\rho_i^2}\,dB_{i,t}, \quad X_{i,0} = 0 \tag{4.50}$$

In figure 67 (see Appendix D), we compare the portfolio loss distribution in the toy model and in this model for a two-sector portfolio, 50 names each, with $\rho_1 = 0.9, \rho_2 = 0.1$, $\mu_1 = \mu_2 = 0, 0.5, 1, 2, 5$. While it still generates a two-humped loss distribution, it appears that adding more fluctuation spreads out the loss distribution.

In summary, we have studied three types of regime-switching models: the barrier-switching model, the correlation-switching model, and the drift-switching model. The barrier-switching model shifts the loss distribution to larger loss. The correlation-switching model puts more weights on both very small and very large losses. The drift-switching model is able to generate a multi-humped loss distribution which apparently occurs during financial crises when there was a significant probability that a larger loss would occur.

4.3.2 Random Drift Models

4.3.2.1 Random Drift with Constant Correlation to the Market We have seen that the drift switching model generates a two-humped loss distribution and we try to find a first-crossing structural model with the desired multi-humped feature that is analytically more tractable. Our idea is to mimic $\int_0^t sgn(W_s)\,ds$, a dynamic arcsin distributed time integral, with $\int_0^t M\,ds$, a relatively more static time integral of an arcsin distributed random variable:

$$d\,X_{i,t} = \rho_i\,\mu_i\,M\,dt + \sigma_i\,\sqrt{1-\rho_i^2}\,dB_{i,t}, \quad X_{i,0} = 0 \tag{4.51}$$

where

$$\Pr(M \in dm) = \frac{1}{\pi\sqrt{1-m^2}}\, dm, \quad m \in (-1,1) \tag{4.52}$$

and

$$\tau_i = \inf\{t > 0 : X_{i,t} < K_i\} \tag{4.53}$$

Let $u(x,t;m)\,dx = \Pr(X_t \in dx, \tau > t | M = m)$ be the transition sub-density of the absorbed process $X_{t\wedge\tau}$ given $M = m$ (we drop the subscript i without confusion), then u satisfies the following Kolmogorov forward equation (see Karatzas and Shreve (1987) [27]):

$$u_t = \frac{1}{2}\,\sigma^2\,(1-\rho^2)\,u_{xx} - \rho\,\mu\,m\,u_x, \quad (x,t) \in (K,\infty)\times(0,\infty) \tag{4.54}$$

$$u(K,t;m) = u(\infty,t;m) = 0, \quad t \in (0,\infty) \tag{4.55}$$

$$u(x,0;m) = \delta(x), \quad x \in (K,\infty) \tag{4.56}$$

The transformation $u(x,t;m) = \exp\{\frac{\rho\mu m}{\sigma^2(1-\rho^2)}x - \frac{\rho^2\mu^2m^2}{2\sigma^2(1-\rho^2)}t\}\,v(x,t)$ leads to a heat equation satisfied by v:

$$v_t = \frac{1}{2}\,\sigma^2\,(1-\rho^2)\,v_{xx}, \quad (x,t) \in (K,\infty)\times(0,\infty) \tag{4.57}$$

$$v(K,t) = v(\infty,t) = 0, \quad t \in (0,\infty) \tag{4.58}$$

$$v(x,0) = \delta(x), \quad x \in (K,\infty) \tag{4.59}$$

with a unique solution given by

$$v(x,t) = \frac{1}{\sqrt{2\pi\sigma^2(1-\rho^2)t}}\,[\exp\{-\frac{x^2}{2\sigma^2(1-\rho^2)t}\} - \exp\{-\frac{(2K-x)^2}{2\sigma^2(1-\rho^2)t}\}] \tag{4.60}$$

Hence,

$$\begin{aligned} u(x,t;m) = {} & \frac{1}{\sqrt{2\pi\sigma^2(1-\rho^2)t}}\,\exp\{\frac{\rho\mu m}{\sigma^2(1-\rho^2)}x - \frac{\rho^2\mu^2m^2}{2\sigma^2(1-\rho^2)}t\} \\ & [\exp\{-\frac{x^2}{2\sigma^2(1-\rho^2)t}\} - \exp\{-\frac{(2K-x)^2}{2\sigma^2(1-\rho^2)t}\}] \end{aligned} \tag{4.61}$$

The individual default probability conditioned on the value of M is

$$
\begin{aligned}
p_i(m) &= \Pr(\tau_i \le T | M = m) \\
&= 1 - \Pr(\tau_i > T | M = m) \\
&= 1 - \int_{K_i}^{\infty} u(x_i, T; m)\, dx_i \\
&= 1 - \int_{K_i}^{\infty} \frac{1}{\sqrt{2\pi\sigma_i^2(1-\rho_i^2)T}} \exp\{\frac{\rho_i\mu_i m}{\sigma_i^2(1-\rho_i^2)}x_i - \frac{\rho_i^2\mu_i^2 m^2}{2\sigma_i^2(1-\rho_i^2)}T\} \\
&\qquad [\exp\{-\frac{x_i^2}{2\sigma_i^2(1-\rho_i^2)T}\} - \exp\{-\frac{(2K_i - x_i)^2}{2\sigma_i^2(1-\rho_i^2)T}\}]\, dx_i \\
&= 1 - \int_{K_i}^{\infty} \frac{1}{\sqrt{2\pi\sigma_i^2(1-\rho_i^2)T}} [\exp\{-\frac{(x_i - \rho_i\mu_i mT)^2}{2\sigma_i^2(1-\rho_i^2)T}\} \\
&\qquad - \exp\{\frac{2\rho_i\mu_i mK_i}{\sigma_i^2(1-\rho_i^2)} - \frac{(x_i - 2K_i - \rho_i\mu_i mT)^2}{2\sigma_i^2(1-\rho_i^2)T}\}]\, dx_i \\
&= 1 - \int_{\frac{K_i - \rho_i\mu_i mT}{\sigma_i\sqrt{(1-\rho_i^2)T}}}^{\infty} \phi(z_i)\, dz_i + \exp\{\frac{2\rho_i\mu_i mK_i}{\sigma_i^2(1-\rho_i^2)}\} \int_{\frac{-K_i - \rho_i\mu_i mT}{\sigma_i\sqrt{(1-\rho_i^2)T}}}^{\infty} \phi(z_i)\, dz_i \\
&= \Phi(\frac{K_i - \rho_i\mu_i mT}{\sigma_i\sqrt{(1-\rho_i^2)T}}) + \exp\{\frac{2\rho_i\mu_i mK_i}{\sigma_i^2(1-\rho_i^2)}\}\, \Phi(\frac{K_i + \rho_i\mu_i mT}{\sigma_i\sqrt{(1-\rho_i^2)T}})
\end{aligned}
\tag{4.62}
$$

The above result is consistent with the first-crossing distribution of a Brownian motion with drift in Shreve (2004) [38] who applied Girsanov's theorem together with the reflection principle of Brownian motion. Let $\hat{\alpha} = -\frac{\rho\mu m}{\sigma\sqrt{1-\rho^2}}$ and $\hat{K} = -\frac{K}{\sigma\sqrt{1-\rho^2}}$. Notice that $\hat{B}_t = -B_t$ is another

Brownian motion on the same probability space. We have

$$
\begin{aligned}
&\Pr(\tau_i \le T | M = m) \\
&= \Pr(\inf\{t > 0 : -\hat{\alpha}t + B_t < -\hat{K}\} \le T) \\
&= \Pr(\inf\{t > 0 : B_t < -\hat{K} + \hat{\alpha}t\} \le T) \\
&= \Pr(\inf\{t > 0 : -B_t > \hat{K} - \hat{\alpha}t\} \le T) \\
&= \Pr(\inf\{t > 0 : \hat{\alpha}t + \hat{B}_t > \hat{K}\} \le T) \\
&= \Pr(\max_{t\in[0,T]} \hat{\alpha}t + \hat{B}_t > \hat{K}) \\
&= 1 - \Pr(\max_{t\in[0,T]} \hat{\alpha}t + \hat{B}_t \le \hat{K}) \\
&= 1 - \Phi(\frac{\hat{K} - \hat{\alpha}T}{\sqrt{T}}) + \exp\{2\hat{\alpha}\hat{K}\}\,\Phi(\frac{-\hat{K} - \hat{\alpha}T}{\sqrt{T}}) \\
&= \Phi(\frac{-\hat{K} + \hat{\alpha}T}{\sqrt{T}}) + \exp\{2\hat{\alpha}\hat{K}\}\,\Phi(\frac{-\hat{K} - \hat{\alpha}T}{\sqrt{T}}) \\
&= \Phi(\frac{K - \rho\mu mT}{\sigma\sqrt{(1-\rho^2)T}}) + \exp\{\frac{2\rho\mu mK}{\sigma^2(1-\rho^2)}\}\,\Phi(\frac{K + \rho\mu mT}{\sigma\sqrt{(1-\rho^2)T}})
\end{aligned}
\tag{4.63}
$$

For a homogeneous portfolio, the loss distribution is

$$
\Pr(L^{(N)} = \frac{n}{N}) = \int_{-1}^{1} \binom{N}{n} p(m)^n \left(1 - p(m)\right)^{N-n} \frac{1}{\pi\sqrt{1-m^2}}\, dm \tag{4.64}
$$

The loss distribution for a two-sector portfolio is given by the following combinatorial formula:

$$
\begin{aligned}
\Pr(L^{(N)} = \frac{n}{N}) = \int_{-1}^{1} &\sum_{n_1=\max(0,n-N_2)}^{\min(n,N_1)} \binom{N_1}{n_1}\binom{N_2}{n-n_1} \\
&p^{(1)}(m)^{n_1}\left(1 - p^{(1)}(m)\right)^{N_1-n_1} p^{(2)}(m)^{n-n_1}\left(1 - p^{(2)}(m)\right)^{N_2-n+n_1} \\
&\frac{1}{\pi\sqrt{1-m^2}}\, dm
\end{aligned}
\tag{4.65}
$$

where $p^{(i)}(m)$ denotes the marginal default probability in sector i given $M = m$.

For a three-sector portfolio,

$$\Pr(L^{(N)} = \frac{n}{N}) = \int_{-1}^{1} \sum_{n_1=\max(0,n-N_2-N_3)}^{\min(n,N_1)} \sum_{n_2=\max(0,n-n_1-N_3)}^{\min(n-n_1,N_2)} \binom{N_1}{n_1} \binom{N_2}{n_2} \binom{N_3}{n-n_1-n_2}$$
$$p^{(1)}(m)^{n_1} \left(1-p^{(1)}(m)\right)^{N_1-n_1} p^{(2)}(m)^{n_2} \left(1-p^{(2)}(m)\right)^{N_2-n_2}$$
$$p^{(3)}(m)^{n-n_1-n_2} \left(1-p^{(3)}(m)\right)^{N_3-n+n_1+n_2} \frac{1}{\pi\sqrt{1-m^2}}\, dm \tag{4.66}$$

Alternatively, we can use the following recursive algorithm (see O'Kane (2008) [34]). Denote $f_{k,n}(m) = \Pr(\sum_{j=1}^{k} I\{\tau_j \le T\} = n | M = m)$ for $k, n = 0, ..., N$, the conditional probability that there are n defaults in the first k names given M. Since defaults are independent conditioned on the value of M, adding new names does not change the previous defaults given $M = m$. Based on the first $k-1$ names, there are two possibilities for the occurrence of n defaults in the first k names: either there are n defaults in the first $k-1$ names and the k^{th} name survives, or there are $n-1$ defaults in the first $k-1$ names and the k^{th} name defaults. We have:

$$\begin{aligned} f_{0,n}(m) &= I\{n=0\} \\ f_{k,n}(m) &= f_{k-1,n}(m)\left(1-p_k(m)\right) + f_{k-1,n-1}(m)\, p_k(m), \quad k = 1, ..., N \end{aligned} \tag{4.67}$$

Hence, the loss distribution is

$$\Pr(L^{(N)} = \frac{n}{N}) = \int_{-1}^{1} f_{N,n}(m) \frac{1}{\pi\sqrt{1-m^2}}\, dm \tag{4.68}$$

Since the order of names in the algorithm does not matter, when there are K sectors, we can order the obligors and take $p_j(m) = p^{(k)}(m)$ for $j = \sum_1^{k-1} N_j + 1, ..., \sum_1^k N_j, \quad k = 1, ..., K$.

It turns out that the recursive algorithm is much faster than the combinatorial formula and is more accurate, especially for large inhomogeneous portfolios. Indeed, figures 68, 69, and 70 (see Appendix D) show the comparison of loss distributions generated by the two different methods in a homogeneous portfolio of 100 names, a two-sector portfolio with 50 names in each sector, and a three-sector portfolio with 50 names in each sector. Tables 7 and 8 (see Appendix D) illustrate the computational time to generate the loss distribution and the total mass of the loss distribution

using the two methods.

The model indeed generates the desired two-humped loss distribution for positive correlations and the two-hump feature is stable across portfolios consisting of various number of sectors in which the correlations to the market are different but positive, as can be seen in figures 71, 72, and 73 (see Appendix D). The loss distribution generated by the arcsin drift and the more dynamic drift switching model are very close even for long maturities such as 30 years (see figure 72), though the arcsin drift approximation puts slightly more weights on small losses.

For a homogeneous portfolio, the two humps almost coincide for small correlation to the market $\rho = 0.1$ and the locations are close to the individual default probability, as the law of large numbers would predict. As correlation increases the two humps spread out, and for large correlation such as $\rho = 0.9$, the two humps are close to 0% loss and 100% loss, respectively. These can be seen in figure 74 (see Appendix D).

For a two-sector portfolio, we fix $\rho_1 = 0.5$ and let ρ_2 vary from -0.9 to 0.9 to study the loss distribution. In figures 75, 76, and 77 (see Appendix D), we can see that when $\rho_2 > 0$, the two humps spread out as ρ_2 increases. On the other hand, when $\rho_2 < 0$, the loss distribution behaves more wildly. In particular, for a two-sector portfolio, if we have a negative asset correlation of medium size, the loss distribution exhibits three humps (see figure 76). Comparing figure 76 and section 2.2.2.4, we can conclude that multi-humps may be generated by both heterogeneity and multiple singularities. We can also see in figure 77 that the arcsin drift model is a good approximation to the drift switching model.

In figures 78, 79, and 80 (see Appendix D), we also compare the loss distributions generated by the drift switching model and the arcsin drift model that is a good approximation for a three-sector portfolio and a five-sector portfolio in which some of the correlations are negative. Comparing with the loss distribution where all correlations are positive, it appears that negative correlations narrow the portfolio loss. Intuitively, negative correlations make it less likely to have joint defaults or joint survivals of a majority of firms, and hence make it less likely to have very small or very large losses.

It seems that when there are an odd number of modest negative asset correlations between different sectors with other parameters fixed, then the arcsin drift model generates three humps; otherwise, it generates two humps. These can be seen in figure 81 (see Appendix D).

This indeed provides a mechanism for generating multi-humps in the portfolio loss. It is expected that a random market factor M with three singularities in the drift could generate three humps for a homogeneous portfolio. For example, the following density for M is able to generate a three-humped loss distribution.

$$\Pr(M \in dm) = \frac{1}{C\sqrt{|m|\,(1-m^2)}}, \quad m \in (-1,0) \cup (0,1) \tag{4.69}$$

where $C = \int_{-1}^{1} \frac{1}{\sqrt{|m|\,(1-m^2)}}\, dm$ is a normalizing constant. This is confirmed by numerical experiments as shown by the following plot. It is interesting to see that for a homogeneous portfolio, the three-humped shape seems to be generated by medium asset correlations (e.g., $\rho = 0.5, 0.7$), similarly to the arcsin drift model where M has two singularities. These can be seen in figure 82 (see Appendix D).

The three-hump feature for modest asset correlations remains the same when there are two sectors, five sectors and six sectors with equal sector sizes (see figures 83, 84, 85, 86, 87, and 88 in Appendix D). Again, the loss distribution with all positive asset correlations is wider than the one with some negative correlations.

4.3.2.2 Random Drift with Local Correlation to the Market

In this subsubsection, we examine a tractable first-crossing model which we call "random drift with local correlation model" that is a special case of the following modeling framework suggested by Metzler (2008) as a direction of future work:

$$d\,X_t^i = \rho_i(M_t)\, M_t\, dt + \sigma_i \sqrt{1-\rho_i^2(M_t)}\, dB_t^i, \tag{4.70}$$

where M_t represents a systematic factor, "the market", and $\rho_i(M_t)$ is interpreted as some sort of stochastic correlation.

In particular, we take $M_t = M$, a random variable rather than a process. Our model then reads

$$d\,X_{i,t} = \rho_i(M)\,M\,dt + \sigma_i\,\sqrt{1-\rho_i^2(M)}\,dB_{i,t}, \quad X_{i,0} = 0, \tag{4.71}$$

If M is an unbounded random variable, we take

$$\rho_i(m) = \frac{\bar{\rho}_i\,exp(-m)}{1\;-\;|\bar{\rho}_i|\;+\;|\bar{\rho}_i|\,exp(-m)} \tag{4.72}$$

This guarantees that $\rho_i(m) \to sgn(\bar{\rho}_i)$ as $m \to -\infty$, $\rho_i(m) \to 0$ as $m \to \infty$ and $\rho_i(0) = \bar{\rho}_i$ with $\bar{\rho}_i \in [-1, 1]$ the equilibrium correlation, and $\rho_i(m) \equiv \bar{\rho}_i$ if $\bar{\rho}_i = 0, \pm 1$.

Notice that conditional on the realization of M, defaults are independent. In the first-crossing setting, we have

$$\begin{aligned} p_i(m) &= P(\tau_i \le T | M = m) \\ &= \Phi(\frac{K_i - \rho_i(m)mt}{\sqrt{1-\rho_i^2(m)}\sqrt{T}}) + \exp\{\frac{2K_i\rho_i(m)m}{\sqrt{1-\rho_i^2(m)}}\}\,\Phi(\frac{K_i + \rho_i(m)mt}{\sqrt{1-\rho_i^2(m)}\sqrt{T}}), \end{aligned} \tag{4.73}$$

By conditional independence, the probability that there are n defaults in a homogeneous portfolio of N credits where $\bar{\rho}_i = \bar{\rho}$ and $K_i = K$ is

$$P(L = \frac{n}{N}) = \int_{-\infty}^{\infty} \binom{N}{n}\,p(m)^n\,(1-p(m))^{N-n}\,f_M(m)\,dm, \tag{4.74}$$

where L is the fraction of loss in the portfolio, $p(m)$ is the conditional default probability of a single name given $M = m$ and $f_M(m)$ is the density of M.

In such a homogeneous portfolio, if $\bar{\rho} = 0$, then defaults are mutually independent. The individual default probability in the first-crossing setting is

$$P(\tau_i \le T) = 2\Phi(\frac{K}{\sqrt{T}}) \tag{4.75}$$

and the loss distribution is

$$p_n^L = P(L = \frac{n}{N}) = \binom{N}{n} (2\Phi(\frac{K}{\sqrt{T}}))^n (1 - 2\Phi(\frac{K}{\sqrt{T}}))^{N-n} \tag{4.76}$$

Using similar arguments as equation (2.17), we conclude that $\frac{p_n^L}{p_{n-1}^L} \geq 1$ if and only if $n \leq 2(N+1)\Phi(\frac{K}{\sqrt{T}})$. Hence, if $\bar{\rho} = 0$, $N = 50$, $K = -3$, and $T = 10$, then the loss probability has a peak when $n = 17$, as is confirmed by numerical example shown below in figure 89 (see Appendix D).

At the other extreme, if $\bar{\rho} = 1$, then defaults are perfectly dependent. The individual default probability is

$$P(\tau_i \leq T) = P(MT \leq K) = P(M \leq \frac{K}{T}) = F_M(\frac{K}{T}) \tag{4.77}$$

where $F_M(m)$ is the cumulative distribution function of M and the loss distribution is

$$P(L = 1) = F_M(\frac{K}{T}), \quad P(L = 0) = 1 - F_M(\frac{K}{T}) \tag{4.78}$$

A plot generated by a numerical example with M a standard Gaussian random variable is shown in figure 89 comparing the exact loss distribution in equation (4.74) and the Monte Carlo simulation in a portfolio of 50 credits for different $\bar{\rho}$ and $K = -3$, $T = 10$.

It may appear from the plot that the probability of no loss, $L = 0$, and the probability of loss in the whole portfolio, $L = 1$, are increasing functions of $\bar{\rho}$. However, this is not true in general. Indeed, from the previous analysis in the cases $\bar{\rho} = 0, 1$, we know that

$$\begin{aligned} P(L = 0|\bar{\rho} = 0) = (1 - 2\Phi(\frac{K}{\sqrt{T}}))^N, \quad P(L = 0|\bar{\rho} = 1) = 1 - F_M(\frac{K}{T}) \\ P(L = 1|\bar{\rho} = 0) = (2\Phi(\frac{K}{\sqrt{T}}))^N, \quad P(L = 1|\bar{\rho} = 1) = F_M(\frac{K}{T}) \end{aligned} \tag{4.79}$$

When $M \sim N(0, 1)$, pick $N = 50, K = 10^4, T = 10^4$, then $P(L = 0|\bar{\rho} = 0) = 1, P(L = 0|\bar{\rho} = 1) = 0.8413$. On the other hand, pick $N = 50, K = 10^{-4}, T = 10^{-4}$, then $P(L = 1|\bar{\rho} = 0) = 0.6700, P(L = 1|\bar{\rho} = 1) = 0.1587$.

In conclusion, the drift switching model and its random drift approximation are able to generate a multi-humped loss distribution which is a desirable feature, and local correlation might be a tool to obtain more financially motivated features.

4.4 RANDOM INITIAL STATE MODELS

In this section, we will address the problem of unrealistically low short-term spread which appears in most structural models (see section 1.2.2 for discussions and literature survey) by randomizing the initial state (i.e., $X_{i,0}$ in equation (2.1)). These models will be calibrated in chapter 6 as applications in the financial market.

4.4.1 Common Random Initial State and Large Portfolio Approximation

We start with a homogeneous random initial state model in which the initial state X_0 with a given distribution is common to all obligors:

$$X_{i,t} = X_0 + \mu\, t + \sigma\, B_{i,t} \tag{4.80}$$

In the first-crossing setup, the conditional marginal probability of default given initial state X_0 is given by the first-crossing probability of a Brownian motion with drift (see similar arguments in equations (4.54)-(4.58) or Shreve (2004) [38]):

$$\Pr(\tau_i \le t | X_0 = x_0) = \Phi(\frac{-x_0 - \mu\, t}{\sigma\, \sqrt{t}}) + \exp\{-\frac{2\, x_0\, \mu}{\sigma^2}\}\, \Phi(\frac{-x_0 + \mu\, t}{\sigma\, \sqrt{t}}) \tag{4.81}$$

The unconditional marginal default probability is given by

$$\Pr(\tau_i \le t) = E[\Pr(\tau_i \le t | X_0)] = \int_0^\infty (\Phi(\frac{-x_0 - \mu\, t}{\sigma\, \sqrt{t}}) + \exp\{-\frac{2\, x_0\, \mu}{\sigma^2}\}\, \Phi(\frac{-x_0 + \mu\, t}{\sigma\, \sqrt{t}}))\, dF_{X_0}(x_0) \tag{4.82}$$

where F_{X_0} is the CDF of the systematic random initial state X_0.

The portfolio loss is taken to be $L_t^{(N)} = \frac{1-R}{N} \sum_{i=1}^{N} I\{\tau_i \leq t\}$ where N is the portfolio size and R is the recovery rate. Conditioned on the systematic factor X_0, the obligors' credit qualities are independent. By the strong law of large numbers, as $N \to \infty$, we have

$$\lim_{N\to\infty} [L_t^{(N)} - E[L_t^{(N)}|X_0]] = 0, \quad \Pr(\cdot\,|X_0) - a.s. \tag{4.83}$$

Let $L_t = \lim_{N\to\infty} L_t^{(N)}$ be the asymptotic loss as the portfolio size grows to infinity, we have that in the first-crossing setup, the asymptotic loss distribution conditioned on X_0 is

$$\begin{aligned} L_t &= \lim_{N\to\infty} E[L_t^{(N)}|X_0] = (1-R)\ \Pr(\tau_i \leq t|X_0) \\ &= (1-R)\,[\Phi(\frac{-X_0 - \mu\, t}{\sigma\,\sqrt{t}}) + \exp\{-\frac{2\,X_0\,\mu}{\sigma^2}\}\,\Phi(\frac{-X_0 + \mu\, t}{\sigma\,\sqrt{t}})] = G(X_0) \end{aligned} \tag{4.84}$$

Since $G(x_0)$ is strictly decreasing in x_0, the CDF of the asymptotic loss fraction is

$$F_{L_t}(l) = \Pr(G(X_0) \leq l) = \Pr(X_0 \geq G^{-1}(l)) = 1 - F_{X_0}(G^{-1}(l)) \tag{4.85}$$

It is worth noting that in the large portfolio setting, in order to allow the possibility of small losses, which is critical for pricing the equity tranche, we should use models with an unbounded initial state distribution.

The large portfolio approximation is useful in pricing portfolio credit derivatives such as Collateralized Debt Obligations (CDO's).

To price the CDO tranches (see the appendix for an introduction to CDO's and their pricing), we need to compute the expected tranche loss. Let $L_t^{[K_A,K_D]}$ be the asymptotic tranche loss of a tranche with attachment point K_A and detachment point K_D, then

$$L_t^{[K_A,K_D]} = \frac{(L_t - K_A)^+ - (L_t - K_D)^+}{K_D - K_A} \tag{4.86}$$

From Appendix A (see equations (A.16)-(A.17)), the CDS spread is given by

$$\begin{aligned} S &= \frac{E[\exp\{-\int_0^\tau r_t dt\}\, I\{\tau \leq T\}\,(1-R)]}{E[\sum_{j=1}^{M}(\exp\{-\int_0^{t_j} r_t dt\}\, I\{\tau > t_j\}\,(t_j - t_{j-1}) + \exp\{-\int_0^\tau r_t dt\}\, I\{t_{j-1} < \tau \leq t_j\}\,(\tau - t_{j-1}))]} \\ &\approx \frac{(1-R)\,\sum_{j=1}^{M} B(0, \frac{t_j + t_{j-1}}{2})\,(\Pr(\tau \leq t_j) - \Pr(\tau \leq t_{j-1}))}{\sum_{j=1}^{M}[(t_j - t_{j-1})\,B(0,t_j)\,(1 - \Pr(\tau \leq t_j)) + \frac{t_j - t_{j-1}}{2}\,B(0, \frac{t_j + t_{j-1}}{2})\,(\Pr(\tau \leq t_j) - \Pr(\tau \leq t_{j-1}))]} \end{aligned} \tag{4.87}$$

and the $[K_A, K_D]$ tranche spread is given by (see equations (A.24)-(A.25) with a zero upfront, $U = 0$)

$$\begin{aligned} S_{CDO} &= \frac{E[\int_0^T \exp\{-\int_0^t r_s\, ds\}\, dL_t^{[K_A,K_D]}]}{E[\sum_{j=1}^M \exp\{-\int_0^{t_j} r_s\, ds\} \int_{t_{j-1}}^{t_j} (1 - L_t^{[K_A,K_D]})\, dt]} \\ &\approx \frac{\sum_{j=1}^M B(0, \frac{t_j + t_{j-1}}{2})\, (E[L_{t_j}^{[K_A,K_D]}] - E[L_{t_{j-1}}^{[K_A,K_D]}])}{\sum_{j=1}^M B(0, t_j)\, (t_j - t_{j-1})\, (1 - E[L_{t_j}^{[K_A,K_D]}])} \end{aligned} \tag{4.88}$$

where $B(0,t) = \exp\{-rt\}$ with r the 3-month treasury yield, $0 = t_0 < t_1 < \cdots < t_{M-1} < t_M = T$ are premium payment dates, and R is the recovery rate (usually prescribed as $R = 0.4$).

The asymptotic expected tranche loss is then

$$\begin{aligned} & E[L_t^{[K_A,K_D]}] \\ &= \int_0^1 \frac{(l - K_A)^+ - (l - K_D)^+}{K_D - K_A}\, dF_{L_t}(l) \\ &= \int_{K_A}^{K_D} \frac{l - K_A}{K_D - K_A}\, dF_{L_t}(l) + \int_{K_D}^1 dF_{L_t}(l) \\ &= \frac{l - K_A}{K_D - K_A} F_{L_t}(l)|_{l=K_A}^{l=K_D} - \int_{K_A}^{K_D} F_{L_t}(l)\, d\frac{l - K_A}{K_D - K_A} + F_{L_t}(l)|_{l=K_D}^{l=1} \\ &= F_{L_t}(K_D) - \frac{1}{K_D - K_A} \int_{K_A}^{K_D} F_{L_t}(l)\, dl + 1 - F_{L_t}(K_D) \\ &= 1 - \frac{1}{K_D - K_A} \int_{K_A}^{K_D} (1 - F_{X_0}(G^{-1}(l)))\, dl \\ &= \frac{1}{K_D - K_A} \int_{K_A}^{K_D} F_{X_0}(G^{-1}(l))\, dl \end{aligned} \tag{4.89}$$

Using the large portfolio approximation as in equation (4.89), it is possible to calibrate this model to CDO tranches. However, since both the marginal default distribution (equation (4.82)) and the expected tranche loss (equation (4.89)) depend on the systematic random initial distribution F_{X_0}, it is more difficult to calibrate the model to both single-name CDS's and CDO tranches simultaneously. In the next two subsections, we will investigate models in which the dependence structure (default correlation) can be separated from the marginal distribution, allowing one to calibrate the marginal to the single-name CDS spreads and the correlation structure to the tranche spreads. This separation of marginals and dependence structure is a standard feature in industry practice.

4.4.2 An Independent Gamma Initial Distribution with Switching Correlation Model

We now extend a univariate model in Valov (2009) [41] to a multivariate default index with independent Gamma initial distribution and switching correlation as follows:

$$d\,X_{i,t} = -\lambda_i\,dt + \rho(W_t)\,dW_t + \sqrt{1-\rho(W_t)^2}\,dB_{i,t}, \quad X_{i,0} \sim Gamma(\alpha_i, \lambda_i) \tag{4.90}$$

where the Gamma distribution has PDF

$$f(x;\alpha,\lambda) = \frac{\lambda^\alpha}{\Gamma(\alpha)}\,x^{\alpha-1}\,\exp\{-\lambda x\} \tag{4.91}$$

with parameters $\alpha > 0$ and $\lambda > 0$. $X_{i,0}$ and $X_{j,0}$ are independent for $i \neq j$. $\rho(W_t)$ is a two-state random variable:

$$\rho(W_t) = \begin{cases} \rho_g, & \text{if } W_t \geq 0 \\ \rho_b, & \text{if } W_t < 0 \end{cases} \tag{4.92}$$

We assume that $\rho_b > \rho_g$. This reflects the empirical observation that correlation tends to be higher in recession ($W_t < 0$) than in normal market conditions ($W_t \geq 0$). In addition, the random initial condition allows one to calibrate the model to short term spreads. As we will see, this model allows a separation of the marginals and the correlation structure. In addition, it is possible to generate a multi-humped loss distribution within the model.

In this model, default is defined as the first time that the default index falls below zero:

$$\tau_i = \inf\{t > 0 | X_{i,t} < 0\} \tag{4.93}$$

Since $\int_0^t \rho(W_s)\,dW_s + \int_0^t \sqrt{1-\rho(W_s)^2}\,dB_{i,s}$ is a Brownian motion, within the first-crossing setting, the marginal probability of default is given in Valov (2009) [41]:

$$\Pr(\tau_i \leq t) = \frac{\gamma(\frac{\alpha_i}{2}, \frac{\lambda_i^2}{2}t)}{\Gamma(\frac{\alpha_i}{2})} \tag{4.94}$$

where $\gamma(s,x) = \int_0^x t^{s-1}\,e^{-t}\,dt$ is the lower incomplete gamma function. Note that we set the drift coefficient to be $-\lambda_i$ to obtain a simple closed-form expression for the default probability. We also notice that the marginal distribution (equation (4.94)) does not depend on the correlation structure ρ, a feature that allows us to easily calibrate the marginal parameters α and λ to the single-name

CDS spreads, which we will carry out in chapter 6.

In our extension to the multi-dimensional model, the portfolio loss distribution is computed by Monte Carlo simulations. In figures 90 and 91 (see Appendix D), we plot the loss density using MC simulations and kernel density estimation for a homogeneous portfolio of 100 names with different parameter values of α, λ, ρ_g, ρ_b. We can see that the model can generate a flexible loss behavior including a multi-humped loss distribution through varying the model parameters.

4.4.3 A Merton-Type Random Initial State Model with a Random Correlation

We extend the "Randomized Merton Model" of Yi et. al. (2011) [45] to the multi-dimensional case:

$$X_{i,t} = X_{i,0} + \mu_i\, t + \sigma_i\, (\rho\, W_t + \sqrt{1-\rho^2}\, B_{i,t}) \tag{4.95}$$

where the initial solvency ratio $X_{i,0}$ is a nonnegative random variable that has a truncated normal distribution with PDF

$$f(x_{i,0}) = \frac{\exp\{-\frac{1}{2}(x_{i,0} - y_{i,0})^2\}}{\sqrt{2\pi}\,\Phi(y_{i,0})}\, I\{x_{i,0} \geq 0\} \tag{4.96}$$

where $X_{i,0}$ and $X_{j,0}$ are independent for $i \neq j$ and are independent of W and $B_1, ..., B_N$, with $W, B_1, ..., B_N$ independent Brownian motions. The correlation ρ is a random variable that has two states: $\rho = \rho_1$ with probability p and $\rho = \rho_2$ with probability $1 - p$. $y_{i,0}$, $\mu_i \leq 0$, and $\sigma_i > 0$ are constants. In this model, we assume that default τ_i occurs within $[0, t]$ if $X_{i,t} < 0$, which is similar to the Merton/Vasicek definition of default. As we will see, this model has a simple structure with separate marginal and dependence structure and can capture important market features such as a multi-humped loss distribution. These properties allow us to calibrate the model to both single-name CDS spreads and tranche spreads simultaneously.

Since $\rho W_t + \sqrt{1-\rho^2}\, B_{i,t}$ is a Brownian motion, the marginal probability of default before t is

$$\begin{aligned} &\Pr(\tau_i \le t) = \Pr(X_{i,t} < 0) = E[\Pr(X_{i,t} < 0 | X_{i,0} = x_{i,0})] \\ &= \int_0^\infty \Phi(-\frac{x_{i,0} + \mu_i t}{\sigma_i \sqrt{t}}) \frac{\exp\{-\frac{1}{2}(x_{i,0} - y_{i,0})^2\}}{\sqrt{2\pi}\, \Phi(y_{i,0})}\, dx_{i,0} \\ &= \frac{\Phi_2(-(y_{i,0} + \mu_i t), y_{i,0}; -\frac{1}{\sqrt{1+\sigma_i^2 t}})}{\Phi(y_{i,0})} \end{aligned} \tag{4.97}$$

where $\Phi_2(x_1, x_2; \rho)$ denotes the two-dimensional normal CDF with mean $[0 \;\; 0]$ and covariance matrix $\begin{bmatrix} 1 & \rho \\ \rho & 1 \end{bmatrix}$. In particular, we force μ_i to be non-positive so that the definition of the default time τ is consistent in the sense that the default probability $\Pr(\tau_i \le t) = \Pr(X_{i,t} < 0)$ is an increasing function of t. Indeed, for $t \ge s > 0$ and $x_{i,0} \ge 0$, we have

$$\begin{aligned} &\Pr(X_{i,t} < 0 | X_{i,0} = x_{i,0}) \\ &= \Phi(-\frac{x_{i,0} + \mu_i t}{\sigma_i \sqrt{t}}) \\ &= \Phi(-\frac{x_{i,0}}{\sigma_i \sqrt{t}} - \frac{\mu_i}{\sigma_i}\sqrt{t}) \\ &\ge \Phi(-\frac{x_{i,0}}{\sigma_i \sqrt{s}} - \frac{\mu_i}{\sigma_i}\sqrt{s}) \\ &= \Phi(-\frac{x_{i,0} + \mu_i s}{\sigma_i \sqrt{s}}) \\ &= \Pr(X_{i,s} < 0 | X_{i,0} = x_{i,0}) \end{aligned} \tag{4.98}$$

In equation (4.97), we have used a lemma in Yi et. al. (2011) [45] which states that if (X, Y) is a bivariate normal with correlation coefficient $\rho_{x,y}$ and marginals $X \sim N(\mu_x, \sigma_x^2)$ and $Y \sim N(\mu_y, \sigma_y^2)$, then the following equation holds:

$$\Phi_2(-\frac{\mu_x}{\sigma_x}, -\frac{\mu_y}{\sigma_y}; \rho_{x,y}) = \int_0^\infty \Phi(\frac{y\rho_{x,y}\frac{\sigma_x}{\sigma_y} + \mu_y \rho_{x,y}\frac{\sigma_x}{\sigma_y} - \mu_x}{\sigma_x \sqrt{1-\rho_{x,y}^2}}) \frac{\exp\{\frac{1}{2}(\frac{y+\mu_y}{\sigma_y})^2\}}{\sqrt{2\pi}}\, dy \tag{4.99}$$

The above marginal default probability (4.97) is obtained by matching the parameters in equation (4.99): $\rho_{x,y}\frac{\sigma_x}{\sigma_y} = -1$, $\mu_y \rho_{x,y}\frac{\sigma_x}{\sigma_y} - \mu_x = -\mu_i t$, $\sigma_x\sqrt{1-\rho_{x,y}^2} = \sigma_i\sqrt{t}$, $\mu_y = -y_{i,0}$, $\sigma_y = 1$. It is easy to see that the above equations are solved by $\rho_{x,y} = -\frac{1}{\sqrt{1+\sigma_i^2 t}}$, $\mu_x = y_{i,0} + \mu_i t$, $\sigma_x = \sqrt{1+\sigma_i^2 t}$, $\mu_y = -y_{i,0}$, $\sigma_y = 1$.

To compute the portfolio loss distribution, we follow the recursive algorithm (see section 4.3.2.1 or O'Kane (2008) [34]). To do this, we need the conditional marginal probability of default before t given the systematic factor W_t. For a given state of correlation $\rho \in [0, 1)$, this is

$$\begin{aligned}
&\Pr(X_{i,t} < 0 | W_t = m\sqrt{t}, \rho) \\
&= E[\Pr(X_{i,t} < 0 | X_{i,0} = x_{i,0}, W_t = m\sqrt{t}, \rho)] \\
&= \int_0^\infty \Phi(-\frac{x_{i,0} + \mu_i t + \rho m\sqrt{t}}{\sigma_i\sqrt{(1-\rho^2)t}}) \frac{\exp\{-\frac{1}{2}(x_{i,0} - y_{i,0})^2\}}{\sqrt{2\pi}\,\Phi(y_{i,0})}\, dx_{i,0} \\
&= \frac{\Phi_2(-(y_{i,0} + \mu_i t + \rho m\sqrt{t}), y_{i,0}; -\frac{1}{\sqrt{1+\sigma_i^2(1-\rho^2)t}})}{\Phi(y_{i,0})}
\end{aligned} \tag{4.100}$$

Again, this is obtained by matching the parameters in the lemma (see equation (4.99)): $\rho_{x,y}\frac{\sigma_x}{\sigma_y} = -1$, $\mu_y\rho_{x,y}\frac{\sigma_x}{\sigma_y} - \mu_x = -(\mu_i t + \rho m\sqrt{t})$, $\sigma_x\sqrt{1-\rho_{x,y}^2} = \sigma_i\sqrt{t}$, $\mu_y = -y_{i,0}$, $\sigma_y = 1$. It is easy to see that the above equations are solved by $\rho_{x,y} = -\frac{1}{\sqrt{1+\sigma_i^2(1-\rho^2)t}}$, $\mu_x = y_{i,0} + \mu_i t + \rho m\sqrt{t}$, $\sigma_x = \sqrt{1+\sigma_i^2(1-\rho^2)t}$, $\mu_y = -y_{i,0}$, $\sigma_y = 1$.

On the other hand, given the correlation state $\rho = 1$, the conditional marginal probability of default before t is

$$\begin{aligned}
&\Pr(X_{i,t} < 0 | W_t = m\sqrt{t}, \rho = 1) \\
&= E[\Pr(X_{i,t} < 0 | X_{i,0} = x_{i,0}, W_t = m\sqrt{t}, \rho = 1)] \\
&= \Pr(X_{i,0} + \mu_i t + \sigma_i m\sqrt{t} < 0) \\
&= \int_0^{\max\{-(\mu_i t + \sigma_i m\sqrt{t}), 0\}} \frac{\exp\{-\frac{1}{2}(x_{i,0} - y_{i,0})^2\}}{\sqrt{2\pi}\,\Phi(y_{i,0})}\, dx_{i,0} \\
&= \frac{\Phi(-(y_{i,0} + \mu_i t + \sigma_i m\sqrt{t})) - \Phi(-y_{i,0})}{\Phi(y_{i,0})}\, I\{m < -\frac{\mu_i}{\sigma_i}\sqrt{t}\}
\end{aligned} \tag{4.101}$$

Using the recursive algorithm, we obtain the conditional portfolio loss distribution before a premium payment date t given the systematic factor $W_t = m\sqrt{t}$ and the state of correlation ρ and we denote it as $F_{L_t|W_t,\rho}(l; m, \rho)$. The unconditional loss distribution is then

$$F_{L_t}(l) = \int_{-\infty}^{\infty} [p\, F_{L_t|W_t,\rho}(l; m, \rho_1) + (1-p)\, F_{L_t|W_t,\rho}(l; m, \rho_2)]\, \phi(m)\, dm \tag{4.102}$$

In the special case where $\rho_1 = 0$ and $\rho_2 = 1$, we can work out the large homogeneous portfolio approximation (assuming a zero recovery rate) as follows:

$$\begin{aligned} L^{(\infty)} &= p\,\frac{\Phi_2(-(y_0+\mu t), y_0; -\frac{1}{\sqrt{1+\sigma^2 t}})}{\Phi(y_0)} \\ &\quad + (1-p)\,\frac{\Phi(-(y_0+\mu t+\sigma m\sqrt{t})) - \Phi(-y_0)}{\Phi(y_0)}\, I\{m < -\frac{\mu}{\sigma}\sqrt{t}\}, \\ &\quad \Pr(\,\cdot\,|W_t = m\sqrt{t}) - a.s. \end{aligned} \tag{4.103}$$

Denote the above conditional asymptotic loss as $G(m)$. Notice that as m varies between $\pm\infty$, $G(m)$ satisfies

$$p\,\frac{\Phi_2(-(y_0+\mu t), y_0; -\frac{1}{\sqrt{1+\sigma^2 t}})}{\Phi(y_0)} \le G(m) \le p\,\frac{\Phi_2(-(y_0+\mu t), y_0; -\frac{1}{\sqrt{1+\sigma^2 t}})}{\Phi(y_0)} + (1-p) \tag{4.104}$$

We obtain the unconditional asymptotic loss CDF as

$$\Pr(L^{(\infty)} \le l) = E[\Pr(L^{(\infty)} \le l)|W_t] = \int_{-\infty}^{\infty} I\{G(m) \le l\}\,\phi(m)\,dm \tag{4.105}$$

Denote $l_1 = p\,\frac{\Phi_2(-(y_0+\mu t), y_0; -\frac{1}{\sqrt{1+\sigma^2 t}})}{\Phi(y_0)}$ and $l_2 = p\,\frac{\Phi_2(-(y_0+\mu t), y_0; -\frac{1}{\sqrt{1+\sigma^2 t}})}{\Phi(y_0)} + (1-p) = l_1 + (1-p)$. It is easy to see that

$$\Pr(L^{(\infty)} \le l) = \begin{cases} 0, & \text{if } \ 0 \le l < l_1 \\ 1, & \text{if } \ l_2 \le l \le 1 \end{cases} \tag{4.106}$$

If $l_1 \leq l < l_2$, then

$$
\begin{aligned}
&\Pr(L^{(\infty)} \leq l) \\
&= \int_{-\infty}^{-\frac{\mu}{\sigma}\sqrt{t}} I\{p\,\frac{\Phi_2(-(y_0+\mu t), y_0; -\frac{1}{\sqrt{1+\sigma^2 t}})}{\Phi(y_0)} + (1-p)\,\frac{\Phi(-(y_0+\mu t+\sigma m\sqrt{t})) - \Phi(-y_0)}{\Phi(y_0)} \leq l\} \\
&\quad \phi(m)\,dm + \int_{-\frac{\mu}{\sigma}\sqrt{t}}^{\infty} \phi(m)\,dm \\
&= \int_{-\frac{1}{\sigma\sqrt{t}}\,[y_0+\mu t+\Phi^{-1}(\frac{\Phi(y_0)l - p\Phi_2(-(y_0+\mu t), y_0; -\frac{1}{\sqrt{1+\sigma^2 t}})}{1-p} + \Phi(-y_0))]}^{-\frac{\mu}{\sigma}\sqrt{t}} \phi(m)\,dm + 1 - \Phi(-\frac{\mu}{\sigma}\sqrt{t}) \\
&= \Phi(-\frac{\mu}{\sigma}\sqrt{t}) - \Phi(-\frac{1}{\sigma\sqrt{t}}\,[y_0+\mu t+\Phi^{-1}(\frac{\Phi(y_0)l - p\Phi_2(-(y_0+\mu t), y_0; -\frac{1}{\sqrt{1+\sigma^2 t}})}{1-p} + \Phi(-y_0))]) \\
&\quad + 1 - \Phi(-\frac{\mu}{\sigma}\sqrt{t}) \\
&= 1 - \Phi(-\frac{1}{\sigma\sqrt{t}}\,[y_0+\mu t+\Phi^{-1}(\frac{\Phi(y_0)l - p\Phi_2(-(y_0+\mu t), y_0; -\frac{1}{\sqrt{1+\sigma^2 t}})}{1-p} + \Phi(-y_0))]) \\
&= \Phi(\frac{1}{\sigma\sqrt{t}}\,[y_0+\mu t+\Phi^{-1}(\frac{\Phi(y_0)l - p\Phi_2(-(y_0+\mu t), y_0; -\frac{1}{\sqrt{1+\sigma^2 t}})}{1-p} + \Phi(-y_0))])
\end{aligned}
\tag{4.107}
$$

Define $F(l) = \Pr(L^{(\infty)} \leq l)$. We have the following one-sided limits:

$$\lim_{l \to {l_1}^+} F(l) = \Phi(\tfrac{\mu}{\sigma}\sqrt{t}) \tag{4.108}$$

$$\lim_{l \to {l_2}^-} F(l) = 1 \tag{4.109}$$

The asymptotic density is thus

$$f(l) = \begin{cases} 0, & \text{if } 0 < l < l_1 \\ 0, & \text{if } l_2 < l < 1 \end{cases} \tag{4.110}$$

If $l_1 < l < l_2$, then

$$
\begin{aligned}
f(l) &= \frac{\Phi(y_0)\,\phi(\frac{1}{\sigma\sqrt{t}}\,[y_0+\mu t+\Phi^{-1}(\frac{\Phi(y_0)l-p\Phi_2(-(y_0+\mu t),y_0;-\frac{1}{\sqrt{1+\sigma^2 t}})}{1-p}+\Phi(-y_0))])}{(1-p)\,\sigma\,\sqrt{t}\,\phi(\Phi^{-1}(\frac{\Phi(y_0)l-p\Phi_2(-(y_0+\mu t),y_0;-\frac{1}{\sqrt{1+\sigma^2 t}})}{1-p}+\Phi(-y_0)))} \\
&= \frac{\Phi(y_0)}{(1-p)\sigma\sqrt{t}}\,\exp\{\frac{1}{2}\,[\Phi^{-1}(\frac{\Phi(y_0)l-p\Phi_2(-(y_0+\mu t),y_0;-\frac{1}{\sqrt{1+\sigma^2 t}})}{1-p}+\Phi(-y_0))]^2 \\
&\quad -\frac{1}{2\sigma^2 t}\,[y_0+\mu t+\Phi^{-1}(\frac{\Phi(y_0)l-p\Phi_2(-(y_0+\mu t),y_0;-\frac{1}{\sqrt{1+\sigma^2 t}})}{1-p}+\Phi(-y_0))]^2\} \\
&= \frac{\Phi(y_0)}{(1-p)\sigma\sqrt{t}} \\
&\quad \exp\{\frac{1}{2}\,[\frac{1}{\sigma\sqrt{t}}\,(y_0+\mu t)+(1+\frac{1}{\sigma\sqrt{t}})\,\Phi^{-1}(\frac{\Phi(y_0)l-p\Phi_2(-(y_0+\mu t),y_0;-\frac{1}{\sqrt{1+\sigma^2 t}})}{1-p}+\Phi(-y_0))] \\
&\quad [-\frac{1}{\sigma\sqrt{t}}\,(y_0+\mu t)+(1-\frac{1}{\sigma\sqrt{t}})\,\Phi^{-1}(\frac{\Phi(y_0)l-p\Phi_2(-(y_0+\mu t),y_0;-\frac{1}{\sqrt{1+\sigma^2 t}})}{1-p}+\Phi(-y_0))]\}
\end{aligned}
\tag{4.111}
$$

Hence, it is easy to see that

$$\lim_{l\to {l_1}^-} f(l) = 0 \tag{4.112}$$

$$\lim_{l\to {l_1}^+} f(l) = \frac{\Phi(y_0)}{(1-p)\sigma\sqrt{t}}\,\exp\{\frac{1}{2}\,(y_0^2-\frac{\mu^2}{\sigma^2}t)\} \tag{4.113}$$

$$\lim_{l\to {l_2}^+} f(l) = 0 \tag{4.114}$$

$$\lim_{l\to {l_2}^-} f(l) = \begin{cases} \infty, & \text{if } \sigma\sqrt{t}>1 \\ \infty, & \text{if } \sigma\sqrt{t}=1 \;\&\; y_0+\mu t<0 \\ \frac{\Phi(y_0)}{1-p}, & \text{if } \sigma\sqrt{t}=1 \;\&\; y_0+\mu t=0 \\ 0, & \text{if } \sigma\sqrt{t}=1 \;\&\; y_0+\mu t>0 \\ 0, & \text{if } \sigma\sqrt{t}<1 \end{cases} \tag{4.115}$$

To study the monotonicity of the asymptotic density, we take the derivative of $f(l)$ with respect to l for $l \in (l_1, l_2)$:

$$
\begin{aligned}
f'(l) = f(l) \{ & \Phi^{-1}(\frac{\Phi(y_0)l - p\Phi_2(-(y_0+\mu t), y_0; -\frac{1}{\sqrt{1+\sigma^2 t}})}{1-p} + \Phi(-y_0)) \\
& \frac{1}{\phi(\Phi^{-1}(\frac{\Phi(y_0)l - p\Phi_2(-(y_0+\mu t), y_0; -\frac{1}{\sqrt{1+\sigma^2 t}})}{1-p} + \Phi(-y_0)))} \frac{\Phi(y_0)}{1-p} \\
& - \frac{1}{\sigma\sqrt{t}} [y_0 + \mu t + \Phi^{-1}(\frac{\Phi(y_0)l - p\Phi_2(-(y_0+\mu t), y_0; -\frac{1}{\sqrt{1+\sigma^2 t}})}{1-p} + \Phi(-y_0))] \\
& \frac{1}{\sigma\sqrt{t}\,\phi(\Phi^{-1}(\frac{\Phi(y_0)l - p\Phi_2(-(y_0+\mu t), y_0; -\frac{1}{\sqrt{1+\sigma^2 t}})}{1-p} + \Phi(-y_0)))} \frac{\Phi(y_0)}{1-p} \} \\
= & \frac{\Phi(y_0)\, f(l)}{(1-p)\,\phi(\Phi^{-1}(\frac{\Phi(y_0)l - p\Phi_2(-(y_0+\mu t), y_0; -\frac{1}{\sqrt{1+\sigma^2 t}})}{1-p} + \Phi(-y_0)))} \\
& \{\Phi^{-1}(\frac{\Phi(y_0)l - p\Phi_2(-(y_0+\mu t), y_0; -\frac{1}{\sqrt{1+\sigma^2 t}})}{1-p} + \Phi(-y_0)) \\
& - \frac{1}{\sigma^2 t} [y_0 + \mu t + \Phi^{-1}(\frac{\Phi(y_0)l - p\Phi_2(-(y_0+\mu t), y_0; -\frac{1}{\sqrt{1+\sigma^2 t}})}{1-p} + \Phi(-y_0))]\} \\
= & \frac{\Phi(y_0)\, f(l)}{(1-p)\,\sigma^2 t\,\phi(\Phi^{-1}(\frac{\Phi(y_0)l - p\Phi_2(-(y_0+\mu t), y_0; -\frac{1}{\sqrt{1+\sigma^2 t}})}{1-p} + \Phi(-y_0)))} \\
& \{(\sigma^2 t - 1)\,\Phi^{-1}(\frac{\Phi(y_0)l - p\Phi_2(-(y_0+\mu t), y_0; -\frac{1}{\sqrt{1+\sigma^2 t}})}{1-p} + \Phi(-y_0)) - (y_0 + \mu t)\}
\end{aligned}
\tag{4.116}
$$

Clearly,

$$
f'(l) > 0 \Leftrightarrow (\sigma^2 t - 1)\,\Phi^{-1}(\frac{\Phi(y_0)l - p\Phi_2(-(y_0+\mu t), y_0; -\frac{1}{\sqrt{1+\sigma^2 t}})}{1-p} + \Phi(-y_0)) > y_0 + \mu t \tag{4.117}
$$

Thus, if $\sigma^2 t > 1$, then

$$
f'(l) > 0 \Leftrightarrow l > \frac{p\,\Phi_2(-(y_0+\mu t), y_0; -\frac{1}{\sqrt{1+\sigma^2 t}}) + (1-p)\,[\Phi(\frac{y_0+\mu t}{\sigma^2 t - 1}) - \Phi(-y_0)]}{\Phi(y_0)} \tag{4.118}
$$

If $\sigma^2 t < 1$, then

$$
f'(l) > 0 \Leftrightarrow l < \frac{p\,\Phi_2(-(y_0+\mu t), y_0; -\frac{1}{\sqrt{1+\sigma^2 t}}) + (1-p)\,[\Phi(\frac{y_0+\mu t}{\sigma^2 t - 1}) - \Phi(-y_0)]}{\Phi(y_0)} \tag{4.119}
$$

If $\sigma^2 t = 1$, then

$$\begin{aligned} f'(l) > 0 &\Leftrightarrow y_0 + \mu\, t < 0 \\ f'(l) = 0 &\Leftrightarrow y_0 + \mu\, t = 0 \\ f'(l) < 0 &\Leftrightarrow y_0 + \mu\, t > 0 \end{aligned} \tag{4.120}$$

Since

$$\frac{\Phi(\frac{y_0+\mu t}{\sigma^2 t-1}) - \Phi(-y_0)}{\Phi(y_0)} \leq \frac{1-\Phi(-y_0)}{\Phi(y_0)} = 1 \tag{4.121}$$

and

$$\frac{\Phi(\frac{y_0+\mu t}{\sigma^2 t-1}) - \Phi(-y_0)}{\Phi(y_0)} \leq 0 \iff \frac{y_0+\mu t}{\sigma^2 t-1} \leq -y_0 \iff \begin{cases} y_0 \leq -\frac{\mu}{\sigma^2}, & \text{if } \sigma^2 t > 1 \\ y_0 \geq -\frac{\mu}{\sigma^2}, & \text{if } \sigma^2 t < 1 \end{cases} \tag{4.122}$$

we can easily deduce that the term

$$\begin{aligned} A(l) &= \frac{p\,\Phi_2(-(y_0+\mu t), y_0; -\frac{1}{\sqrt{1+\sigma^2 t}}) + (1-p)\,[\Phi(\frac{y_0+\mu t}{\sigma^2 t-1}) - \Phi(-y_0)]}{\Phi(y_0)} \\ &= l_1 + (1-p)\,\frac{\Phi(\frac{y_0+\mu t}{\sigma^2 t-1}) - \Phi(-y_0)}{\Phi(y_0)} \end{aligned} \tag{4.123}$$

on the right-hand side of equations (4.118)-(4.119) satisfies the following: $A(l) \in (l_1, l_2]$ if $\sigma\sqrt{t}-1$ and $y_0 + \frac{\mu}{\sigma^2}$ have the same sign, and $A(l) \leq l_1$ if $\sigma\sqrt{t}-1$ and $y_0 + \frac{\mu}{\sigma^2}$ have opposite signs.

Combining the properties of $f(l)$ and $f'(l)$, we can easily see that the model is flexible in generating different shapes of loss distributions including multi-humped loss distributions for $l \in (l_1, l_2)$:

if $\sigma\sqrt{t} > 1$ & $y_0 > -\frac{\mu}{\sigma^2}$, then $f(l)$ first decreases and then increases to ∞.

If $\sigma\sqrt{t} > 1$ & $y_0 \leq -\frac{\mu}{\sigma^2}$, then $f(l)$ increases to ∞.

If $\sigma\sqrt{t} < 1$ & $y_0 < -\frac{\mu}{\sigma^2}$, then $f(l)$ first increases and then decreases to 0.

If $\sigma\sqrt{t} < 1$ & $y_0 \geq -\frac{\mu}{\sigma^2}$, then $f(l)$ decreases to 0.

If $\sigma\sqrt{t} = 1$ & $y_0 + \mu t < 0$, then $f(l)$ increases to ∞.

If $\sigma\sqrt{t} = 1$ & $y_0 + \mu t = 0$, then $f(l)$ is a constant and stays at $\frac{\Phi(y_0)}{1-p}$.

If $\sigma\sqrt{t} = 1$ & $y_0 + \mu t > 0$, then $f(l)$ decreases to 0.

This can be illustrated by the following plot (figure 92 in Appendix D) of the asymptotic loss density $f(l)$ with $y_0 = 3$, $p = 0.5$, $t = 5$ and varying μ and σ.

In figure 93 (see Appendix D), we also notice that with other parameters fixed, changing p changes the location of the humps but does not change the shape of the loss distribution.

For verification and comparison purposes, we also compare the analytic asymptotic loss PDF (using equations (4.110)-(4.111)) with the infinite-dimensional kernel density estimation using Monte Carlo (first generate the systematic factor $W_t = m\sqrt{t}$ and then generate the asymptotic loss using equation (4.103)). In figures 94-100 (see Appendix D), the red, green, blue, black curves represent the asymptotic loss PDF using analytic formulas (4.110)-(4.111), MC with 10000 simulations, MC with 100000 simulations, and MC with 1000000 simulations, respectively. The MC simulations have verified the analytic formulas.

4.5 MEAN-REVERTING MODELS

In this section, we will study mean-reverting models where certain variates such as correlation and global economy exhibit cyclical behavior and revert back to the long-term means.

4.5.1 A Mean-Reverting Stochastic Correlation Model

The model is inspired by Delbaen and Shirakawa (2002) [7] who studied an interest rate dynamical model with bounded interest rates. Their interest rate dynamics satisfies the SDE:

$$d\,r_t = \alpha\,(r_\mu - r_t)\,dt + \beta\,\sqrt{(r_t - r_m)\,(r_M - r_t)}\,dW_t \tag{4.124}$$

where the interest rate r_t is bounded in $[r_m, r_M]$ and tends asymptotically to r_μ.

In analogy, we study a stochastic correlation model for a homogeneous portfolio as follows:

$$d\,X_{i,t} = \rho_t\,dW_t + \sqrt{1-\rho_t^2}\,dB_{i,t}, \quad X_{i,0} = 0 \tag{4.125}$$

$$d\,\rho_t = \kappa\,(\bar{\rho} - \rho_t)\,dt - \sigma\,\sqrt{\rho_t(1-\rho_t)}\,dW_t \tag{4.126}$$

where $\kappa > 0$, $\sigma > 0$, and ρ is bounded in $[0,1]$ (recall that only nonnegative ρ is considered in the homogeneous case).

This model reflects the phenomenon that correlation is mean-reverting and anti-cyclical; i.e., the correlation ρ increases as the market gets worse ($dW_t < 0$) by observing the minus sign in front of σ in equation (4.126).

In addition, any $\rho \in [0,1]$ ensures that the instantaneous covariance matrix of $X_1, ..., X_N$ is nonnegative definite:

$$\begin{pmatrix} 1 & \rho^2 & ... & \rho^2 \\ \rho^2 & 1 & ... & \rho^2 \\ & ..... & & \\ \rho^2 & \rho^2 & ... & 1 \end{pmatrix} \geq 0 \iff (1-\rho^2)^{n-1}\,(1+(n-1)\rho^2) \geq 0, \quad n = 2, ..., N \tag{4.127}$$

$$\iff \rho^2 \in [0,1]$$

In figure 101 (see Appendix D), we compare the FtD probability for two names with varying σ and parameters $\rho_0 = \bar{\rho} = 0, ..., 1$, $\kappa = 1$, $K = -3$, $T = 5$. The red, green, blue, cyan and magenta curves represent the FtD probability with $\sigma = 0, 0.25, 0.5, 0.75, 1$, respectively.

We also compare the loss distribution for a homogeneous portfolio of 100 names with varying σ and parameters $\rho_0 = \bar{\rho} = 0.5$, $\kappa = 1$, $K = -3$, $T = 5$ in figure 102 (see Appendix D). The red, green, blue, cyan and magenta curves represent the loss distribution with $\sigma = 0, 0.25, 0.5, 0.75, 1$, respectively. It appears that increasing the volatility of ρ increases the probability of small-size loss and very large loss and decreases the probability of mid-size loss.

4.5.2 A Model with a Cyclical Economy

We now consider a model with a mean-reverting economy:

$$d\,X_{i,t} = \rho_i\,dM_t + \sqrt{1-\rho_i^2}\,dB_{i,t}, \quad X_{i,0} = 0 \tag{4.128}$$

$$d\,M_t = -\kappa_{cy}\,M_t\,dt + dW_t, \quad M_0 = m_0 \tag{4.129}$$

where ρ_i and $\kappa_{cy} > 0$ are constants. In this model, the systematic factor (the market or the economy) has the tendency to return to the normal state $M = 0$ whenever it deviates from the normal. Thus, the model is intended to reflect business cycles.

By Ito's formula,

$$d\left(\exp\{\kappa_{cy}t\}\,M_t\right) = \exp\{\kappa_{cy}t\}\left(\kappa_{cy}\,M_t\,dt + dM_t\right) = \exp\{\kappa_{cy}t\}\,dW_t \tag{4.130}$$

This implies

$$\begin{aligned}\exp\{\kappa_{cy}t\}\,M_t &= \exp\{\kappa_{cy}0\}\,m_0 + \int_0^t \exp\{\kappa_{cy}s\}\,dW_s \\ &= m_0 + \int_0^t \exp\{\kappa_{cy}s\}\,dW_s\end{aligned} \tag{4.131}$$

Hence, we have

$$\begin{aligned}X_{i,t} &= \rho_i\left(M_t - m_0\right) + \sqrt{1-\rho_i^2}\,B_{i,t} \\ &= \rho_i\left[m_0\left(\exp\{-\kappa_{cy}t\} - 1\right) + \int_0^t \exp\{\kappa_{cy}(s-t)\}\,dW_s\right] + \sqrt{1-\rho_i^2}\,B_{i,t}\end{aligned} \tag{4.132}$$

Since W and B are independent, we have

$$\begin{aligned}p_i^{Vasicek}(m) &= \Pr(X_{i,T} < K_i | \int_0^T \exp\left\{\kappa_{cy}(t-T)\right\} dW_t = m) \\ &= \Phi(\frac{K_i + \rho_i\,m_0\left(1 - \exp\{-\kappa_{cy}T\}\right) - \rho_i\,m}{\sqrt{(1-\rho_i^2)T}})\end{aligned} \tag{4.133}$$

Since $\int_0^T \exp\{\kappa_{cy}(t-T)\}\,dW_t$ is Gaussian with mean 0 and variance

$$Var[\int_0^T \exp\{\kappa_{cy}(t-T)\}\,dW_t] = \int_0^T \exp\{2\kappa_{cy}(t-T)\}\,dt = \frac{1}{2\kappa_{cy}}\left(1-\exp\{-2\kappa_{cy}T\}\right) \tag{4.134}$$

we obtain the portfolio loss distribution and the n^{th}-to-default probability in the Vasicek setting,

$$P^{Vasicek}(L=\frac{n}{N}) = \sqrt{\frac{\kappa_{cy}}{\pi\left(1-\exp\left\{-2\kappa_{cy}T\right\}\right)}}\int_{-\infty}^{\infty}\sum_{1\leq i_1<\ldots<i_n\leq N}\prod_{k=1}^{n}p_{i_k}^{Vasicek}(m) \\ \prod_{l\neq i_1,\ldots,i_n}\left(1-p_l^{Vasicek}(m)\right)\exp\left\{-\frac{\kappa_{cy}\,m^2}{1-\exp\left\{-2\kappa_{cy}T\right\}}\right\}dm \tag{4.135}$$

$$P^{Vasicek}(L\geq\frac{n}{N}) = \sqrt{\frac{\kappa_{cy}}{\pi\left(1-\exp\left\{-2\kappa_{cy}T\right\}\right)}}\int_{-\infty}^{\infty}\sum_{j=n}^{N}\sum_{1\leq i_1<\ldots<i_j\leq N}\prod_{k=1}^{j}p_{i_k}^{Vasicek}(m) \\ \prod_{l\neq i_1,\ldots,i_j}\left(1-p_l^{Vasicek}(m)\right)\exp\left\{-\frac{\kappa_{cy}\,m^2}{1-\exp\left\{-2\kappa_{cy}T\right\}}\right\}dm \tag{4.136}$$

If the portfolio is homogeneous, i.e., $p_i^{Vasicek}(m) = p^{Vasicek}(m),\ i = 1,\ldots,n$, we obtain simpler expressions:

$$P^{Vasicek}(L=\frac{n}{N}) = \sqrt{\frac{\kappa_{cy}}{\pi\left(1-\exp\left\{-2\kappa_{cy}T\right\}\right)}}\int_{-\infty}^{\infty}\binom{N}{n}p^{Vasicek}(m)^n \\ \left(1-p^{Vasicek}(m)\right)^{N-n}\exp\{-\frac{\kappa_{cy}\,m^2}{1-\exp\left\{-2\kappa_{cy}T\right\}}\}\,dm \tag{4.137}$$

$$P^{Vasicek}(L\geq\frac{n}{N}) = \sqrt{\frac{\kappa_{cy}}{\pi\left(1-\exp\left\{-2\kappa_{cy}T\right\}\right)}}\int_{-\infty}^{\infty}\sum_{j=n}^{N}\binom{N}{j}p^{Vasicek}(m)^j \\ \left(1-p^{Vasicek}(m)\right)^{N-j}\exp\{-\frac{\kappa_{cy}\,m^2}{1-\exp\left\{-2\kappa_{cy}T\right\}}\}\,dm \tag{4.138}$$

In figure 103 (see Appendix D), we compare the loss distribution in this model in both the first-crossing and the Vasicek setting for a homogeneous portfolio of 50 names with $\rho = 0.5$, $m_0 = 0$, $K = -3$, $T = 5$ and different levels of $\kappa_{cy} = 0, 0.05, 0.1, 0.2, 0.5, 1$, represented by the red, green, blue, cyan, magenta and yellow curves, respectively (the loss distributions for $\kappa_{cy} = 0.1$ and $\kappa_{cy} = 0.2$ are indistinguishable). Note that as κ_{cy}, the frequency of the business cycle increases, the loss distribution seems to be more and more concentrated. Intuitively, when κ_{cy} is small, the market returns to its mean slowly, and the effects of the systematic randomness are significant. This combined with the idiosyncratic randomness spreads out the loss distribution. On the other

hand, when κ_{cy} becomes very large, the economy is "pinned" at the normal state and only the idiosyncratic randomness is presented. Indeed, as $\kappa_{cy} \to \infty$, we have

$$\lim_{\kappa_{cy}\to\infty} X_{i,t} = -\rho_i\, m_0 + \sqrt{1-\rho_i^2}\, B_{i,t} \tag{4.139}$$

Here, we have used the fact that

$$\lim_{\kappa_{cy}\to\infty} \exp\{-\kappa_{cy} t\} = 0 \tag{4.140}$$

and

$$\lim_{\kappa_{cy}\to\infty} \int_0^t \exp\{\kappa_{cy}(s-t)\}\, dW_s = 0, \quad a.s. \tag{4.141}$$

since $\int_0^t \exp\{\kappa_{cy}(s-t)\}\, dW_s$ is Gaussian with mean 0 and vanishing variance (see equation (4.134)):

$$\lim_{\kappa_{cy}\to\infty} \frac{1}{2\kappa_{cy}} \left(1 - \exp\{-2\kappa_{cy} T\}\right) = 0 \tag{4.142}$$

Hence, in the large κ_{cy} limit, the individual default probabilities in the first-crossing and in the Vasicek settings are $p_i = 2\Phi(\frac{\rho_i m_0 + K_i}{\sqrt{(1-\rho_i^2)T}})$ and $p_i^{Vasicek} = \Phi(\frac{\rho_i m_0 + K_i}{\sqrt{(1-\rho_i^2)T}})$, respectively. In addition, the exact portfolio loss distributions for a homogeneous portfolio with $\rho_i = \rho$ and $K_i = K$ in the first-crossing and in the Vasicek settings are:

$$P(L = \frac{n}{N}) = \binom{N}{n} (2\Phi(\frac{\rho m_0 + K}{\sqrt{(1-\rho^2)T}}))^n\, (1 - 2\Phi(\frac{\rho m_0 + K}{\sqrt{(1-\rho^2)T}}))^{N-n} \tag{4.143}$$

and

$$P^{Vasicek}(L = \frac{n}{N}) = \binom{N}{n} \Phi(\frac{\rho m_0 + K}{\sqrt{(1-\rho^2)T}})^n\, (1 - \Phi(\frac{\rho m_0 + K}{\sqrt{(1-\rho^2)T}}))^{N-n} \tag{4.144}$$

Denote $p_n^L = P(L = \frac{n}{N})$ and $p_n^{L,Vasicek} = P^{Vasicek}(L = \frac{n}{N})$. Using similar arguments as equations (2.19)-(2.22), we have

$$\frac{p_n^L}{p_{n-1}^L} = \frac{N-n+1}{n} \frac{2\Phi(\frac{\rho m_0 + K}{\sqrt{(1-\rho^2)T}})}{1 - 2\Phi(\frac{\rho m_0 + K}{\sqrt{(1-\rho^2)T}})} \tag{4.145}$$

and

$$\frac{p_n^{L,Vasicek}}{p_{n-1}^{L,Vasicek}} = \frac{N-n+1}{n} \frac{\Phi(\frac{\rho m_0 + K}{\sqrt{(1-\rho^2)T}})}{1 - \Phi(\frac{\rho m_0 + K}{\sqrt{(1-\rho^2)T}})} \tag{4.146}$$

So

$$\frac{p_n^L}{p_{n-1}^L} \geq 1 \iff n \leq 2(N+1)\Phi(\frac{\rho m_0 + K}{\sqrt{(1-\rho^2)T}}) \tag{4.147}$$

and

$$\frac{p_n^{L,Vasicek}}{p_{n-1}^{L,Vasicek}} \geq 1 \iff n \leq (N+1)\Phi(\frac{\rho m_0 + K}{\sqrt{(1-\rho^2)T}}) \tag{4.148}$$

Thus, for a homogeneous portfolio of 50 obligors with $\rho = 0.5$, $m_0 = 0$, $K = -3$, $T = 5$, the loss distribution in the large κ_{cy} limit attains a peak at $n = 6$ in the first-crossing setup and a peak at $n = 3$ in the Vasicek setup. Figure 104 (see Appendix D) confirms the above theoretical results, where the red, green and blue curves represent the loss distribution with the above model parameters and $\kappa_{cy} = 1, 10, 100$, respectively, and the plain and asterisk shape represent the first-crossing and Vasicek settings, respectively.

In figure 105 (see Appendix D), we also plot the loss distribution in the first-crossing setting for a two-sector portfolio with 50 names in each sector, with $\rho_1 = 0.9$, $\rho_2 = 0.1$, $m_0 = 0$, $K = -3$, $T = 5$, $\kappa_{cy} = 0, 0.05, 0.1, 0.2, 0.5, 1$, represented by the red, green, blue, cyan, magenta and yellow curves, respectively.

4.6 CHAPTER SUMMARY

In this chapter, we have investigated structural models where systematic factor related dynamics are modeled to capture financially motivated features. In particular, the drift switching model and its random drift approximation provide a mechanism through multiple singularities in the systematic factor to generate a multi-humped loss distribution that the finance industry is interested in. This mechanism can be combined with heterogeneity (see section 2.2.2.4) to obtain a more flexible loss distribution. On the other hand, having a random initial state in the model can resolve the problem of low short-term spreads, which might be combined with appropriate dependence structure such as a random correlation to calibrate to single-name CDS's and tranche data simultaneously, as will be seen in chapter 6. In the next chapter, we will examine another approach to

modeling the dependence structure, namely, contagion models.

5.0 CONTAGION MODELS

As mentioned before, cyclical dependence and default contagion are endemic in the market. While cyclical dependence correlates the credit qualities of different obligors through macroeconomic factors, contagion links the default indices of different companies in the same sector (industry) through direct business interactions. For example, default of a parent company can cause its subsidiaries to default. As another example, credit events on General Motors (e.g., default or credit downgrade) may increase the default risk of Ford. In this chapter, we study examples of first-crossing models with contagion and the effect of contagion on loss distributions.

5.1 A CONTAGION MODEL WITH INFECTIOUS VOLATILITY

The model we study in this section is inspired by Haworth (2006) [19] who proposed a structural model with contagion where the firm value V_i follows the dynamics:

$$d\,V_{i,t} = (r_f - q_i)\,V_{i,t}\,dt + \sigma_i\,V_{i,t}\,dW_{i,t} \tag{5.1}$$

Here, r_f is the risk-free interest rate, q_i is the dividend rate, $\sigma_i > 0$ is the volatility, and $W_1, ..., W_N$ are correlated Brownian motions with $dW_{i,t}\,dW_{j,t} = \rho_{i,j}\,dt$ for $i \neq j$.

Contagion is introduced in Haworth (2006) [19] by increasing the volatilities of the surviving firms whenever there is a default. More precisely, Haworth (2006) [19] related the direction and

size of the increase in volatility to the degree of correlation between the firms. So for correlation parameter $\rho_{i,j}$, if company i defaults, the volatility of company j jumps by

$$\sigma_j \;\rightarrow\; \sigma_j \, F^{\rho_{i,j}} \tag{5.2}$$

for some constant $F \geq 1$. Haworth (2006) [19] implemented this model in two and three dimensions by numerically solving a system of pricing partial differential equations for basket default swaps, and studied the effect of contagion through the volatility factor F on their pricing.

In this section, we study a contagion model with the first-crossing definition of default similar to Haworth (2006) by increasing the volatility of the firms in the sector if a default event occurs. We use Monte Carlo simulations to study the loss distributions for a portfolio with a large number of obligors (100-125 dimensions).

The dynamics of the firm's credit index is as follows:

$$d\,X_{i,t} = \rho_j \, dW_t + \sigma_{j,t} \sqrt{1-\rho_j^2}\, dB_{i,t}, \qquad X_{i,0} = 0 \tag{5.3}$$

$$\sigma_{j,t} = 1 + \kappa_{co}^{j} \, \tfrac{N_{j,t-}}{N_j} \tag{5.4}$$

where ρ_j is the correlation between obligor in sector j and the market, $\sigma_{j,t}$ is the volatility of the idiosyncratic component that is a increasing function of the fraction of loss in sector j and κ_{co}^{j} controls the level of contagion in sector j. $N_{j,t-} = \sum_{i \in S_j} I\{\tau_i < t\}$ is the number of defaults in sector j up to just before time t, and N_j is the number of names in sector j. This model captures the contagion phenomenon that default events in a sector can increase the risk of default of other companies in the same sector.

In figure 106 (see Appendix E), we compare the portfolio loss distribution in the model for a two-sector portfolio with 50 names in each sector, with $\rho_1 = 0.9, \rho_2 = 0.1$ and different levels of contagion effects κ_{co}. It appears that the pure contagion effect in our model does not generate a two-humped loss distribution.

5.2 A JUMP-DIFFUSION CONTAGION MODEL WITH INFECTIOUS JUMP SIZE

In this section, we develop a contagion model by adding jumps to the toy model with infectious jump size:

$$d\,X_{i,t} = \rho_j\,dW_t + \sqrt{1-\rho_j^2}\,dB_{i,t} + (1-\kappa_j^u\,\frac{N_{j,t-}}{N_j})\,dJ_{i,t}^u - (1+\kappa_j^d\,\frac{N_{j,t-}}{N_j})\,dJ_{i,t}^d \tag{5.5}$$

where standard Poisson processes J_t^u and J_t^d represent up and down jumps, κ_j^u and κ_j^d are levels of contagion in sector j.

In figure 107 (see Appendix E), we compare the portfolio loss distribution for a homogeneous portfolio of 100 names in the toy model against the contagion model with infectious jump size with $\rho = 0.5$, $\kappa^u = 0$, $K = -3$, $T = 5$ and varying κ^d. The red, green, blue, cyan, magenta and yellow curves represent the loss distribution with $\kappa^d = 0, 0.5, 1, 2, 5$, respectively. It appears that adding a downsize contagion makes large portfolio loss more likely, as expected. However, once again, there is no two-humped loss distribution in this infectious jump size model.

Next, we compare an inhomogeneous portfolio with 50 names in each of the two sectors, with the same set of parameters except $\rho_1 = 0.9$ and $\rho_2 = 0.1$. In figure 108 (see Appendix E), the red, green, blue, cyan, magenta and yellow curves represent the loss distribution with $\kappa^d = 0, 0.5, 1, 2, 5$, respectively. Again, adding a downsize contagion makes large portfolio loss more likely, but there is no two-humped loss distribution.

In addition, we compare an inhomogeneous portfolio with 50 names in each of the two sectors, with the same set of parameters except that we fix $\kappa_1^d = 1$ and let κ_2^d vary. In figure 109 (see Appendix E), the red, green, blue and cyan curves represent the the loss distribution with $\kappa_2^d = 0, 0.5, 1, 2$, respectively. It appears that increasing κ_2^d only shifts the loss distribution to larger portfolio loss.

5.3 A JUMP-DIFFUSION CONTAGION MODEL WITH INFECTIOUS INTENSITY

We now study a jump-diffusion model with contagion that increases the intensity of the down-size jumps when defaults accumulate:

$$d\,X_{i,t} = \rho_j\,dW_t + \sqrt{1-\rho_j^2}\,dB_{i,t} + dJ^u_{i,t} - dJ^d_{i,H_{j,t-}} \tag{5.6}$$

where $H_{j,t} = \int_0^t (1 + \kappa_j^d \frac{N_{j,s}}{N_j})ds$ represent the cumulative hazard process of the down-size jump in sector j with intensity $1 + \kappa_j^d \frac{N_{j,t}}{N_j}$.

We compare the loss distribution in the toy model and in the jump-diffusion with infectious intensity model for a homogeneous portfolio of 100 names with $\rho = 0.5$, $K = -3$, $T = 5$: In figure 110 (see Appendix E), the red, green, blue, cyan, magenta and yellow curves represent the loss distributions for the toy model and the jump-diffusion with infectious intensity model with $\kappa^d = 0, 0.5, 1, 2, 5$, respectively. It seems that increasing the intensity as defaults accumulate increases the probability of large portfolio loss.

Next, we look at the loss distribution in the toy model and in the jump-diffusion with infectious intensity model for an inhomogeneous portfolio with 50 names in each of the two sectors with the same parameters except $\rho_1 = 0.9$, $\rho_2 = 0.1$, $\kappa_1^d = \kappa_2^d = 0, 0.5, 1, 2, 5$ (see figure 111 in Appendix E). Again, intensity infection increases the probability of large loss.

Moreover, we fix $\kappa_1^d = 1$, and compare the loss distributions with $\kappa_2^d = 0, 0.5, 1$. Again, we see the shifting effect of varying κ_2^d in figure 112 (see Appendix E).

In addition, we look at a homogeneous portfolio of 100 names and see how the loss distribution depends on the correlation ρ. In figure 113 (see Appendix E), the red, green and blue curves represent the loss distributions with $\rho = 0.1, 0.5, 0.9$, respectively. It is clear that increasing the correlation spreads out the loss distribution.

5.4 COMBINING CYCLICAL DEPENDENCE AND CONTAGION

In order to generate a multi-humped loss distribution as we did in section 4.3 and incorporate the contagion effect, we propose a model that combines these feature in the following subsection.

5.4.1 A Contagion Model with Drift Switching, Cyclical Economy, and Infectious Volatility

In this section, we combine drift switching, cyclical economy, and default contagion into a simple "hybrid" model in which the dynamics of the firm's credit index is as follows:

$$d\,X_{i,t} = \rho_j\,(\mu_j\,sgn(M_t)\,dt + dM_t) + \sigma_{j,t}\,\sqrt{1-\rho_j^2}\,dB_{i,t}, \quad X_{i,0} = 0 \tag{5.7}$$

$$d\,M_t = -\kappa_{cy}\,M_t\,dt + dW_t, \quad M_0 = m_0 \tag{5.8}$$

$$\sigma_{j,t} = 1 + \kappa_{co}^{j}\,\tfrac{N_{j,t-}}{N_j} \tag{5.9}$$

where ρ_j is the correlation between obligors in sector j and the market, κ_{co}^{j} controls the level of contagion in sector j. N_t^j is the number of defaults in sector j up to time t, and N_j is the number of names in sector j. This model reveals the contagion phenomenon that default events in a sector can increase the risk of default of other companies in the same sector.

We compare the portfolio loss distribution in the model for a homogeneous portfolio of 100 names, starting with normal initial market condition $m_0 = 0$, with different levels of cyclical and contagion effects. In figure 114 (see Appendix E), the red, green, blue, cyan, magenta, yellow and black curves represent the portfolio loss distribution in the toy model and in the contagion model with $\mu_i = 1$, $\rho_1 = 0.9$, $\rho_2 = 0.1$, $K = -3$, $T = 5$, $(\kappa_{cy}, \kappa_{co}) = (0,0)$, $(0.5,0)$,$(0,2)$,$(0.5,2)$,$(0.5,5)$,$(0.05,5)$, respectively. It appears that the contagion model generates a two-humped loss distribution that the finance industry is interested in.

In figures 115, 116, and 117 (see Appendix E), we compare the portfolio loss distribution in the model for a two-sector portfolio of 100 names with 50 names in each of the two sectors, starting

from different initial market condition $m_0 = 0, 1, -1$ (market expansion, normal market and market recession), with different levels of cyclical and contagion effects. The red, green, blue, cyan, magenta, yellow and black curves represent the portfolio loss distribution in the toy model and in the contagion model with $\mu_i = 1$, $\rho_1 = 0.9$, $\rho_2 = 0.1$, $K = -3$, $T = 5$, $(\kappa_{cy}, \kappa_{co}^1, \kappa_{co}^2) = (0, 0, 0)$, $(0.5, 0, 0)$,$(0, 2, 2)$,$(0.5, 2, 2)$,$(0.5, 5, 5)$,$(0.05, 5, 5)$, respectively. Again, the contagion model generates a two-humped loss distribution with a flexible location of the humps. Moreover, the probability of larger losses increases as the market deteriorates.

5.5 CHAPTER SUMMARY

In this chapter, we have investigated structural models with contagion that have the effect of shifting the loss distribution to larger losses. By combining cyclical dependence with contagion, one is able to generate a multi-humped loss distribution with flexibilities on hump sizes and locations. In the next chapter, we will apply our models to the financial market by calibrating the models in section 4.4.

6.0 CALIBRATION

In this chapter, we will detail the applications of our models to the financial market by calibrating the models in section 4.4. Section 6.1 is an introduction that describes the dislocation between single-name CDS's and CDO tranches, and provides a preliminary calibration of the common random initial state model in section 4.4.1 to market tranche quotes. Section 6.2 will introduce the pre-crisis market standard (Gaussian) copula model including the mixing copula model in O'Kane (2008) [34] which we will use to generate data that our models in sections 4.4.2 and 4.4.3 will calibrate to. Sections 6.3 and 6.4 will calibrate the switching correlation model and the random correlation model both with random initial state introduced in sections 4.4.2 and 4.4.3 to the data generated by the mixing copula model in O'Kane (2008) [34]. Section 6 is the conclusion.

6.1 INTRODUCTION AND CALIBRATION OF THE COMMON RANDOM INITIAL STATE MODEL

An ambitious goal of studying the financially motivated models in chapters 4 and 5 is to price consistently the single-name CDS's and CDO tranches over different times and maturities. Naturally, we would like to apply our models directly to the financial market by calibrating them to both single-name data (CDS spreads) and multi-name data (CDO tranche spreads). However, it is difficult to obtain the actual data (we need CDS data for all of the 125 companies in the CDX index and the tranche data) from non-commercial sources. More importantly, it is known that there are discrepancies between single-name CDS spreads and CDX tranche spreads, due to liquidity and specific investor preferences that any model will find difficult to capture. For example, the 2012

JPMorgan Chase trading loss was caused by a credit derivatives trader (the "London Whale") who created a disparity between the price of the CDX index and the average price of credit default swaps on the individual companies through aggressive trades. As a result, calibrating our models to actual market quotes will never account for these subjective trading discrepancies. Instead, we will calibrate our models to data generated by widely-accepted models. Although we focus on structural models through the thesis, there are other models (see section 1.2.1) that have previously been popular in the finance world. For instance, copula models, especially Gaussian copula models, had been extensively used in practice before the credit crisis. We will calibrate our models to O'Kane's mixing copula model (O'Kane (2008) [34]) which was an industry standard before the financial crisis.

Before we describe O'Kane's mixing copula model, we would like to illustrate that, although we will focus in the following on a bespoke, 5-dimensional portfolio, it is possible to calibrate our models in the full 125 dimensions by calibrating the homogeneous common random initial state model in section 4.1 to the Markit CDX tranche (a standard credit index derivative consisting of 125 companies in the financial market) quotes on April 15, 2010.

With a gamma initial state distribution $X_0 \sim Gamma(\alpha, \lambda)$ having the PDF

$$f_{X_0}(x_0; \alpha, \lambda) = \frac{\lambda^\alpha}{\Gamma(\alpha)} x_0^{\alpha-1} \exp\{-\lambda x_0\} \tag{6.1}$$

and the CDF

$$F_{X_0}(x_0; \alpha, \lambda) = \frac{\gamma(\alpha, \lambda x_0)}{\Gamma(\alpha)} \tag{6.2}$$

the asymptotic expected tranche loss in equation (4.89) is then

$$\begin{aligned} & E[L_t^{[K_A, K_D]}] \\ &= \frac{1}{K_D - K_A} \int_{K_A}^{K_D} F_{X_0}(G^{-1}(l))\, dl \\ &= \frac{1}{K_D - K_A} \int_{K_A}^{K_D} \frac{\gamma(\alpha, \lambda G^{-1}(l))}{\Gamma(\alpha)}\, dl \end{aligned} \tag{6.3}$$

We calibrate the model with the above common Gamma initial distribution to minimize the mean relative error (MRE) of the tranche upfront with a fixed running spread of $S = 100\ bps$:

$$MRE = \frac{1}{5}\sum_{j=1}^{5} |\frac{U_j^{Model} - U_j^{Actual}}{U_j^{Actual}}| \tag{6.4}$$

where U_j are tranche upfronts. The model upfront U with attachment point K_A, detachment point K_D, and running spread S is given in Appendix A (see equations (A.26)-(A.27)):

$$\begin{aligned} U &= E[\int_0^T \exp\{-\int_0^t r_s\, ds\}\, dL_t^{[K_A,K_D]}] - S\, E[\sum_{j=1}^{M} \exp\{-\int_0^{t_j} r_s\, ds\} \int_{t_{j-1}}^{t_j} (1 - L_t^{[K_A,K_D]})\, dt] \\ &\approx \sum_{j=1}^{M} B(0, \frac{t_j + t_{j-1}}{2})\, (E[L_{t_j}^{[K_A,K_D]}] - E[L_{t_{j-1}}^{[K_A,K_D]}]) - S \sum_{j=1}^{M} B(0,t_j)\, (t_j - t_{j-1})\, (1 - E[L_{t_j}^{[K_A,K_D]}]) \end{aligned} \tag{6.5}$$

Here, $B(0,t) = \exp\{-rt\}$ where r is the 3-month treasury yield that is $16\ bps$ in April 2010, and we take the recovery rate to be $R = 40\%$.

It turns out that using the large portfolio approximation (6.3), we are able to calibrate the model to the 5-year CDX tranches on April 15, 2010 with a reasonable MRE. Table 9 (see Appendix F) shows the calibrated parameters α, λ, and μ (notice that the inverse function G^{-1} in equation (6.3) depends on μ where G is defined in equation (4.84)) as well as the relative error in each tranche upfront and the MRE on average. Table 10 (see Appendix F) shows the comparison between the actual and model spreads. We can see that the common random initial state model is able to capture the market tranche quotes except the junior-mezzanine tranche and the super-senior tranche.

6.2 THE O'KANE MIXING COPULA MODEL

We begin with a brief description of the copula approach (see Schönbucher (2003) [37] or O'Kane (2008) [34]). A copula function separates the dependence structure from the marginal distributions. An N-dimensional copula function C is a multivariate cumulative distribution function with N uniform marginals with probabilities $u_1, ..., u_N$. We can write the copula as

$$\Pr(U_1 \leq u_1, ..., U_N \leq u_N) = C(u_1, ..., u_N) \tag{6.6}$$

Through the choice of the copula C, we can model the dependence structure of the default times of N credits as follows. Define a random variable $U_i = F_i(\tau_i)$, where F_i is the CDF of τ_i. We notice that U_i is uniformly distributed in $[0, 1]$, since for $u_i \in [0, 1]$,

$$\Pr(U_i \leq u_i) = \Pr(F_i(\tau_i) \leq u_i) = \Pr(\tau_i \leq F_i^{-1}(u_i)) = F_i(F_i^{-1}(u_i)) = u_i \tag{6.7}$$

where $F_i^{-1}(u) = \inf\{x | F_i(x) \geq u\}$ is a generalized inverse function (the quantile function in this case) of F_i.

We can then model the joint distribution of the default times through C by

$$\Pr(\tau_1 \leq t_1, ...\tau_N \leq t_N) = \Pr(U_1 \leq F_1(t_1), ..., U_N \leq F_N(t_N)) = C(F_1(t_1), ..., F_N(t_N)) \tag{6.8}$$

Sklar's theorem ensures that the above definition of joint default distribution is reasonable.

Theorem (Sklar) Let $X_1, ..., X_N$ be random variables with marginal distribution functions $F_1, ..., F_N$ and joint distribution function F. Then there exists an N-dimensional copula function C such that for all $(x_1, ..., x_N) \in \mathbf{R}^N$:

$$F(x_1, ..., x_N) = C(F_1(x_1), ..., F_N(x_N)) \tag{6.9}$$

i.e., C is the distribution function of $F_1(X_1), ..., F_N(X_N)$. If $F_1, ..., F_N$ are continuous, then C is unique. Otherwise, C is uniquely determined on $RanF_1 \times \cdots \times RanF_N$, where $RanF_i$ denotes the range of F_i for $i = 1, .., N$.

The Gaussian copula, which plays an important role in credit derivatives practices, is defined in the following:

Definition (Gaussian Copula) Let $X_1, ..., X_N$ be normally distributed random variables with means $\mu_1, ..., \mu_N$, standard deviations $\sigma_1, ..., \sigma_N$ and correlation matrix Σ. Then the distribution function $C_\Sigma(u_1, ..., u_N)$ of the random variables

$$U_i = \Phi(\frac{X_i - \mu_i}{\sigma_i}), \quad i \in \{1, ..., N\} \tag{6.10}$$

is a copula and it is called the Gaussian copula for the correlation matrix Σ.

Recall that the one-factor Vasicek Gaussian latent variable model is

$$X_i = \rho_i \, M + \sqrt{1 - \rho_i^2} \, Z_i \tag{6.11}$$

where the systematic factor M and idiosyncratic factor Z_i are standard normal random variables and are independent. Default τ_i occurs in $[0, t]$ if $X_i < K_i(t)$ where $K_i(t)$ is a time-dependent default barrier.

The one-factor Vasicek Gaussian latent variable model is already such a Gaussian copula model and is called a one-factor Gaussian copula model. To see this, we need to verify the conditions in the definition of the Gaussian copula. First notice that $M, Z_1, ..., Z_N$ is an $N + 1$-dimensional standard normal vector whose mean is a zero vector and whose covariance matrix is an identity matrix. Hence, the affine transformation $\mathbf{X} = (X_1, ..., X_N) = A\,(M, Z_1, ..., Z_N)^T$ is jointly normal with mean 0 and covariance matrix Σ where

$$A = \begin{pmatrix} \rho_1 & \sqrt{1-\rho_1^2} & 0 & ... & 0 \\ \rho_2 & 0 & \sqrt{1-\rho_2^2} & ... & 0 \\ & & ..... & & \\ \rho_N & 0 & 0 & ... & \sqrt{1-\rho_N^2} \end{pmatrix} \tag{6.12}$$

$$\Sigma = A\,A^T = \begin{pmatrix} 1 & \rho_1\rho_2 & \rho_1\rho_3 & ... & \rho_1\rho_N \\ \rho_1\rho_2 & 1 & \rho_2\rho_3 & ... & \rho_2\rho_N \\ & & ..... & & \\ \rho_1\rho_N & \rho_2\rho_N & \rho_3\rho_N & ... & 1 \end{pmatrix} \tag{6.13}$$

Since the marginal default probability in the model is

$$F_i(t_i) = \Pr(\tau_i \le t_i) = \Pr(X_i \le K_i(t_i)) = \Phi(K_i(t)) \tag{6.14}$$

the joint default distribution is thus

$$\begin{aligned} &\Pr(\tau_1 \le t_1, ..., \tau_N \le t_N) \\ &= \Pr(X_1 \le K_1(t_1), ..., X_N \le K_N(t_N)) \\ &= \Phi_N(K_1(t_1), ..., K_N(t_N); \Sigma) \\ &= \Phi_N(\Phi^{-1}(F_1(t_1)), ..., \Phi^{-1}(F_N(t_N)); \Sigma) \\ &= C_\Sigma(F_1(t_1), ..., F_N(t_N)) \end{aligned} \tag{6.15}$$

where $\Phi_N(x_1, ..., x_N; \Sigma)$ is the N-dimensional Gaussian CDF with mean 0 and covariance matrix Σ, and $C_\Sigma(u_1, ..., u_N) = \Phi_N(\Phi^{-1}(u_1), ..., \Phi^{-1}(u_N); \Sigma)$ is the Gaussian copula function. The distribution of the portfolio loss $L_t = \frac{1-R}{N} \sum_{i=1}^{N} I\{\tau_i \le t\}$ with recovery rate R can then be calculated.

An overview of applications of copula models, especially the Gaussian copula, can be found in Schöbucher (2003) [37] or O'Kane (2008) [34]. In the simplified case of the one-factor Gaussian copula model where $\rho_i = \rho$ (i.e., the dependence structure is flat), we can reverse out the "implied correlation" ρ from the tranche spreads; namely, we can solve for ρ in $PV(K_A, K_D; \rho) = 0$, where K_A and K_D are attachment and detachment points of the tranche, and

$$\begin{aligned} &PV(K_A, K_D; \rho) \\ &= U + E[\sum_{j=1}^{M} \exp\{-\int_0^{t_j} r_s\,ds\}\, S \int_0^{t_j} (1 - L_t^{[K_A,K_D]})\,dt] - E[\int_0^{T} \exp\{-\int_0^{t} r_s\,ds\}\, dL_t^{[K_A,K_D]}] \end{aligned} \tag{6.16}$$

where $t_j : j = 1, ..., M$ are premium payment dates, U is an upfront payment, S is an annualized premium, r a risk-free interest rate, and $L_t^{[K_A,K_D]} = \frac{(L_t-K_A)^+-(L_t-K_D)^+}{K_D-K_A}$ is the tranche loss.

Given K_A, K_D, r, U, S and the marginal distributions, the implied correlation ρ can be solved for by using a one-dimensional root searching algorithm.

A drawback of the one-factor Gaussian copula model is that it does not capture the implied correlation smile: the market is implying different correlation values for different tranches on the same portfolio. One of the well-known models in the literature that captures the implied correlation smile is the mixing copula model (see O'Kane (2008) [34]). The mixing copula model is essentially a one-factor Gaussian copula model with a random correlation that has a finite number of states. The default index in the model is:

$$X_i = \sqrt{\rho}\, M + \sqrt{1-\rho}\, Z_i \tag{6.17}$$

where the correlation ρ has a finite number of states $\rho_j : j = 1, ..., S$ each with probability p_j satisfying $\sum_{j=1}^{S} p_j = 1$. The model with a three-state correlation is calibrated in O'Kane (2008) [34] to actual CDS spreads over different maturities and the 5-year CDX tranche data simultaneously on a single day with a close fit to both data (although it underestimates the most senior tranche spread, which is typical during the credit crisis for many of the models). Table 11 (see Appendix F) shows the fit of the tranche data with the mean relative error (MRE) given by

$$MRE = \frac{1}{5}\sum_{j=1}^{5} \frac{|S_j^{Model} - S_j^{Actual}|}{S_j^{Actual}} \tag{6.18}$$

where S_j are tranche spreads (in bps), and S_j^{Model} can be calculated using equations (A.24)-(A.25) in Appendix A.

We use this mixing copula model to generate tranche data for a bespoke portfolio of 5 names: AIG, Amgen, American Express, First Energy, Wal-Mart. We choose these five companies since they represent different industries (sectors) and have different credit qualities. Moreover, this resembles a model for the entire portfolio of 125 names in the CDX index, except that we model the

sectors instead of the individual companies.

The model is implemented as follows.

First, we will back out a forward default hazard rate $h_i(t)$ that is piecewise constant between premium payment dates. The survival probability and then the default boundary $K_i(t)$ are determined from actual CDS quotes on March 18, 2011 for each name using a bootstrapping method. More specifically,

$$\Pr(\tau_i > t) = \exp\{-\int_0^t h_i(s)\,ds\}, \quad \text{where } h_i(t) = h_{i,j} \text{ if } t \in (t_{j-1}, t_j] \tag{6.19}$$

$$\begin{aligned} \Pr(\tau_i > t) &= \Pr(X_i \geq K_i(t)) = \Phi(-K_i(t)) \\ \Rightarrow \; K_i(t) &= -\Phi^{-1}(\exp\{-\int_0^t h_i(s)\,ds\}) \end{aligned} \tag{6.20}$$

where $t_j : \; j = 1, ..., M$ are premium payment dates and the Merton/Vasicek definition of default has been applied.

Second, given the systematic factor M, calculate the conditional loss distribution recursively from the conditional default probability (see section 4.3.2 or O'Kane (2008) [34])

$$\Pr(\tau_i \leq t|M) = \Phi(\frac{K_i(t) - \sqrt{\rho}\,M}{\sqrt{1-\rho}}) \tag{6.21}$$

and then calculate the unconditional loss distribution by taking the expectation over the systematic factor M.

Third, from the unconditional loss distribution, we generate tranche spreads for the bespoke portfolio with the correlation structure $\rho_1 = 0$, $\rho_2 = 0.1463$, $\rho_3 = 1$, with probabilities $p_1 = 0.4852$, $p_2 = 0.4385$, and $p_3 = 1 - p_1 - p_2 = 0.0726$ as given in O'Kane (2008) [34] who derived the parameters from actual data, for the $0\% - 20\%$, $20\% - 40\%$ and $40\% - 60\%$ tranches. The more senior tranches (i.e., $60\% - 80\%$ and $80\% - 100\%$) have essentially zero spreads. The tranche spreads generated by this procedure are 491.45 bps for the $0\% - 20\%$ tranche, 41.13 bps for the $20\% - 40\%$ tranche, and 5.95 bps for the $40\% - 60\%$ tranche.

6.3 CALIBRATING THE CORRELATION SWITCHING MODEL WITH RANDOM INITIAL STATE

For the Independent Gamma Initial Distribution with Switching Correlation Model in section 4.4.2, the default index follows:

$$d\,X_{i,t} = -\lambda_i\,dt + \rho(W_t)\,dW_t + \sqrt{1-\rho(W_t)^2}\,dB_{i,t}, \quad X_{i,0} \sim Gamma(\alpha_i, \lambda_i) \tag{6.22}$$

where the Gamma distribution has the PDF $f(x;\alpha,\lambda) = \frac{\lambda^\alpha}{\Gamma(\alpha)}\,x^{\alpha-1}\,\exp\{-\lambda x\}$ with parameters $\alpha > 0$ and $\lambda > 0$. $X_{i,0}$ and $X_{j,0}$ are independent for $i \neq j$, and $\rho(W_t)$ is a two-state random variable:

$$\rho(W_t) = \begin{cases} \rho_g, & \text{if } W_t \geq 0 \\ \rho_b, & \text{if } W_t < 0 \end{cases} \tag{6.23}$$

We focus on the special case where $\rho_b = 1$; that is, all firms become perfectly correlated with each other when the economy is in recession. This is widely believed to be a central feature contributing to a credit crisis.

We first notice that the model can be successfully calibrated to the term-structure of single-name CDS spreads within one second for each name with a mean relative error (MRE) of less than 5% and relatively stable parameters as the initiation date evolves over a period of a week.

As a preliminary exercise, we calibrate the single-name model with marginal default probability $\Pr(\tau_i \leq t) = \frac{\gamma(\frac{\alpha_i}{2}, \frac{\lambda_i^2}{2}t)}{\Gamma(\frac{\alpha_i}{2})}$ to the CDS spreads of a "good" company IBM and of a "bad" company AIG from April 12, 2010 to April 16, 2010. We choose these two companies in this time period because at the time, the AIG spreads are significantly higher than the IBM spreads. The calibration is carried out by minimizing the mean relative error (MRE)

$$MRE(\alpha,\lambda) = \frac{1}{7}\sum_{j=1}^{7} \frac{|S_j^{Model}(\alpha,\lambda) - S_j^{Actual}|}{S_j^{Actual}} \tag{6.24}$$

over admissible values $\alpha > 0$ and $\lambda > 0$, where $S_1, ..., S_7$ are CDS spreads with maturities $T = 1, 2, 3, 4, 5, 7, 10$. Here, the model CDS spread with maturity T is given by (see equations (A.16)-(A.17) in Appendix A)

$$S = \frac{E[\exp\{-\int_0^\tau r_t dt\}\, I\{\tau \le T\}\, (1-R)]}{E[\sum_{j=1}^M (\exp\{-\int_0^{t_j} r_t dt\}\, I\{\tau > t_j\}\, (t_j - t_{j-1}) + \exp\{-\int_0^\tau r_t dt\}\, I\{t_{j-1} < \tau \le t_j\}\, (\tau - t_{j-1}))]}$$
$$\approx \frac{(1-R)\, \sum_{j=1}^M B(0, \frac{t_j + t_{j-1}}{2})\, (\Pr(\tau \le t_j) - \Pr(\tau \le t_{j-1}))}{\sum_{j=1}^M [(t_j - t_{j-1})\, B(0, t_j)\, (1 - \Pr(\tau \le t_j)) + \frac{t_j - t_{j-1}}{2}\, B(0, \frac{t_j + t_{j-1}}{2})\, (\Pr(\tau \le t_j) - \Pr(\tau \le t_{j-1}))]} \tag{6.25}$$

where the default-free zero-coupon bond price $B(0,t) = \exp\{-rt\}$ for constant interest-rate r, $0 = t_0 < t_1 < \cdots < t_{M-1} < t_M = T$ are premium payment dates (typically once a quarter), and R is a constant recovery rate. In our calibration, we take r to be the 3-month treasury yield that is 16 bps in April 2010. The time interval between successive premium dates is $\Delta t = t_j - t_{j-1} = 0.25$ (year) so that $t_j = j\Delta t$. The recovery rate is assumed to be $R = 40\%$ (as specified by Bloomberg).

The calibration results with parameter values of α_i and λ_i and MRE as well as actual vs. model spreads in bps are shown in tables 12-23 (see Appendix F).

Then, we compare this model to the mixing copula model in O'Kane (2008). To do this, we first calibrate the two parameters α_i and λ_i to fit the seven CDS spreads for each of the five names on March 18, 2011 (AIG, Amgen, American Express, First Energy, and Wal-Mart) when the 3-month treasury yield fell to 6 bps. The calibrated parameter values, MREs, and actual vs. model spreads are shown as follows (see tables 24-29 in Appendix F).

Finally, we calibrate the correlation state parameter ρ_g in a good market (assuming $\rho_b = 1$) to fit the tranche spreads generated by the mixing copula model in O'Kane (2008) [34]. The objective function is the MRE given by

$$MRE(\rho_g) = \frac{1}{3} \sum_{j=1}^{3} \frac{|S_j^{Model}(\rho_g) - S_j^{O'Kane}|}{S_j^{O'Kane}} \tag{6.26}$$

where S_1, S_2, S_3 are spreads for the $0\% - 20\%$, $20\% - 40\%$, and $40\% - 60\%$ tranches. Here, the model tranche spreads are calculated using Monte Carlo simulations, by simulating the loss process L_t, and calculating (see equations (A.24)-(A.25))

$$\begin{aligned} S &= \frac{E[\int_0^T \exp\{-\int_0^t r_s\, ds\}\, dL_t^{[K_A,K_D]}]}{E[\sum_{j=1}^M \exp\{-\int_0^{t_j} r_s\, ds\}\, \int_{t_{j-1}}^{t_j} (1 - L_t^{[K_A,K_D]})\, dt]} \\ &\approx \frac{\sum_{j=1}^M B(0, \frac{t_j + t_{j-1}}{2})\, (E[L_{t_j}^{[K_A,K_D]}] - E[L_{t_{j-1}}^{[K_A,K_D]}])}{\sum_{j=1}^M B(0,t_j)\, (t_j - t_{j-1})\, (1 - E[L_{t_j}^{[K_A,K_D]}])} \end{aligned} \tag{6.27}$$

Again, $B(0,t) = \exp\{-rt\}$ where r is the 3-month treasury yield that is 6 bps in March 2011, and we take the recovery rate to be $R = 40\%$.

The parameter and relative errors as well as O'Kane vs. model spreads are shown in tables 30 and 31 (see Appendix F). Spreads generated by a model with constant average correlation $\rho_{Avg} = (\rho_g + \rho_b)/2$ are also given for comparison. It appears that the correlation switching model with Gamma initial data captures the $0\% - 20\%$ and $20\% - 40\%$ tranches relatively well but does not capture the most senior $40\% - 60\%$ tranche. The correlation switching model performs better than the model with constant average correlation.

6.4 CALIBRATING THE RANDOM CORRELATION MODEL

We calibrate the Zero-One Random Correlation Model with a truncated normal initial state studied in section 4.4.3. Recall that the model has the form (see equation (4.95)):

$$X_{i,t} = X_{i,0} + \mu_i\, t + \sigma_i\, (\rho\, W_t + \sqrt{1 - \rho^2}\, B_{i,t}) \tag{6.28}$$

where $X_{i,0}$ is a nonnegative random variable that has a truncated normal distribution with PDF

$$f(x_{i,0}) = \frac{\exp\{-\frac{1}{2}(x_{i,0} - y_{i,0})^2\}}{\sqrt{2\pi}\, \Phi(y_{i,0})}\, I\{x_{i,0} \geq 0\} \tag{6.29}$$

$X_{i,0}$ and $X_{j,0}$ are independent for $i \neq j$ and are independent of $W, B_1, ..., B_N$. The correlation ρ is a two-state random variable: $\rho = 0$ with probability p and $\rho = 1$ with probability $1 - p$.

Recall that the marginal default probability at t is:

$$\Pr(X_{i,t} < 0) = \frac{\Phi_2(-(y_{i,0} + \mu_i t), y_{i,0}; -\frac{1}{\sqrt{1+\sigma_i^2 t}})}{\Phi(y_{i,0})} \tag{6.30}$$

There are 3 parameters to calibrate to the single-name CDS spreads over 7 maturities (1, 2, 3, 4, 5, 7, 10 years) for each obligor: $y_{i,0}$, μ_i, σ_i so that the MRE defined below is minimized.

$$MRE(y_0, \mu, \sigma) = \frac{1}{7} \sum_{j=1}^{7} \frac{|S_j^{Model}(y_0, \mu, \sigma) - S_j^{Actual}|}{S_j^{Actual}} \tag{6.31}$$

Again, the model CDS spread with maturity T is given by (see equation (A.17) in Appendix A)

$$S \approx \frac{(1-R) \sum_{j=1}^{M} B(0, \frac{t_j + t_{j-1}}{2}) \left(\Pr(\tau \leq t_j) - \Pr(\tau \leq t_{j-1})\right)}{\sum_{j=1}^{M} [(t_j - t_{j-1}) B(0, t_j) (1 - \Pr(\tau \leq t_j)) + \frac{t_j - t_{j-1}}{2} B(0, \frac{t_j + t_{j-1}}{2}) \left(\Pr(\tau \leq t_j) - \Pr(\tau \leq t_{j-1})\right)]} \tag{6.32}$$

Table 32 (see Appendix E) shows the calibrated parameters for each obligor and the corresponding mean relative error (MRE), and tables 33-37 (see Appendix E) demonstrate the comparison of actual and model CDS spreads (in bps).

With these marginal parameters, we calibrate p to obtain the dependence structure that fits the tranche spreads generated by the mixing copula model in O'Kane (2008). The objective function is the MRE given by

$$MRE(p) = \frac{1}{3} \sum_{j=1}^{3} \frac{|S_j^{Model}(p) - S_j^{O'Kane}|}{S_j^{O'Kane}} \tag{6.33}$$

where S_1, S_2, S_3 are spreads for the $0\% - 20\%$, $20\% - 40\%$, and $40\% - 60\%$ tranches. Here, the model tranche spreads are calculated according to the following formula (see equation (A.25) in Appendix A), with the portfolio loss distribution calculated using the recursive algorithm,

$$S \approx \frac{\sum_{j=1}^{M} B(0, \frac{t_j + t_{j-1}}{2}) \left(E[L_{t_j}^{[K_A, K_D]}] - E[L_{t_{j-1}}^{[K_A, K_D]}]\right)}{\sum_{j=1}^{M} B(0, t_j) (t_j - t_{j-1}) (1 - E[L_{t_j}^{[K_A, K_D]}])} \tag{6.34}$$

The value of the parameter p and MRE and the comparison of actual (O'Kane) and model spreads are shown in tables 38 and 39 (see Appendix E). Tranche spreads generated by the model with one-state average correlation $\rho_{avg} = 1 - p = 0.2418$ are also shown for comparison purposes.

The implied 10 year tranche spreads using the calibrated 5 year correlation structure are shown in table 40 (see Appendix E). Clearly, the dynamic Zero-One Random Correlation Model generates higher spreads especially for the more senior tranches than the static mixing copula model in O'Kane (2008), which is desirable especially in recession and crisis times.

Finally, this calibration may be extended to 125 names by applying the large portfolio approximation in section 4.4.3 (see equations (4.107) - (4.115) and section 6.1 for an illustration) which will be included in our future work.

6.5 CHAPTER SUMMARY

In this chapter, we calibrated the models in section 4.4 to O'Kane's mixing copula model. Our calibration showed that the random correlation model with a random initial state is able to simultaneously capture both single-name and multi-name features in the CDS and CDO tranches and is superior to the pre-crisis market standard mixing copula model in generating higher spreads for senior tranches.

7.0 CONCLUSIONS AND FUTURE WORK

Throughout the thesis, we have studied the effect of the cyclical dependence and the contagion within the hierarchical structural modeling framework. The main original contributions of the thesis are:

- We have identified mechanisms for generating a multi-humped distribution of portfolio loss which is of interest in the finance industry (sections 2.2.2.4, 3.2.2.3, 4.3, 4.4.2, 4.4.3, 5.4).
- We have been able to incorporate the effect of contagion in the model (sections 5.2, 5.3, 5.4).
- We have been able to simultaneously price single-name CDS's and multi-name CDO's by calibrating some of the new models to the standard market model (sections 6.3, 6.4).

As a follow-up to this research, we intend in the future to:

- Calibrate the models in the full 125 dimensions and calibrate the contagion models.
- Prove that the random correlation model in which ρ has two states, 0 and 1, appearing in sections 4.4.3 and 6.4, has positive tail dependence.
- Analyze the hierarchical structural model with uncertain parameters using the worst-case scenario analysis to reduce model risk (see Avellaneda et. al. (1995) [1] and Avellaneda and Parás (1996) [2] for references in this direction).

APPENDIX A

AN INTRODUCTION TO CREDIT DERIVATIVES

In this appendix, we will describe two of the most liquid credit derivatives in the market and which appear in this thesis: credit default swaps (CDS's) and collateralized debt obligations (CDO's). These contracts and their pricing are well described in the literature (e.g., Schönbucher (2003) [37] or O'Kane (2008) [34]).

A.1 CREDIT DEFAULT SWAP

Roughly speaking, a single-name credit default swap (CDS) is an insurance contract that protects credit investors from loss due to the default of a single firm. In a single-name CDS contract, a protection buyer buys credit protection from a protection seller so that when a default event occurs for the underlying (reference) credit (corporate debts, defaultable bonds, etc.), the protection seller will pay the protection buyer to compensate for the credit loss at a prescribed recovery rate. In return, the protection buyer makes periodic (typically once a quarter) premium payments to the protection seller until the occurrence of the default event or the maturity of the contract, whichever comes first.

In a typical CDS contract, the default compensation is referred to as the protection leg and the premium payment is referred to as the premium leg. The premium payment size is quoted in the

market as an annualized spread, called the "default swap spread". Consider a hypothetical example of a CDS contract in which the reference credit is $\$10,000$ worth of Ford corporate bonds. The maturity is $T = 5$ years and the spread is $S = 6\%$ (equivalently, $S = 600\ bps$) annually which would correspond to quarterly payments of $\$10,000 \times 6\%/4 = \$150$. If the underlying bond did not default until the maturity, the protection buyer would be required to pay to the protection seller a total of $\$150 \times 20 = \$3000$ during the lifetime of the contract. Should a default occur one month after the sixth payment date (i.e., 19 months after the inception date), a compensation equal to the loss amount, for instance, $\$6,000$ (corresponding to a recovery rate $R = 40\%$) would be made to the protection buyer. On the other hand, the protection buyer would pay $\$150 \times 6 = \$900$ plus a final "accrual" payment of $\$10,000 \times 6\% \times \frac{1}{12} = \$50$ to account for the fact that he was "protected" between the last payment date and the time of default.

Valuation of CDS contracts is similar to valuation of futures contracts. From the protection buyer perspective, the present value of the CDS is the difference between the (risk-neutral) expected value of the discounted protection leg (expected present value of the protection leg) and the (risk-neutral) expected value of the premium leg (expected present value of the premium leg). The protect seller perspective is the opposite. The "fair spread" is set so that there is no initial payment at the time of inception. This can only occur if the (risk-neutral) expected present values of the protection leg and the premium leg are equal.

Let S be the fair CDS spread, r_t be the instantaneous risk-free rate process, R be the recovery rate (typically 40% as prescribed in Bloomberg), T be the maturity, and $0 = t_0 < t_1 < \cdots < t_{M-1} < t_M = T$ be the premium payment dates. Denote τ as the (random) default time. Without loss of generality, assume that the notional of the reference credit is 1.

The present value of the protection leg is

$$PV_{Prot} = \exp\{-\textstyle\int_0^\tau r_t dt\}\, I\{\tau \le T\}\, (1-R) \tag{A.1}$$

$$= \textstyle\sum_{j=1}^{M} \exp\{-\int_0^\tau r_t dt\}\, I\{t_{j-1} < \tau \le t_j\}\, (1-R) \tag{A.2}$$

On the other hand, the present value of the premium leg is

$$\begin{aligned} PV_{Prem} = \sum_{j=1}^{M} (&\exp\{-\int_0^{t_j} r_t dt\}\, I\{\tau > t_j\}\, (t_j - t_{j-1})\, S \\ &+ \exp\{-\int_0^{\tau} r_t dt\}\, I\{t_{j-1} < \tau \leq t_j\}\, (\tau - t_{j-1})\, S) \end{aligned} \tag{A.3}$$

where the second term in equation (A.3) represents the present value of the final "accrual".

The following approximations of (risk-neutral) expectations of present values of the protection leg and the premium leg are valid assuming that the interest rate r, the default time τ, and the (constant) recovery rate R are independent, and default occurs half-way between successive premium payment dates; i.e., $\tau \in \{\frac{t_1+t_0}{2}, \frac{t_2+t_1}{2}, ..., \frac{t_M+t_{M-1}}{2}\}$.

$$E[PV_{Prot}] = (1-R)\, \textstyle\sum_{j=1}^{M} E[\exp\{-\int_0^{\tau} r_t dt\}\, I\{t_{j-1} < \tau \leq t_j\}] \tag{A.4}$$

$$= (1-R)\, \textstyle\sum_{j=1}^{M} E[E[\exp\{-\int_0^{\tau} r_t dt\}\, I\{t_{j-1} < \tau \leq t_j\} | \tau]] \tag{A.5}$$

$$= (1-R)\, \textstyle\sum_{j=1}^{M} E[\exp\{-\int_0^{\tau} r_t dt\} | t_{j-1} < \tau \leq t_j]\, \Pr(t_{j-1} < \tau \leq t_j) \tag{A.6}$$

$$= (1-R)\, \textstyle\sum_{j=1}^{M} E[\exp\{-\int_0^{\tau} r_t dt\} | \tau = \frac{t_j+t_{j-1}}{2}]\, \Pr(t_{j-1} < \tau \leq t_j) \tag{A.7}$$

$$= (1-R)\, \textstyle\sum_{j=1}^{M} E[\exp\{-\int_0^{\frac{t_j+t_{j-1}}{2}} r_t dt\}]\, \Pr(t_{j-1} < \tau \leq t_j) \tag{A.8}$$

$$= (1-R)\, \textstyle\sum_{j=1}^{M} B(0, \frac{t_j+t_{j-1}}{2})\, (\Pr(\tau \leq t_j) - \Pr(\tau \leq t_{j-1})) \tag{A.9}$$

and

$$PV_{Prem} = S \sum_{j=1}^{M} (E[\exp\{-\int_0^{t_j} r_t dt\}\, I\{\tau > t_j\}\, (t_j - t_{j-1})] + E[\exp\{-\int_0^{\tau} r_t dt\}\, I\{t_{j-1} < \tau \le t_j\}\, (\tau - t_{j-1})]) \tag{A.10}$$

$$= S \sum_{j=1}^{M} (E[E[\exp\{-\int_0^{t_j} r_t dt\}\, I\{\tau > t_j\}\, (t_j - t_{j-1})|\tau]] + E[E[\exp\{-\int_0^{\tau} r_t dt\}\, I\{t_{j-1} < \tau \le t_j\}\, (\tau - t_{j-1})|\tau]]) \tag{A.11}$$

$$= S \sum_{j=1}^{M} ((t_j - t_{j-1})\, E[\exp\{-\int_0^{t_j} r_t dt\}|\tau > t_j]\, Pr(\tau > t_j) + E[\exp\{-\int_0^{\tau} r_t dt\}\, (\tau - t_{j-1})|t_{j-1} < \tau \le t_j])\, Pr(t_{j-1} < \tau \le t_j) \tag{A.12}$$

$$= S \sum_{j=1}^{M} ((t_j - t_{j-1})\, E[\exp\{-\int_0^{t_j} r_t dt\}|\tau > t_j]\, Pr(\tau > t_j) + E[\exp\{-\int_0^{\tau} r_t dt\}\, (\tau - t_{j-1})|\tau = \frac{t_j + t_{j-1}}{2}]\, Pr(t_{j-1} < \tau \le t_j)) \tag{A.13}$$

$$= S \sum_{j=1}^{M} ((t_j - t_{j-1})\, E[\exp\{-\int_0^{t_j} r_t dt\}]\, Pr(\tau > t_j) + E[\exp\{-\int_0^{\frac{t_j+t_{j-1}}{2}} r_t dt\}\, (\frac{t_j + t_{j-1}}{2} - t_{j-1})]\, Pr(t_{j-1} < \tau \le t_j)) \tag{A.14}$$

$$= S \sum_{j=1}^{M} [(t_j - t_{j-1})\, B(0, t_j)\, (1 - \Pr(\tau \le t_j)) + \frac{t_j - t_{j-1}}{2}\, B(0, \frac{t_j + t_{j-1}}{2})\, (\Pr(\tau \le t_j) - \Pr(\tau \le t_{j-1}))] \tag{A.15}$$

where $B(0,t) = E[\exp\{-\int_0^t r_s ds\}]$ is the price of the zero-coupon risk-free bond. Note that equations (A.7) and (A.13) are based on the assumption that default occurs half-way between successive premium payment dates, and equations (A.8) and (A.14) are based on the assumption that the default time τ and the risk-free rate r are independent.

Equating the expected protection leg and premium leg, we obtain the fair CDS spread:

$$S = \frac{E[\exp\{-\int_0^{\tau} r_t dt\}\, I\{\tau \le T\}\, (1-R)]}{E[\sum_{j=1}^{M} (\exp\{-\int_0^{t_j} r_t dt\}\, I\{\tau > t_j\}\, (t_j - t_{j-1}) + \exp\{-\int_0^{\tau} r_t dt\}\, I\{t_{j-1} < \tau \le t_j\}\, (\tau - t_{j-1}))]} \tag{A.16}$$

$$\approx \frac{(1-R)\, \sum_{j=1}^{M} B(0, \frac{t_j + t_{j-1}}{2})\, (\Pr(\tau \le t_j) - \Pr(\tau \le t_{j-1}))}{\sum_{j=1}^{M} [(t_j - t_{j-1})\, B(0,t_j)\, (1 - \Pr(\tau \le t_j)) + \frac{t_j - t_{j-1}}{2}\, B(0, \frac{t_j + t_{j-1}}{2})\, (\Pr(\tau \le t_j) - \Pr(\tau \le t_{j-1}))]} \tag{A.17}$$

In practice, equation (A.17) may be further approximated using $B(0,t) \approx \exp\{-rt\}$ with the (constant) risk-free rate r taken to be the 3-month treasury yield. With quarterly premium payments, $t_j = j\Delta t$ where $\Delta t = t_j - t_{j-1} = 0.25$ (year) is the time interval between successive premium dates.

A.2 COLLATERALIZED DEBT OBLIGATION

In a collateralized debt obligation (CDO), an underlying (reference) portfolio of credits is defined, along with several "tranches" that restructure the credit risk profile of the portfolio associated with different credit ratings. Among other CDO's, the most liquid CDO's traded in the market are synthetic tranches (for which the underlying are portfolios of CDS contracts) on standardized CDS indices such as the CDX and the iTraxx series.

A tranche with attachment point K_A and detachment point K_D (e.g., 3% and 7%) has the following payoff structure. A protection buyer of the tranche is not reimbursed for any loss due to defaults until the portfolio loss reaches the attachment point 3%. Starting from the attachment point, the protection buyer will be compensated until the detachment point 7% of portfolio loss is reached. In return, the protection buyer makes periodic (typically quarterly) payments on the outstanding tranche notional (which is the initial amount covered less the compensation already paid out) until the detachment point is reached (the outstanding tranche notional is then zero).

For example, suppose that the initial tranche notional is $\$10,000$. After 8 months, a tranche loss of $\$5,000$ occurs (no loss occurred before that). Suppose that the tranche spread is $600\ bps = 6\%$. The protection buyer will be compensated with $\$5,000$. In return, he has to pay $\$10,000 \times 6\% \times \frac{6}{12} = \$300$ for the protection during the first 6 months, plus an "accrual" payment of $\$10,000 \times 6\% \times \frac{2}{12} = \$100$ for the protection during the 2-month period between the last premium and the time that the loss occurs. After that, the tranche notional becomes $\$10,000 - \$5,000 = \$5,000$. If the tranche should not assume further loss, a premium payment of $\$5,000 \times 6\% \times \frac{3}{12} = \$75$ based

on the reduced notional would be due on the next premium date (i.e., 9 months after the inception of the tranche).

Mathematically, let $\tau_i : \ i = 1, ..., N$ be the default time for firm i, and define the portfolio loss process (assuming a notional of 1 without loss of generality)

$$L_t = \frac{1}{N} \sum_{i=1}^{N} I\{\tau_i \leq t\} \, (1 - R) \tag{A.18}$$

where R (typically, $R = 40\%$) is the recovery rate. The loss of a tranche with attachment point K_A and detachment point K_D is defined as

$$L_t^{[K_A, K_D]} = \frac{(L_t - K_A)^+ - (L_t - K_D)^+}{K_D - K_A} \tag{A.19}$$

With instantaneous risk-free rate r_t, the "fair spread" of the tranche with attachment point K_A and detachment point K_D can be found by equating the (risk-neutral) expected present values of the protection leg and the premium leg. With a running (annualized) spread S and possibly an upfront U (usually quoted in percentages), the present value of the protection leg is

$$PV_{Prot} = \int_0^T \exp\{-\int_0^t r_s \, ds\} \, dL_t^{[K_A, K_D]} \tag{A.20}$$

$$\approx \sum_{j=1}^{M} \exp\{-\int_0^{\frac{t_j + t_{j-1}}{2}} r_s \, ds\} \, (L_{t_j}^{[K_A, K_D]} - L_{t_{j-1}}^{[K_A, K_D]}) \tag{A.21}$$

where equation (A.21) is the midpoint approximation of the Riemann-Stieltjes integral (A.20).

Ignoring the final "accrual" and assuming that the premium is paid on the average notional, the present value of the premium leg is

$$PV_{Prem} = U + \sum_{j=1}^{M} \exp\{-\int_0^{t_j} r_s \, ds\} \, S \, (t_j - t_{j-1}) \int_{t_{j-1}}^{t_j} \frac{1 - L_t^{[K_A, K_D]}}{t_j - t_{j-1}} \, dt \tag{A.22}$$

$$\approx U + S \sum_{j=1}^{M} \exp\{-\int_0^{t_j} r_s \, ds\} \, (1 - E[L_{t_j}^{[K_A, K_D]}]) \tag{A.23}$$

where $\int_{t_{j-1}}^{t_j} \frac{1 - L_t^{[K_A, K_D]}}{t_j - t_{j-1}} \, dt$ represents the average outstanding tranche notional, and $1 - E[L_{t_j}^{[K_A, K_D]}]$ is the top-right corner approximation of the Riemann integral $\int_{t_{j-1}}^{t_j} 1 - L_t^{[K_A, K_D]} \, dt$.

Using similar approximations as in appendix A.1, we have that, given U, the fair spread is

$$S = \frac{E[\int_0^T \exp\{-\int_0^t r_s\,ds\}\,dL_t^{[K_A,K_D]}] - U}{E[\sum_{j=1}^M \exp\{-\int_0^{t_j} r_s\,ds\}\int_{t_{j-1}}^{t_j}(1-L_t^{[K_A,K_D]})\,dt]} \tag{A.24}$$

$$\approx \frac{\sum_{j=1}^M B(0,\frac{t_j+t_{j-1}}{2})\,(E[L_{t_j}^{[K_A,K_D]}]-E[L_{t_{j-1}}^{[K_A,K_D]}]) - U}{\sum_{j=1}^M B(0,t_j)\,(t_j-t_{j-1})\,(1-E[L_{t_j}^{[K_A,K_D]}])} \tag{A.25}$$

On the other hand, given S, the fair upfront is

$$\begin{aligned} U &= E[\int_0^T \exp\{-\int_0^t r_s\,ds\}\,dL_t^{[K_A,K_D]}] \\ &\quad - S\,E[\sum_{j=1}^M \exp\{-\int_0^{t_j} r_s\,ds\}\int_{t_{j-1}}^{t_j}(1-L_t^{[K_A,K_D]})\,dt] \end{aligned} \tag{A.26}$$

$$\begin{aligned} &\approx \sum_{j=1}^M B(0,\frac{t_j+t_{j-1}}{2})\,(E[L_{t_j}^{[K_A,K_D]}] - E[L_{t_{j-1}}^{[K_A,K_D]}]) \\ &\quad - S\sum_{j=1}^M B(0,t_j)\,(t_j-t_{j-1})\,(1-E[L_{t_j}^{[K_A,K_D]}]) \end{aligned} \tag{A.27}$$

Again, equations (A.25) and (A.27) may be further approximated using $B(0,t) \approx \exp\{-rt\}$ with the (constant) risk-free rate r taken to be the 3-month treasury yield. With quarterly premium payments, $t_j = j\Delta t$ where $\Delta t = t_j - t_{j-1} = 0.25$ (year) is the time interval between successive premium dates.

It is expected that when there is only 1 company in the portfolio, a tranche with attachment point 0% and detachment point 100% and zero upfront payment should have a spread that is equal to the single-name CDS spread. This is indeed true by comparing equations (A.1)-(A.17) with equations (A.20)-(A.25). In this case, we have

$$L_t^{[0\%,100\%]} = L_t = I\{\tau \le t\}\,(1-R) \tag{A.28}$$

Thus, equation (A.20) is reduced to equation (A.1)

$$PV_{Prot} = \int_0^T \exp\{-\int_0^t r_s\,ds\}\,dL_t^{[0\%,100\%]} = \exp\{-\int_0^\tau r_t dt\}\,I\{\tau \le T\}\,(1-R) \tag{A.29}$$

and equation (A.21) with $U = 0$ is reduced to

$$\begin{aligned} PV_{Prem} &= \sum_{j=1}^{M} \exp\{-\int_0^{t_j} r_s\, ds\}\, S\,(t_j - t_{j-1}) \int_{t_{j-1}}^{t_j} \frac{1 - L_t^{[0\%,100\%]}}{t_j - t_{j-1}}\, dt \\ &= \sum_{j=1}^{M} \exp\{-\int_0^{t_j} r_s\, ds\}\, S\,[I\{\tau > t_j\}\,(t_j - t_{j-1}) + I\{t_{j-1} < \tau \le t_j\}\,(\tau - t_{j-1})] \end{aligned} \tag{A.30}$$

The difference between equation (A.3) and equation (A.30) is usually small (we may assume that r_t is bounded, since it is typically small):

$$\begin{aligned} \text{Difference} &= \sum_{j=1}^{M} (\exp\{-\int_0^{\tau} r_s ds\} - \exp\{-\int_0^{t_j} r_s ds\})\, S\, I\{t_{j-1} < \tau \le t_j\}\,(\tau - t_{j-1}) \\ &\le \max_{1\le j\le M} (\exp\{-\int_0^{t_{j-1}} r_s ds\} - \exp\{-\int_0^{t_j} r_s ds\})\, S\,(t_j - t_{j-1}) \\ &= \max_{1\le j\le M} \exp\{-\int_0^{t_j} r_s ds\}\,(\exp\{\int_{t_{j-1}}^{t_j} r_s ds\} - 1)\, S\,(t_j - t_{j-1}) \\ &\le \max_{1\le j\le M} (\exp\{\int_{t_{j-1}}^{t_j} r_s ds\} - 1)\, S\,(t_j - t_{j-1}) \\ &\le \max_{1\le j\le M} (\exp\{(t_j - t_{j-1}) \sup_{t\in[0,T]} r_t\} - 1)\, S\,(t_j - t_{j-1}) \\ &\approx \max_{1\le j\le M} S\,(t_j - t_{j-1})^2 \sup_{t\in[0,T]} r_t \end{aligned} \tag{A.31}$$

The (approximate) fair spread from equation (A.25) with $U = 0$ is reduced to

$$\begin{aligned} S &\approx \frac{\sum_{j=1}^{M} B(0, \frac{t_j + t_{j-1}}{2})\,(E[L_{t_j}^{[0\%,100\%]}] - E[L_{t_{j-1}}^{[0\%,100\%]}])}{\sum_{j=1}^{M} B(0,t_j)\,(t_j - t_{j-1})\,(1 - E[L_{t_j}^{[0\%,100\%]}])} \\ &= \frac{(1-R)\sum_{j=1}^{M} B(0, \frac{t_j + t_{j-1}}{2})\,(\Pr(\tau \le t_j) - \Pr(\tau \le t_{j-1}))}{\sum_{j=1}^{M} (t_j - t_{j-1})\, B(0,t_j)\,(1 - \Pr(\tau \le t_j))} \end{aligned} \tag{A.32}$$

which is equal to equation (A.17) without the final "accrual".

APPENDIX B

CHPATER 2 TABLES AND FIGURES

Table 1: Asymptotic Loss Density in the Toy Model for Homogeneous Portfolio with $\rho = 0.6$ and Different Values of $x \approx 0$

x	ρ	K	T	Asymptotic Loss Density
10^{-1}	0.6	-3	5	2.637494641944723
10^{-2}	0.6	-3	5	13.720427416221783
10^{-3}	0.6	-3	5	26.769586547296061
10^{-4}	0.6	-3	5	33.012696379816177
10^{-5}	0.6	-3	5	30.861689176001754
10^{-6}	0.6	-3	5	23.871713251337059
10^{-7}	0.6	-3	5	16.058449408375573
10^{-8}	0.6	-3	5	9.694448950897250
10^{-9}	0.6	-3	5	5.365125317518422
10^{-10}	0.6	-3	5	2.763512799104135
10^{-11}	0.6	-3	5	1.339848554577622
10^{-12}	0.6	-3	5	0.616743229128958
10^{-13}	0.6	-3	5	0.271359882150280
10^{-14}	0.6	-3	5	0.114745430509819
10^{-15}	0.6	-3	5	0.046837785751293
10^{-16}	0.6	-3	5	0.018523429051423

Table 2: Asymptotic Loss Density in the Toy Model for Homogeneous Portfolio with $\rho = 0.6$ and Different Values of $x \approx 1$

x	ρ	K	T	Asymptotic Loss Density
$1 - 10^{-1}$	0.6	-3	5	0.001266032042814
$1 - 10^{-2}$	0.6	-3	5	0.000012971280277
$1 - 10^{-3}$	0.6	-3	5	0.000000266119887
$1 - 10^{-4}$	0.6	-3	5	0.000000007723196
$1 - 10^{-5}$	0.6	-3	5	0.000000000278562
$1 - 10^{-6}$	0.6	-3	5	0.000000000011702
$1 - 10^{-7}$	0.6	-3	5	0.000000000000551
$1 - 10^{-8}$	0.6	-3	5	0.000000000000028
$1 - 10^{-9}$	0.6	-3	5	0.000000000000002
$1 - 10^{-10}$	0.6	-3	5	0
$1 - 10^{-11}$	0.6	-3	5	0
$1 - 10^{-12}$	0.6	-3	5	0
$1 - 10^{-13}$	0.6	-3	5	0
$1 - 10^{-14}$	0.6	-3	5	0
$1 - 10^{-15}$	0.6	-3	5	0
$1 - 10^{-16}$	0.6	-3	5	0

Table 3: Asymptotic Loss Density in the Toy Model for Homogeneous Portfolio with $\rho = 0.8$ and Different Values of $x \approx 0$

x	ρ	K	T	Asymptotic Loss Density
10^{-1}	0.8	-3	5	1.31951
10^{-2}	0.8	-3	5	11.20066
10^{-3}	0.8	-3	5	72.37687
10^{-4}	0.8	-3	5	407.21963
10^{-5}	0.8	-3	5	2099.18689
10^{-6}	0.8	-3	5	10173.42993
10^{-7}	0.8	-3	5	47062.25957
10^{-8}	0.8	-3	5	209863.29787
10^{-9}	0.8	-3	5	908257.77211
10^{-10}	0.8	-3	5	3833808.07474
10^{-11}	0.8	-3	5	15842009.24101
10^{-12}	0.8	-3	5	64268217.14544
10^{-13}	0.8	-3	5	256553591.48223
10^{-14}	0.8	-3	5	1009617174.67530
10^{-15}	0.8	-3	5	3922754373.04159
10^{-16}	0.8	-3	5	15067151949.66244

Table 4: Asymptotic Loss Density in the Toy Model for Homogeneous Portfolio with $\rho = 0.8$ and Different Values of $x \approx 1$

x	ρ	K	T	Asymptotic Loss Density
$1 - 10^{-1}$	0.8	-3	5	0.052518848549356
$1 - 10^{-2}$	0.8	-3	5	0.032188914445154
$1 - 10^{-3}$	0.8	-3	5	0.030445137606181
$1 - 10^{-4}$	0.8	-3	5	0.035220826103427
$1 - 10^{-5}$	0.8	-3	5	0.045988974456140
$1 - 10^{-6}$	0.8	-3	5	0.065214876207861
$1 - 10^{-7}$	0.8	-3	5	0.098263303808370
$1 - 10^{-8}$	0.8	-3	5	0.155174238798868
$1 - 10^{-9}$	0.8	-3	5	0.254448018665415
$1 - 10^{-10}$	0.8	-3	5	0.430387031100073
$1 - 10^{-11}$	0.8	-3	5	0.747262809405284
$1 - 10^{-12}$	0.8	-3	5	1.326838910999168
$1 - 10^{-13}$	0.8	-3	5	2.402015494827477
$1 - 10^{-14}$	0.8	-3	5	4.425183783832114
$1 - 10^{-15}$	0.8	-3	5	8.274828462550902
$1 - 10^{-16}$	0.8	-3	5	15.228836116926827

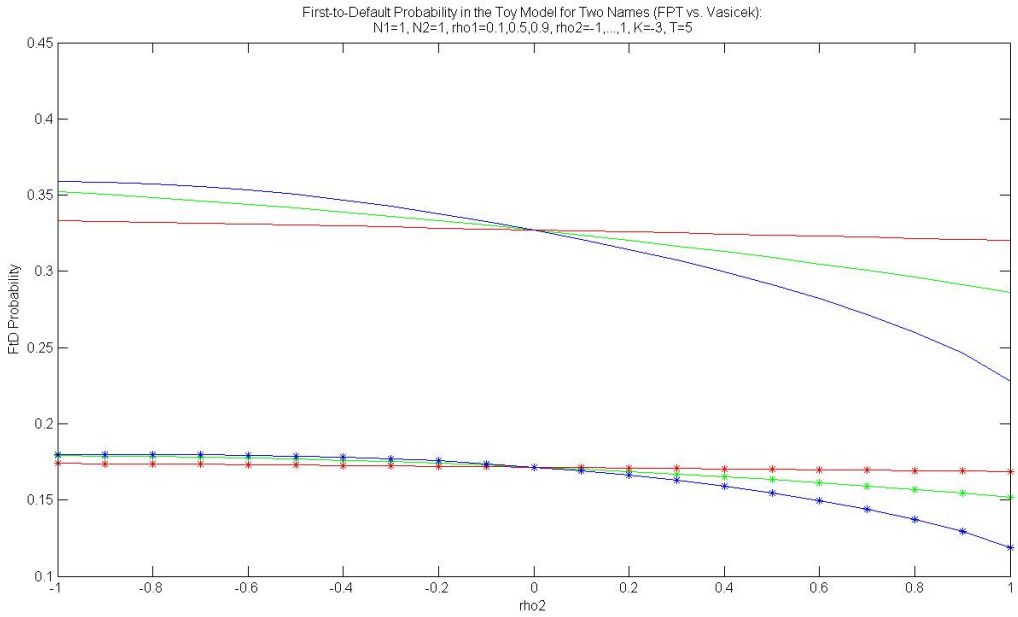

Figure 1: FPT vs. Vasicek First-to-Default Probability in the Toy Model for Two Firms with Different Values of ρ

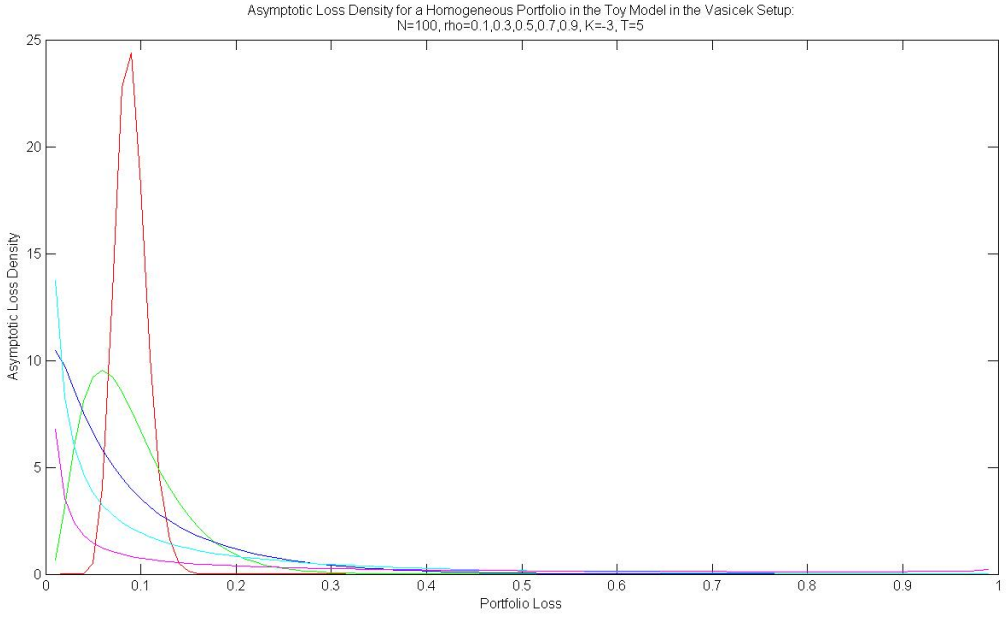

Figure 2: Asymptotic Loss Density in the Toy Model for Homogeneous Portfolio with $K = -3$ and Different Values of ρ

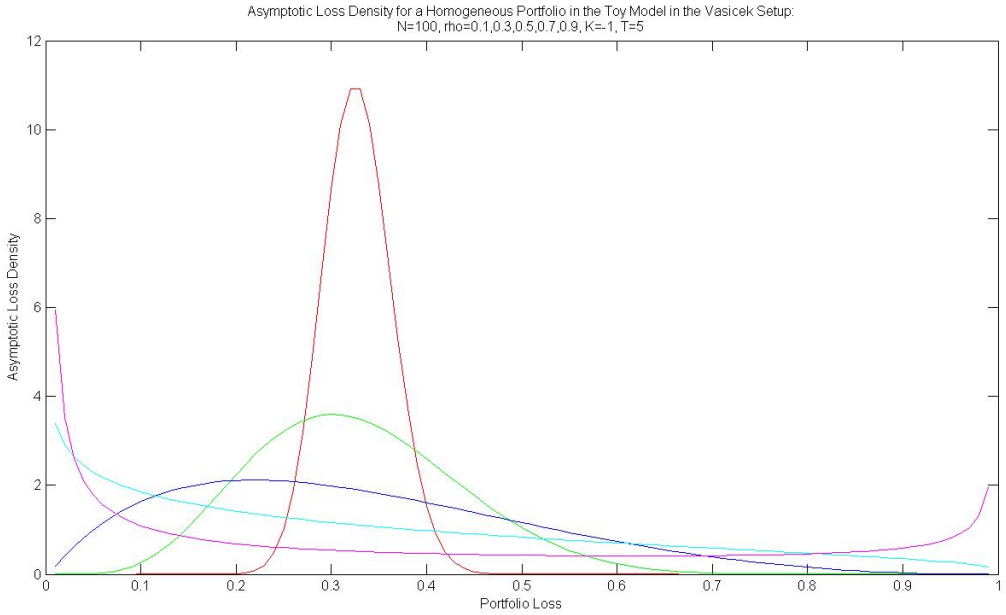

Figure 3: Asymptotic Loss Density in the Toy Model for Homogeneous Portfolio with $K = -1$ and Different Values of ρ

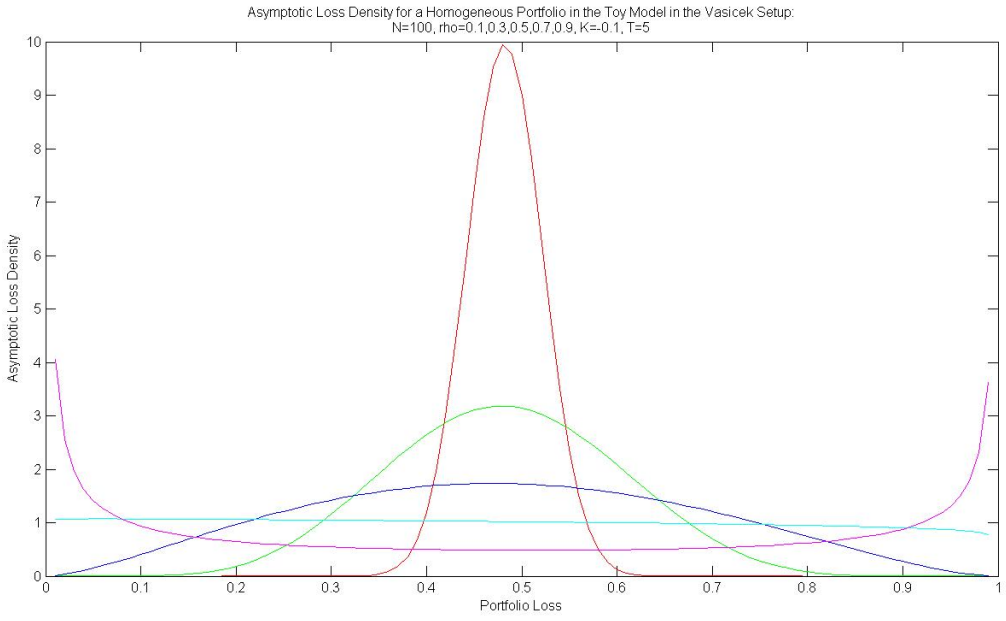

Figure 4: Asymptotic Loss Density in the Toy Model for Homogeneous Portfolio with $K = -0.1$ and Different Values of ρ

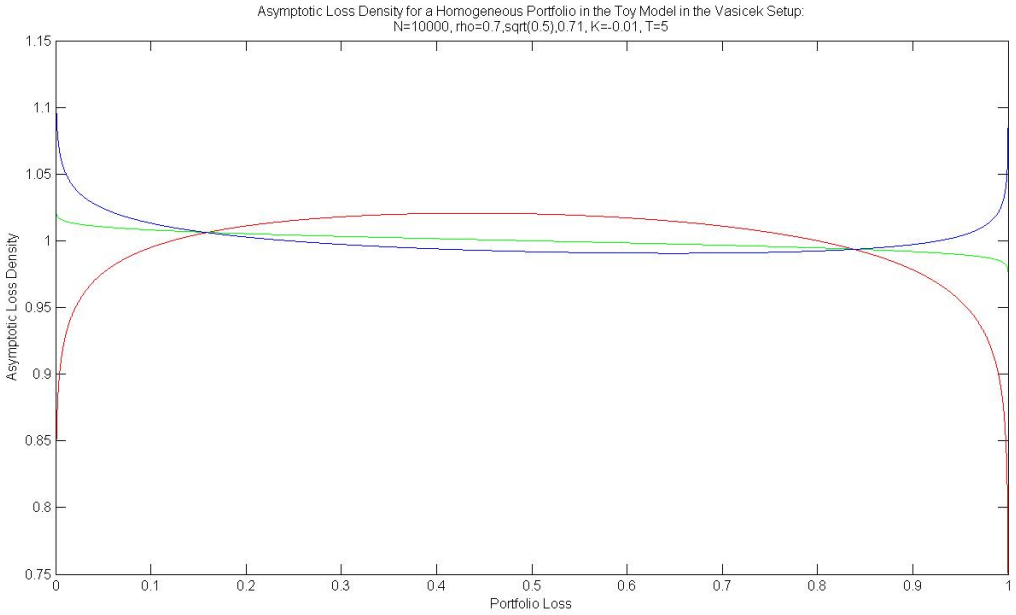

Figure 5: Asymptotic Loss Density in the Toy Model for Homogeneous Portfolio with Different Values of $\rho \approx \sqrt{0.5}$

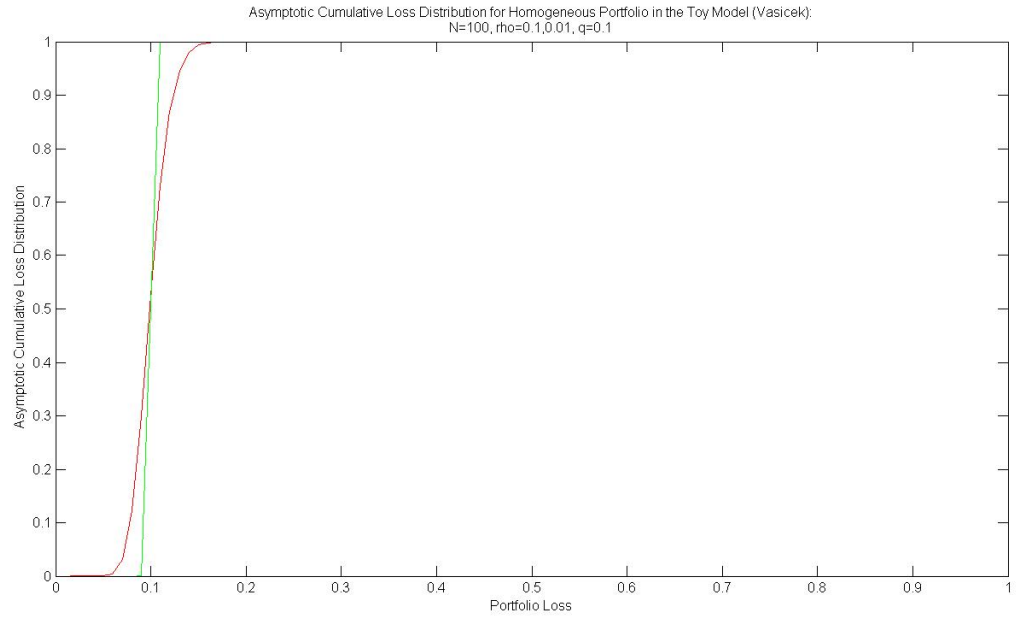

Figure 6: Asymptotic Loss CDF in the Toy Model for Homogeneous Portfolio with Different Values of $\rho \approx 0$

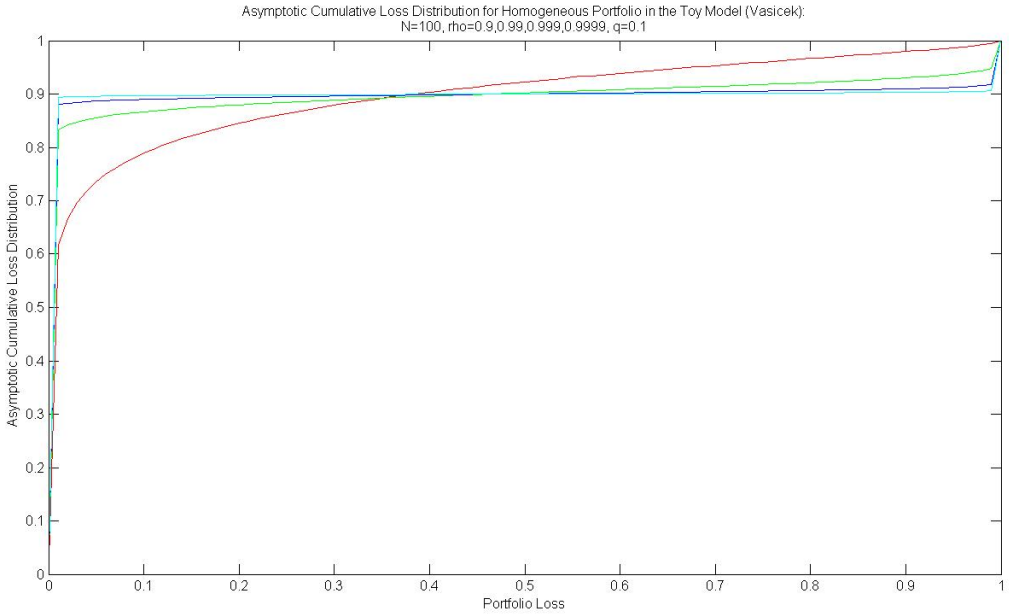

Figure 7: Asymptotic Loss CDF in the Toy Model for Homogeneous Portfolio with Different Values of $\rho \approx 1$

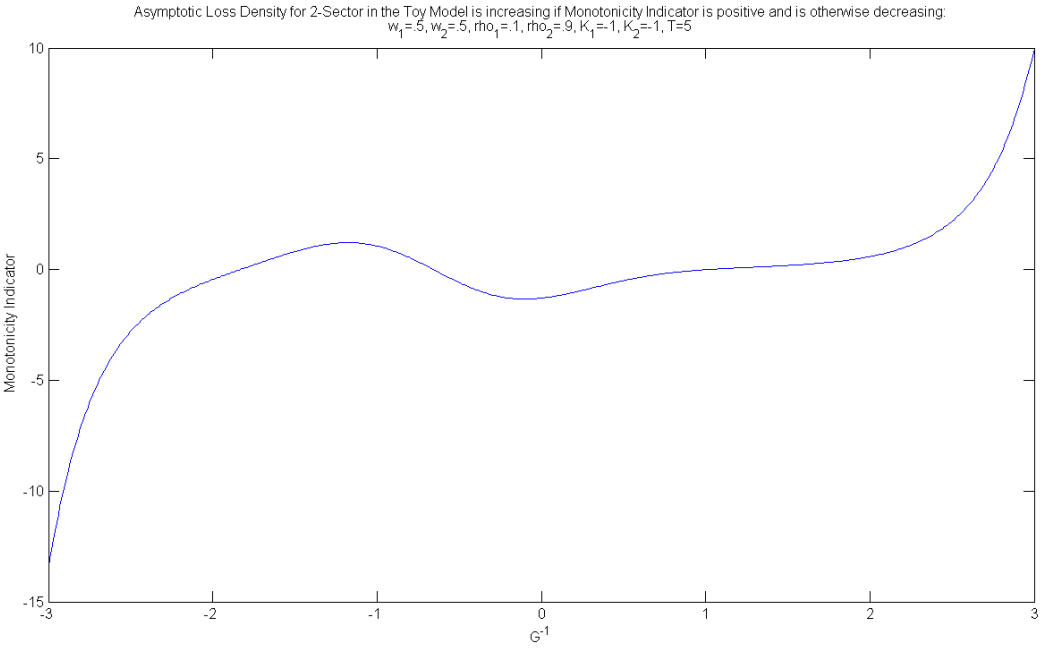

Figure 8: Monotonicity of the Asymptotic Loss PDF for Two-Sector Portfolio

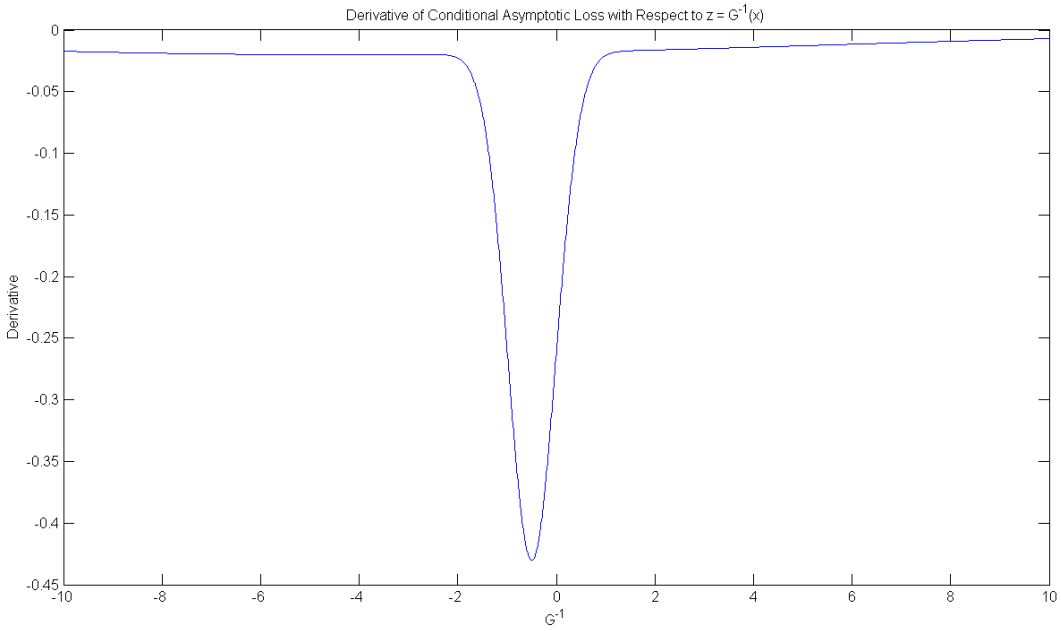

Figure 9: Denominator $G'(G^{-1}(x))$ in the Asymptotic Loss PDF for Two-Sector Portfolio

APPENDIX C

CHAPTER 3 TABLES AND FIGURES

Table 5: l^{∞} Error of a Homogeneous Portfolio of 100 Firms

Stepsize	Number of Simulations	l^{∞} Error
0.25	10000	0.0657
0.01	10000	0.0022
0.001	10000	0.003
0.25	50000	0.0727
0.01	50000	0.0031
0.001	50000	0.0014

Table 6: l^{∞} Error of a Heterogeneous Portfolio of Two Firms

ρ_1	Stepsize	Number of Simulations	l^{∞} Error
0.1	0.25	10000	0.0097
0.1	0.01	10000	0.0091
0.1	0.25	50000	0.0072
0.1	0.01	50000	0.004
0.5	0.25	10000	0.0141
0.5	0.01	10000	0.01
0.5	0.25	50000	0.0065
0.5	0.01	50000	0.0046
0.9	0.25	10000	0.0164
0.9	0.01	10000	0.008
0.9	0.25	50000	0.0091
0.9	0.01	50000	0.0041

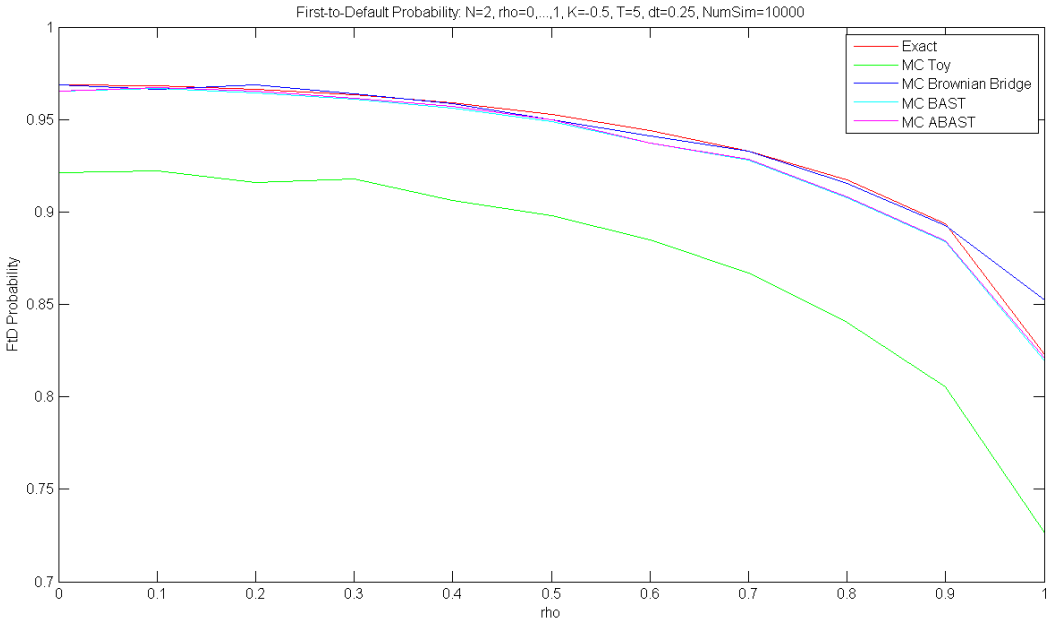

Figure 10: First-to-Default Probability in the Toy Model for Two Firms with $K = -0.5$, $\delta t = 0.25$ and $NumSim = 10000$

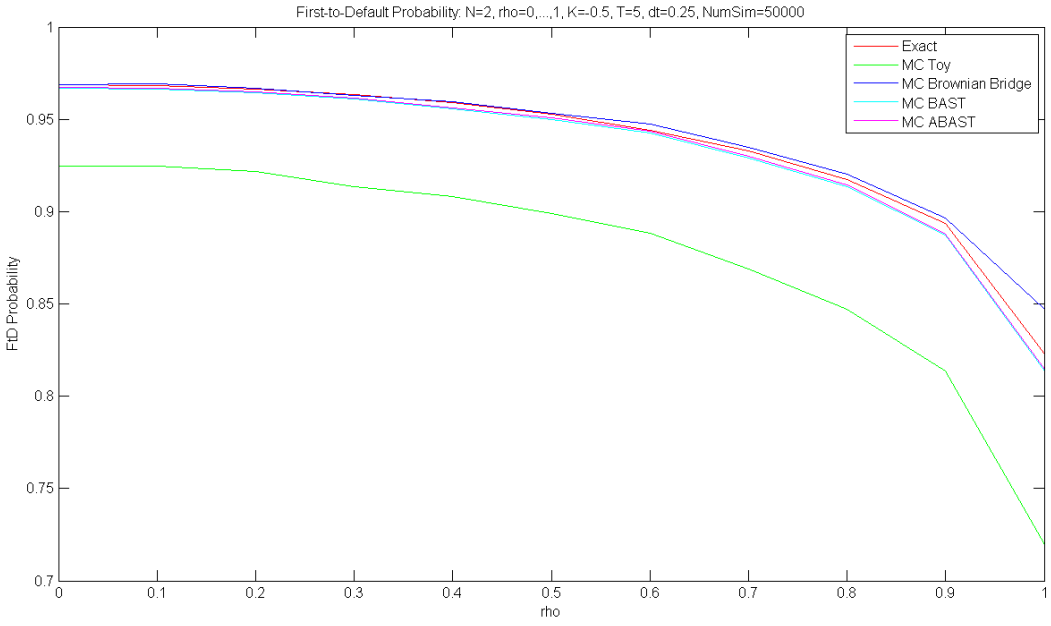

Figure 11: First-to-Default Probability in the Toy Model for Two Firms with $K = -0.5$, $\delta t = 0.25$ and $NumSim = 50000$

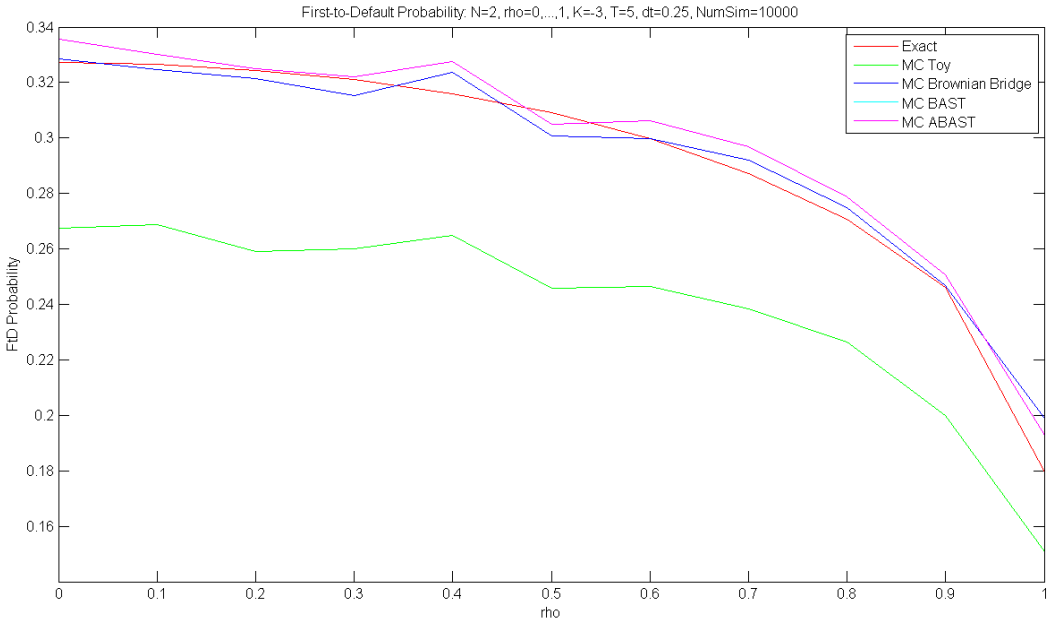

Figure 12: First-to-Default Probability in the Toy Model for Two Firms with $K = -3$, $\delta t = 0.25$ and $NumSim = 10000$

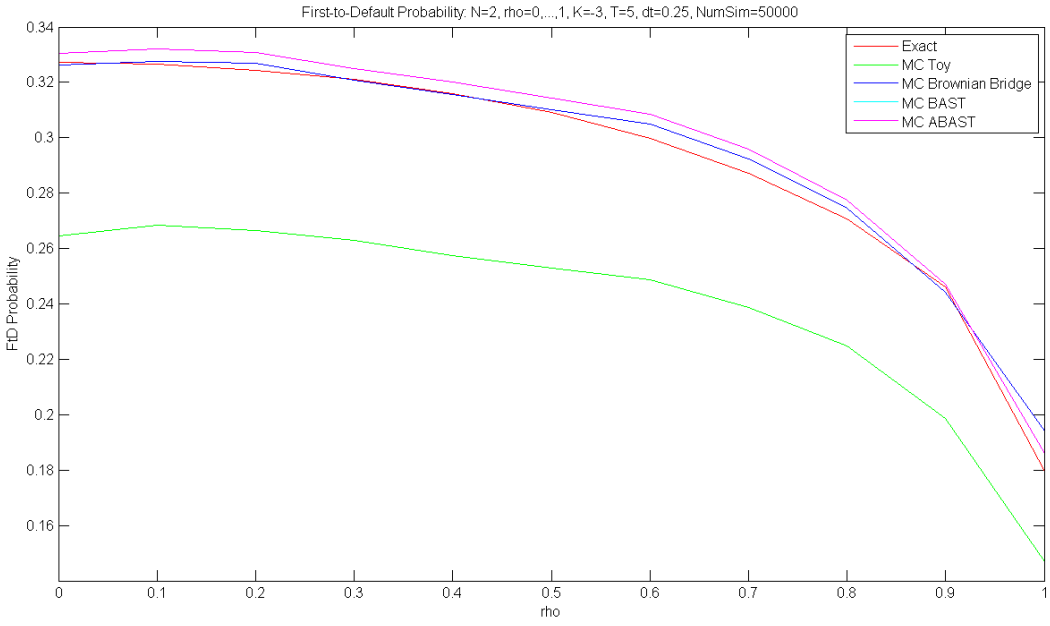

Figure 13: First-to-Default Probability in the Toy Model for Two Firms with $K = -3$, $\delta t = 0.25$ and $NumSim = 50000$

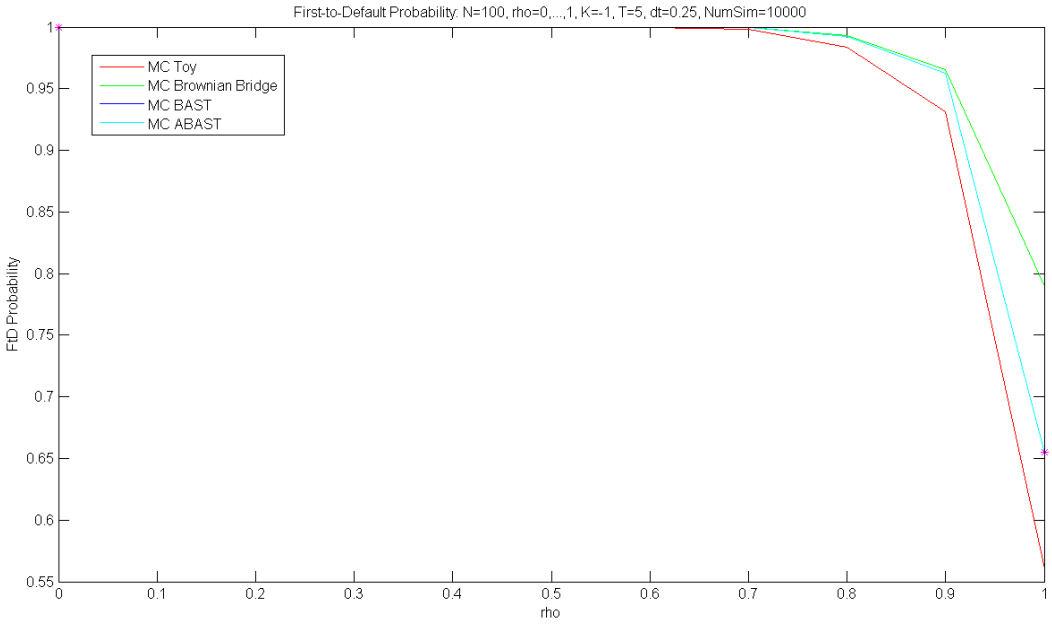

Figure 14: First-to-Default Probability in the Toy Model for Homogeneous Portfolio with $K = -1$, $\delta t = 0.25$ and $NumSim = 10000$

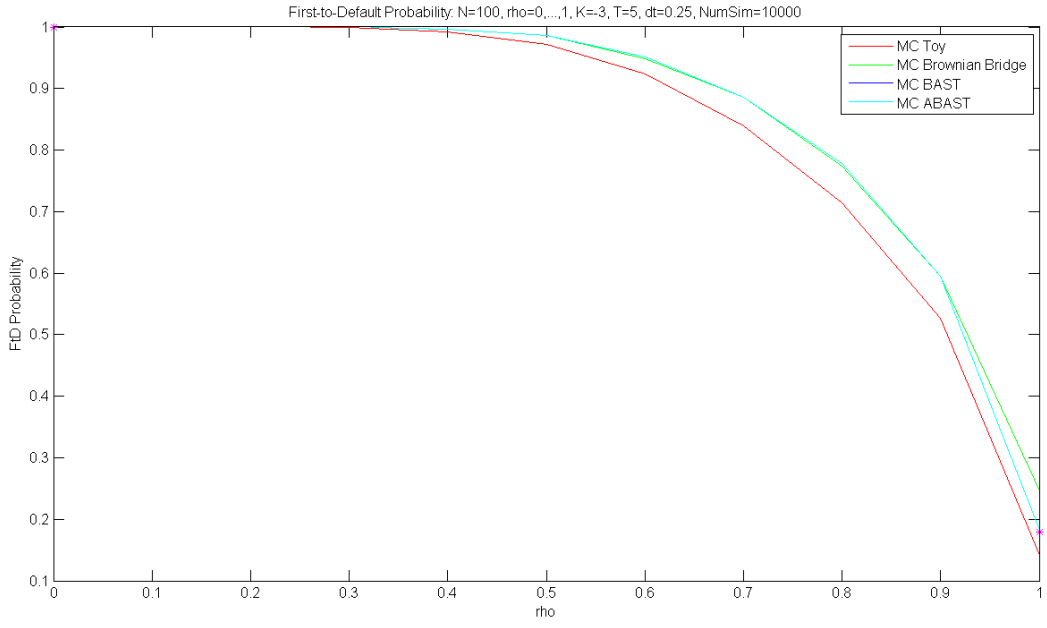

Figure 15: First-to-Default Probability in the Toy Model for Homogeneous Portfolio with $K = -3$, $\delta t = 0.25$ and $NumSim = 10000$

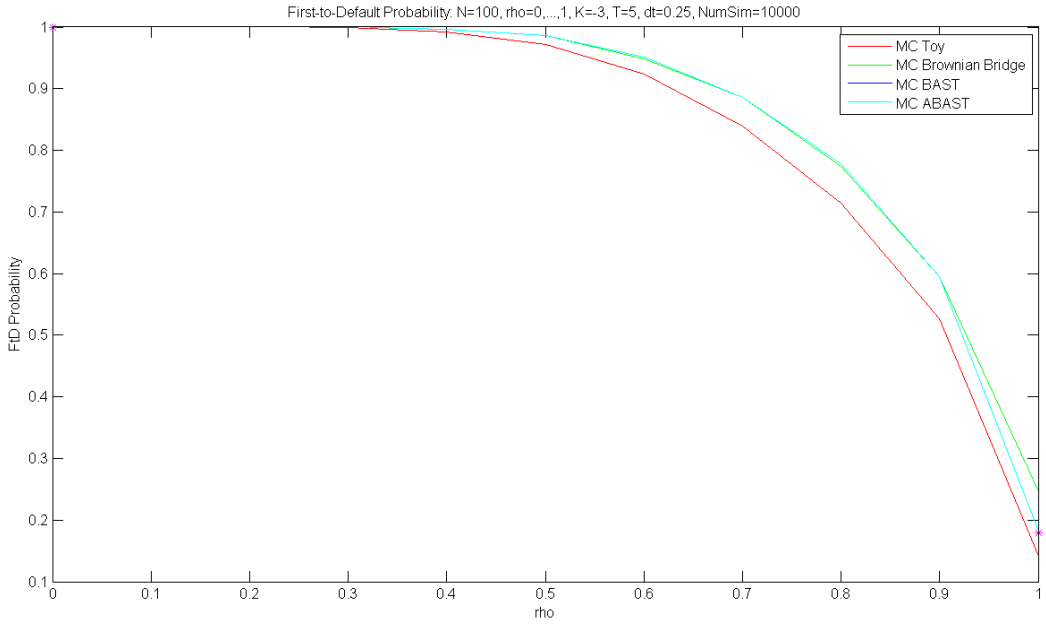

Figure 16: First-to-Default Probability in the Toy Model for Homogeneous Portfolio with $K = -3$, $\delta t = 0.25$ and $NumSim = 10000$

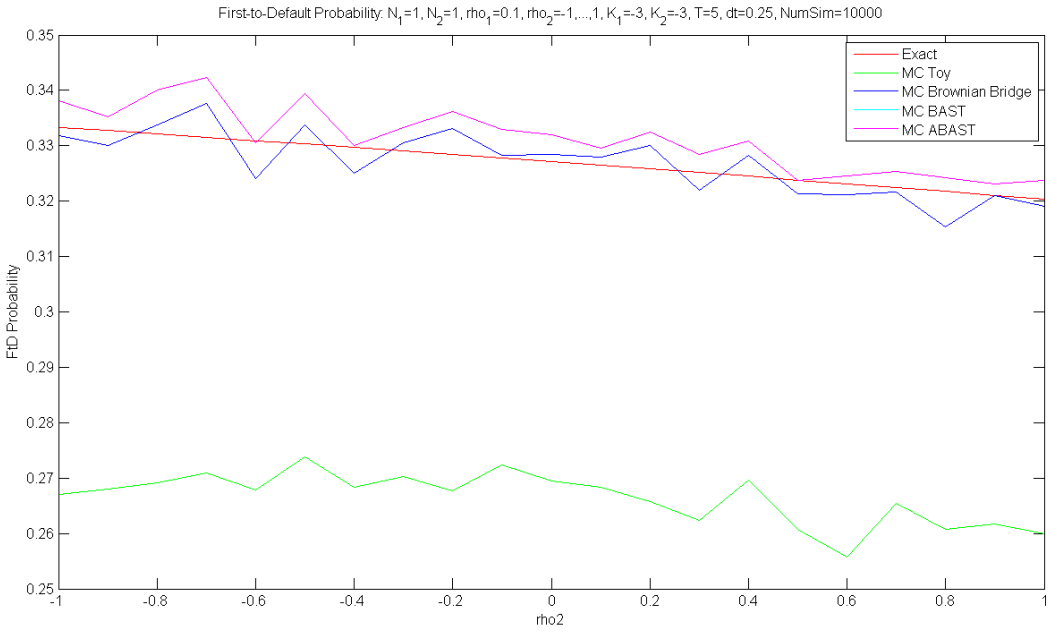

Figure 17: First-to-Default Probability in the Toy Model for Two Firms with $K = -3$, $\rho_1 = 0.1$, $\delta t = 0.25$ and $NumSim = 10000$

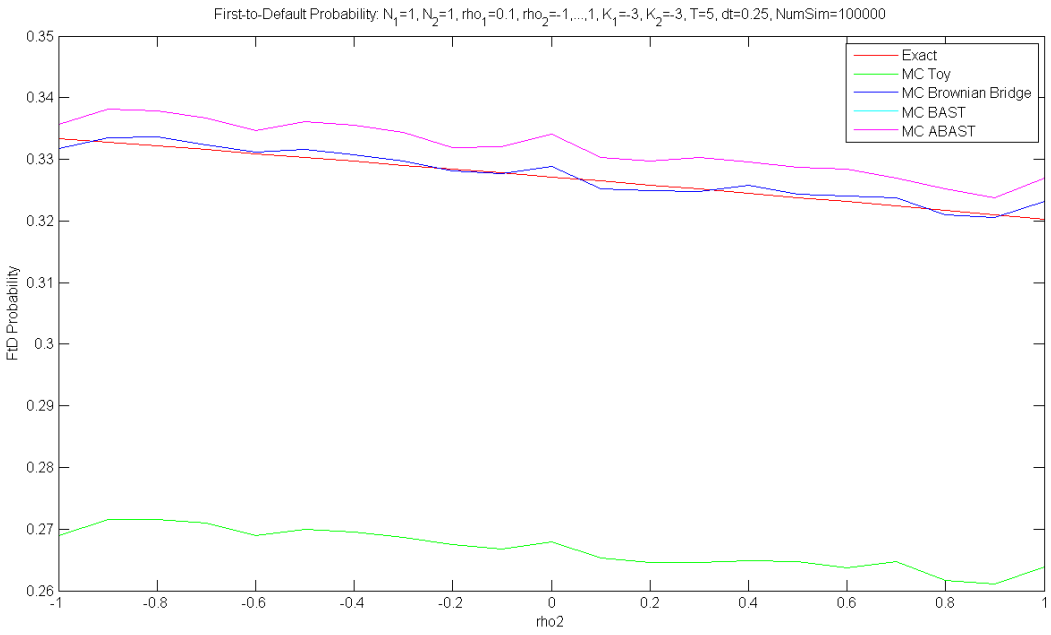

Figure 18: First-to-Default Probability in the Toy Model for Two Firms with $K = -3$, $\rho_1 = 0.1$, $\delta t = 0.25$ and $NumSim = 100000$

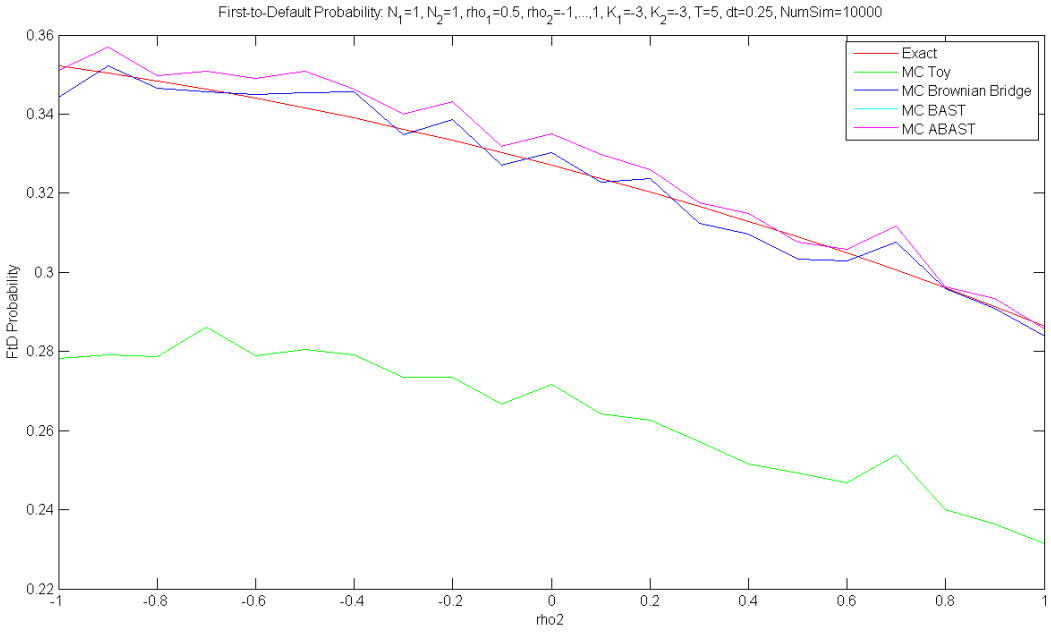

Figure 19: First-to-Default Probability in the Toy Model for Two Firms with $K = -3$, $\rho_1 = 0.5$, $\delta t = 0.25$ and $NumSim = 10000$

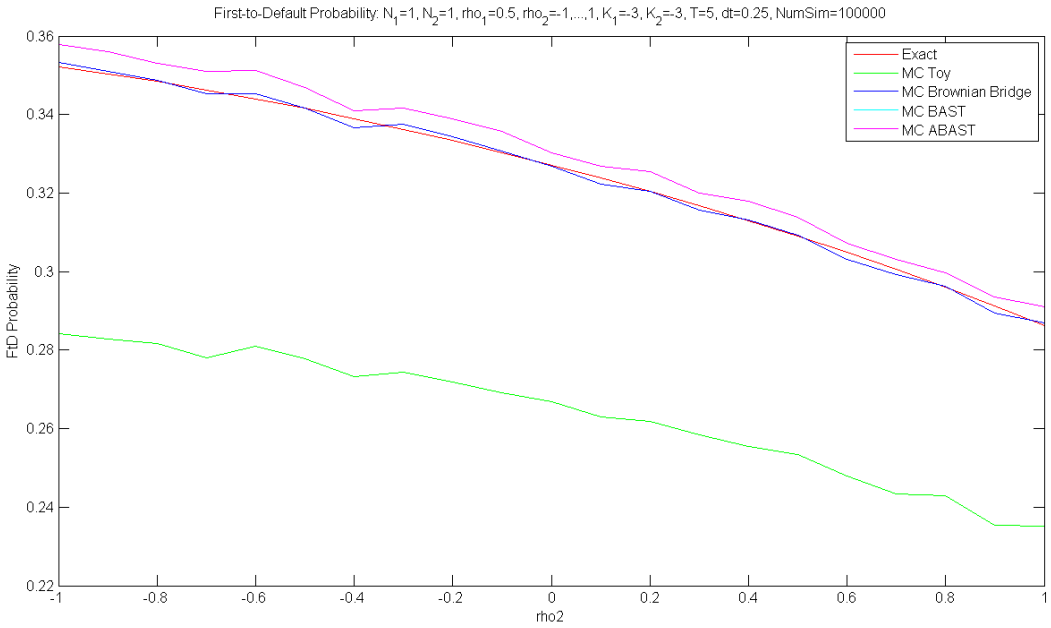

Figure 20: First-to-Default Probability in the Toy Model for Two Firms with $K = -3$, $\rho_1 = 0.5$, $\delta t = 0.25$ and $NumSim = 100000$

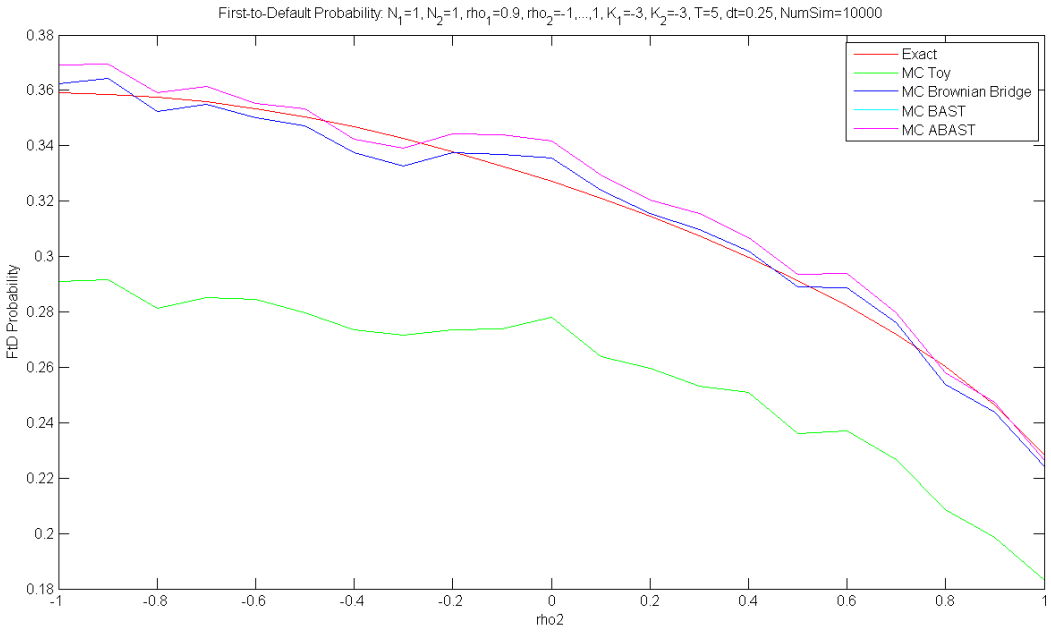

Figure 21: First-to-Default Probability in the Toy Model for Two Firms with $K = -3$, $\rho_1 = 0.9$, $\delta t = 0.25$ and $NumSim = 10000$

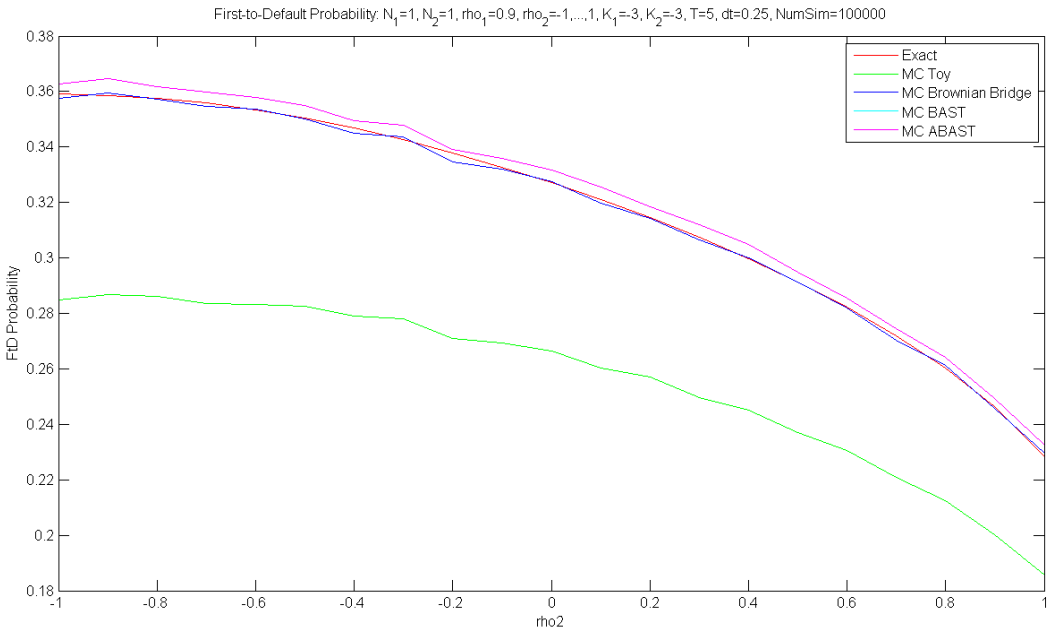

Figure 22: First-to-Default Probability in the Toy Model for Two Firms with $K = -3$, $\rho_1 = 0.9$, $\delta t = 0.25$ and $NumSim = 100000$

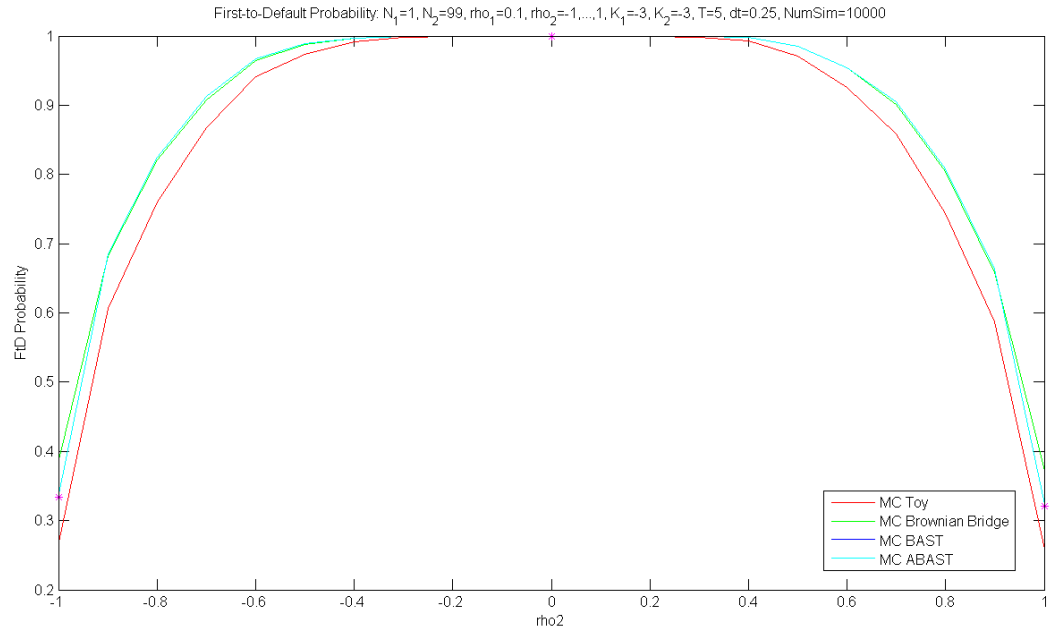

Figure 23: First-to-Default Probability in the Toy Model for Two-Sector Portfolio with $N_1 = 1$, $N_2 = 99$, $K = -3$, $\rho_1 = 0.1$, $\delta t = 0.25$ and $NumSim = 10000$

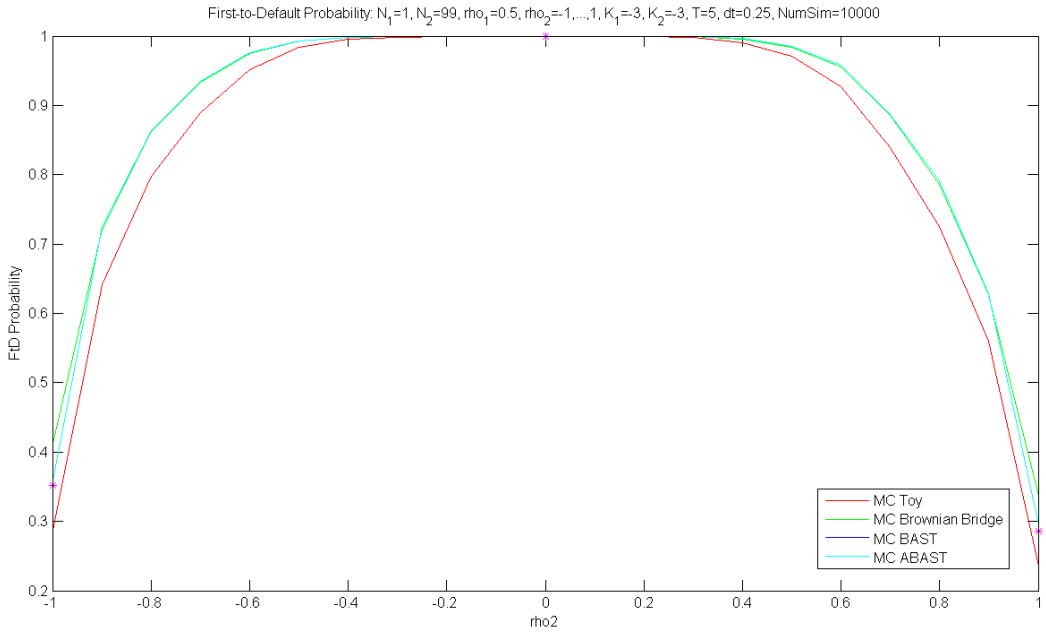

Figure 24: First-to-Default Probability in the Toy Model for Two-Sector Portfolio with $N_1 = 1$, $N_2 = 99$, $K = -3$, $\rho_1 = 0.5$, $\delta t = 0.25$ and $NumSim = 10000$

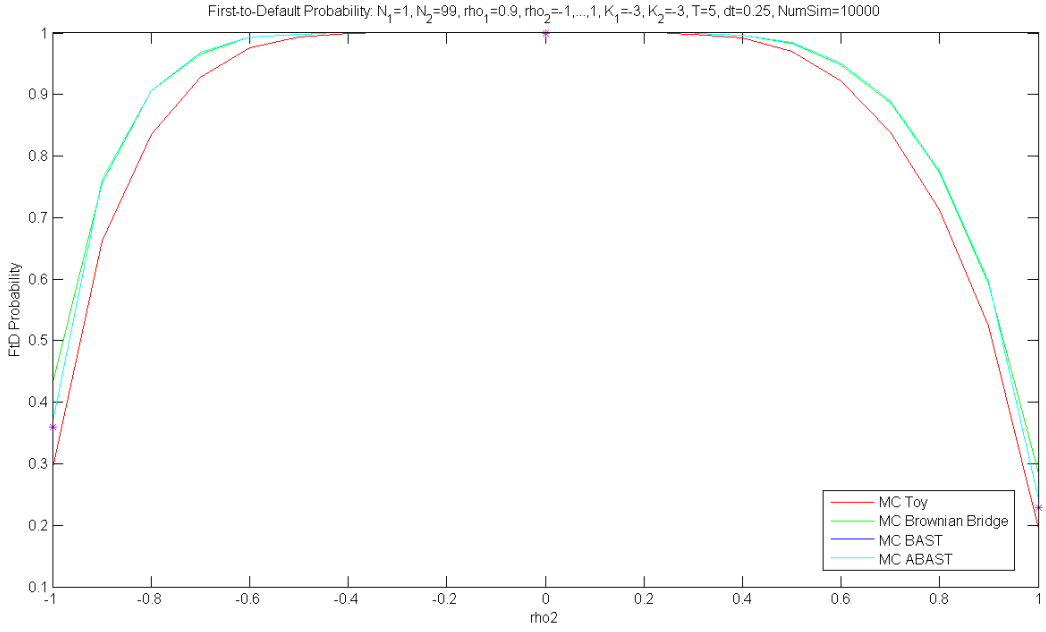

Figure 25: First-to-Default Probability in the Toy Model for Two-Sector Portfolio with $N_1 = 1$, $N_2 = 99$, $K = -3$, $\rho_1 = 0.9$, $\delta t = 0.25$ and $NumSim = 10000$

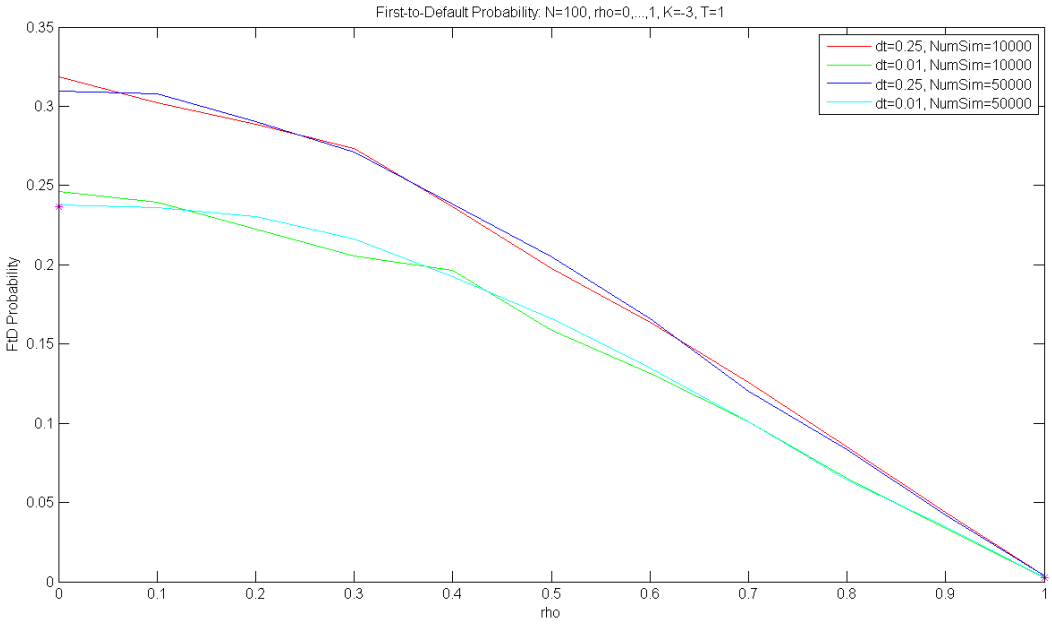

Figure 26: First-to-Default Probability in the Toy Model for Homogeneous Portfolio with $\delta t = 0.25, 0.01$ and $NumSim = 10000, 50000$

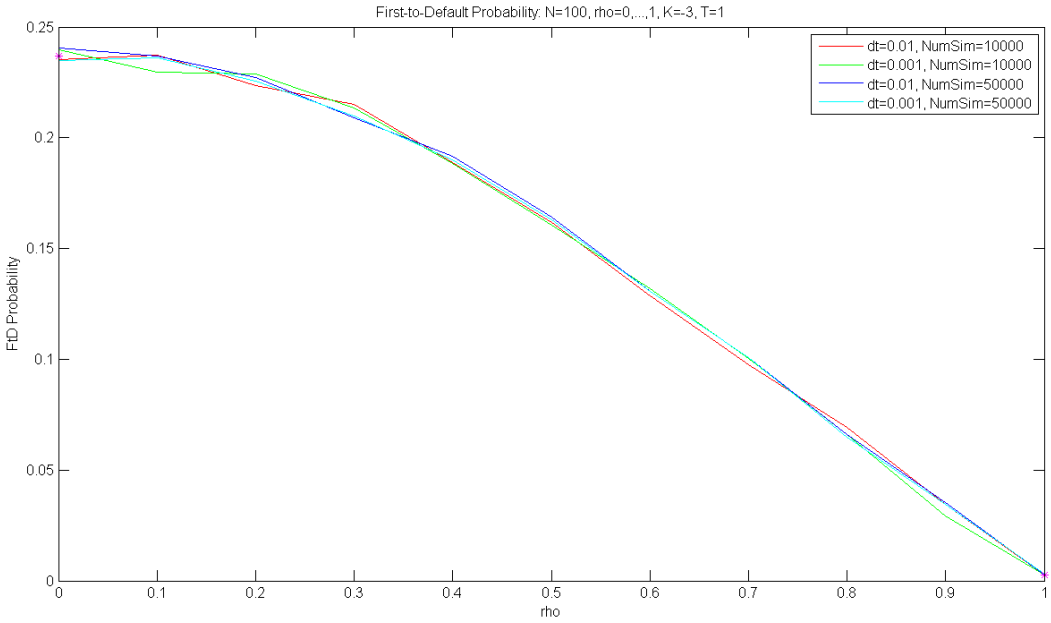

Figure 27: First-to-Default Probability in the Toy Model for Homogeneous Portfolio with $\delta t = 0.01, 0.001$ and $NumSim = 10000, 50000$

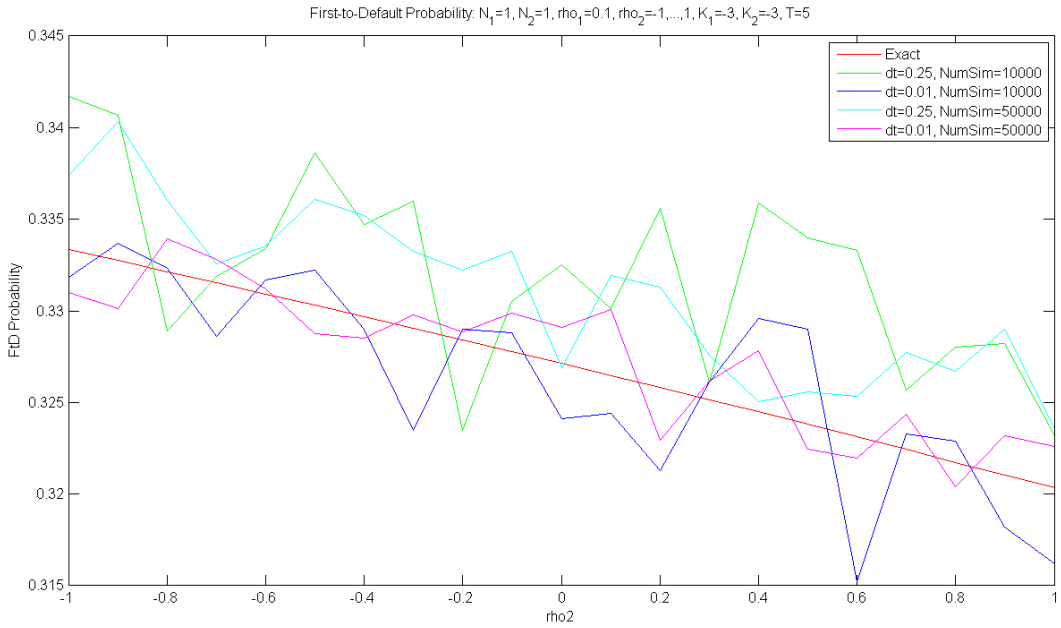

Figure 28: First-to-Default Probability in the Toy Model for Two Firms with $\rho_1 = 0.1$, $\delta t = 0.25, 0.01$ and $NumSim = 10000, 50000$

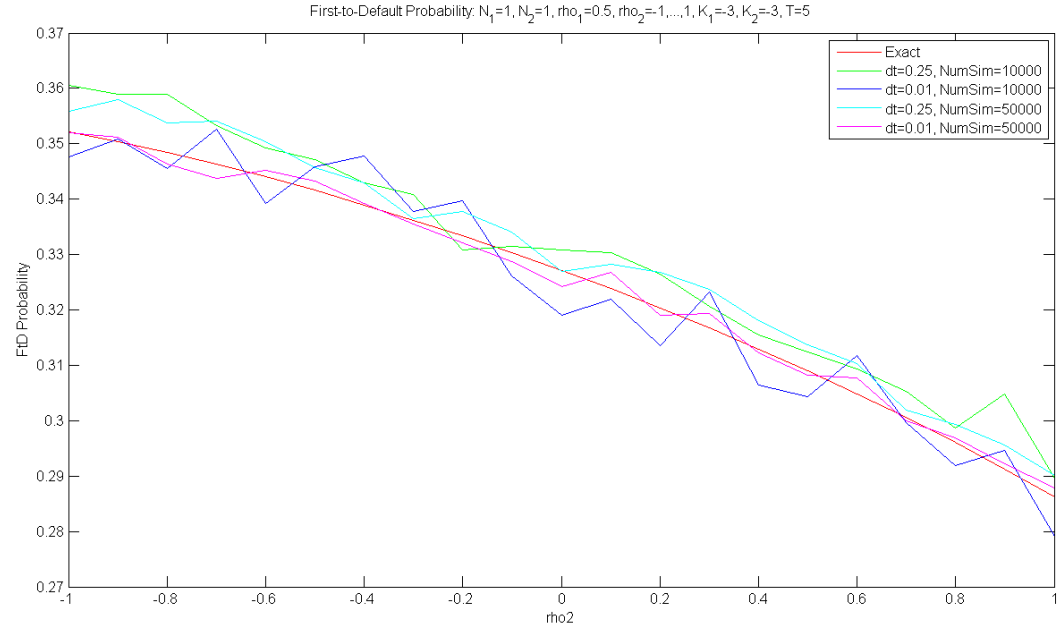

Figure 29: First-to-Default Probability in the Toy Model for Two Firms with $\rho_1 = 0.5$, $\delta t = 0.25, 0.01$ and $NumSim = 10000, 50000$

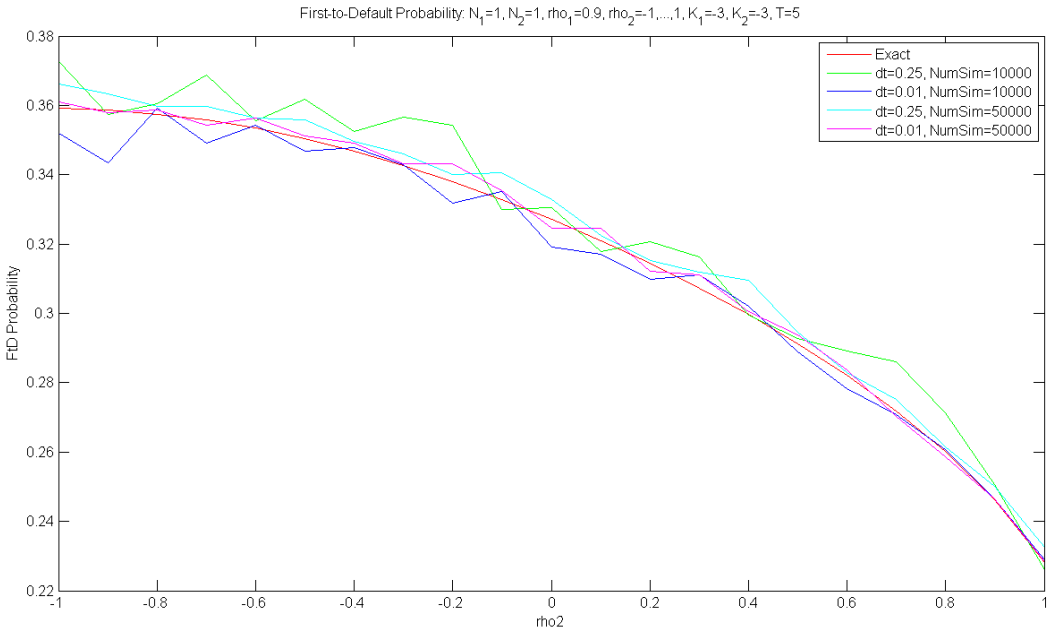

Figure 30: First-to-Default Probability in the Toy Model for Two Firms with $\rho_1 = 0.9$, $\delta t = 0.25, 0.01$ and $NumSim = 10000, 50000$

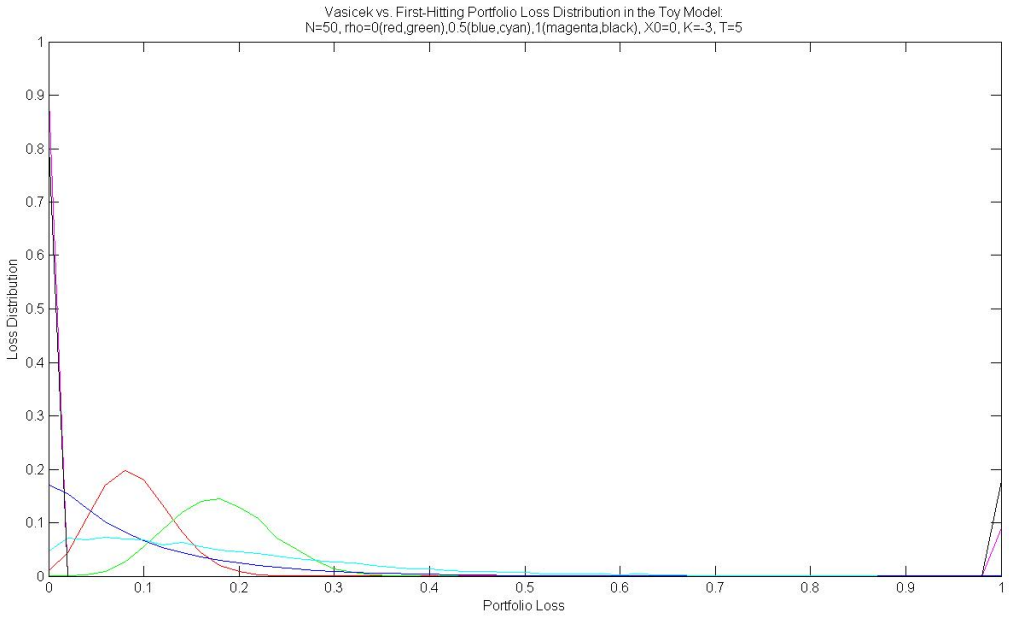

Figure 31: Loss Distribution in the Toy Model for Homogeneous Portfolio with Different Values of ρ

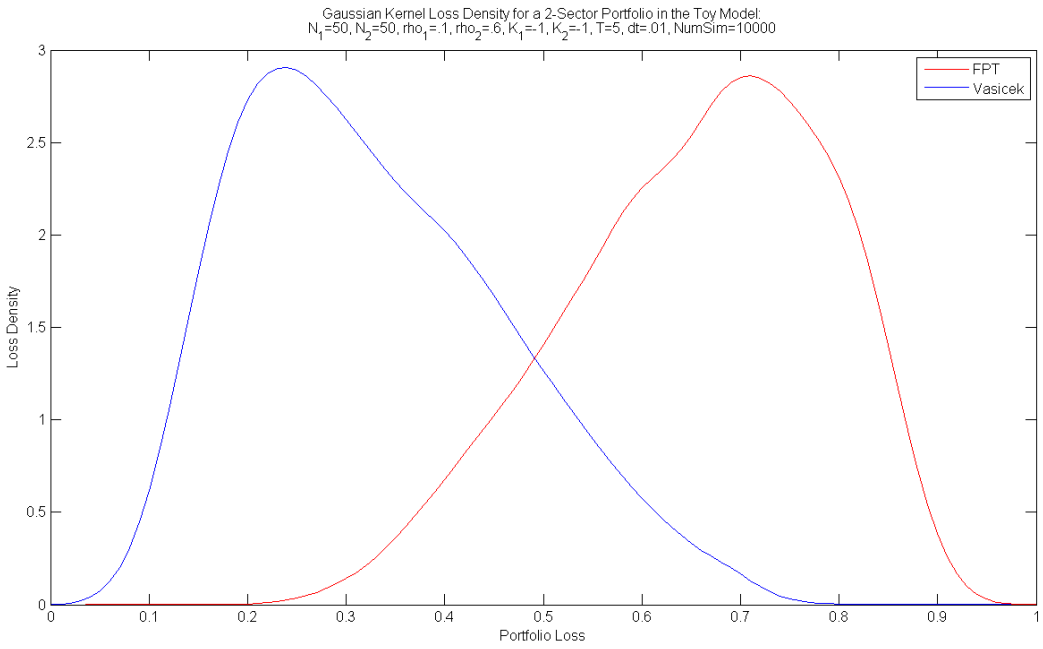

Figure 32: MC Loss PDF in the Toy Model for Two-Sector Portfolio with $\rho_1 = 0.1$ and $\rho_2 = 0.6$

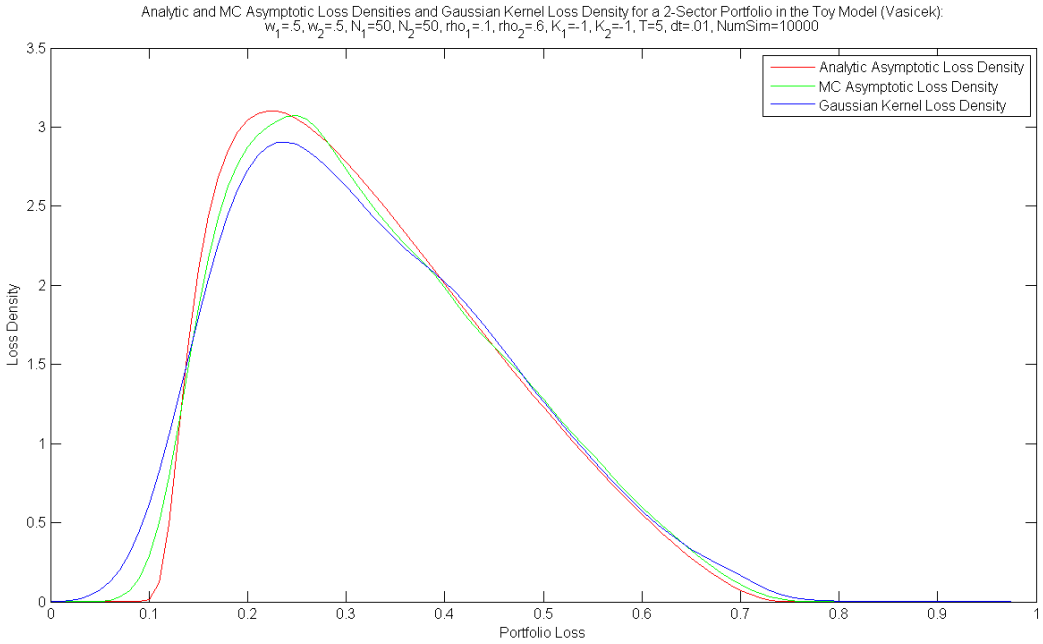

Figure 33: MC vs. Asymptotic Loss PDF in the Toy Model for Two-Sector Portfolio with $\rho_1 = 0.1$ and $\rho_2 = 0.6$

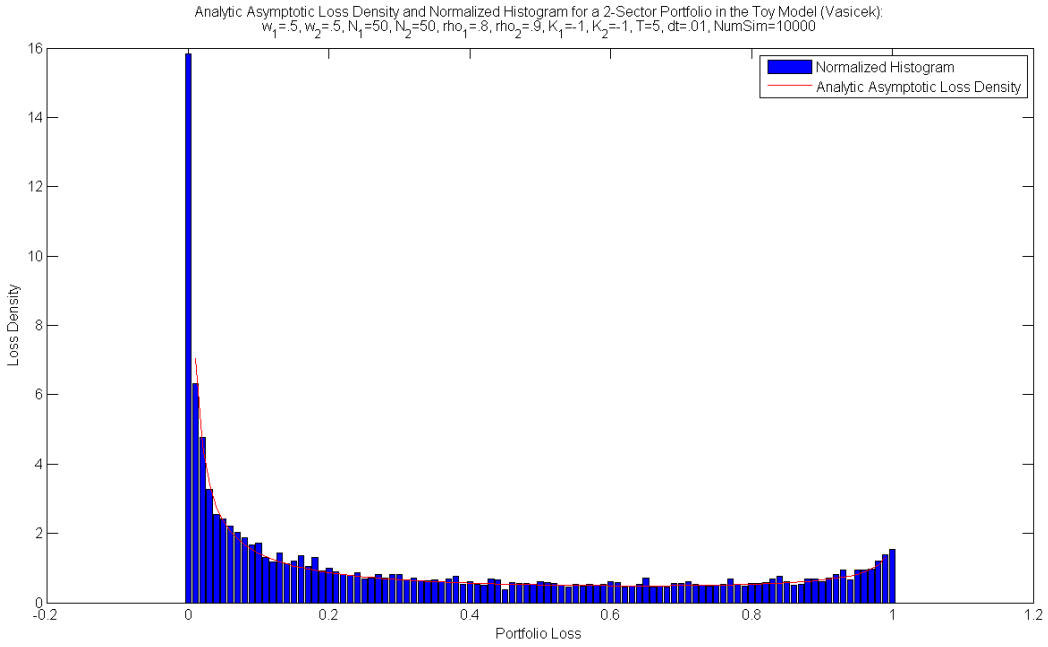

Figure 34: MC vs. Asymptotic Loss PDF in the Toy Model for Two-Sector Portfolio with $\rho_1 = 0.8$ and $\rho_2 = 0.9$

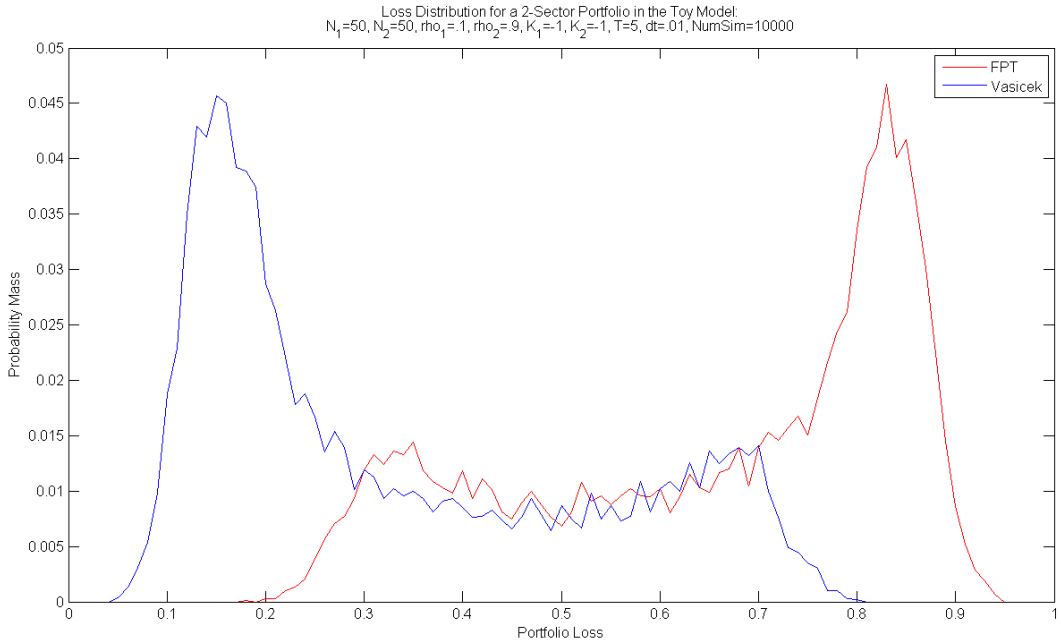

Figure 35: MC Loss Distribution in the Toy Model for Two-Sector Portfolio with $\rho_1 = 0.1$ and $\rho_2 = 0.9$

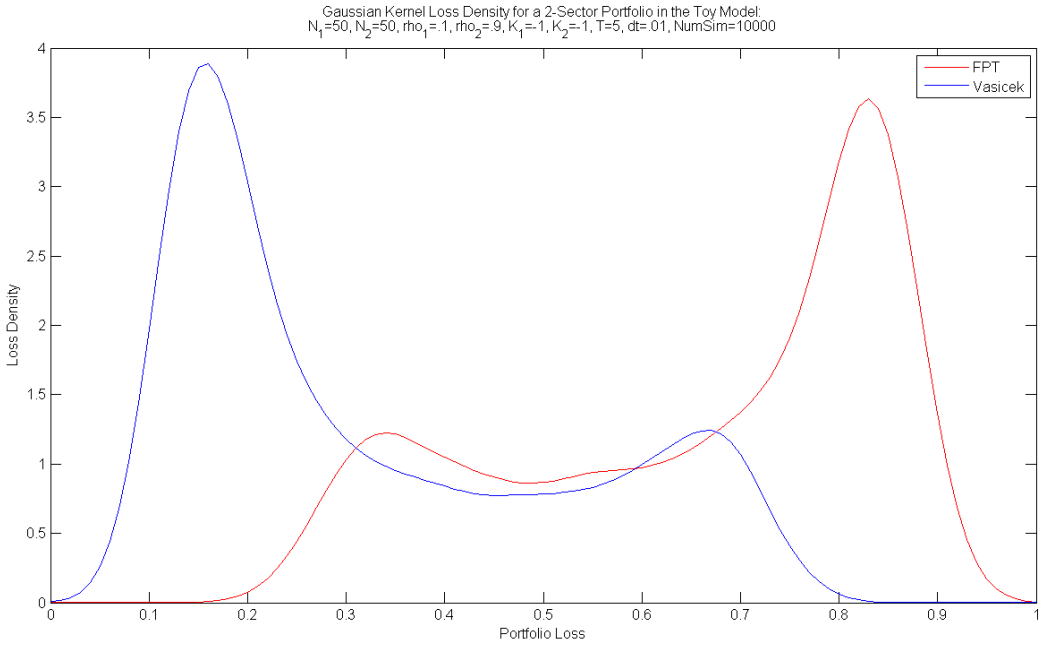

Figure 36: MC Loss PDF in the Toy Model for Two-Sector Portfolio with $\rho_1 = 0.1$ and $\rho_2 = 0.9$

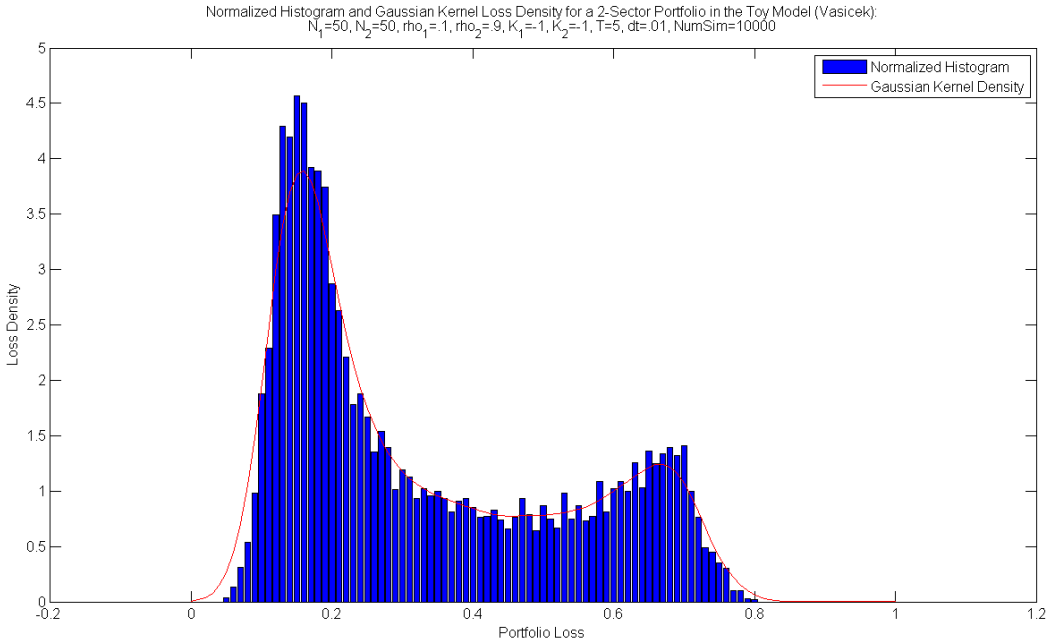

Figure 37: Histogram vs. Kernel PDF in the Toy Model for Two-Sector Portfolio with $\rho_1 = 0.1$ and $\rho_2 = 0.9$

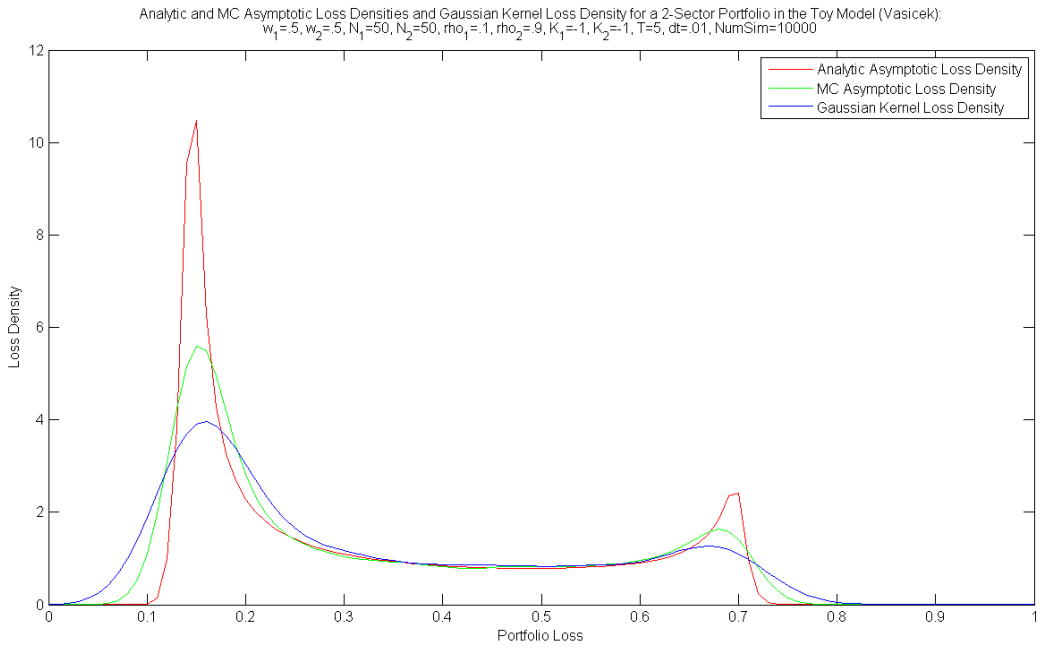

Figure 38: MC vs. Asymptotic Loss PDF in the Toy Model for Two-Sector Portfolio with $\rho_1 = 0.1$ and $\rho_2 = 0.9$

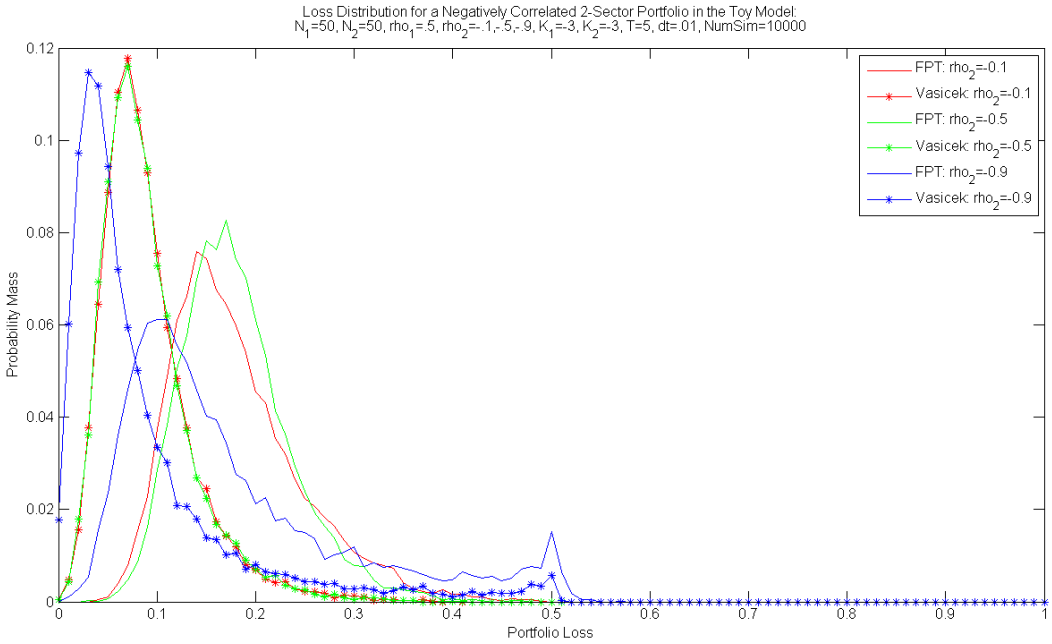

Figure 39: MC Loss Distribution in the Toy Model for Two-Sector Portfolio with $\rho_1 = 0.5$ and $\rho_2 = -0.1, -0.5, -0.9$

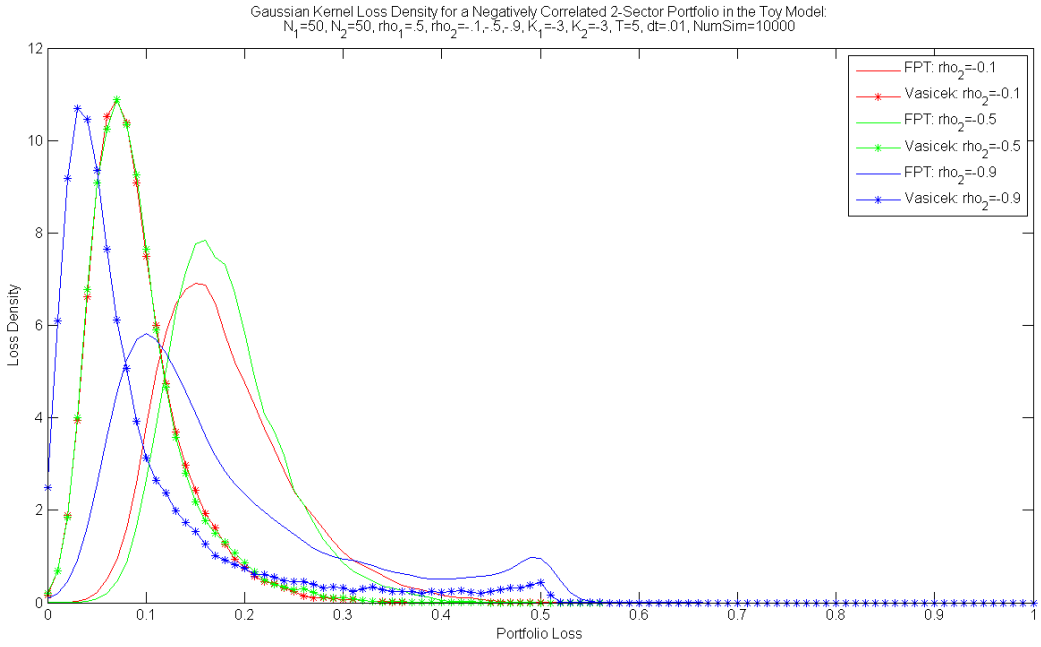

Figure 40: MC Loss PDF in the Toy Model for Two-Sector Portfolio with $\rho_1 = 0.5$ and $\rho_2 = -0.1, -0.5, -0.9$

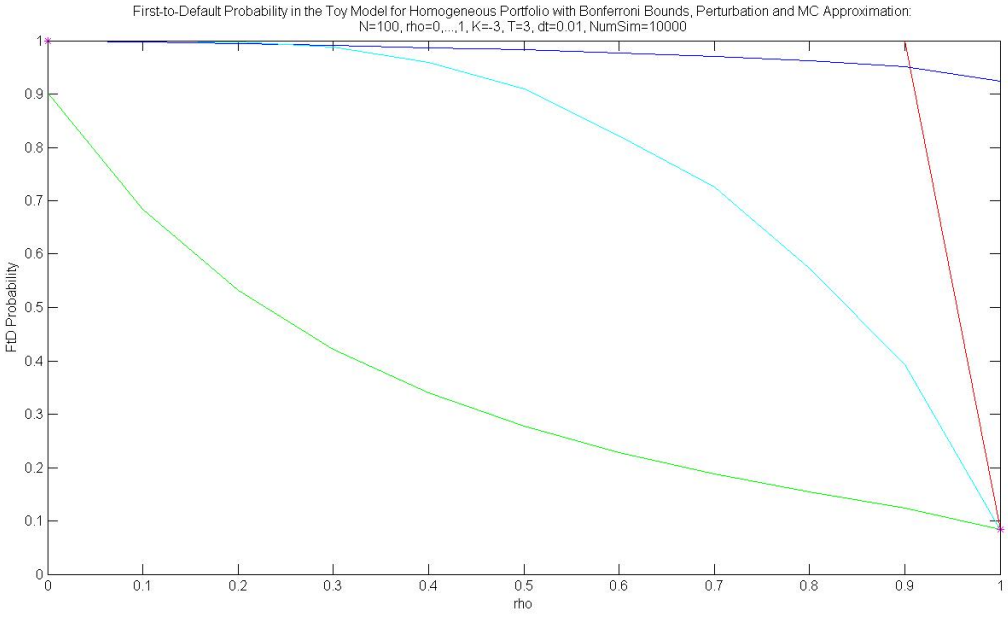

Figure 41: MC vs. Perturbation vs. Bonferroni in the Toy Model for Homogeneous Portfolio

APPENDIX D

CHAPTER 4 TABLES AND FIGURES

Table 7: Computational Time (in seconds) of Loss Distribution in the Arcsin Drift Model - Combinatorial Formula vs. Recursive Algorithm

Number of Sectors	Combinatorial Formula	Recursive Algorithm
1	1.490528	0.134404
2	30.850787	0.199113
3	1604.200699	0.349201

Table 8: Total Mass of Loss Distribution in the Arcsin Drift Model - Combinatorial Formula vs. Recursive Algorithm

Number of Sectors	Combinatorial Formula	Recursive Algorithm
1	1.0006	1.0001
2	1.0031	1.0002
3	1.1146	1.0002

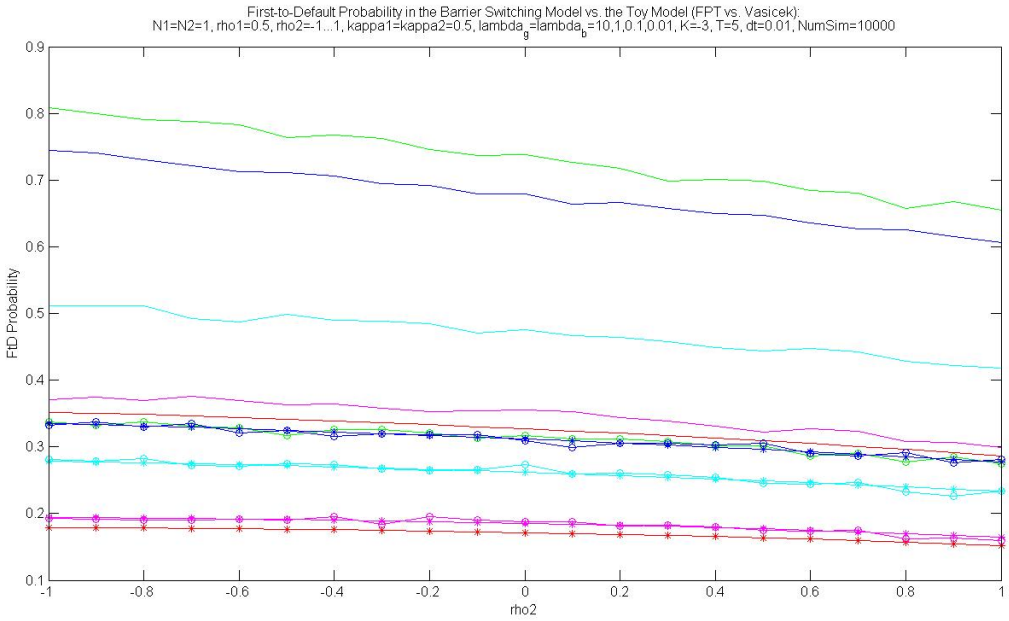

Figure 42: First-to-Default Probability in the Barrier Switching Model for Two Firms with Different Values of $\lambda_g = \lambda_b$

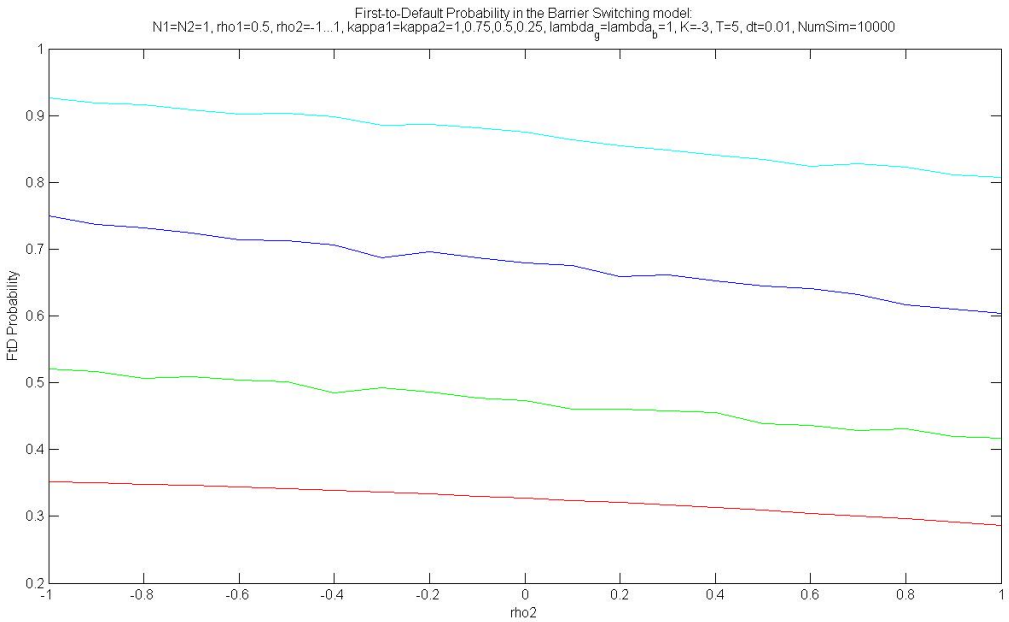

Figure 43: First-to-Default Probability in the Barrier Switching Model for Two Firms with Different Values of $\kappa_1 = \kappa_2$

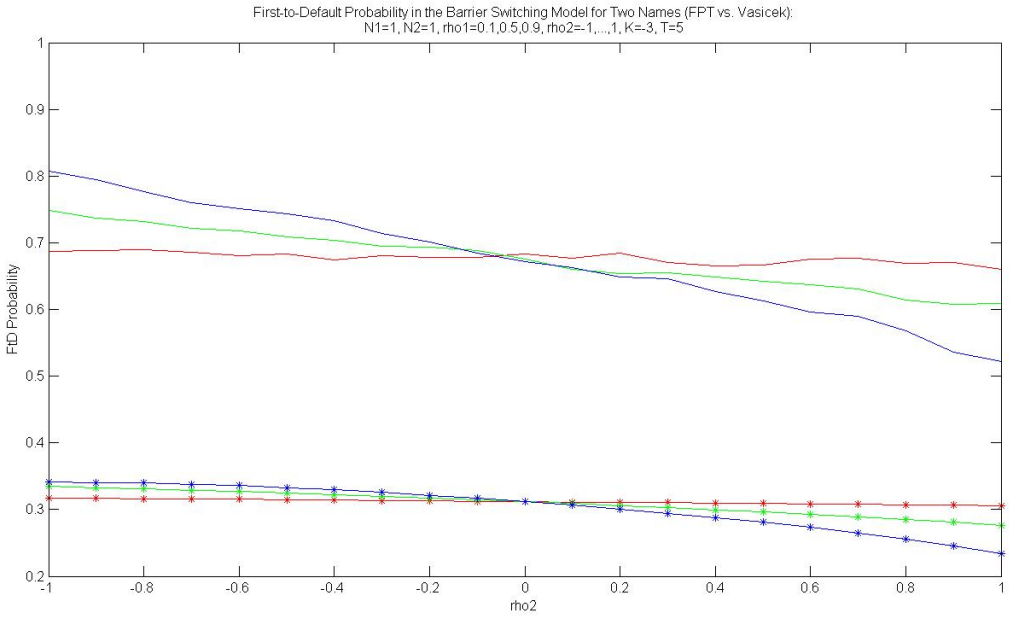

Figure 44: First-to-Default Probability in the Barrier Switching Model for Two Firms with Different Values of ρ_1

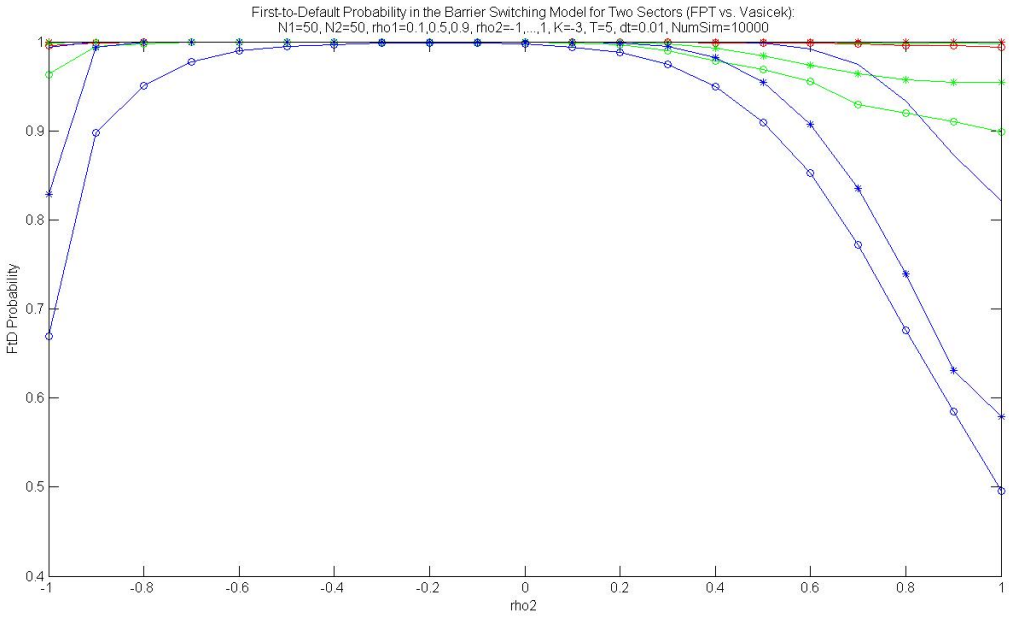

Figure 45: First-to-Default Probability in the Barrier Switching Model for Two-Sector Portfolio with Different Values of ρ_1

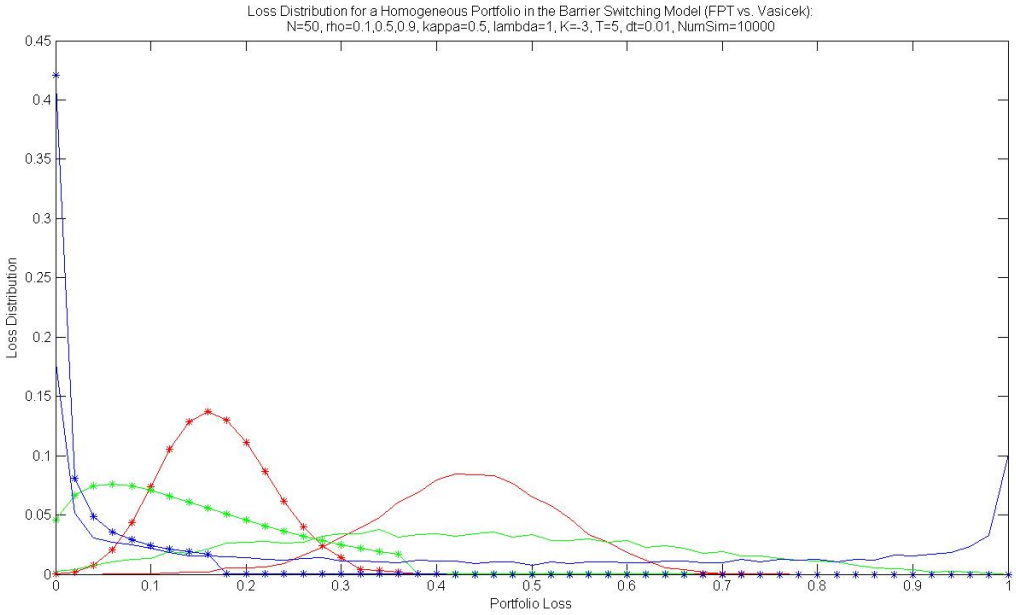

Figure 46: Loss Distribution in the Barrier Switching Model for Homogeneous Portfolio with Different Values of ρ_1

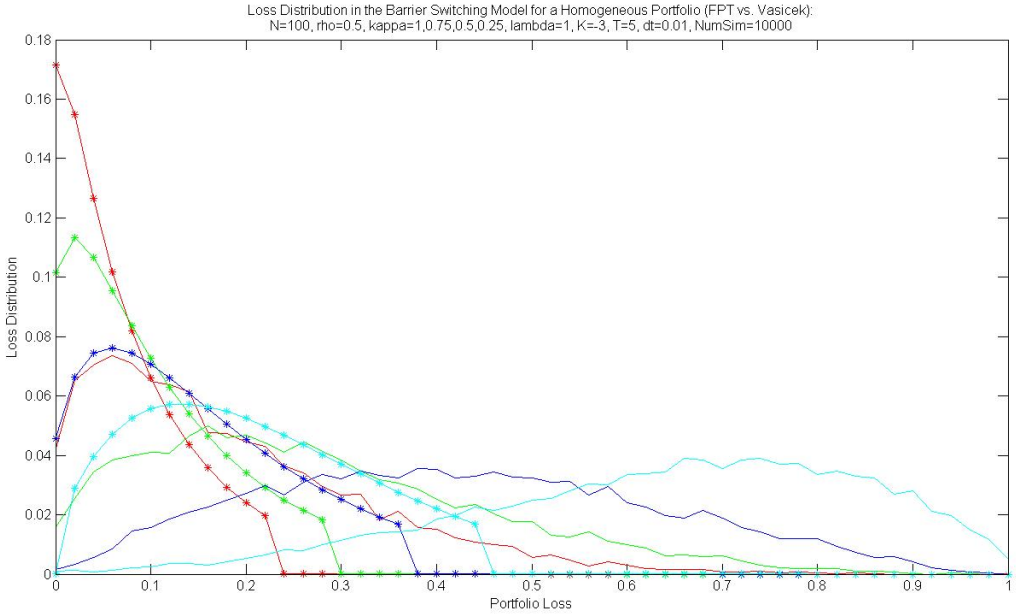

Figure 47: Loss Distribution in the Barrier Switching Model for Homogeneous Portfolio with Different Values of κ

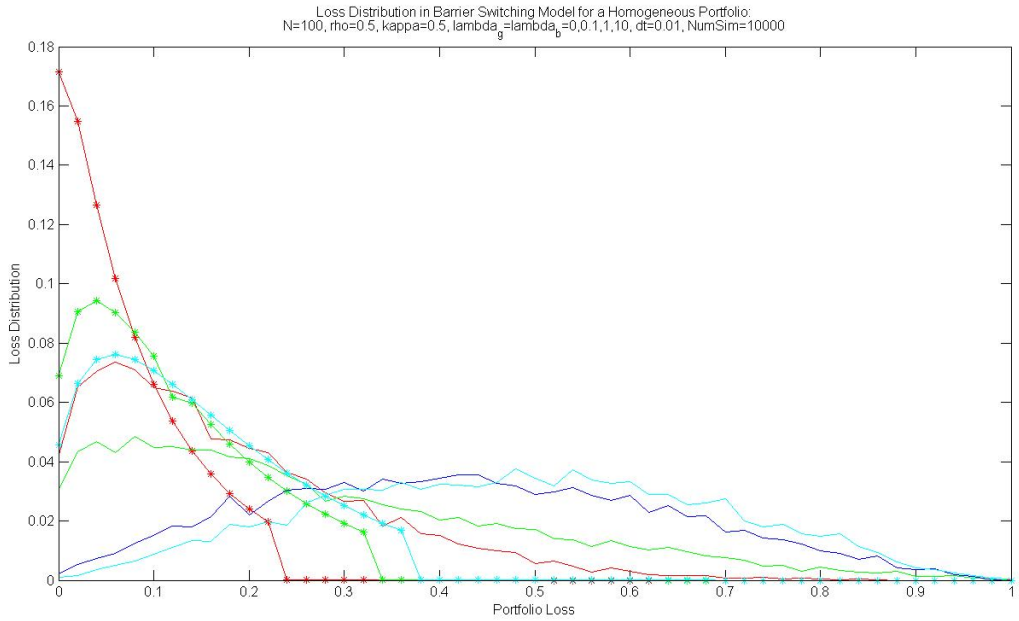

Figure 48: Loss Distribution in the Barrier Switching Model for Homogeneous Portfolio with Different Values of λ

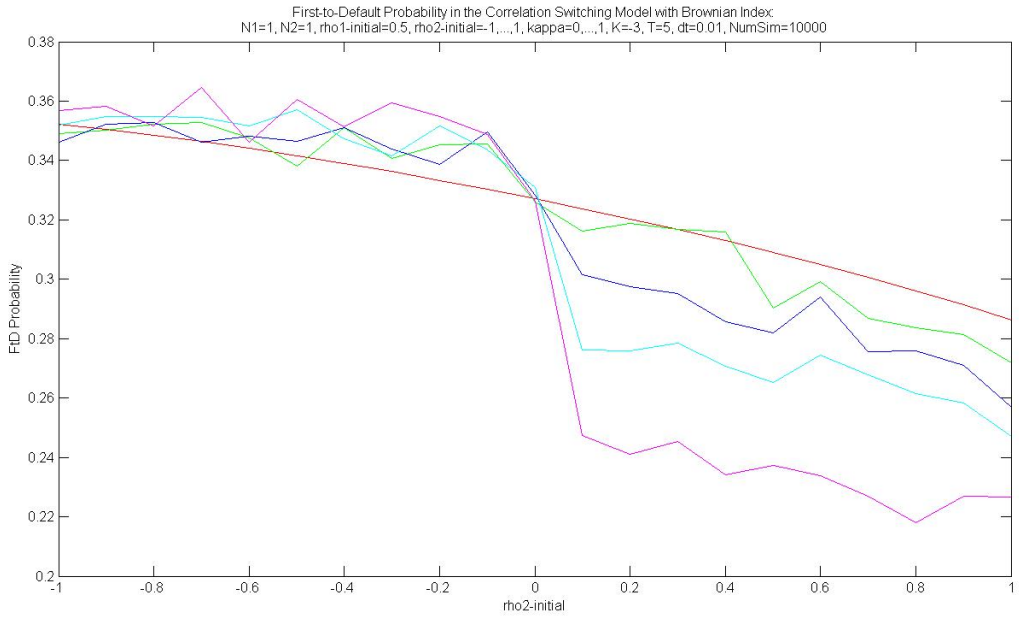

Figure 49: First-to-Default Probability in the Correlation Switching Model with Brownian Market for Two Firms with Different Values of κ

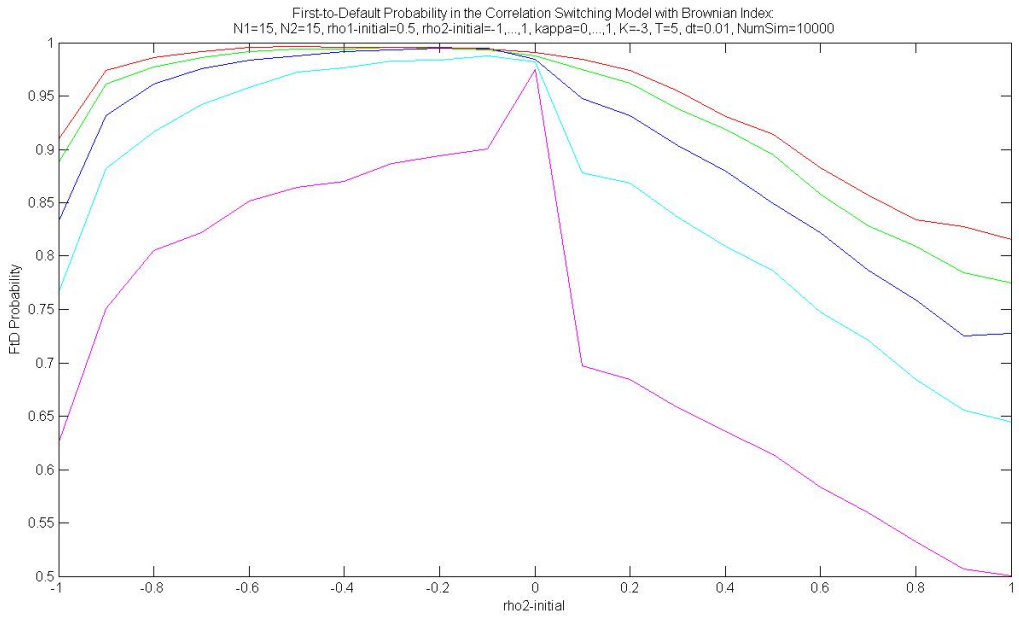

Figure 50: First-to-Default Probability in the Correlation Switching Model with Brownian Market for Two-Sector Portfolio with Different Values of κ

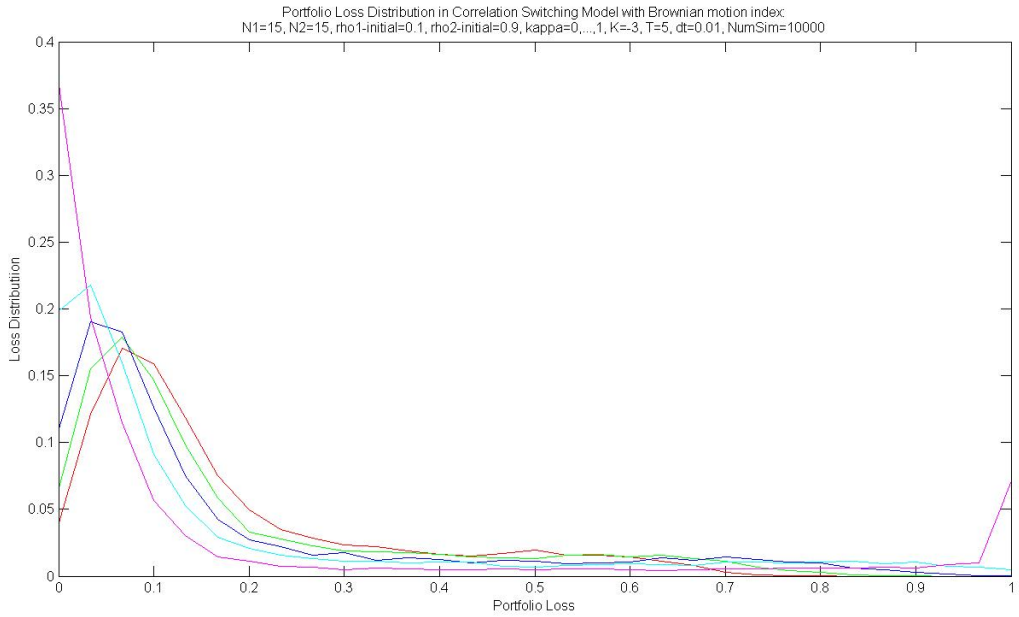

Figure 51: Loss Distribution in the Correlation Switching Model with Brownian Market for Two-Sector Portfolio with Different Values of κ

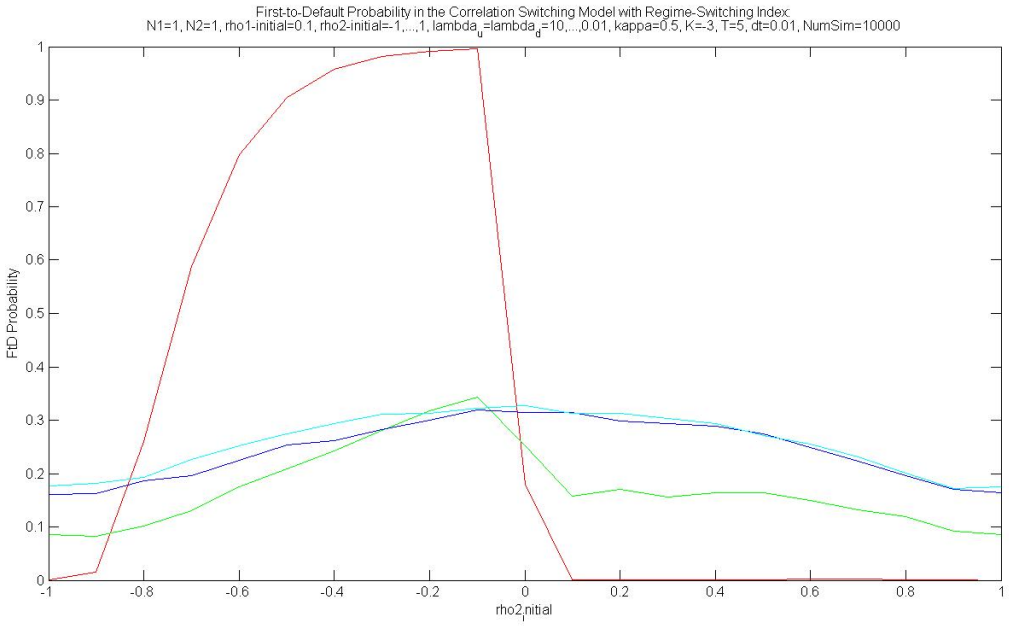

Figure 52: First-to-Default Probability in the Correlation Switching Model with Jump Market for Two Firms with $\rho_1 = 0.1$ and Different Values of $\lambda_u = \lambda_d$

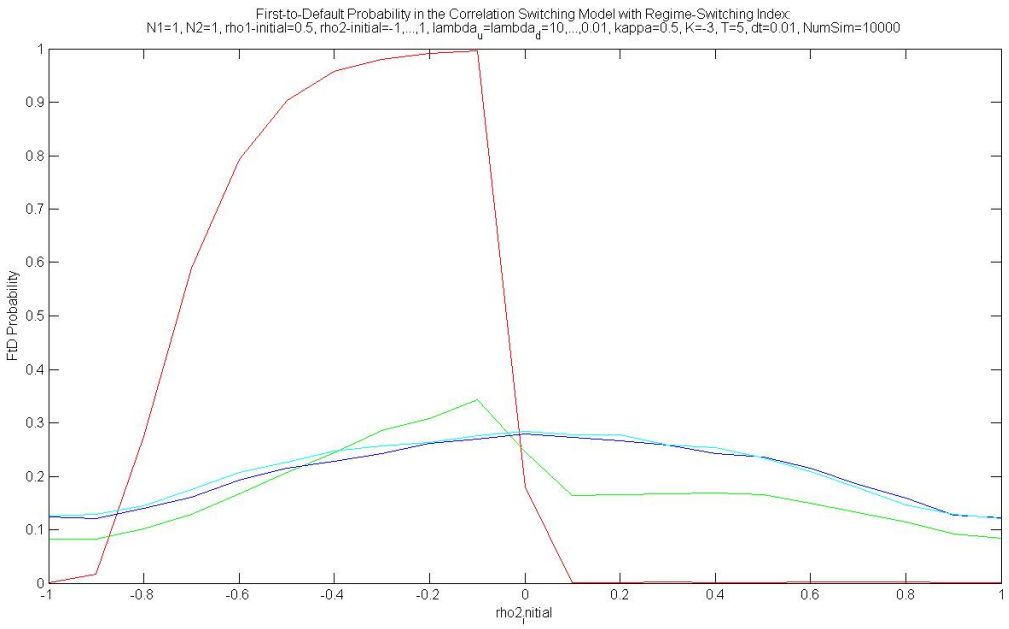

Figure 53: First-to-Default Probability in the Correlation Switching Model with Jump Market for Two Firms with $\rho_1 = 0.5$ and Different Values of $\lambda_u = \lambda_d$

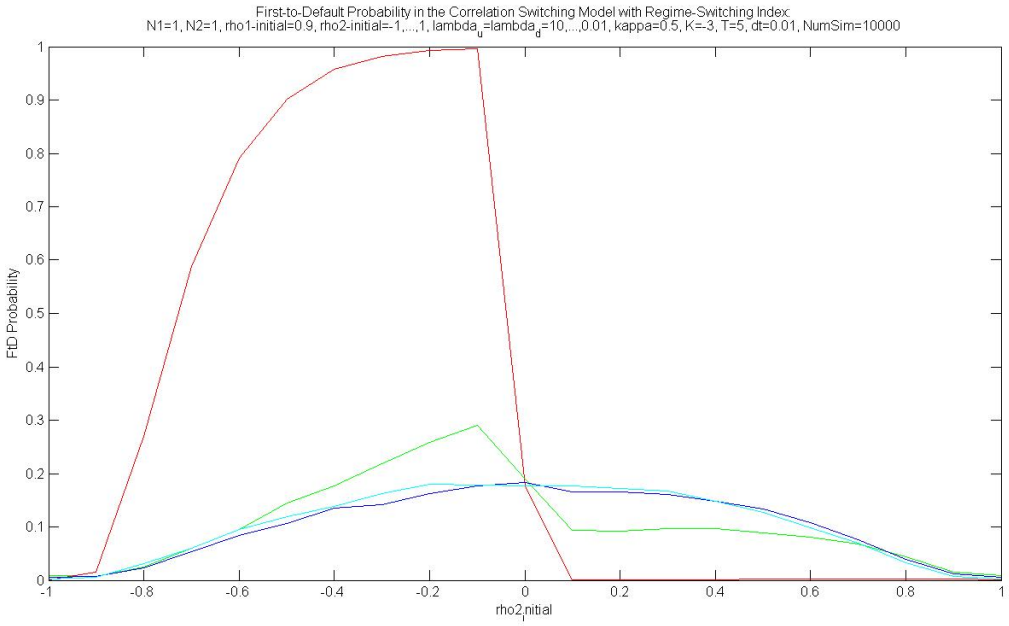

Figure 54: First-to-Default Probability in the Correlation Switching Model with Jump Market for Two Firms with $\rho_1 = 0.9$ and Different Values of $\lambda_u = \lambda_d$

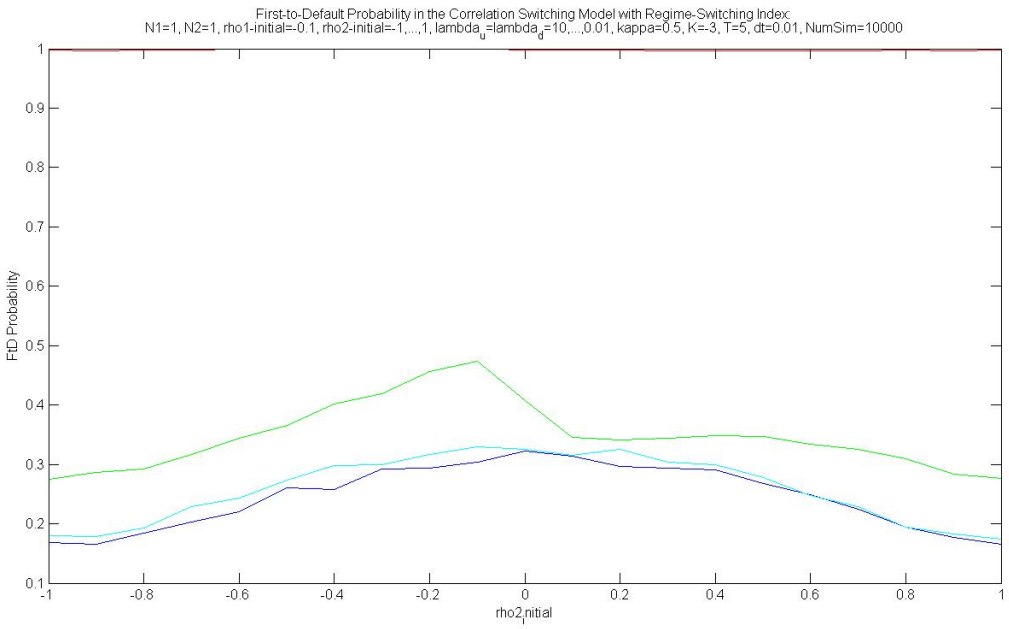

Figure 55: First-to-Default Probability in the Correlation Switching Model with Jump Market for Two Firms with $\rho_1 = -0.1$ and Different Values of $\lambda_u = \lambda_d$

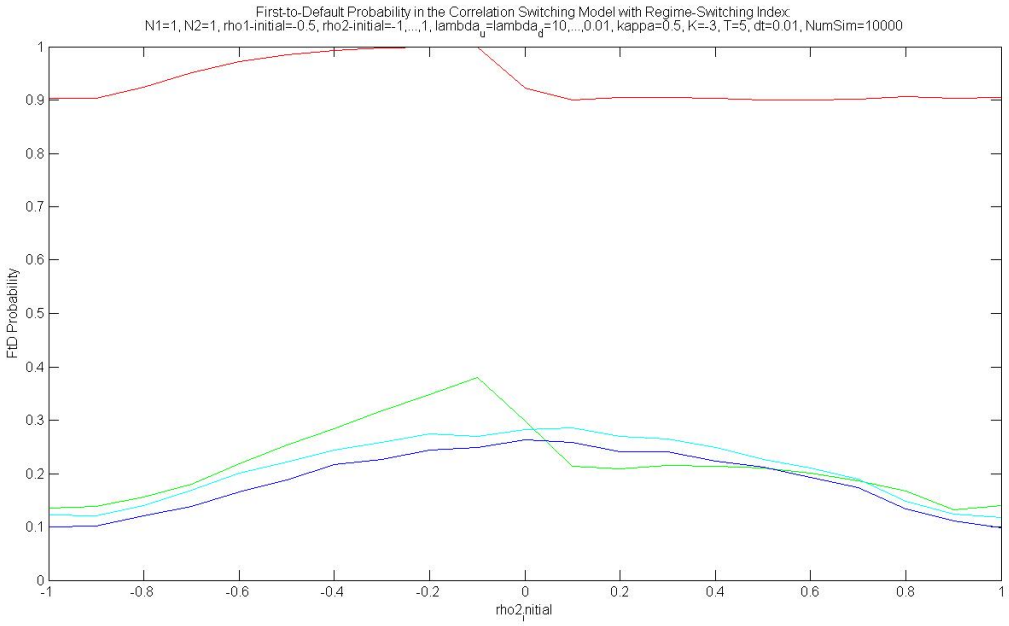

Figure 56: First-to-Default Probability in the Correlation Switching Model with Jump Market for Two Firms with $\rho_1 = -0.5$ and Different Values of $\lambda_u = \lambda_d$

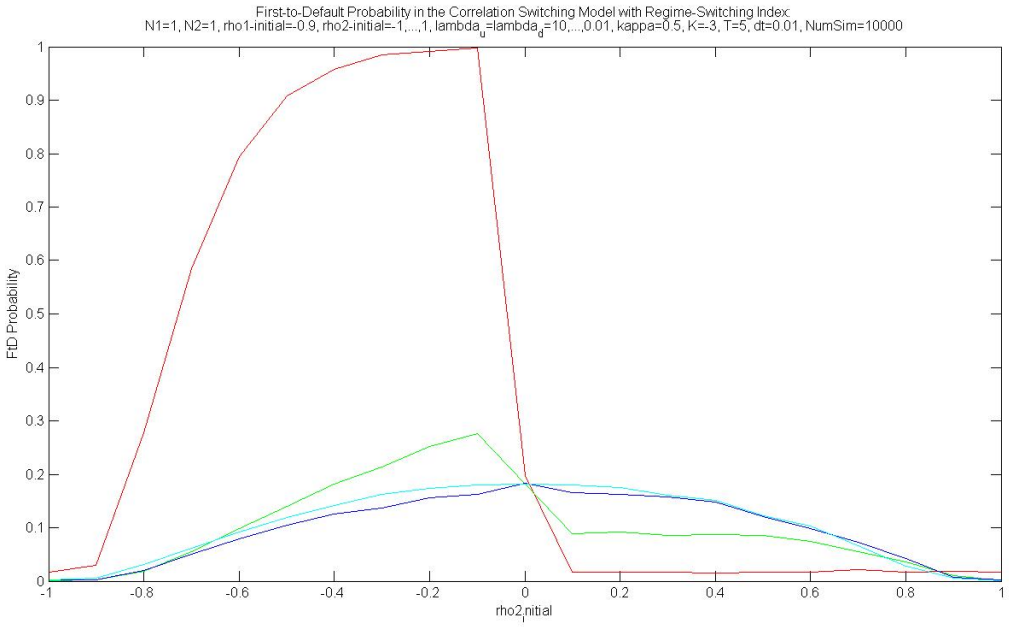

Figure 57: First-to-Default Probability in the Correlation Switching Model with Jump Market for Two Firms with $\rho_1 = -0.9$ and Different Values of $\lambda_u = \lambda_d$

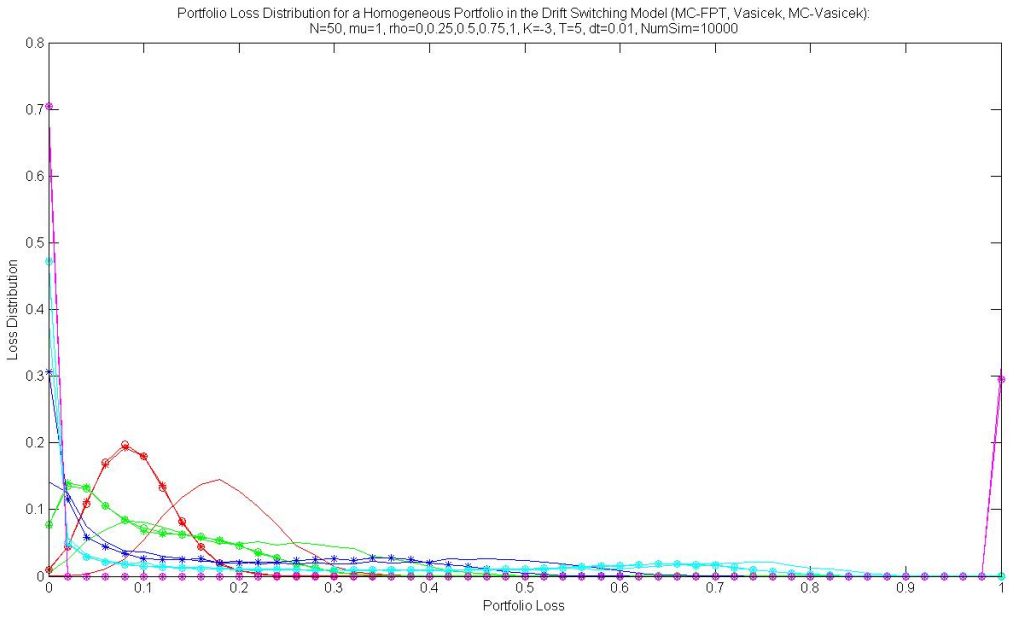

Figure 58: Loss Distribution in the Drift Switching Model for Homogeneous Portfolio with Different Values of ρ

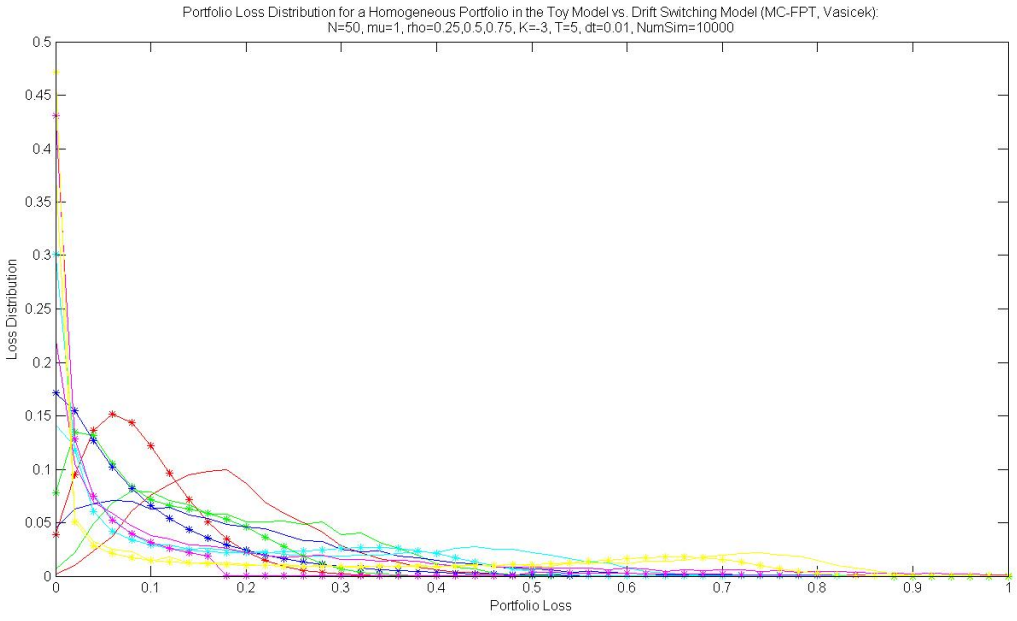

Figure 59: Loss Distribution in the Toy Model vs. the Drift Switching Model for Homogeneous Portfolio with Different Values of ρ

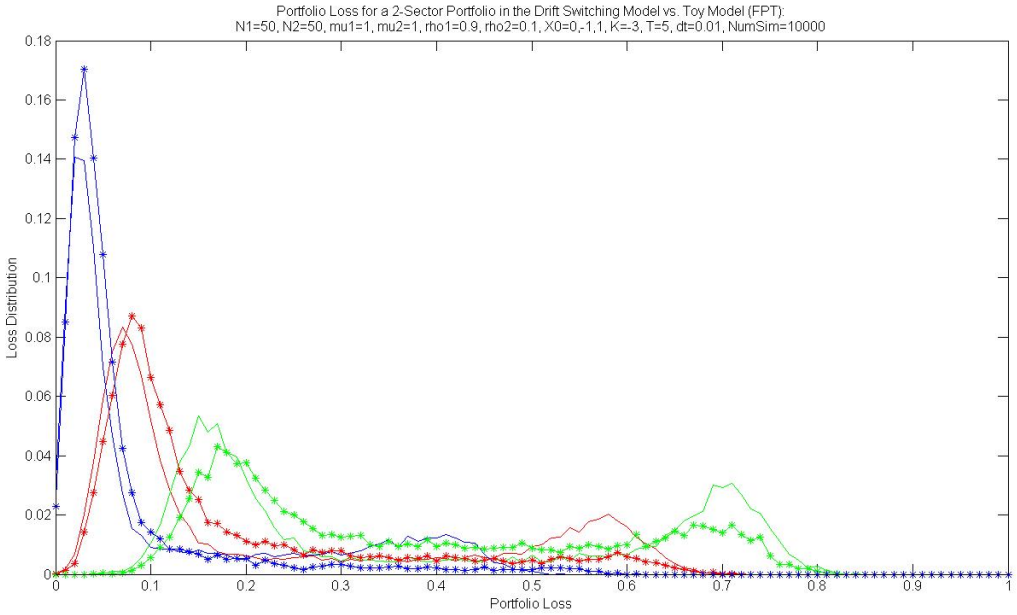

Figure 60: Loss Distribution in the Toy Model vs. the Drift Switching Model for Two-Sector Portfolio with Different Values of ρ

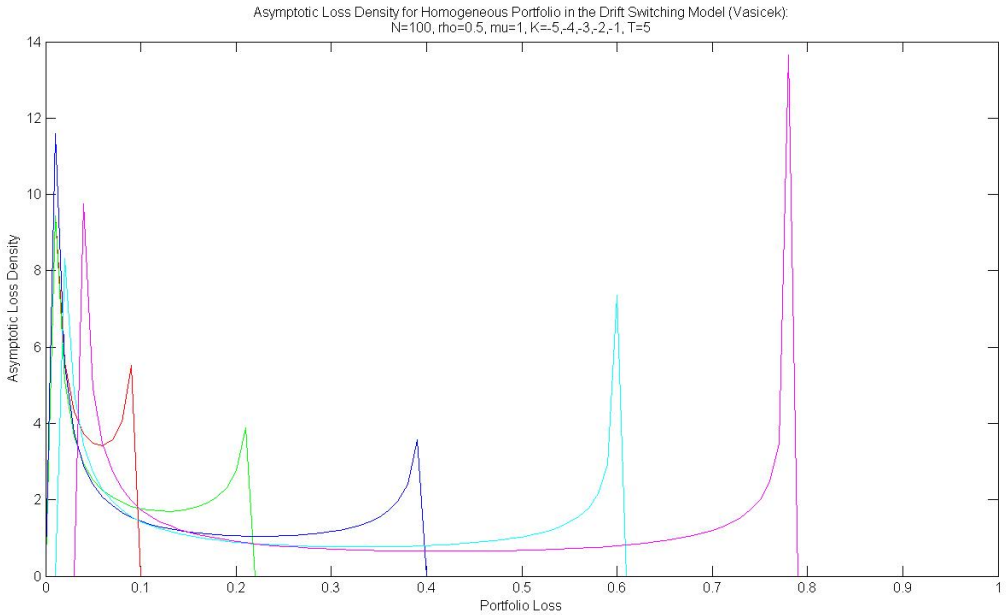

Figure 61: Asymptotic Loss Density in the Drift Switching Model for Homogeneous Portfolio with Different Values of K

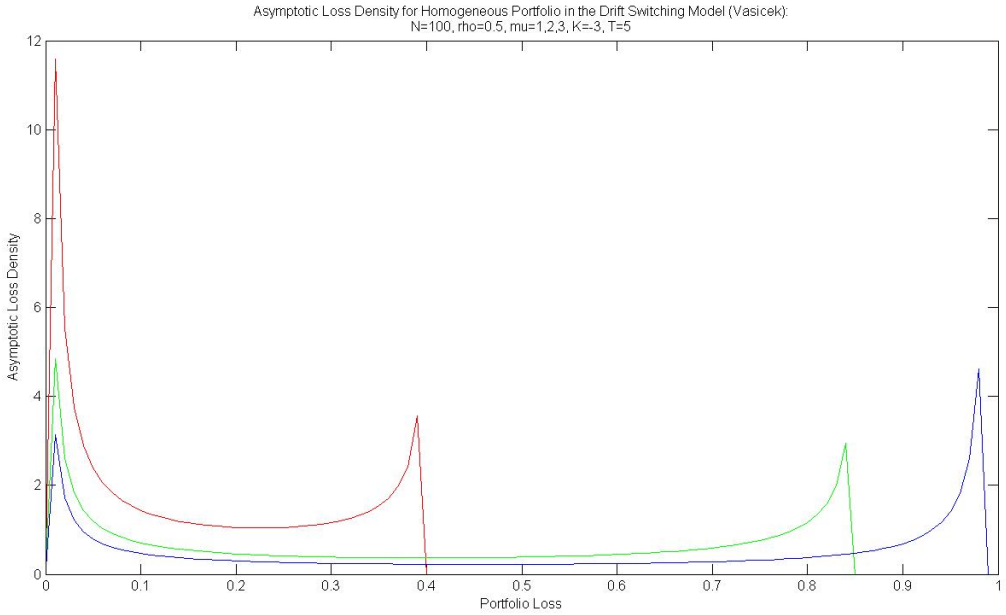

Figure 62: Asymptotic Loss Density in the Drift Switching Model for Homogeneous Portfolio with Different Values of μ

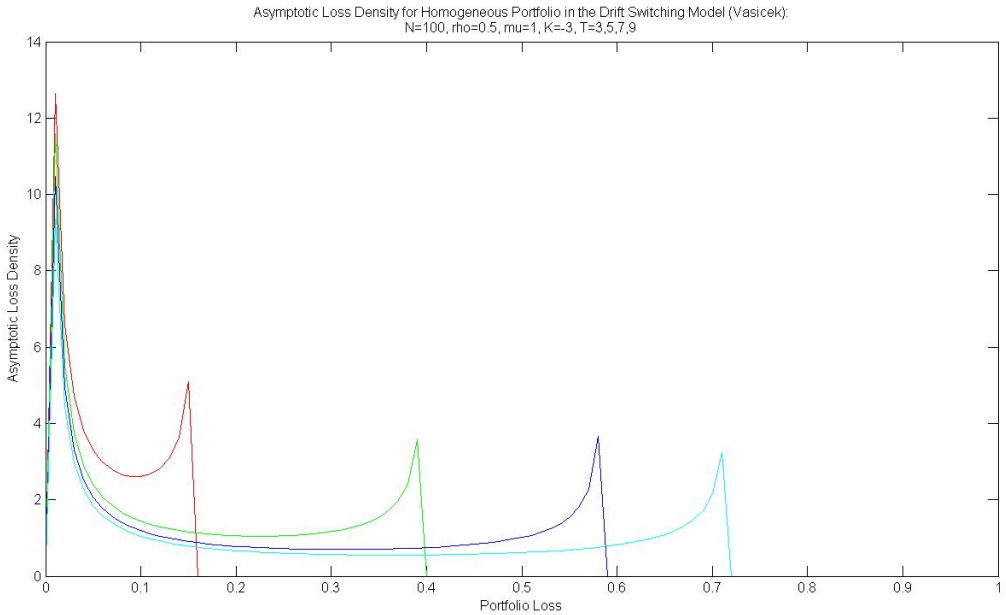

Figure 63: Asymptotic Loss Density in the Drift Switching Model for Homogeneous Portfolio with Different Values of T

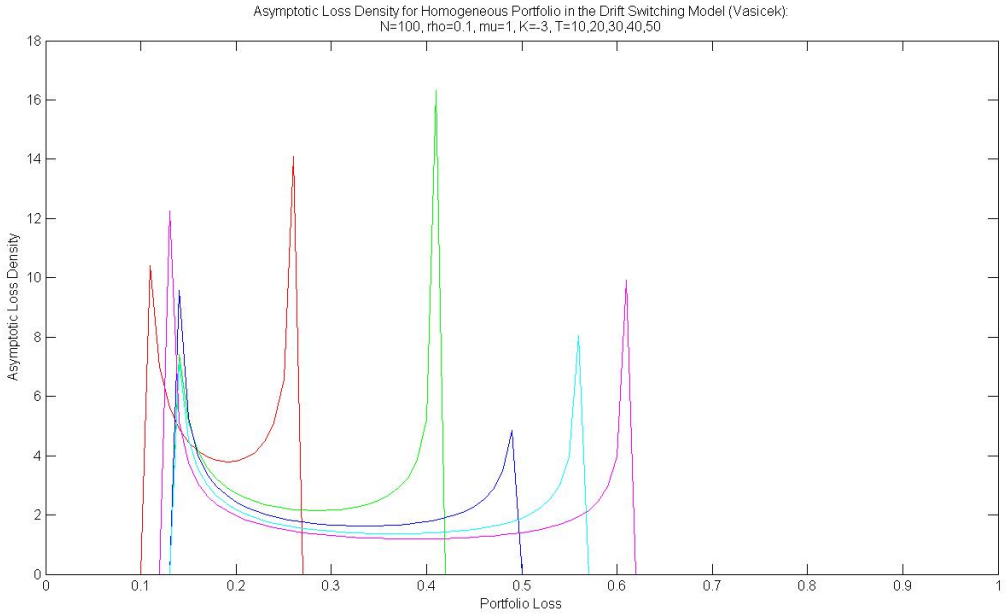

Figure 64: Asymptotic Loss Density in the Drift Switching Model for Homogeneous Portfolio with Different Values of Long T

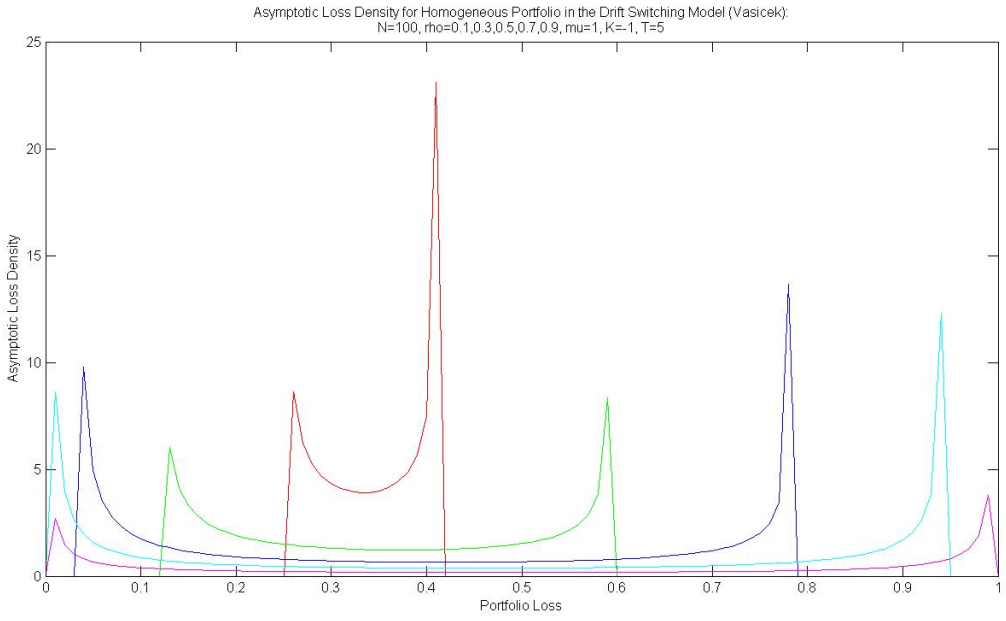

Figure 65: Asymptotic Loss Density in the Drift Switching Model for Homogeneous Portfolio with $K = -1$ and Different Values of ρ

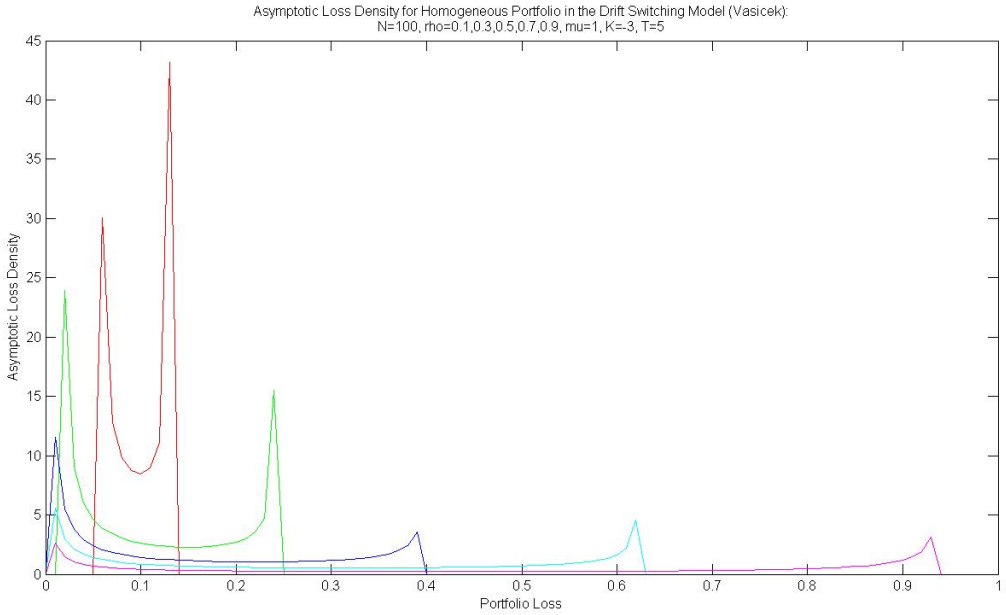

Figure 66: Asymptotic Loss Density in the Drift Switching Model for Homogeneous Portfolio with $K = -3$ and Different Values of ρ

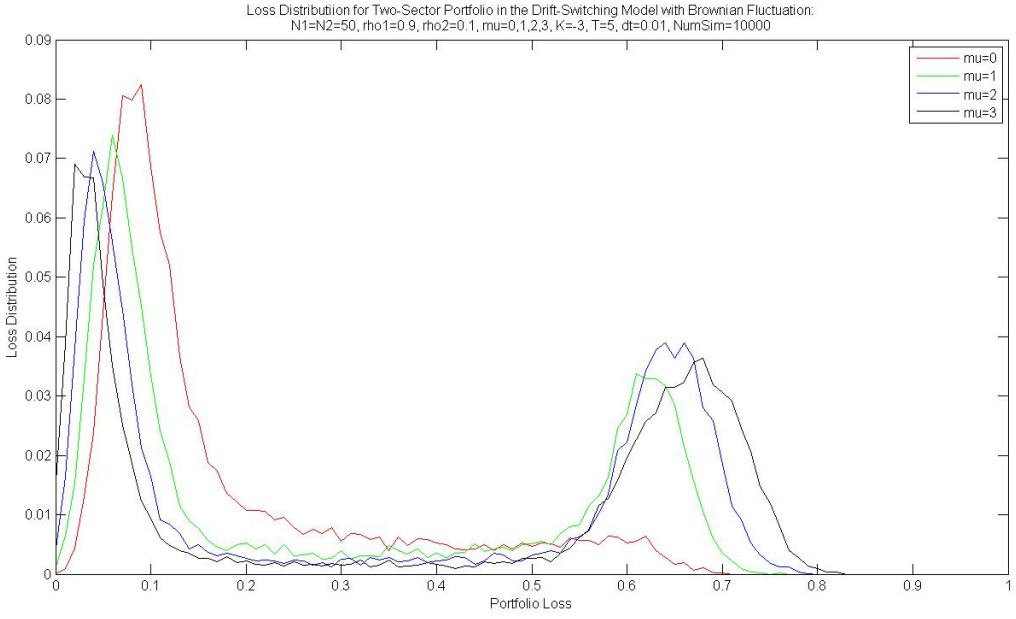

Figure 67: Asymptotic Loss Density in the Toy Model vs. the Drift Switching Model with Brownian Market for Two-Sector Portfolio with Different Values of $\mu_1 = \mu_2$

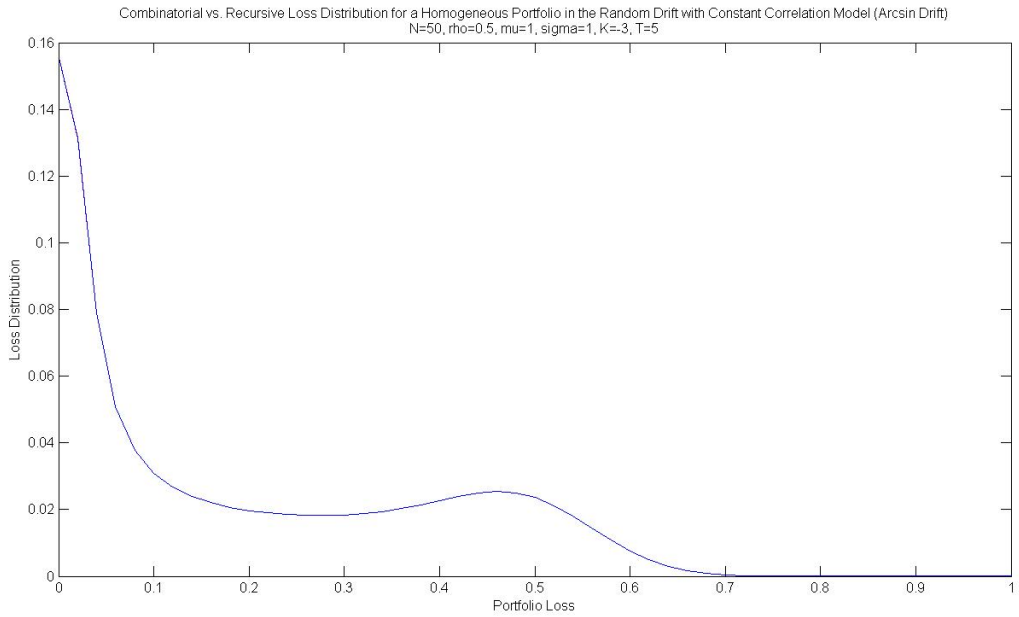

Figure 68: Loss Distribution in the Arcsin Drift Model for Homogeneous Portfolio - Combinatorial Formula vs. Recursive Algorithm

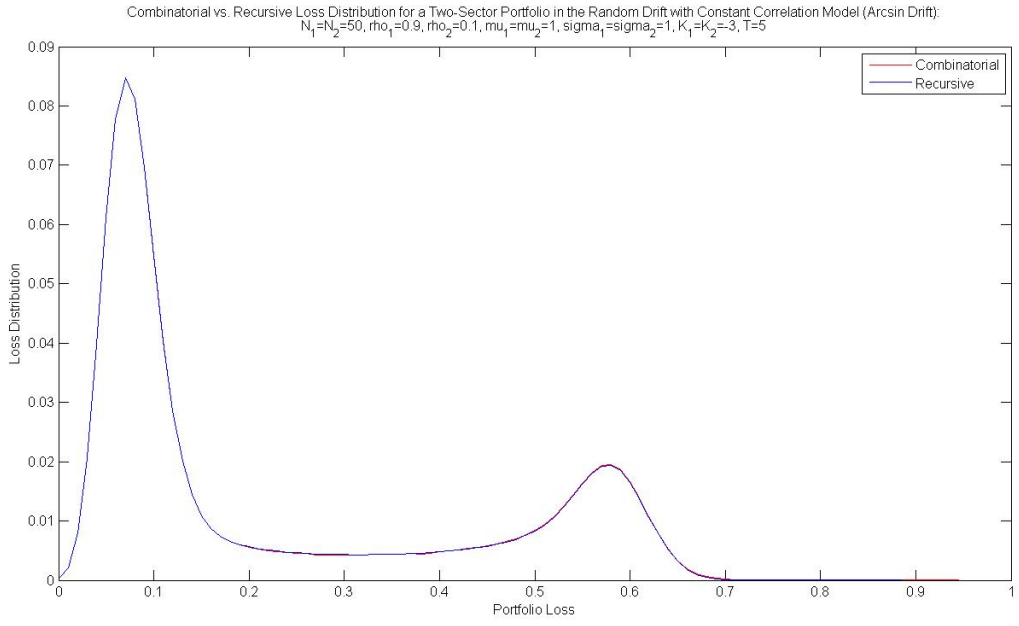

Figure 69: Loss Distribution in the Arcsin Drift Model for Two-Sector Portfolio - Combinatorial Formula vs. Recursive Algorithm

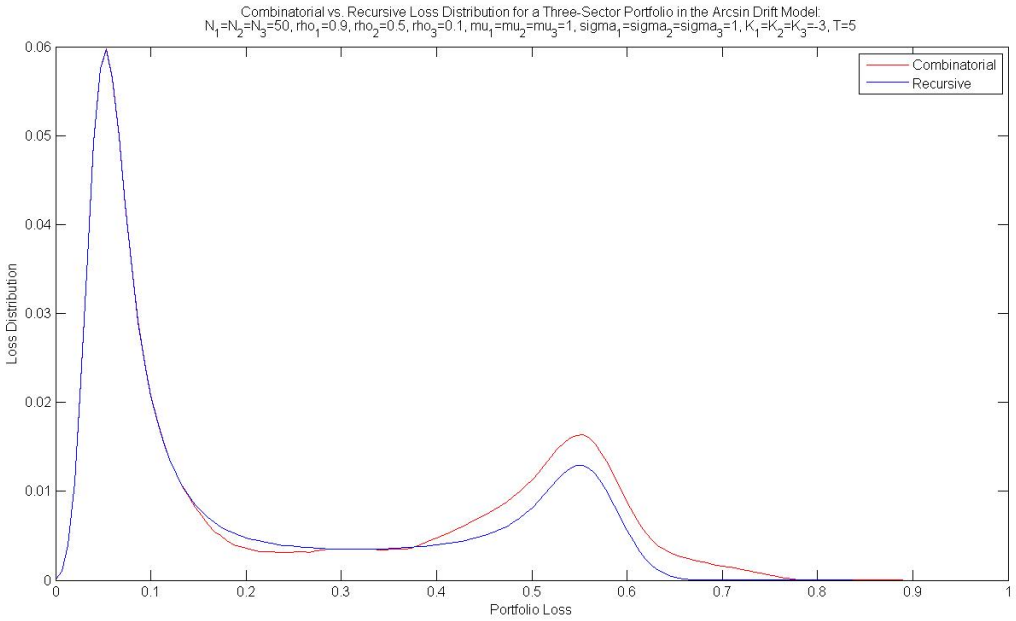

Figure 70: Loss Distribution in the Arcsin Drift Model for Three-Sector Portfolio - Combinatorial Formula vs. Recursive Algorithm

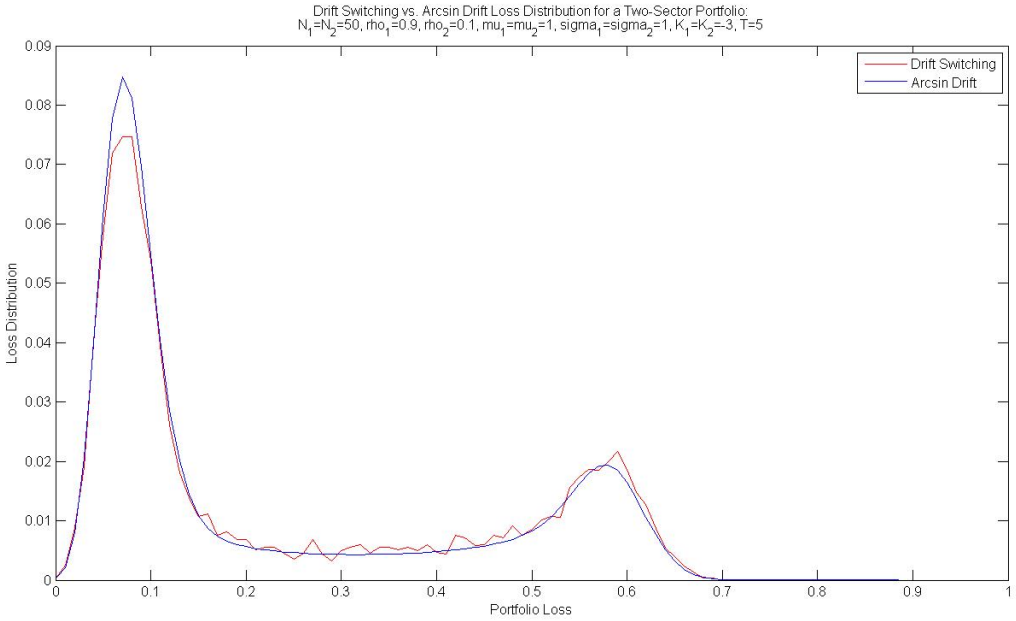

Figure 71: Loss Distribution in the Drift Switching Model vs. the Arcsin Drift Model for Two-Sector Portfolio

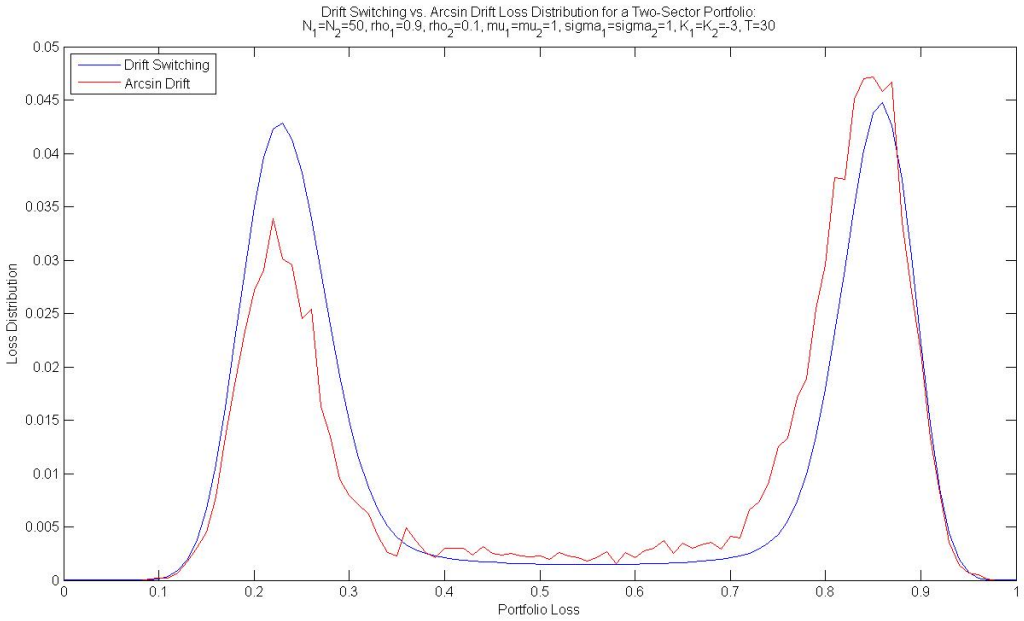

Figure 72: Loss Distribution in the Drift Switching Model vs. the Arcsin Drift Model for Two-Sector Portfolio with Long Maturity

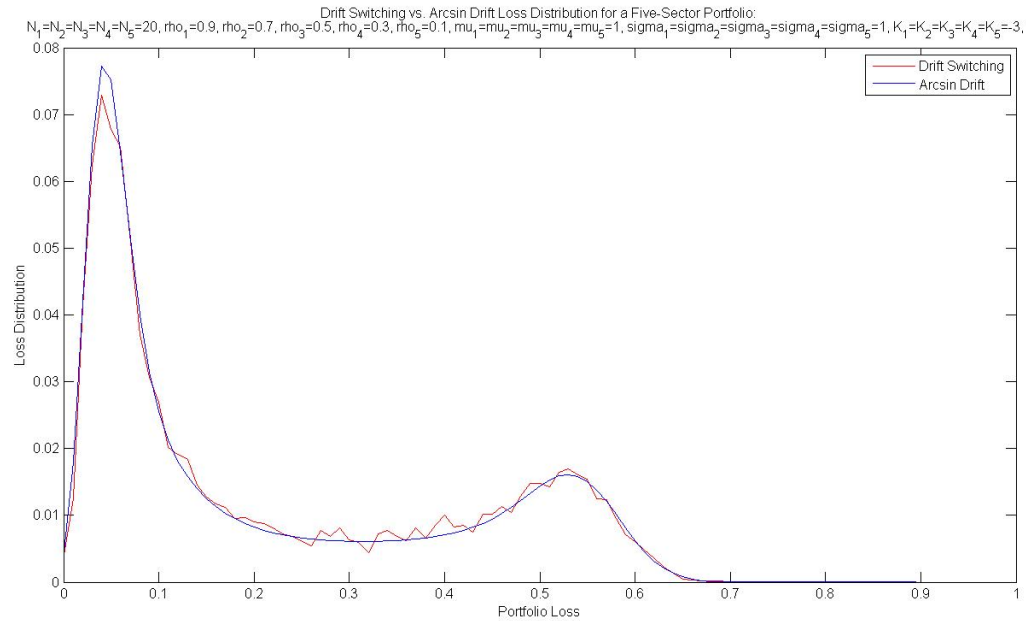

Figure 73: Loss Distribution in the Drift Switching Model vs. the Arcsin Drift Model for Five-Sector Portfolio

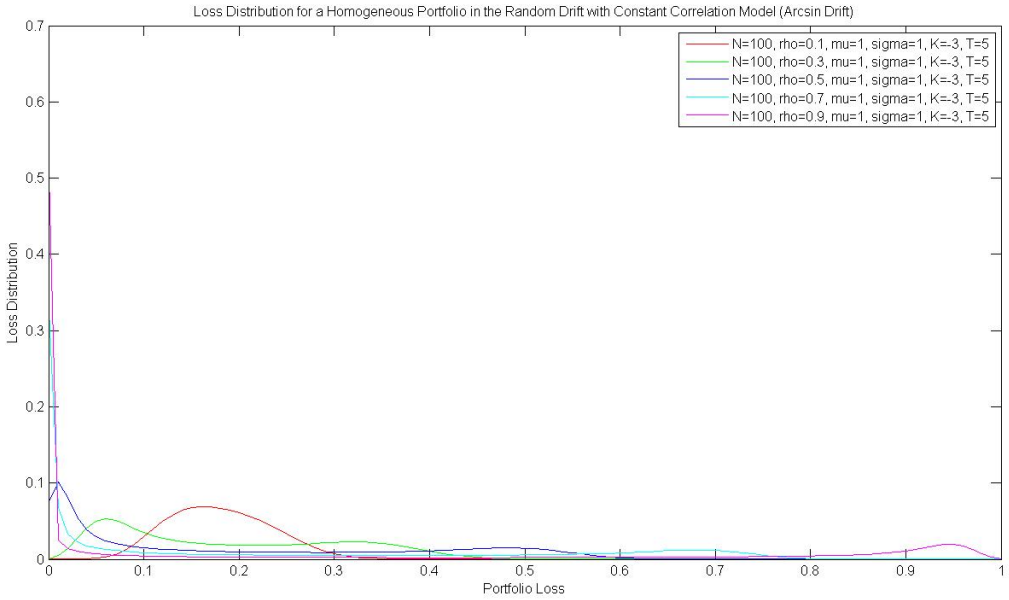

Figure 74: Loss Distribution in the Arcsin Drift Model for Homogeneous Portfolio with Different Values of ρ

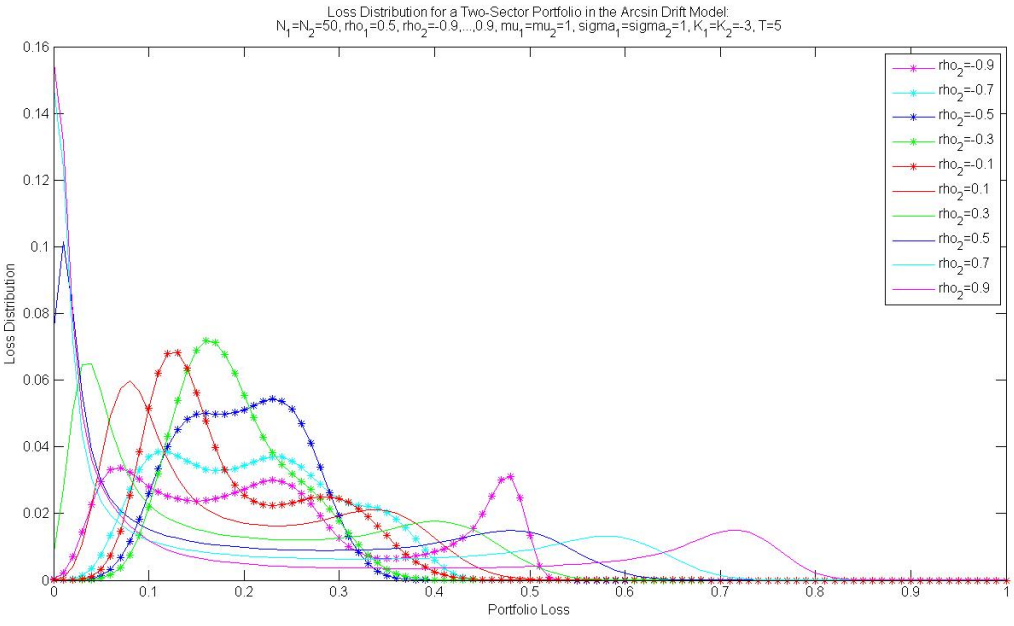

Figure 75: Loss Distribution in the Arcsin Drift Model for Two-Sector Portfolio with $\rho_1 = 0.5$ and Both Positive and Negative Values of ρ_2

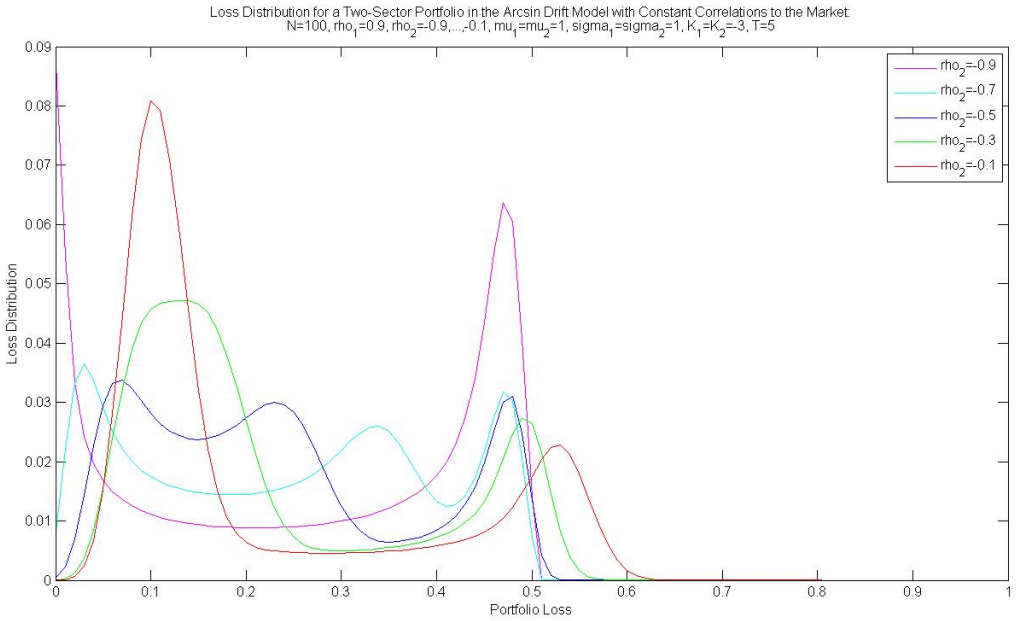

Figure 76: Loss Distribution in the Arcsin Drift Model for Two-Sector Portfolio with $\rho_1 = 0.5$ and Negative Values of ρ_2

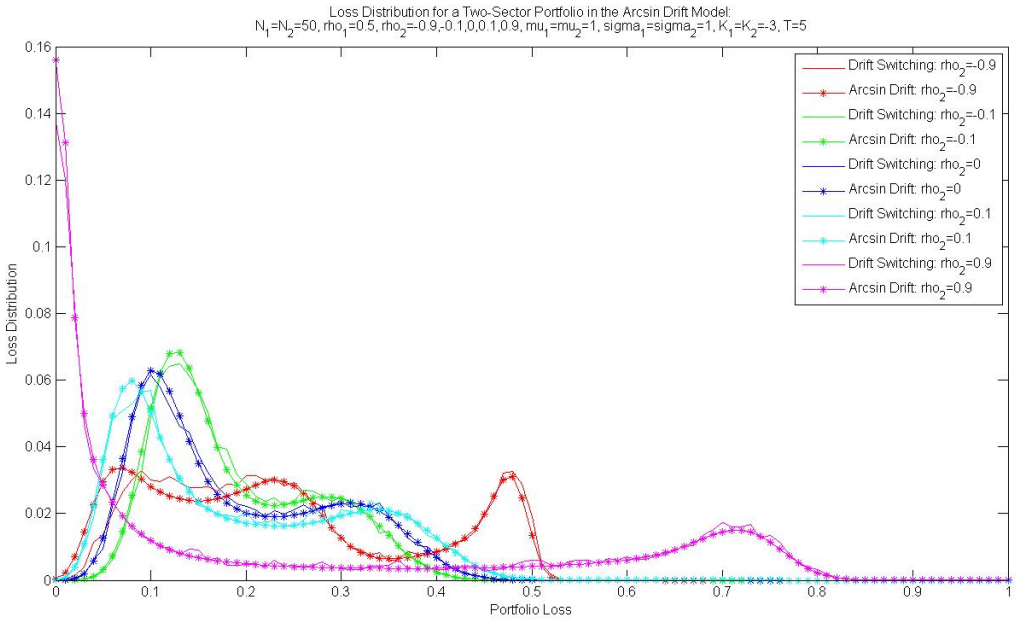

Figure 77: Loss Distribution in the Drift Switching Model vs. the Arcsin Drift Model for Two-Sector Portfolio with $\rho_1 = 0.5$ and Both Positive and Negative Values of ρ_2

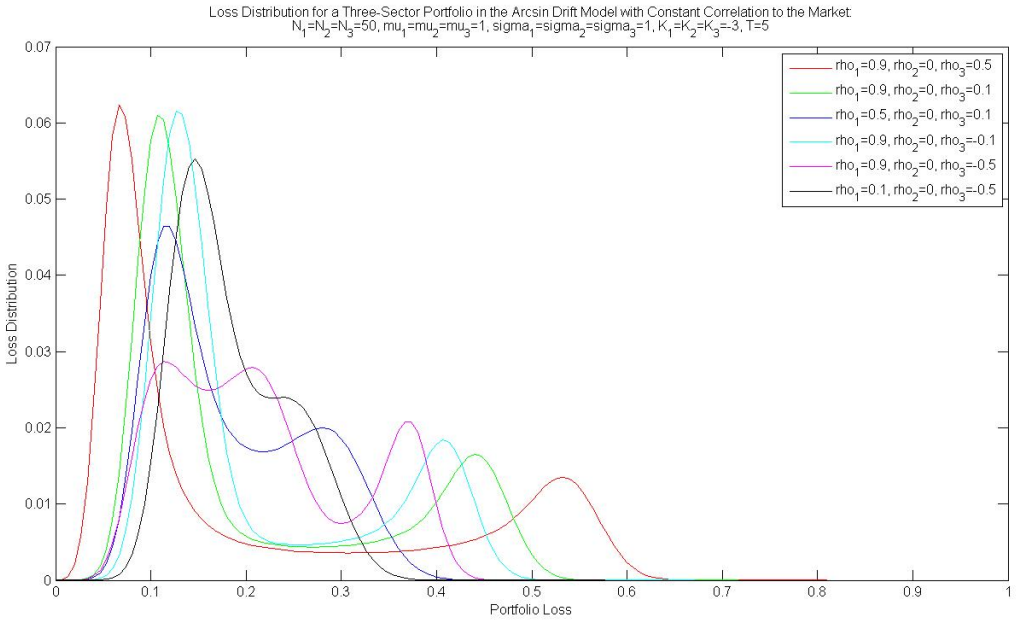

Figure 78: Loss Distribution in the Arcsin Drift Model for Three-Sector Portfolio with $\rho_1 > 0$, $\rho_2 = 0$ and Both Positive and Negative Values of ρ_3

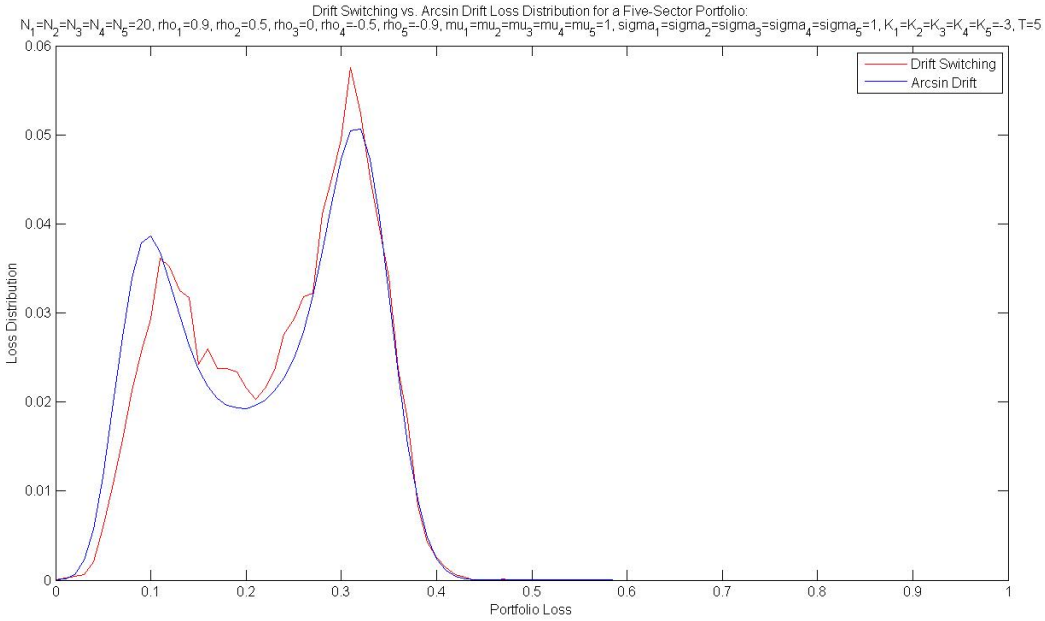

Figure 79: Loss Distribution in the Drift Switching Model vs. the Arcsin Drift Model for Five-Sector Portfolio

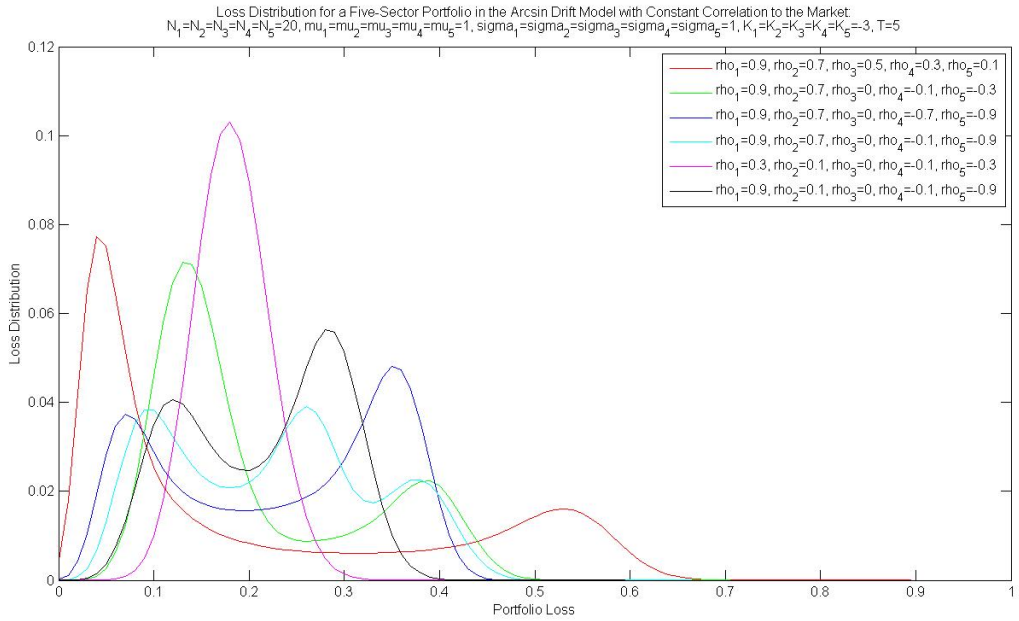

Figure 80: Loss Distribution in the Arcsin Drift Model for Five-Sector Portfolio with Both Positive and Negative Values of ρ_4 and ρ_5

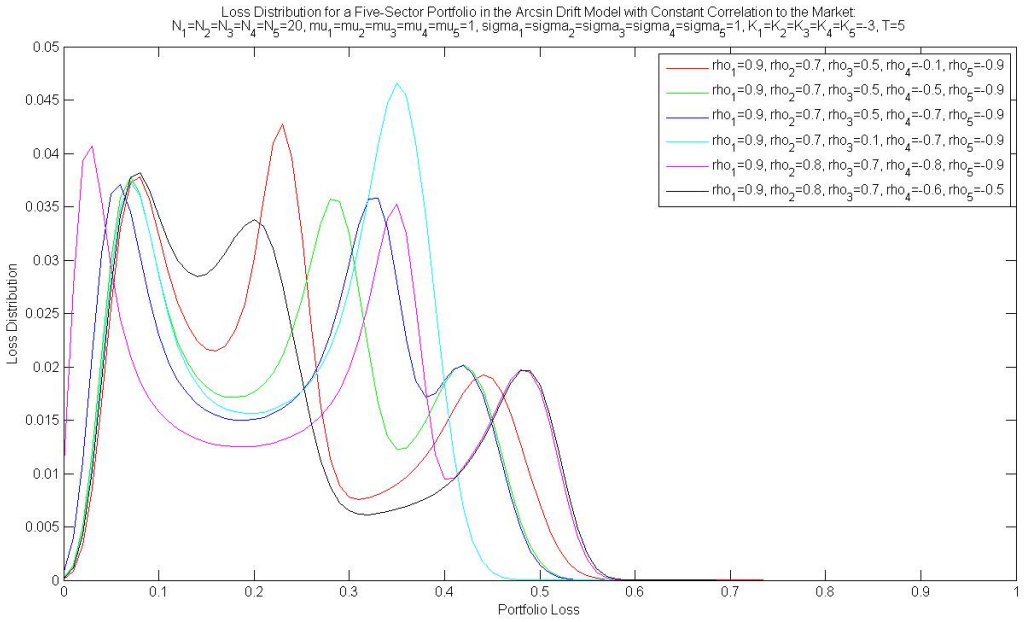

Figure 81: Loss Distribution in the Arcsin Drift Model for Five-Sector Portfolio with Modest Negative Values of ρ_4 and ρ_5

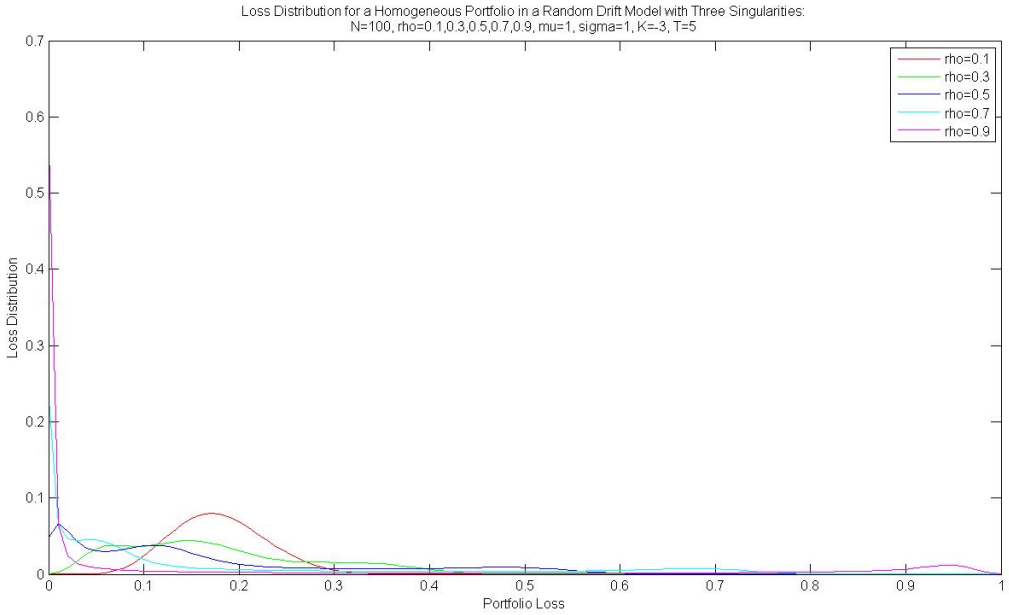

Figure 82: Loss Distribution in the Three Singular Drift Model for Homogeneous Portfolio with $\rho = 0.1, 0.3, 0.5, 0.7, 0.9$

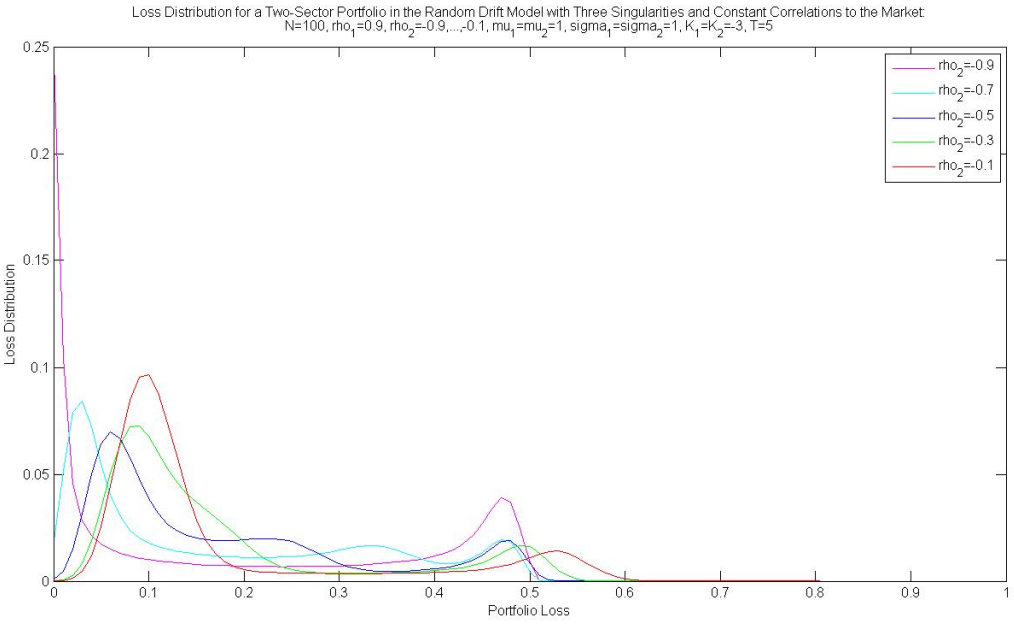

Figure 83: Loss Distribution in the Three Singular Drift Model for Two-Sector Portfolio with $\rho_1 = 0.9$ and $\rho_2 = -0.1, -0.3, -0.5, -0.7, -0.9$

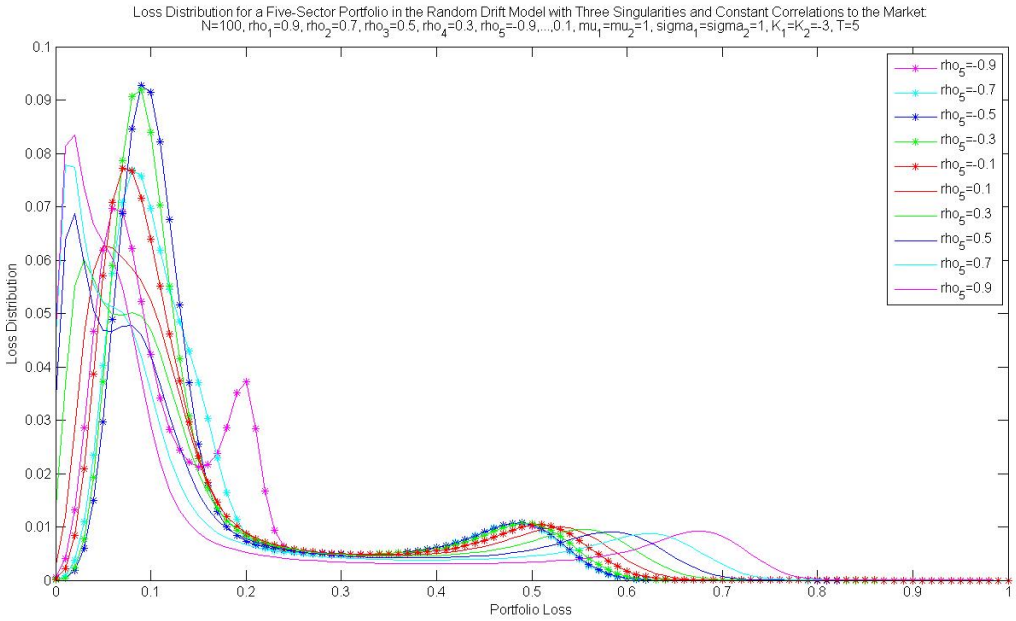

Figure 84: Loss Distribution in the Three Singular Drift Model for Five-Sector Portfolio with $\rho_1 > 0$, $\rho_2 > 0$, $\rho_3 > 0$, $\rho_4 > 0$, and Different Values of ρ_5

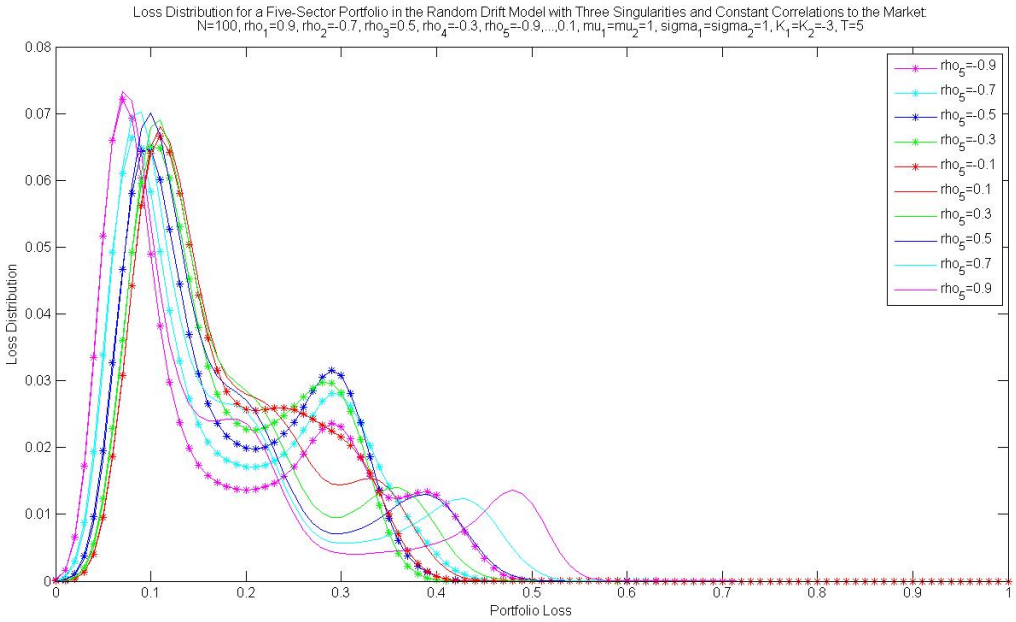

Figure 85: Loss Distribution in the Three Singular Drift Model for Five-Sector Portfolio with $\rho_1 > 0$, $\rho_2 < 0$, $\rho_3 > 0$, $\rho_4 < 0$, and Different Values of ρ_5

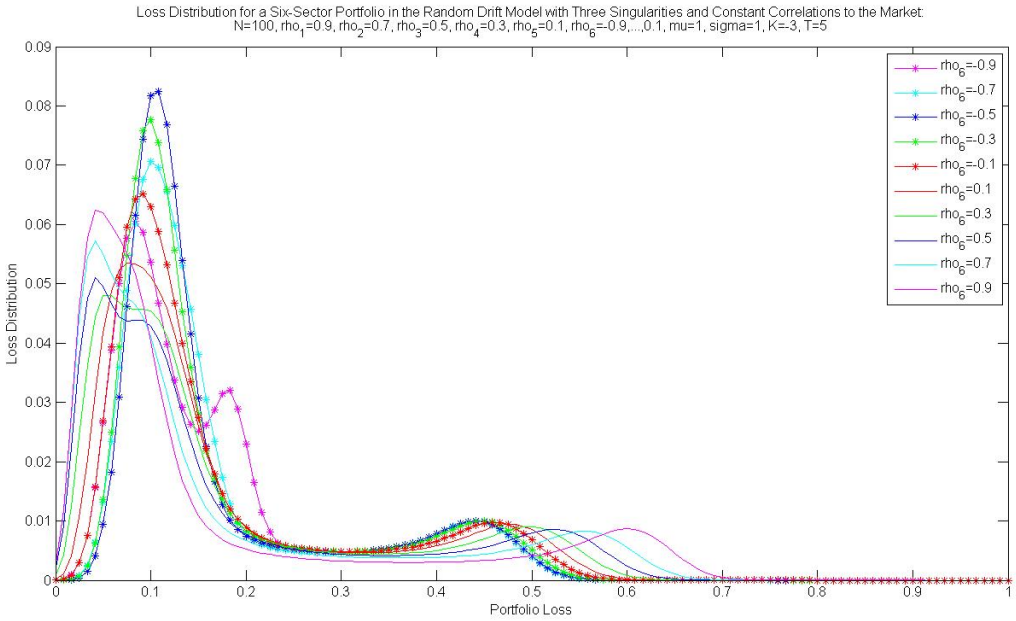

Figure 86: Loss Distribution in the Three Singular Drift Model for Six-Sector Portfolio with $\rho_1 > 0$, $\rho_2 > 0$, $\rho_3 > 0$, $\rho_4 > 0$, $\rho_5 > 0$, and Different Values of ρ_6

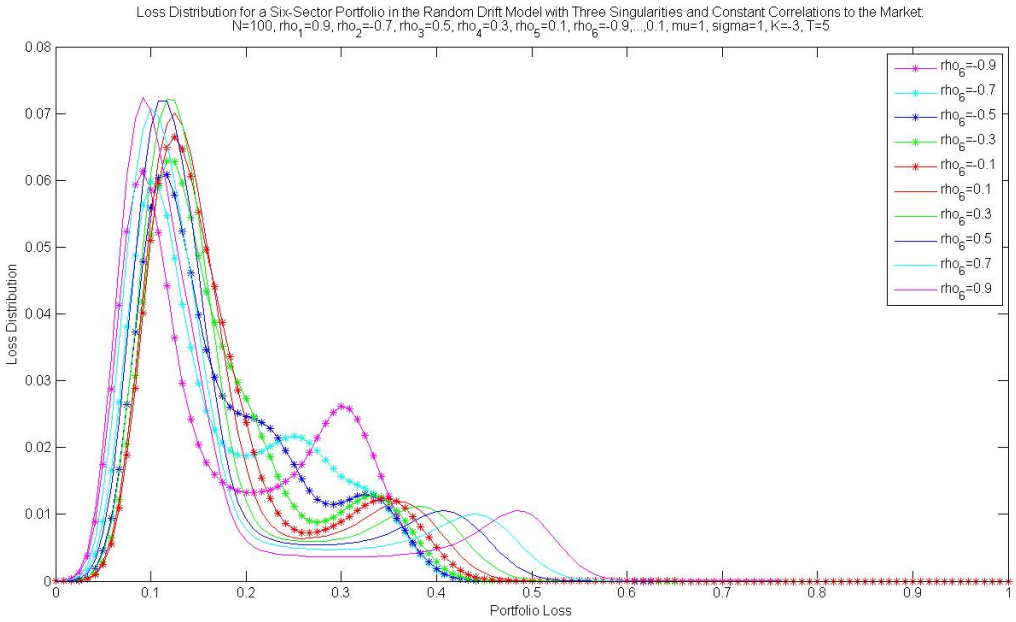

Figure 87: Loss Distribution in the Three Singular Drift Model for Six-Sector Portfolio with $\rho_1 > 0$, $\rho_2 < 0$, $\rho_3 > 0$, $\rho_4 > 0$, $\rho_5 > 0$, and Different Values of ρ_6

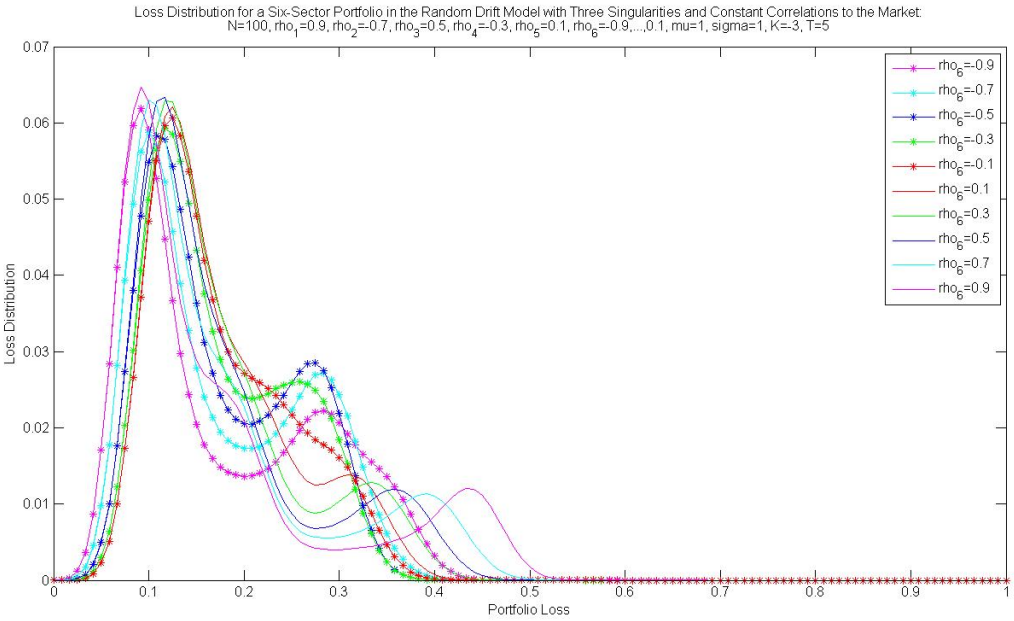

Figure 88: Loss Distribution in the Three Singular Drift Model for Six-Sector Portfolio with $\rho_1 > 0$, $\rho_2 < 0$, $\rho_3 > 0$, $\rho_4 < 0$, $\rho_5 > 0$, and Different Values of ρ_6

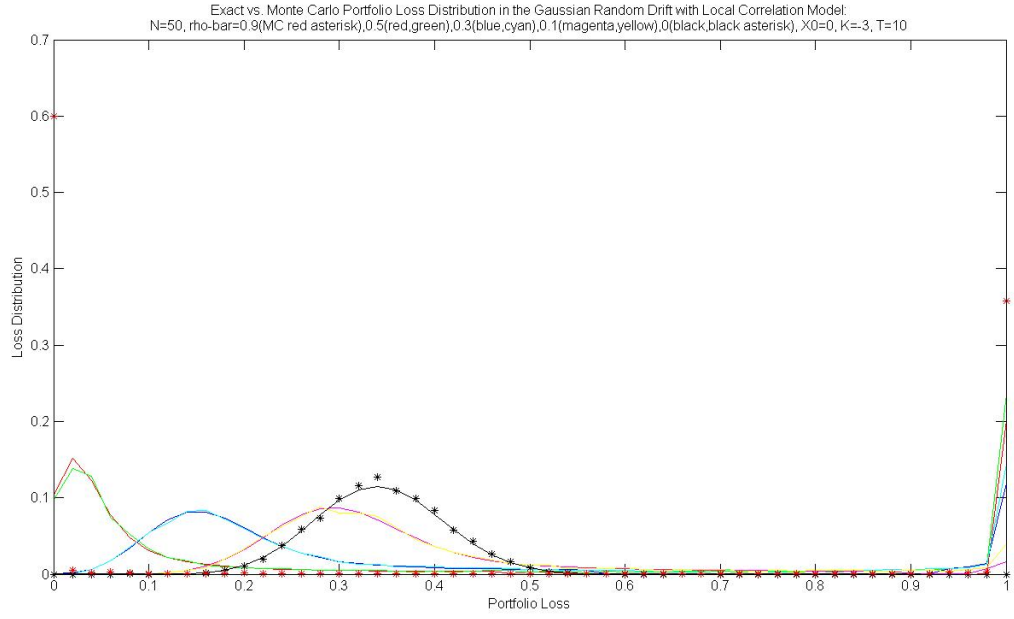

Figure 89: Loss Distribution in the Gaussian Drift Local Correlation Model for Homogeneous Portfolio with Different Values of $\bar{\rho}$

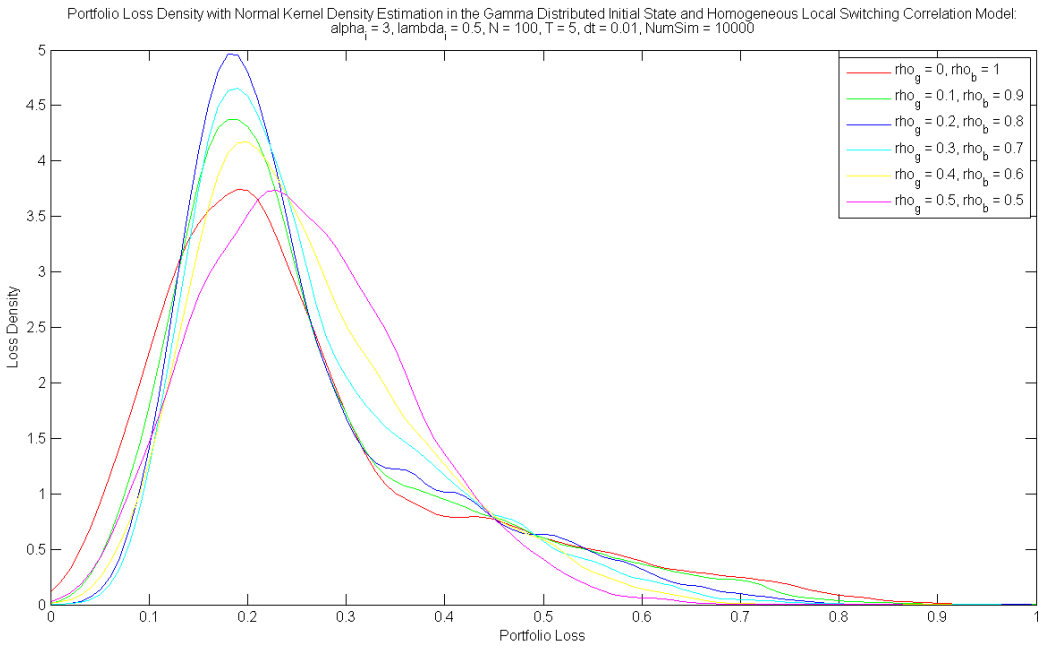

Figure 90: Loss Distribution in the Gamma Initial Switching Correlation Model for Homogeneous Portfolio with $\alpha = 3$, $\lambda = 0.5$ and Different Values of ρ_g and ρ_b

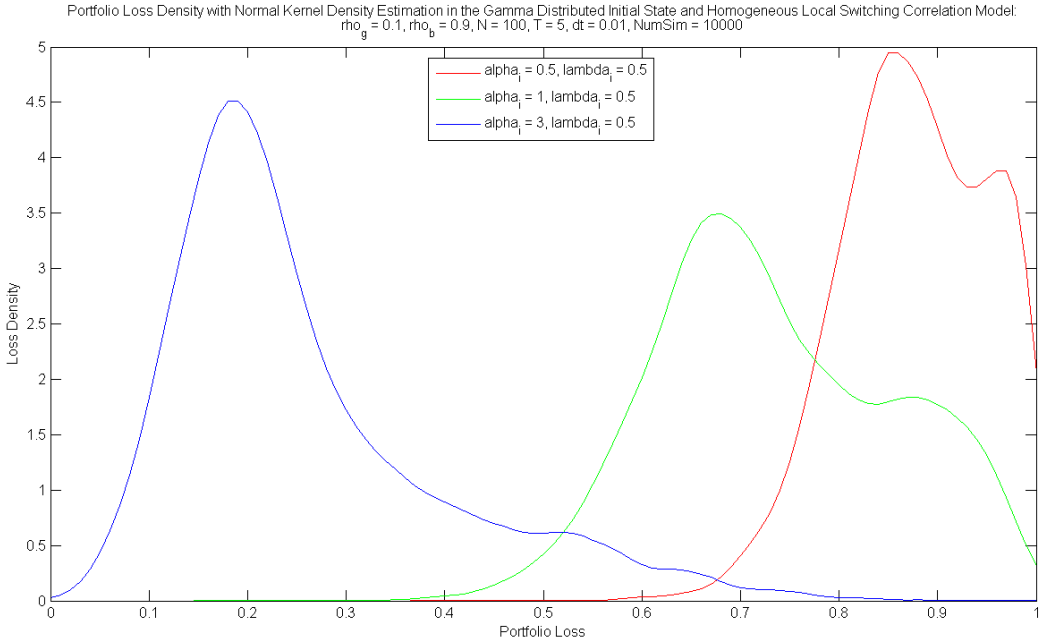

Figure 91: Loss Distribution in the Gamma Initial Switching Correlation Model for Homogeneous Portfolio with $\rho_g = 0.1$, $\rho_b = 0.9$ and Different Values of α and λ

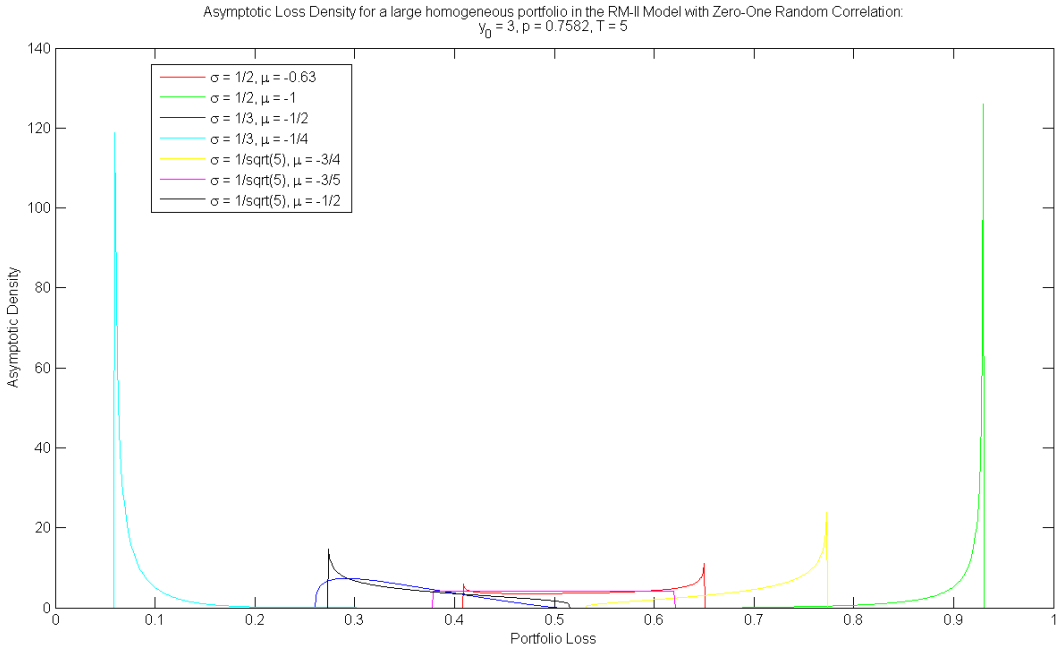

Figure 92: Asymptotic Loss Density of the Random Correlation Model with Random Initial State and Different Values of μ and σ

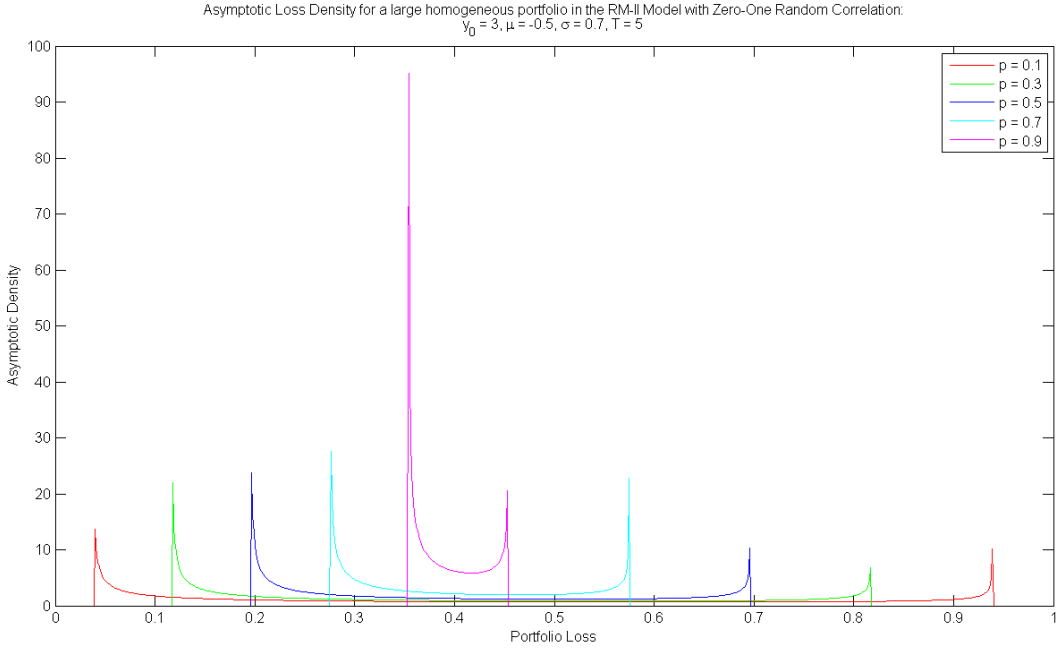

Figure 93: Asymptotic Loss Density of the Random Correlation Model with Random Initial State and Different Values of p

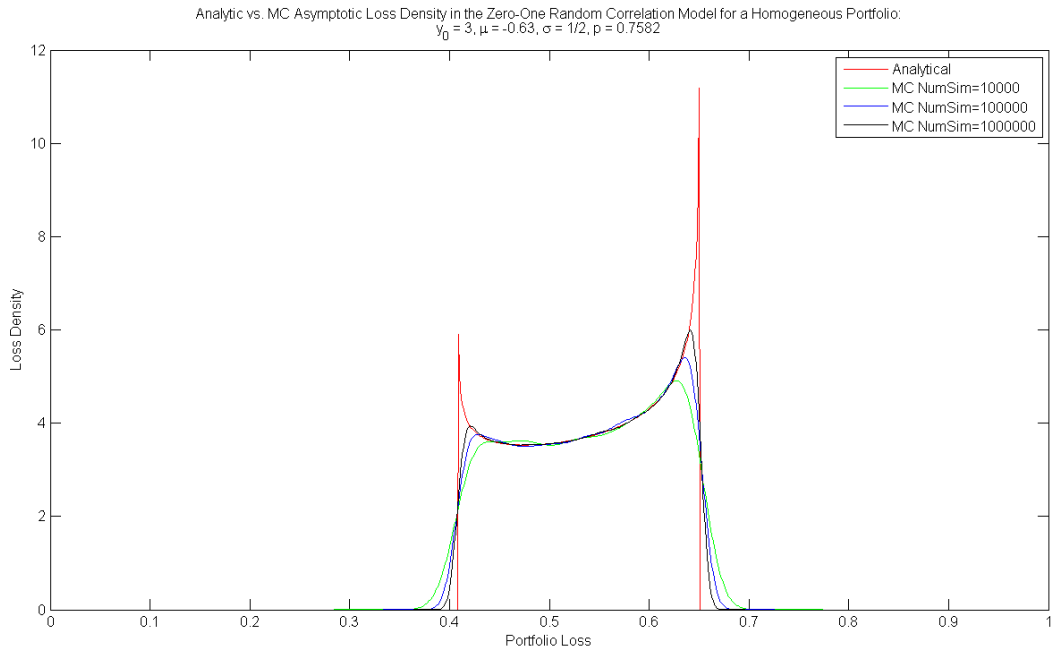

Figure 94: Analytic vs. Monte Carlo Asymptotic Loss Density of the Random Correlation Model with Random Initial State: $y_0 = 3$, $\mu = -0.63$, $\sigma = 1/2$, $p = 0.7852$, $T = 5$

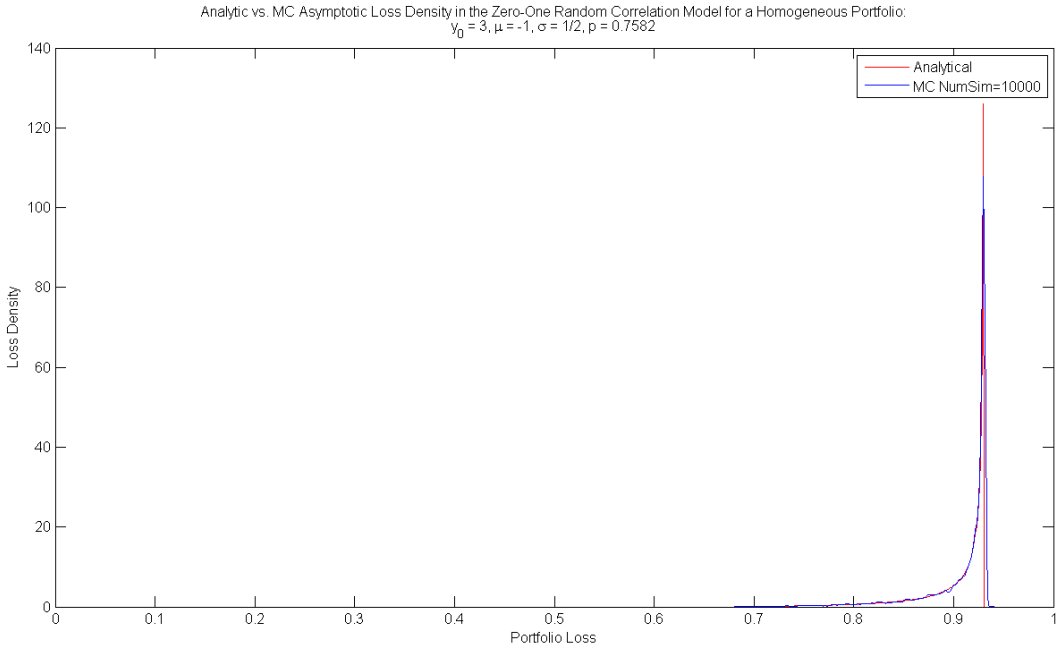

Figure 95: Analytic vs. Monte Carlo Asymptotic Loss Density of the Random Correlation Model with Random Initial State: $y_0 = 3$, $\mu = -1$, $\sigma = 1/2$, $p = 0.7852$, $T = 5$

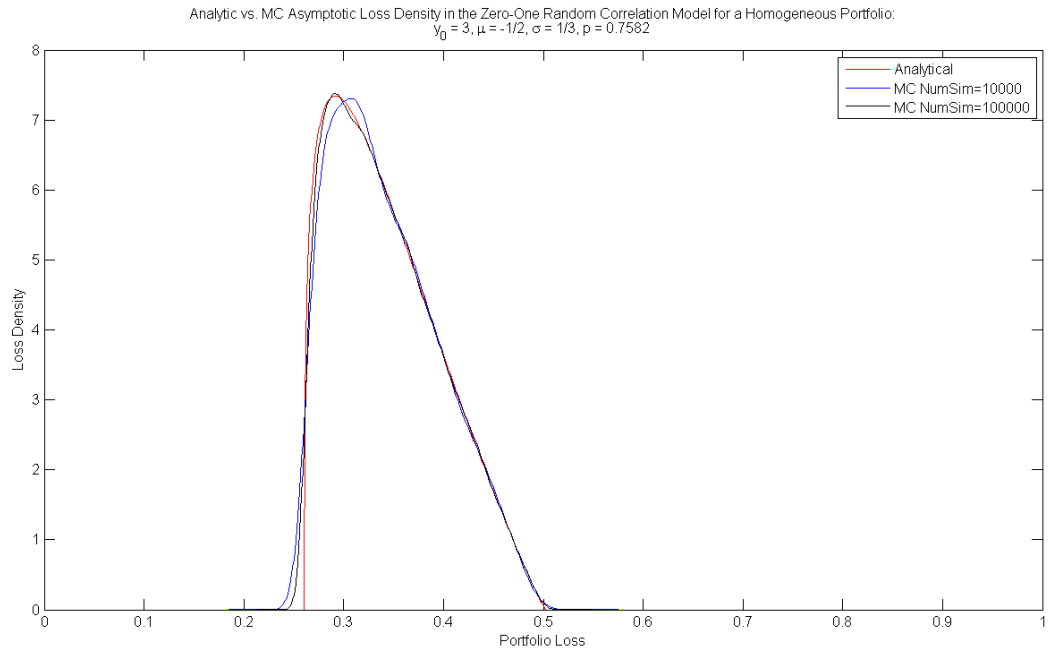

Figure 96: Analytic vs. Monte Carlo Asymptotic Loss Density of the Random Correlation Model with Random Initial State: $y_0 = 3$, $\mu = -1/2$, $\sigma = 1/3$, $p = 0.7852$, $T = 5$

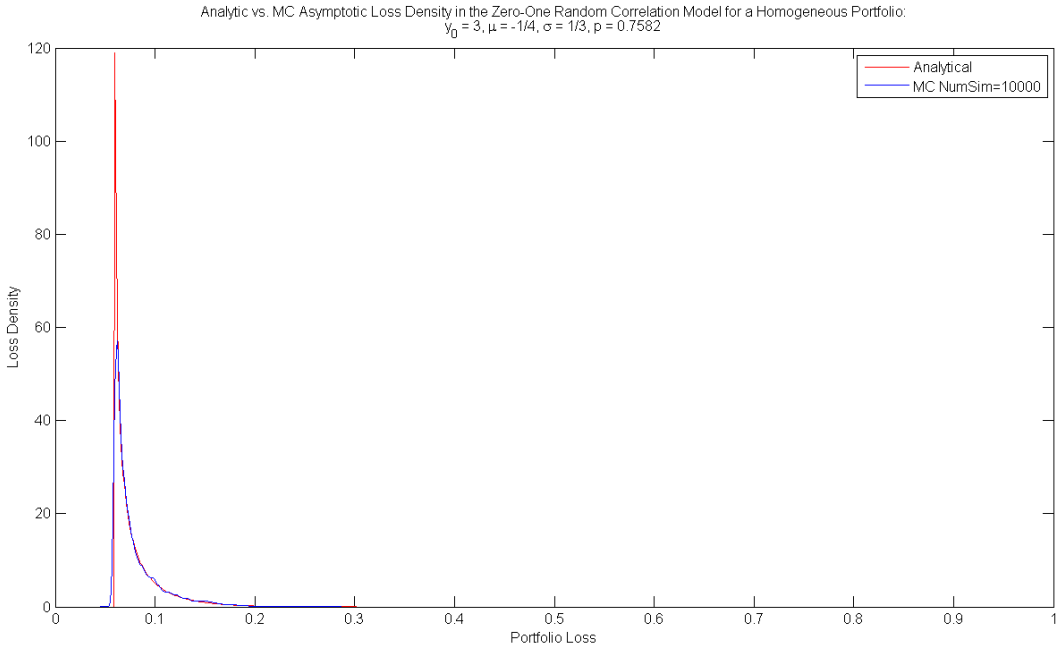

Figure 97: Analytic vs. Monte Carlo Asymptotic Loss Density of the Random Correlation Model with Random Initial State: $y_0 = 3$, $\mu = -1/4$, $\sigma = 1/3$, $p = 0.7852$, $T = 5$

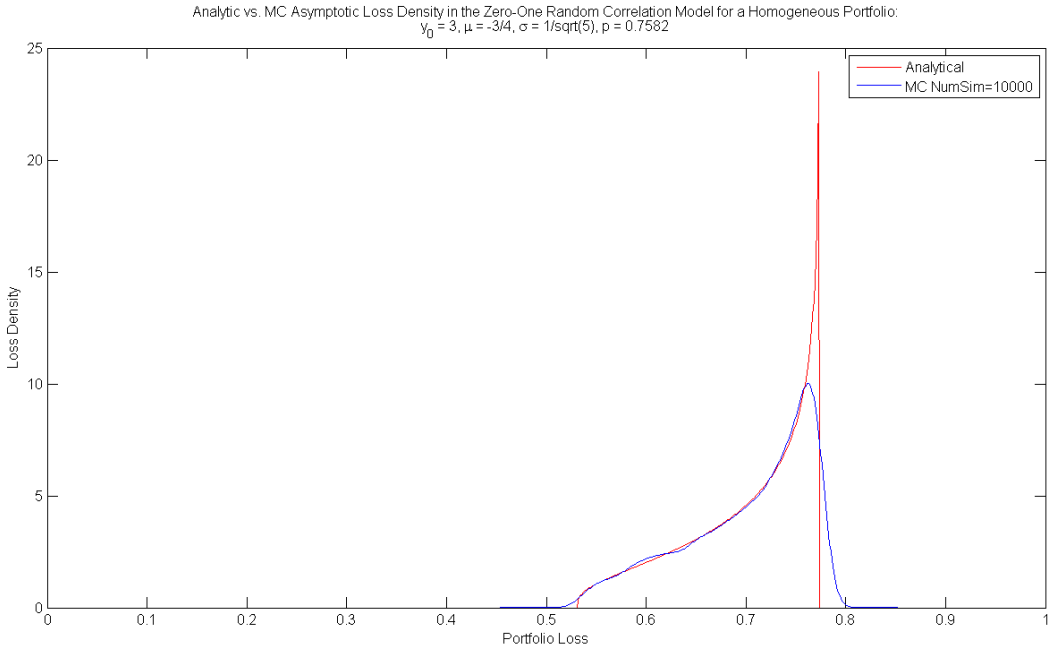

Figure 98: Analytic vs. Monte Carlo Asymptotic Loss Density of the Random Correlation Model with Random Initial State: $y_0 = 3$, $\mu = -3/4$, $\sigma = 1/\sqrt{5}$, $p = 0.7852$, $T = 5$

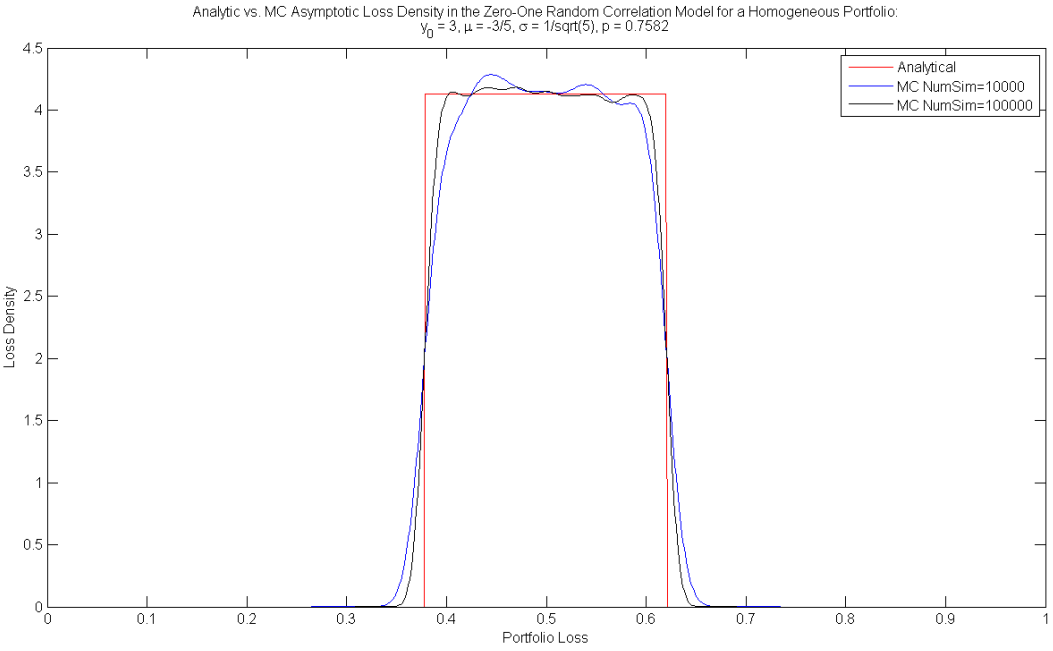

Figure 99: Analytic vs. Monte Carlo Asymptotic Loss Density of the Random Correlation Model with Random Initial State: $y_0 = 3$, $\mu = -3/5$, $\sigma = 1/\sqrt{5}$, $p = 0.7852$, $T = 5$

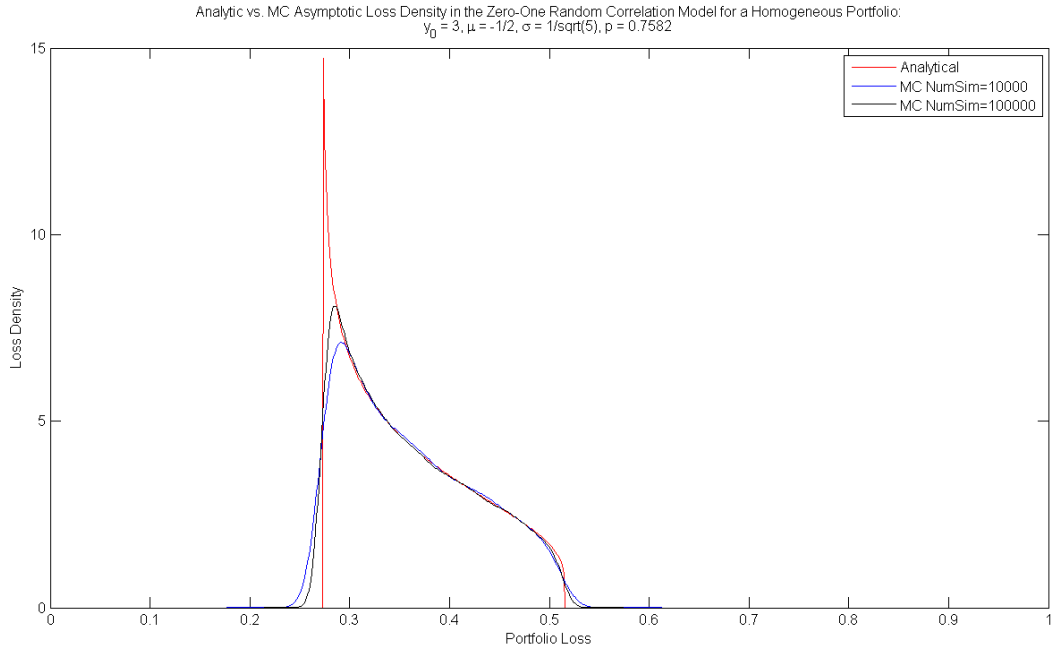

Figure 100: Analytic vs. Monte Carlo Asymptotic Loss Density of the Random Correlation Model with Random Initial State: $y_0 = 3$, $\mu = -1/2$, $\sigma = 1/\sqrt{5}$, $p = 0.7852$, $T = 5$

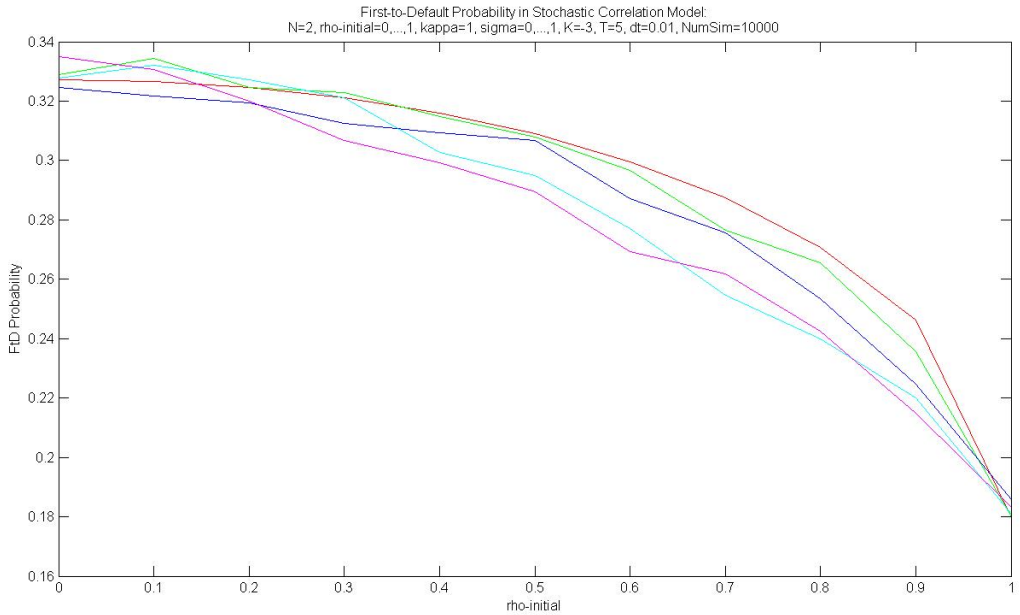

Figure 101: First-to-Default Probability in the Mean-Reverting Stochastic Correlation Model for Two Firms with Different Values of σ

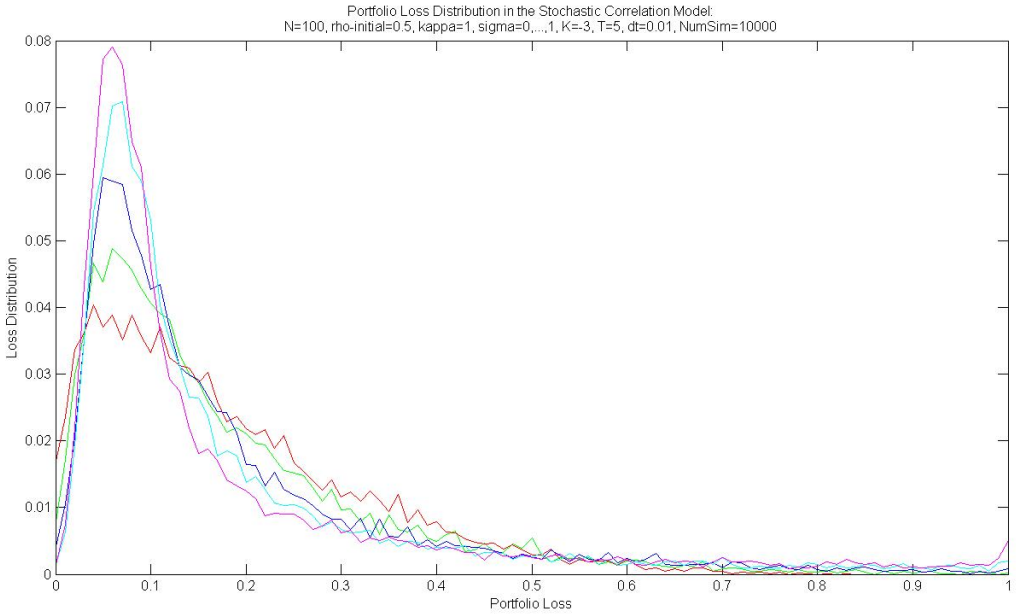

Figure 102: Loss Distribution in the Mean-Reverting Stochastic Correlation Model for Two Firms with Different Values of σ

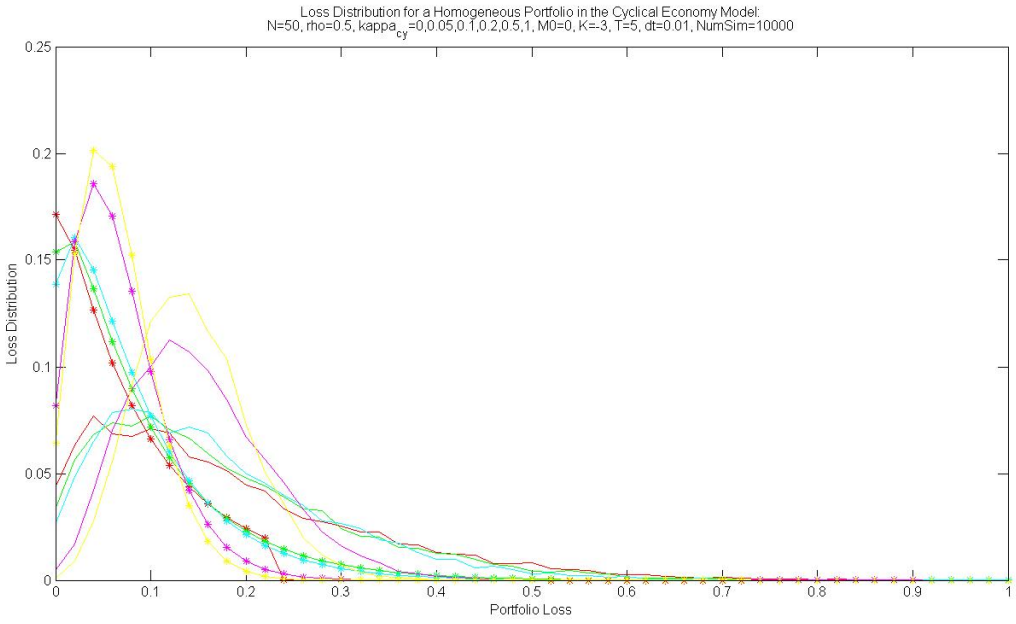

Figure 103: Loss Distribution in the Cyclical Economy Model for Homogeneous Portfolio with Different Values of κ_{cy}

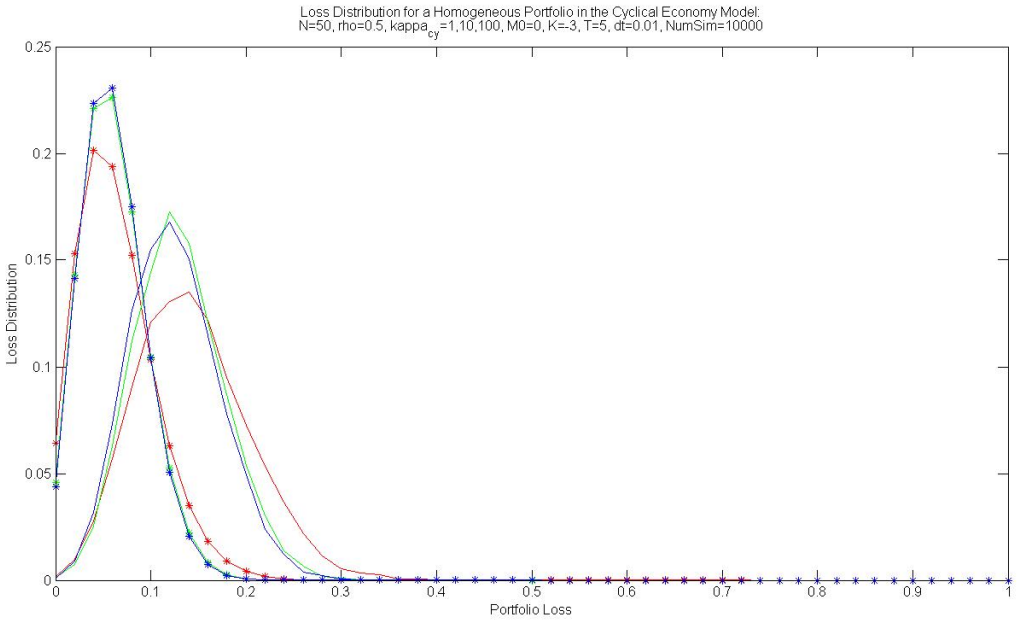

Figure 104: Loss Distribution in the Cyclical Economy Model for Homogeneous Portfolio with Large κ_{cy}

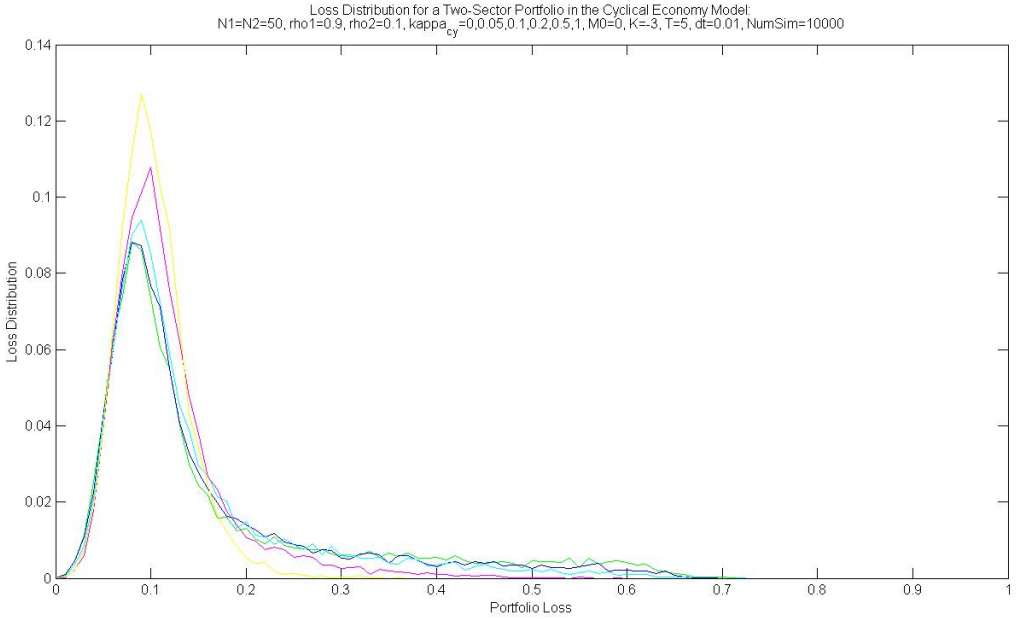

Figure 105: Loss Distribution in the Cyclical Economy Model for Two-Sector Portfolio with Different Values of κ_{cy}

APPENDIX E

CHAPTER 5 FIGURES

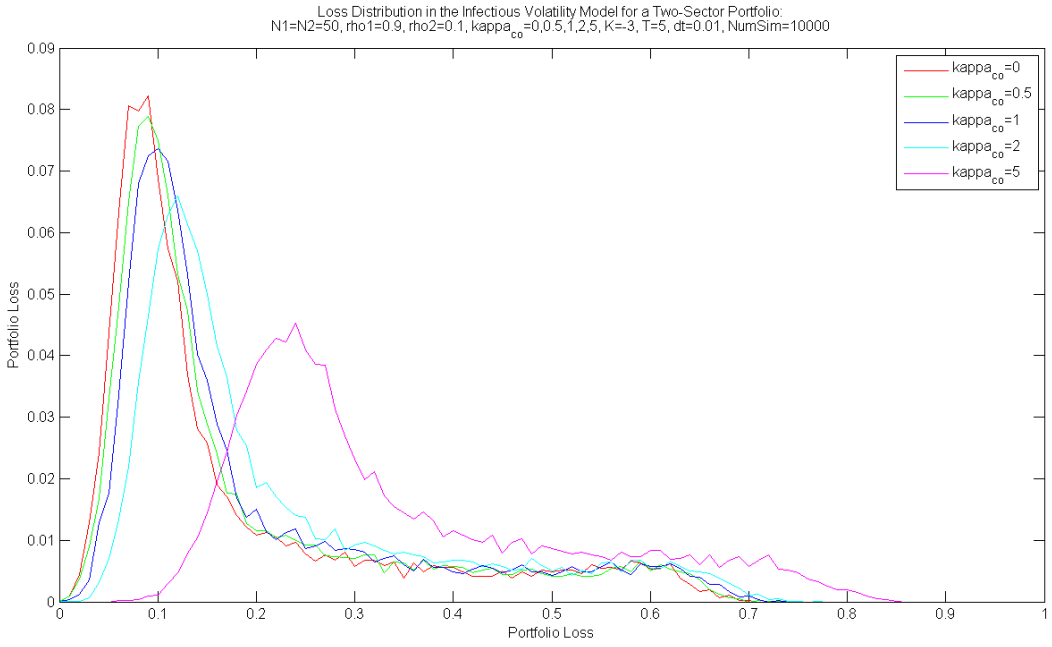

Figure 106: Loss Distribution in the Infectious Volatility Model

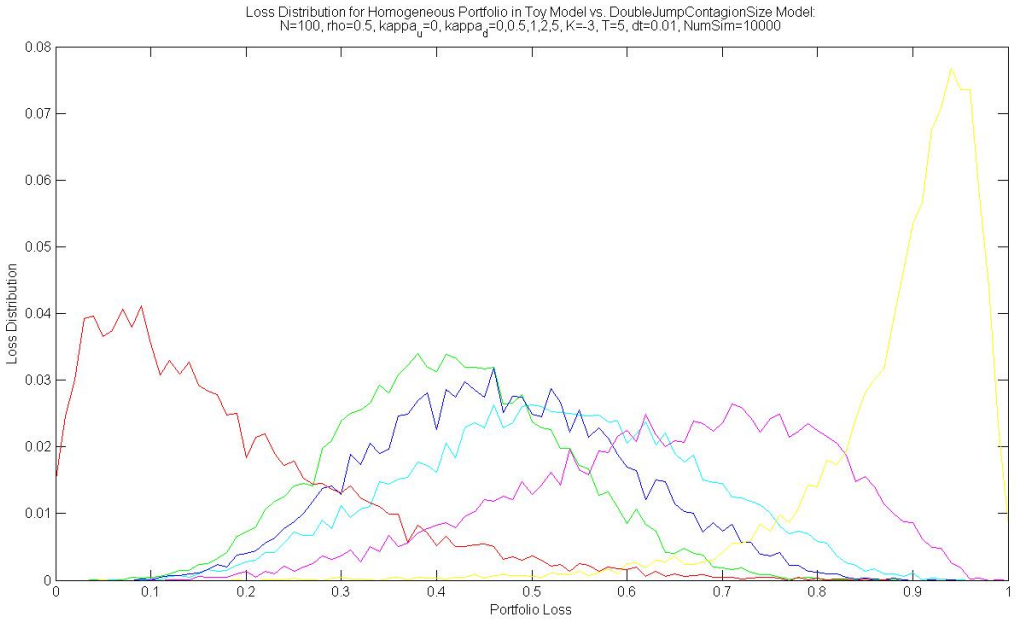

Figure 107: Loss Distribution in the Toy Model vs. Infectious Jump Size Model for Homogeneous Portfolio with Different Values of κ^d

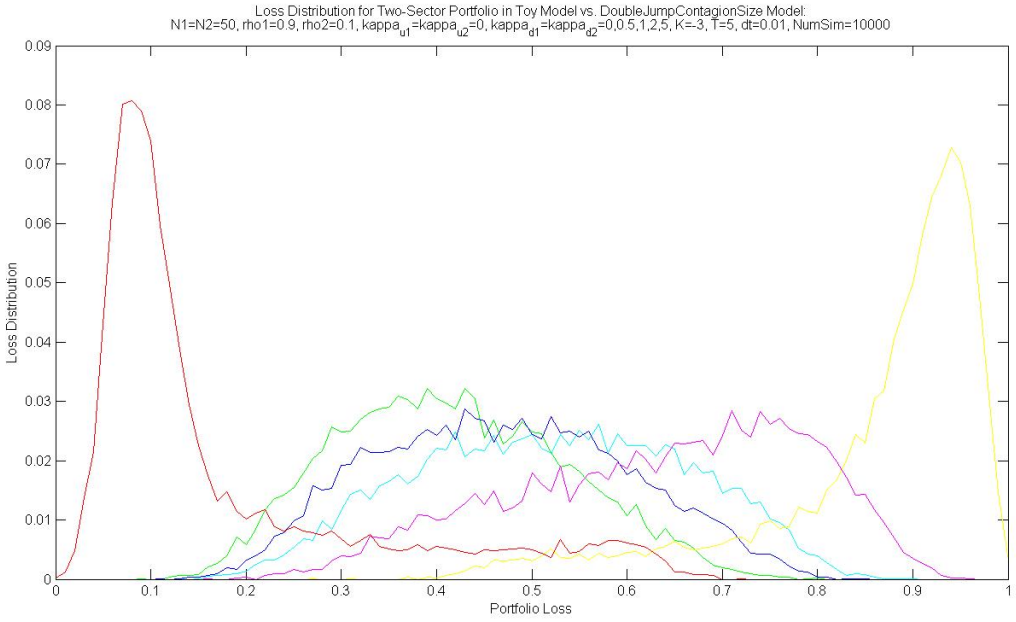

Figure 108: Loss Distribution in the Toy Model vs. Infectious Jump Size Model for Heterogeneous Portfolio with Different Values of $\kappa_1^d = \kappa_2^d$

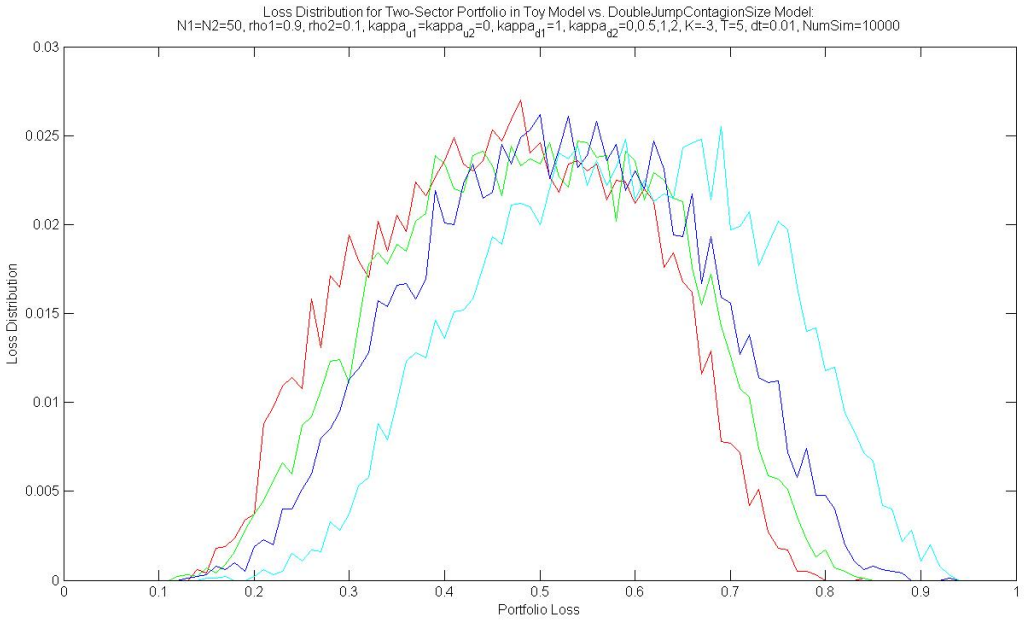

Figure 109: Loss Distribution in the Toy Model vs. Infectious Jump Size Model for Heterogeneous Portfolio with $\kappa_1^d = 1$ and Different Values of κ_2^d

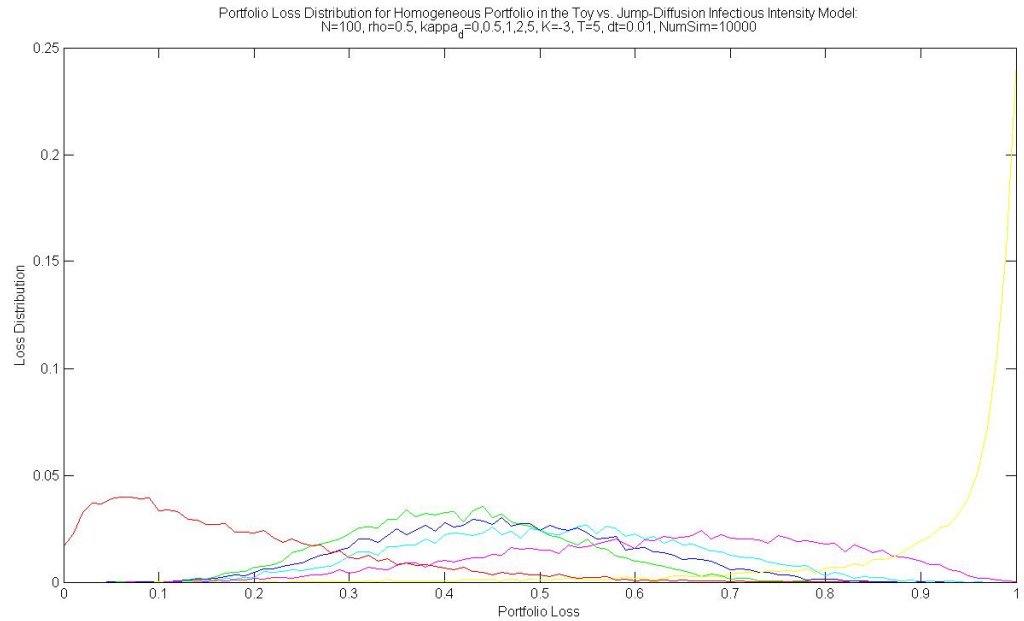

Figure 110: Loss Distribution in the Infectious Jump Intensity Model for Homogeneous Portfolio with Different Values of κ^d

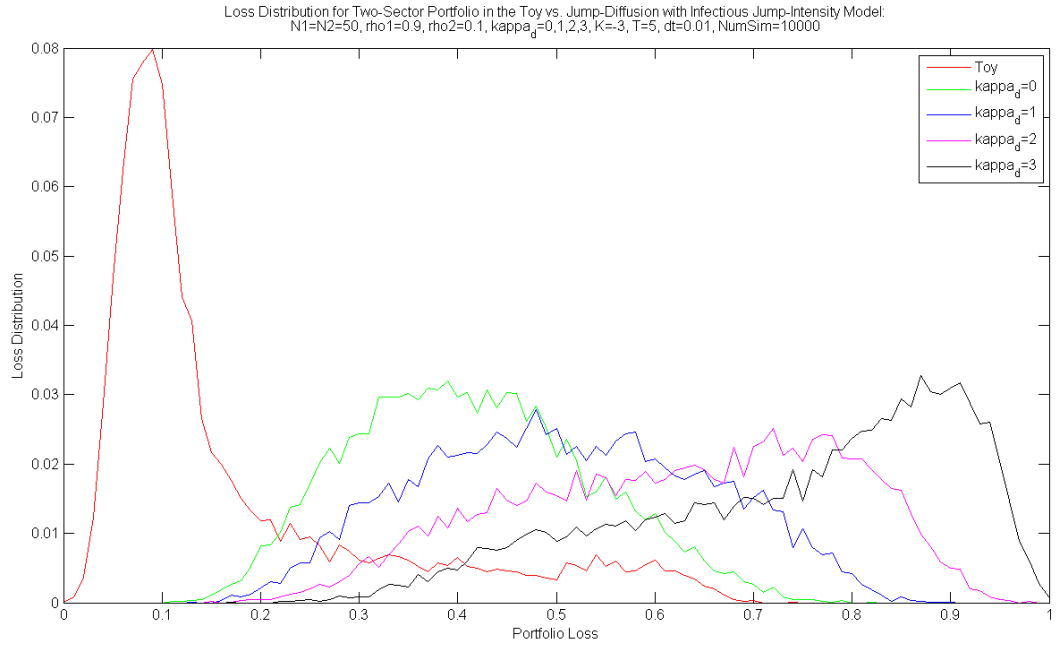

Figure 111: Loss Distribution in the Infectious Jump Intensity Model for Heterogeneous Portfolio with Different Values of $\kappa_1^d = \kappa_2^d$

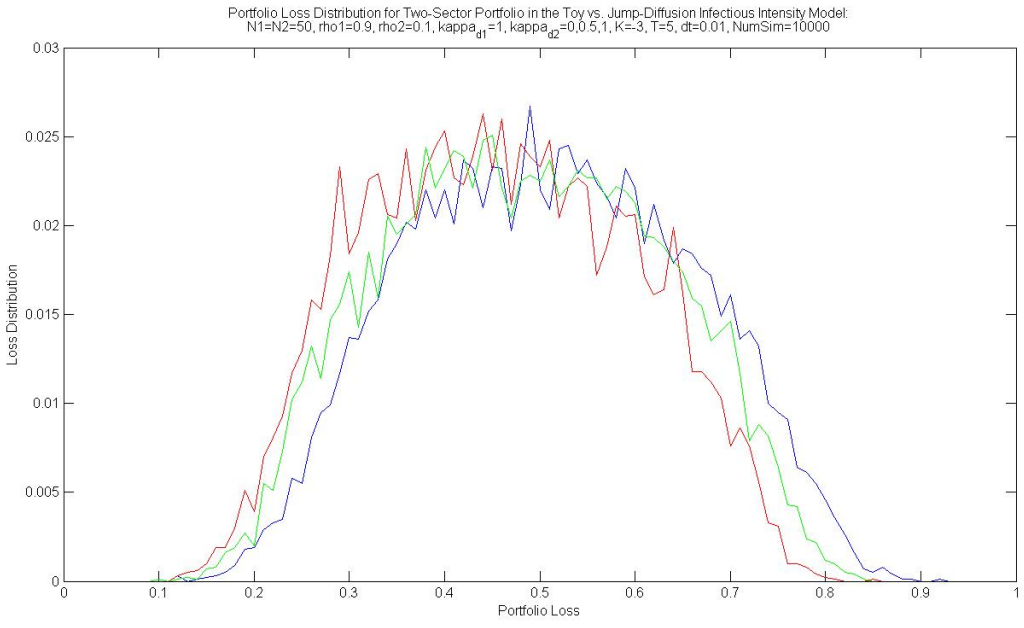

Figure 112: Loss Distribution in the Infectious Jump Intensity Model for Heterogeneous Portfolio with $\kappa_1^d = 1$ and Different Values of κ_2^d

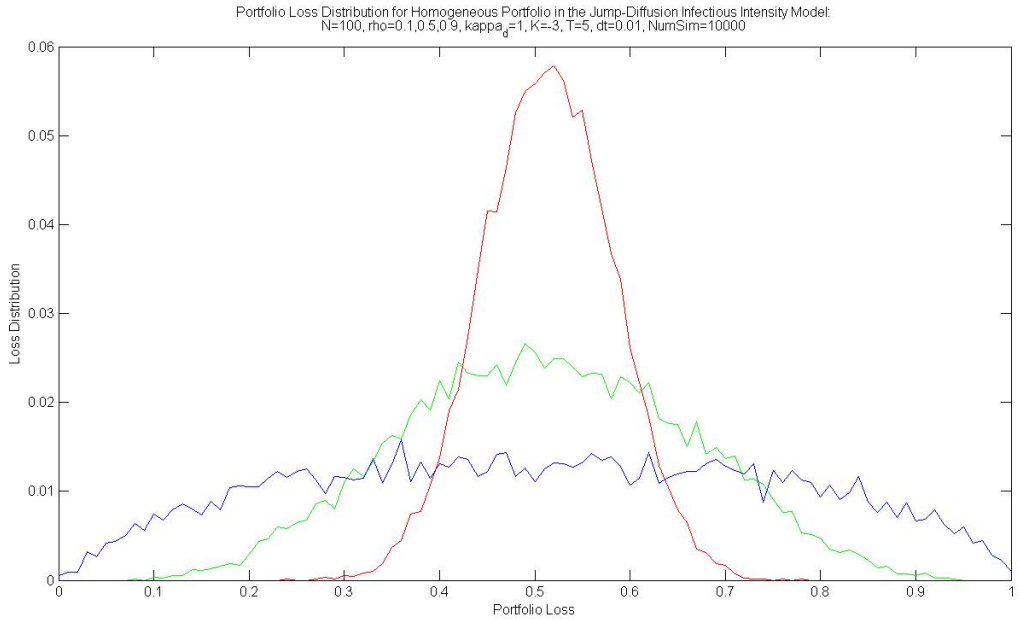

Figure 113: Loss Distribution in the Infectious Jump Intensity Model for Homogeneous Portfolio with Different Values of ρ

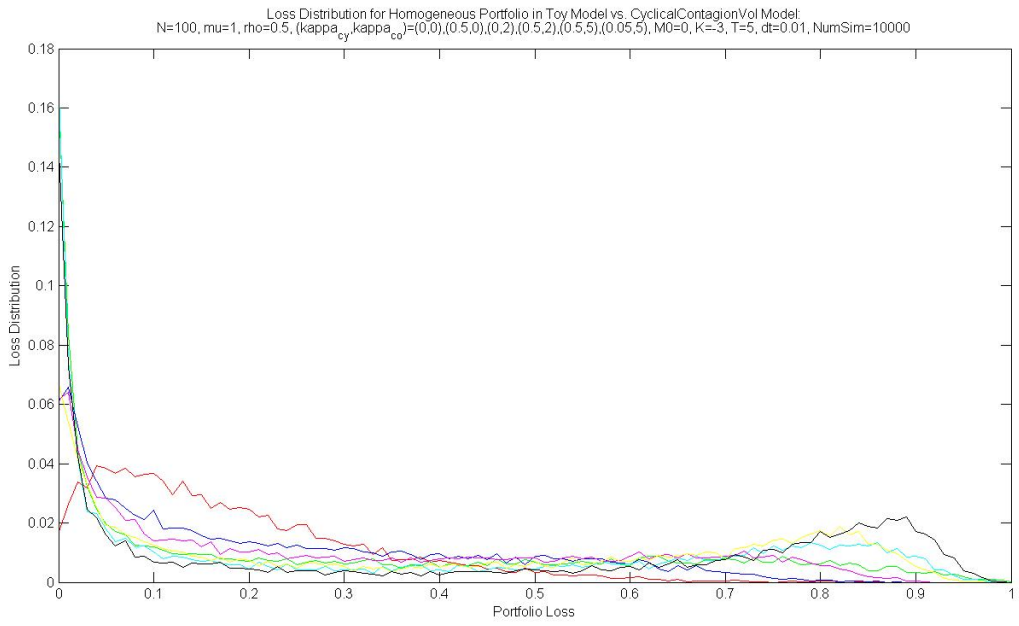

Figure 114: Loss Distribution in the Hybrid Model for Homogeneous Portfolio with Different Values of κ_{cy} and κ_{co}

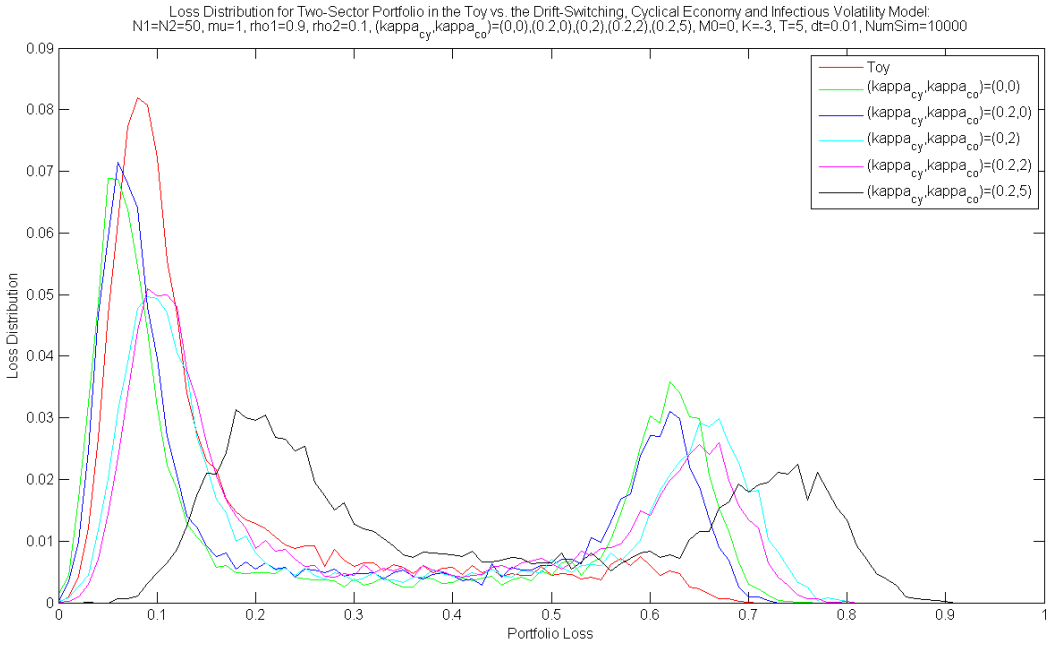

Figure 115: Loss Distribution in the Hybrid Model for Heterogeneous Portfolio with $M = 0$ and Different Values of κ_{cy} and $\kappa_{co}^1 = \kappa_{co}^2$

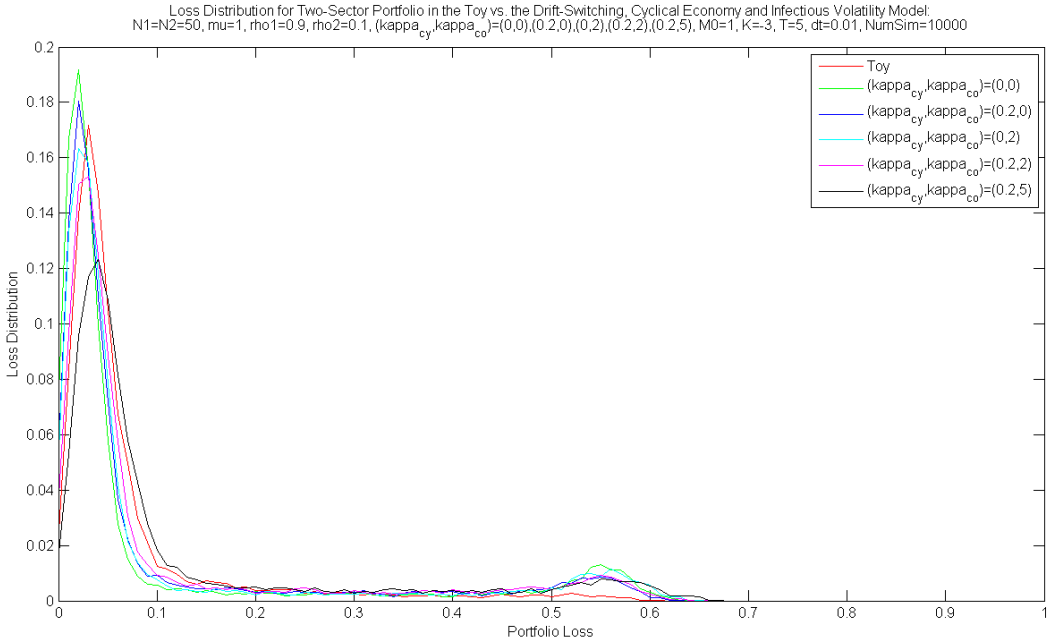

Figure 116: Loss Distribution in the Hybrid Model for Heterogeneous Portfolio with $M = 1$ and Different Values of κ_{cy} and $\kappa_{co}^1 = \kappa_{co}^2$

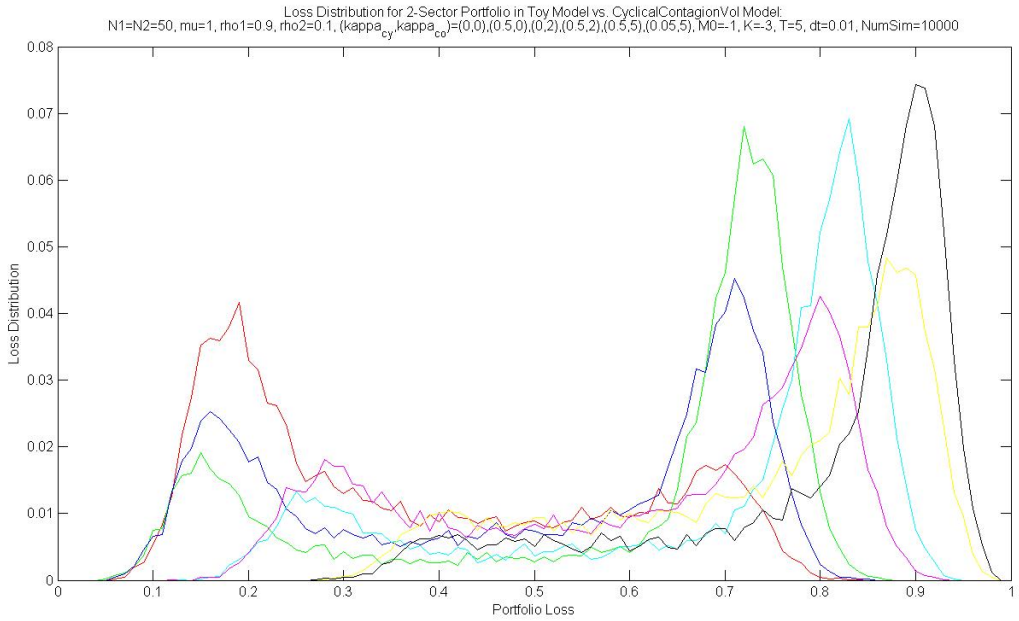

Figure 117: Loss Distribution in the Hybrid Model for Heterogeneous Portfolio with $M = -1$ and Different Values of κ_{cy} and $\kappa_{co}^1 = \kappa_{co}^2$

APPENDIX F

CHAPTER 6 TABLES

Table 9: Parameter Values and Relative Errors of Common Random Initial State Model Calibrated to CDO Tranches

α	λ	μ	$0\% - 3\%$	$3\% - 7\%$	$7\% - 10\%$	$10\% - 15\%$	$15\% - 30\%$	MRE
11.2987	37.421	6.403	2.23%	27.26%	0%	0%	50.23%	15.94%

Table 10: Actual vs. Model Upfront for the Common Random Initial State Model Calibrated to CDO Tranches

Tranche	$0\% - 3\%$	$3\% - 7\%$	$7\% - 10\%$	$10\% - 15\%$	$15\% - 30\%$
Actual	52.185%	16.605%	5.345%	-0.855%	-2.88%
Model	51.019%	21.131%	5.345%	-0.855%	-4.327%

Table 11: Actual vs. Model Spreads in O'Kane Mixing Copula Model Calibrated to Market Quotes

Tranche	$0\% - 3\%$	$3\% - 7\%$	$7\% - 10\%$	$10\% - 15\%$	$15\% - 30\%$	MRE
Actual	500	90	18.25	8	3.5	
O'Kane	500	90.25	18.25	5.97	2.38	11.53%

Table 12: Parameter Values and Mean Relative Error for IBM in the Switching Correlation Model with Random Initial State Calibrated to CDS Quotes

IBM	α	λ	MRE
04/12/2010	3.5269	0.295	4.17%
04/13/2010	3.5149	0.2928	3.61%
04/14/2010	3.529	0.2931	3.69%
04/15/2010	3.5997	0.2973	3.83%
04/16/2010	3.6193	0.2969	3.82%

Table 13: Parameter Values and Mean Relative Error for AIG in the Switching Correlation Model with Random Initial State Calibrated to CDS Quotes

AIG	α	λ	MRE
04/12/2010	3.2236	0.4691	3.87%
04/13/2010	3.2229	0.4689	3.89%
04/14/2010	3.2584	0.4701	3.51%
04/15/2010	3.3027	0.4749	4.05%
04/16/2010	3.2249	0.4597	4.4%

Table 14: Actual vs. Model Spreads for IBM in the Switching Correlation Model with Random Initial State Calibrated to CDS Quotes on April 12, 2010

IBM 04/12/2010	$1Y$	$2Y$	$3Y$	$4Y$	$5Y$	$7Y$	$10Y$
Actual	16.92	23.45	29.24	36.15	42.01	53.34	64.06
Switch. Corr.	14.27	23.45	30.98	37.44	43.12	52.71	63.94

Table 15: Actual vs. Model Spreads for IBM in the Switching Correlation Model with Random Initial State Calibrated to CDS Quotes on April 13, 2010

IBM 04/13/2010	$1Y$	$2Y$	$3Y$	$4Y$	$5Y$	$7Y$	$10Y$
Actual	16.82	23.31	29.26	35.67	42.45	52.11	63.36
Switch. Corr.	14.24	23.31	30.73	37.1	42.68	52.11	63.15

Table 16: Actual vs. Model Spreads for IBM in the Switching Correlation Model with Random Initial State Calibrated to CDS Quotes on April 14, 2010

IBM 04/14/2010	$1Y$	$2Y$	$3Y$	$4Y$	$5Y$	$7Y$	$10Y$
Actual	16.36	22.86	28.72	34.98	41.79	51.51	62.73
Switch. Corr.	13.9	22.86	30.22	36.54	42.1	51.51	62.54

Table 17: Actual vs. Model Spreads for IBM in the Switching Correlation Model with Random Initial State Calibrated to CDS Quotes on April 15, 2010

IBM 04/15/2010	$1Y$	$2Y$	$3Y$	$4Y$	$5Y$	$7Y$	$10Y$
Actual	15.41	21.37	27.45	33.53	40.21	50	61.32
Switch. Corr.	12.69	21.37	28.62	34.92	40.49	50	61.25

Table 18: Actual vs. Model Spreads for IBM in the Switching Correlation Model with Random Initial State Calibrated to CDS Quotes on April 16, 2010

IBM 04/16/2010	$1Y$	$2Y$	$3Y$	$4Y$	$5Y$	$7Y$	$10Y$
Actual	15.34	20.6	26.63	33.44	39.35	48.84	60.19
Switch. Corr.	12.15	20.6	27.69	33.88	39.4	48.76	59.9

Table 19: Actual vs. Model Spreads for AIG in the Switching Correlation Model with Random Initial State Calibrated to CDS Quotes on April 12, 2010

AIG 04/12/2010	$1Y$	$2Y$	$3Y$	$4Y$	$5Y$	$7Y$	$10Y$
Actual	111.79	161.18	198.85	232.94	267.36	272.67	275.17
Switch. Corr.	111.79	161.18	195.92	222.47	243.61	275.21	306.25

Table 20: Actual vs. Model Spreads for AIG in the Switching Correlation Model with Random Initial State Calibrated to CDS Quotes on April 13, 2010

AIG 04/13/2010	$1Y$	$2Y$	$3Y$	$4Y$	$5Y$	$7Y$	$10Y$
Actual	111.76	161.11	199.6	232.83	262.44	271.05	272.99
Switch. Corr.	111.76	161.11	195.82	222.34	243.46	275.04	306.05

Table 21: Actual vs. Model Spreads for AIG in the Switching Correlation Model with Random Initial State Calibrated to CDS Quotes on April 14, 2010

AIG 04/14/2010	$1Y$	$2Y$	$3Y$	$4Y$	$5Y$	$7Y$	$10Y$
Actual	106.63	155.7	190.97	226.18	252.15	264.61	268.4
Switch. Corr.	106.82	155.7	190.38	217.01	238.3	270.23	301.71

Table 22: Actual vs. Model Spreads for AIG in the Switching Correlation Model with Random Initial State Calibrated to CDS Quotes on April 15, 2010

AIG 04/15/2010	$1Y$	$2Y$	$3Y$	$4Y$	$5Y$	$7Y$	$10Y$
Actual	103.14	152.44	189.99	224.5	251.43	261.41	265.28
Switch. Corr.	103.21	152.44	187.69	214.9	236.71	269.53	301.94

Table 23: Actual vs. Model Spreads for AIG in the Switching Correlation Model with Random Initial State Calibrated to CDS Quotes on April 16, 2010

AIG 04/16/2010	$1Y$	$2Y$	$3Y$	$4Y$	$5Y$	$7Y$	$10Y$
Actual	104.77	150.96	189.11	224.98	258.2	260.15	263.46
Switch. Corr.	104.77	151.39	184.33	209.6	229.8	260.15	290.19

Table 24: Parameter Values and Mean Relative Error in the Switching Correlation Model with Random Initial State Calibrated to CDS Quotes

Name	α	λ	MRE
AIG	3.7779	0.4883	4.59%
Amgen	3.7929	0.3196	4.22%
American Express	3.8708	0.3706	6.08%
First Energy	4.261	0.5076	5.91%
Wal-Mart	3.8864	0.3342	5.83%

Table 25: Actual vs. Model Spreads for AIG in the Switching Correlation Model with Random Initial State Calibrated to CDS Quotes

AIG	$1Y$	$2Y$	$3Y$	$4Y$	$5Y$	$7Y$	$10Y$
Actual	55.41	93.99	128.37	167.87	202.16	219.29	232.61
Switch. Corr.	55.41	95.81	128.87	156.72	180.57	219.29	267.7

Table 26: Actual vs. Model Spreads for Amgen in the Switching Correlation Model with Random Initial State Calibrated to CDS Quotes

Amgen	$1Y$	$2Y$	$3Y$	$4Y$	$5Y$	$7Y$	$10Y$
Actual	11.31	18.94	26.42	35.76	45.59	58.37	69.03
Switch. Corr.	11.31	20.4	28.46	35.76	42.45	54.32	69.25

Table 27: Actual vs. Model Spreads for American Express in the Switching Correlation Model with Random Initial State Calibrated to CDS Quotes

American Express	$1Y$	$2Y$	$3Y$	$4Y$	$5Y$	$7Y$	$10Y$
Actual	18.25	28.9	43.88	58.1	71.98	83.59	92.72
Switch. Corr.	17.06	31.28	43.89	55.24	65.54	83.59	105.67

Table 28: Actual vs. Model Spreads for First Energy in the Switching Correlation Model with Random Initial State Calibrated to CDS Quotes

First Energy	$1Y$	$2Y$	$3Y$	$4Y$	$5Y$	$7Y$	$10Y$
Actual	30.91	61.89	98.61	131.16	158.97	181.23	203.88
Switch. Corr.	30.91	62.39	91.36	117.55	141.1	181.23	227.51

Table 29: Actual vs. Model Spreads for Wal-Mart in the Switching Correlation Model with Random Initial State Calibrated to CDS Quotes

Wal-Mart	$1Y$	$2Y$	$3Y$	$4Y$	$5Y$	$7Y$	$10Y$
Actual	14.86	20.78	28.24	37.38	46.19	60.94	71.83
Switch. Corr.	11.19	20.78	29.45	37.39	44.7	57.78	74.28

Table 30: Parameter Value and Relative Errors in the Switching Correlation Model with Random Initial State Calibrated to O'Kane Tranche Spreads

ρ_g	$0\% - 20\%$	$20\% - 40\%$	$40\% - 60\%$	MRE
0.4	12.47%	9.48%	48.25%	23.48%

Table 31: O'Kane vs. Model Tranche Spreads in the Switching Correlation Model with Random Initial State

Model Name	$0\% - 20\%$	$20\% - 40\%$	$40\% - 60\%$
O'Kane	491.45	41.13	5.95
Switch. Corr.	429.02	45.03	3.08
Avg. Corr.	456.36	33.94	0.76

Table 32: Parameter Values and Mean Relative Error in the Random Correlation Model with Random Initial State Calibrated to CDS Spreads

Name	y_0	μ	σ	MRE
AIG	3.2672	-0.212	0.8374	3.53%
Amgen	3.419	-0.0823	0.599	1.97%
American Express	3.3706	-0.0989	0.6709	3.68%
First Energy	3.5457	-0.2085	0.8386	2.54%
Wal-Mart	3.1942	-0.0899	0.5241	2.72%

Table 33: Actual vs. Model Spreads in the Random Correlation Model with Random Initial State for AIG

AIG	$1Y$	$2Y$	$3Y$	$4Y$	$5Y$	$7Y$	$10Y$
Actual	55.41	93.99	128.37	167.87	202.16	219.29	232.61
Rand. Corr.	55.41	99.97	137.93	167.32	189.55	219.14	242.56

Table 34: Actual vs. Model Spreads in the Random Correlation Model with Random Initial State for Amgen

Amgen	$1Y$	$2Y$	$3Y$	$4Y$	$5Y$	$7Y$	$10Y$
Actual	11.31	18.94	26.42	35.76	45.59	58.37	69.03
Rand. Corr.	11.31	18.94	27.42	35.76	43.48	56.51	70.52

Table 35: Actual vs. Model Spreads in the Random Correlation Model with Random Initial State for American Express

American Express	$1Y$	$2Y$	$3Y$	$4Y$	$5Y$	$7Y$	$10Y$
Actual	18.25	28.9	43.88	58.1	71.98	83.59	92.72
Rand. Corr.	18.25	31.4	44.82	56.97	67.44	83.59	98.96

Table 36: Actual vs. Model Spreads in the Random Correlation Model with Random Initial State for First Energy

First Energy	$1Y$	$2Y$	$3Y$	$4Y$	$5Y$	$7Y$	$10Y$
Actual	30.91	61.89	98.61	131.16	158.97	181.23	203.88
Rand. Corr.	30.91	65.63	99.06	127.08	149.51	181.23	208.39

Table 37: Actual vs. Model Spreads in the Random Correlation Model with Random Initial State for Wal-Mart

Wal-Mart	$1Y$	$2Y$	$3Y$	$4Y$	$5Y$	$7Y$	$10Y$
Actual	14.86	20.78	28.24	37.38	46.19	60.94	71.83
Rand. Corr.	14.86	21.74	29.53	37.38	44.88	58.19	73.64

Table 38: Parameter Value and Mean Relative Error in the Random Correlation Model with Random Initial State Calibrated to O'Kane Tranche Spreads

p	MRE
0.7582	5.54%

Table 39: Actual vs. Model Tranche Spreads in the Random Correlation Model with Random Initial State

Model Name	$0\% - 20\%$	$20\% - 40\%$	$40\% - 60\%$
O'Kane	491.45	41.13	5.95
Rand. Corr.	463.83	45.65	5.95
Avg. Corr.	491.14	28.06	0.19

Table 40: Implied $10Y$ Tranche Spreads in the Random Correlation Model with Random Initial State Calibrated to O'Kane Tranche Spreads

Model Name	$0\% - 20\%$	$20\% - 40\%$	$40\% - 60\%$
O'Kane	624.77	100.53	12.35
Rand. Corr.	626.53	116.6	19.53

BIBLIOGRAPHY

[1] M. Avellaneda, A. Levy, A. Parás (1995). Pricing and hedging derivative securities in markets with uncertain volatilities. *Applied Mathematical Finance*, 2, 73-88.

[2] M. Avellaneda and A. Parás (1996). Managing the volatility risks of portfolios of derivative securities: the Lagrangian uncertain volatility model. *Applied Mathematical Finance*, 3, 21-52.

[3] F. Black and J. C. Cox (1976). Valuing Corporate Securities: Some Effects of Bond Indenture Provisions. *Journal of Finance*, 31(2), 351-367.

[4] M. Broadie, P. Glasserman, S. Kou (1997). A Continuity Correction For Discrete Barrier Options. *Mathematical Finance*, 7(4), 325-348.

[5] U. Çetin, R. Jarrow, P. Protter, Y. Yildirim (2004). Modeling Credit Risk With Partial Information. *Annals of Applied Probability*, 14(3), 1167-1178.

[6] D. A. Dawson and D. Sankoff (1967). An Inequality For Probabilities. *Proceedings of the American Mathematical Society*, 18(3), 504-507.

[7] F. Delbaen and H. Shirakawa (2002). An Interest Rate Model with Upper and Lower Bounds. Working Paper.

[8] D. Duffie and K. Singleton (1999). Simulating Correlated Defaults. Working Paper.

[9] D. Duffie and D. Lando (2001). Term Structure Of Credit Spreads With Incomplete Accounting Information. *Econometrica*, 69(3), 633-664.

[10] J. P. Fouque, R. Sircar, K. Sølna (2006). A first-passage-time model under regime-switching market environment. *Applied Mathematical Finance*, 13(3), 215-244.

[11] J. P. Fouque, B. C. Wignall, X. Zhou (2008). Modeling correlated defaults: first passage model under stochastic volatility. *Journal of Computational Finance*, 11(3), 43-78.

[12] R. Frey and A. J. McNeil (2003). Dependent Defaults in Models of Portfolio Credit Risk. Working Paper.

[13] R. Frey and T. Schmidt (2010). Filtering and Incomplete Information in Credit Risk. Working Paper.

[14] K. Giesecke and S. Weber (2004). Cyclical correlations, credit contagion, and portfolio losses. *Journal of Banking & Finance*, 28, 3009-3036.

[15] K. Giesecke (2006). Default and information. *Journal of Economic Dynamics & Control*, 30, 2281-2303.

[16] P. Glasserman (2004). *Monte Carlo Methods in Financial Engineering*. Springer.

[17] E. Gobet (2008). Advanced Monte Carlo methods for barrier and related exotic options. Working Paper.

[18] X. Guo, R. A. Jarrow, Y. Zeng (2009). Credit Risk Models with Incomplete Information. *Mathematics Of Operations Research*, 34(2), 320-332.

[19] H. Haworth (2006). Structural Models of Credit with Default Contagion. Ph.D. Dissertation, Oxford University.

[20] J. Hull, M. Predescu, A. White (2005). The Valuation of Correlation-Dependent Credit Derivatives Using a Structural Model. Working Paper.

[21] D. Hunter (1976). An Upper Bound For The Probability Of A Union. *Journal of Applied Probability*, 13(3), 597-603.

[22] T. R. Hurd (2009). Credit Risk Modeling Using Time-Changed Brownian Motion. *International Journal of Theoretical and Applied Finance*, 12(8), 1213-1230.

[23] S. Iyengar (1985). Hitting lines with two-dimensional brownian motion. *SIAM Journal on Applied Mathematics*, 45(6), 983-989.

[24] K. Jackson, A. Kreinin, W. Zhang (2009). Randomization in the first hitting time problem. *Statistics and Probability Letters*, 79, 2422-2428.

[25] R. A. Jarrow and P. Protter (2004). Structural Versus Reduced Form Models: A New Information Based Prospective. *Journal of Investement Management*, 2(2), 1-10.

[26] R. A. Jarrow, P. Protter, A. D. Sezer (2007). Information reduction via level crossings in a credit risk model. *Finance and Stochastics*, 11, 195-212.

[27] I. Karatzas and S. E. Shreve (1987). *Brownian Motion and Stochastic Calculus*. Springer.

[28] Y. A. Katz and N. V. Shokhirev (2010). Default risk modeling beyond the first-passage approximation: Extended Black-Cox model. *Physical Review*, 82(1).

[29] M. A. Kim, B. G. Jang, H. S. Lee (2008). A first-passage-time model under regime-switching market environment. *Journal of Banking & Finance*, 32, 2617-2627.

[30] S. M. Kwerel (1975). Stringent Bounds on Aggregated Probabilities of Partially Specified Dependent Probability Systems. *Journal of the American Statistical Association*, 70(350), 472-470.

[31] D. L. McLeish and A. Metzler (2011). A multiname first-passage model for credit risk. *Journal of Credit Risk*, 7(1), 35-64.

[32] R. Merton (1974). On the Pricing of Corporate Debt: The Risk Structure of Interest Rates. *Journal of Finance*, 29(2), 449-470.

[33] A. Metzler (2008). Multivariate First-Passage Models in Credit Risk. Ph.D. Dissetation, University of Waterloo.

[34] D. O'Kane (2008). *Modelling Single-name and Multi-name Credit Derivatives*. The Wiley Finance Series.

[35] J. Ruf and M. Scherer (2009). Pricing corporate bonds in an arbitrary jump-diffusion model based on an improved Brownian-bridge algorithm. Working Paper.

[36] P. J. Schöbucher (2002). Taken To The Limit: Simple And Not-So-Simple Loan Loss Distributions. Working Paper.

[37] P. J. Schönbucher (2003). *Credit Derivatives Pricing Models*. John Wiley & Sons Ltd.

[38] S. E. Shreve (2004). *Stochastic Calculus for Finance II: Continuous-Time Models*. Springer Finance.

[39] T. K. Siu, C. Erlwein, R. S. Mamon (2008). The Pricing Of Credit Default Swaps Under A Markov-Modulated Merton'S Structural Model. *North American Actuarial Journal*, 12(1), 19-46.

[40] J. M. Steele (2000). *Stochastic Calculus and Financial Applications*. Springer.

[41] A. V. Valov (2009). First Passage Times: Integral Equations, Randomization and Analytical Approximations. Ph.D. Dissertation, University of Toronto.

[42] M. Valužis (2008). On the Probabilities of Correlated Defaults: a First Passage Time Approach. Working Paper.

[43] O. Vasicek (1987). Probability of loss on loan portfolio. Working Paper, KMV Corporation.

[44] M. B. Wise and V. Bhansali (2008). Correlated Random Walks and the Joint Survival Probability. Working Paper.

[45] C. Yi, A. Tchernitser, T. Hurd (2011). Randomized structural models of credit spreads. *Quantitative Finance*, 11(9), 1301-1313.

[46] Y. Yildirim (2006). Modelling Default Risk: A New Structural Approach. Working Paper.

[47] C. Zhou (2001). An analysis of default correlations and multiple defaults. *Review of Financial Studies*, 14(2), 555-576.

[48] C. Zhou (2001). The Term Structure of Credit Spreads with Jump Risk. *Journal of Banking & Finance*, 25, 2015-2040.